APPLICATION OF MULTIPROXY TRACERS TO RECONSTRUCT PALEOENVIRONMENTAL PERTURBATIONS ON THE MID-ATLANTIC MARGIN ACROSS THE PALEOCENE-EOCENE THERMAL MAXIMUM

By

MARIA MAKAROVA

A dissertation submitted to the

School of Graduate Studies

Rutgers, The State University of New Jersey

In partial fulfillment of the requirements

For the degree of

Doctor of Philosophy

Graduate Program in Geological Sciences

Written under the direction of

Dr. Kenneth G. Miller

And approved by

_____

_____

_____

_____

New Brunswick, New Jersey

October, 2018

ABSTRACT OF THE DISSERTATION

Application of multiproxy tracers to reconstruct paleoenvironmental perturbations on the mid-Atlantic margin across the Paleocene-Eocene thermal maximum

By MARIA MAKAROVA

Dissertation Director:

Dr. Kenneth G. Miller

The Paleocene-Eocene Thermal Maximum (PETM) was an abrupt warming event (~56 Ma) characterized by a global temperature increase estimated to be on the order of 4-9°C and associated with a carbon isotope excursion of 2-7‰ requiring a substantial addition of light carbon (^{12}C) into global reservoirs. This dissertation presents an integrated view of the spatial and temporal environmental perturbations caused by the PETM on the mid-Atlantic continental shelf by the use of multiple paleoproxies. The approach used here to resolve regional from global ecological and hydrographic responses is to construct a cross-shelf transect with sites that range in coastal proximity and environmental influence. I show new records from Millville and Medford cores and sample the PETM in a shelf transect of five drillsites from the New Jersey Coastal Plain (NJCP): Medford, Wilson Lake, Ancora, Millville, and Bass River.

Application of the multiproxy approach reveals a warming of 6-7°C on the New Jersey paleoshelf during the PETM. Surface dwelling foraminifera recorded smaller $\delta^{18}O$ anomalies, caused by changes in shelf hydrography and/or calcification preclusion of foraminifera at temperatures above the survival limit of ~33°C. The organic paleothermometer TEX_{86}-based temperature estimates show comparable warming anomalies among the NJCP sections with a slightly larger warming recorded in the nearshore sites. The study of the Medford cores, the most expanded section of the PETM onset from the NJCP, indicated no warming prior to the CIE onset, rejecting the precursor warming hypothesis. Bulk sediment records together with trace elemental ratios in foraminifera suggested rapid mud deposition on the shelf accompanied by a decrease in the water column oxygen content.

The significance of this work is a detailed chemostratigraphic correlation that integrates planktonic and benthic foraminiferal stable isotopic data, temperature records from independent proxies (TEX_{86} and foraminiferal Mg/Ca ratio), and an evaluation of salinity variations on the shelf. Lastly, this study utilizes the novel paleoredox proxy (foraminiferal I/Ca ratio) to evaluate water column deoxygenation on the New Jersey paleoshelf during the PETM.

DEDICATION

To my parents Elena and Alexander

ACKNOWLEDGEMENTS

First and furthermost, I would like to thank my advisor Dr. Ken Miller. I was very fortunate to have you as my mentor during seven years at Rutgers. I am grateful for sharing your enormous passion for science with me and thankful for the opportunity to continue my M.S. research and develop it into Ph.D. dissertation. Your inspiring enthusiasm and endless support kept pushing me further in my research, my career, and personal growth. I would not have completed this journey without such mentor by my side!

I am thankful to my committee member Dr. Jim Wright for always asking insightful questions and sharing bright ideas. That long waiting time by your office door was totally worth it, because I really enjoyed our scientific discussions that fundamentally shaped my outlook on academic research. Large amounts of data I present here was generated at Jim Wright's lab, and I am grateful for his tremendous help with stable isotope analyses.

I would like to thank my committee member Dr. Yair Rosenthal for always welcoming me in his lab and encouraging me in my research. I am grateful for your thoughtful comments and revisions that greatly improved this manuscript. Thanks for asking "Masha kak dela?" that always made me smile. Large amounts of my data was generated at Yair Rosenthal's lab, and I am thankful for helping me with trace elemental analyses.

My gratitude goes to Dr. Tim Herbert for providing support and valuable feedback as my external committee member and the opportunity to do exciting research at Brown University. I would like to thank the research team from Brown, Dr. Marcelo Da Rosa Alexandre, Dr. Rafael Tarozo, Dr. Alexandrina Tzanova, and Shuo Yang, who helped me perform lipid biomarker analyses.

I also would like to thank Dr. Jim Browning for your unconditional support and advice, as well as for helping me in the core repository, providing manuscript edits, and of course the best yoga sessions.

I am grateful to Dr. Rick Mortlock, Dr. Nicole Abdul, and Dr. Linda Godfrey for their tremendous help with stable isotope analyses.

I would like to thank Dr. Tali Babila, Dr. Xiaoli Zhou, and Dr. Ryan Bu for helping with trace elemental analyses and valuable discussions. Tali thanks for sharing your endless inspiration and being my all-time cheerleader.

I am also grateful to Dr. Richard Olsson, Dr. William Berggren, and Dr. Marie-Pierre Aubry for their help with foraminiferal taxonomy, helpful discussions, and introduction to micropaleontology, that I felt in love with.

I am grateful to Dr. Dennis Kent and Dr. Morgan Schaller for helpful discussions.

I also would like to thank my Marlboro Clay comrades, Dr. Chris Lombardi and Luca Podrecca, for help in the core repository and sharing the PETM struggles.

I thank Dr. Vadim Levin for always providing your advice and support, Russian conversations in department hallways, and cottage cheese pancakes!

I would like to thank all faculty, staff, and students from the Department of Earth and Planetary Sciences for their help, friendships and good times we spent together. Thank you all for making me feel like being home at Rutgers! In particular, thanks to my dear friends César, Linda, and Max G. and his family. Huge thanks go to my current and past lab mates and grad students from the Earth and Planetary Sciences Department. This list is so long, forgive me all for not listing your names. You literally rocked my world!

I also would like to thank my mentors and friends from my alma mater Moscow State University, especially Natasha, Vika, Inessa, Marina, Alyona, Yulya, Lenar,

Andrey, Sasha, Seryoja, and Dima. I always feel your love and support despite great distances separating us.

Special thanks go to my soul sister Katerina Speir and her family for your love, support, friendship, and never ending Russian feast.

My very special thanks go to Kevin Faroni for your endless love, acceptance, and unconditional support and the Faroni family for happy moments we shared and the warmest welcome I could possibly wish for.

Last but not least, I want to thank my family: mom Lena, dad Sanya, and sister Ira. You are the core of my confidence and strength! Thanks for your unconditional love, prayers, and support during my journey at Rutgers. I love you to the Moon and back!

This work would not be possible without support by fellowships, scholarships, and research grants. I would like to express my gratitude to the Department of Earth and Planetary Sciences and School of Arts and Sciences for excellence fellowships, the Department of Earth and Planetary Sciences for travel support, and School of Graduate Studies, New Brunswick for the special study award. I am grateful to the Cushman Foundation for Foraminifera Research and the Geological Society of America for providing research grants. I would like to thank the National Science Foundation for providing funds to attend summer courses, IsoCamp and Urbino Summer School in Paleoclimatology. I also thank the ExxonMobil Russian Scholars Program and personally Bob Stewart, Brenda Roper, and Enam Haddad for providing scholarship to pursue a M.S. degree at Rutgers and support during my first three years in the U.S.

TABLE OF CONTENTS

ABSTRACT OF THE DISSERTATION ii

DEDICATION iv

ACKNOWLEDGEMENTS v

TABLE OF CONTENTS viii

LIST OF TABLES AND APPENDICES xii

LIST OF FIGURES xiv

I. Chapter One: Introduction to the dissertation 1

1.1. Introduction 1

1.2. References 7

II. Chapter Two: Hydrographic and ecologic implications of foraminiferal stable isotopic response across the mid-Atlantic U.S. continental shelf during the Paleocene-Eocene Thermal Maximum 10

2.1. Abstract 11

2.2. Introduction 12

2.3. ODP Leg 174AX Millville site 15

2.4. Methods 17

2.4.1. Analyses 17

2.4.2. Correction for test size 18

2.4.3. Planktonic foraminiferal depth habitats 20

2.5. Results 21

2.5.1. Millville foraminiferal isotopic records 21

2.5.2. Foraminiferal isotopic records from the New Jersey paleoshelf 23

2.6. Discussion 26

2.6.1. Environmental and biotic controls on stable isotope records of foraminifera 26

2.6.2. Environmental response of other plankton 33

2.7. Conclusions 36

2.8. Acknowledgments 37

2.9. References 37

2.10. Figures 49

2.11. Tables 56

2.12. Supporting information 64

III. Chapter Three: Blackout of planktonic foraminifera: seasonality effects on surface ocean climate reconstructions at the Paleocene-Eocene thermal maximum 75

3.1. Abstract 75

3.2. Introduction 76

3.3. Geological Setting and Methods 77

3.3.1. Lipid biomarker analyses (TEX_{86}) 78

3.3.2. Trace element analyses of foraminifera 79

3.4. Results 79

3.4.1. TEX_{86}-based temperature estimates 79

3.4.2. Mg/Ca-based temperature estimates 81

3.5. Discussion 81
3.5.1. Sea surface temperature anomaly at Millville, NJ 81
3.5.1.1. Oxygen isotopes of foraminifera 81
3.5.1.2. TEX_{86}-derived temperature estimates 85
3.5.1.3. Mg/Ca-derived temperature estimates 87
3.5.2. Spatial distribution of temperature anomalies on the New Jersey paleoshelf during the PETM: intersites comparison of TEX_{86}-based estimates 88
3.5.3. Temperature estimates in other PETM sections from low-mid latitudes .. 92
3.5.4. Salinity evaluations on the New Jersey paleoshelf during the PETM 95
3.6. Conclusions 97
3.7. Acknowledgments 98
3.8. References 99
3.9. Figures 107
3.10. Tables 121

IV. Chapter Four: Proximity does it: Reconstructions of the PETM onset at Medford, New Jersey (USA) 126
4.1. Abstract 126
4.2. Introduction 127
4.3. Geological Setting and Methods 131
4.3.1. Lithological description of the MAP 3A, 3B, and 5A cores 132
4.3.2. Methods 133
4.3.3. Paleoredox reconstructions from I/Ca in foraminifera 135

4.4. Results 136
4.4.1. Bulk sediment isotopic records from Medford Sites MAP 3A and 3B 136
4.4.2. Foraminiferal assemblages at MAP 3A, Medford, NJ 137
4.4.3. Foraminiferal stable isotopes from multiple-specimen analysis at MAP 3A, Medford, NJ 139
4.4.4. Preliminary results of foraminiferal stable isotopes from single-specimen measurements at MAP 3A, Medford, NJ 140
4.4.5. Trace elements (Mg/Ca, I/Ca) in foraminifera at MAP 3A, Medford, NJ 141
4.4.6. TEX_{86} derived temperature estimates at MAP 3B, Medford, NJ 142
4.5. Discussion 143
4.5.1. Depositional model for the New Jersey paleoshelf during the PETM 143
4.5.2. Precursor warming? Results of multi proxy temperature estimates at Medford, NJ 144
4.5.3. Paleoredox evaluation from trace metals in planktonic and benthic foraminifera from Medford, NJ 147
4.6. Conclusions 148
4.7. Acknowledgements 150
4.8. References 150
4.9. Figures 156
4.10. Tables 181

V. Conclusions and Dissertation Final Remarks 194

VI. Appendices..... 198

LIST OF TABLES AND APPENDICES

Table 2.1. Measured stable isotopic values of planktonic and benthic foraminifera at Millville, NJ. Table includes adjusted for core expansion depths and corrected for test size $\delta^{13}C$ values. Samples from the core expansion are marked in quotes 56

Table 2.S1. Paleowater depths estimates for the Vincentown Formation at the New Jersey coastal plain sites (WL – Wilson Lake; AN – Ancora; MV – Millville; BR – Bass River) using possible end-member assumptions of the paleoslope gradient and errors in the anchor point at Medford (MD), NJ and site projections to a dip profile (±5 m in the relative placement) 74

Table 2.S2. Stable carbon isotopic values of *Subbotina roesnaesensis* from the 150-212 μm and 300-350 μm size fractions at Wilson Lake Hole B, NJ with indicated offset in $\delta^{13}C$ values between small (150-212 μm) and large specimens (300-350 μm) due to the vital effect 74

Table 3.1. GDGT abundances and TEX_{86} estimated temperatures [Kim et al., 2010] from Millville, NJ 121

Table 3.2. GDGT abundances and BIT values from Millville, NJ 123

Table 3.3. Mg/Ca ratios in *Morozovella*, *Acarinina*, and *Subbotina* spp. at Millville, NJ. Mg/Ca values calibrated to temperatures using Anand et al. [2003] multispecies equation (calibration error is ±1°C) and seawater Mg/Ca of 2.5 mmol/mol 124

Table 4.1. Percent coarse (>63 μm) fraction at MAP 3A, 3B, and 5A, Medford, NJ. Table includes modified for core expansion depths (mcd). Samples from the core expansion are marked in quotes 181

Table 4.2. Stable isotopic values measured in multi-specimen samples of planktonic and benthic foraminifera at MAP 3A, Medford, NJ. Table includes modified for core expansion depths (mcd). Samples from the core expansion are marked in quotes 184

Table 4.3. Stable isotopic values measured in single specimens of planktonic and benthic foraminifera at MAP 3A, Medford, NJ. Table includes modified for core expansion depths (mcd) 186

Table 4.4. Trace elemental ratios in planktonic and benthic foraminifera at the MAP 3A core, Medford, NJ. Table includes modified for core expansion depths (mcd). Samples from the core expansion are marked in quotes 188

Table 4.5. GDGT abundances and TEX_{86} estimated temperatures [Kim et al., 2010] from the MAP 3B core at Medford, NJ. Table includes modified for core expansion depths (mcd) 191

Table 4.6. GDGT abundances and BIT values from the MAP 3B core at Medford, NJ. Table includes modified for core expansion depths (mcd) 193

Appendix 1. Trace elements ratios in in *Morozovella*, *Acarinina*, and *Subbotina* spp. at Millville, NJ 198

Appendix 2. Percent coarse (>63 μm) fraction at Millville, NJ (Chapter Two). Table includes modified for core expansion depths (mcd). Samples from the core expansion are marked in quotes 199

Appendix 3. Bulk sediment $\delta^{13}C$, $\delta^{18}O$, and % $CaCO_3$ at Millville, NJ (Chapter Two). Table includes modified for core expansion depths (mcd). Samples from the core expansion are marked in quotes 201

Appendix 4. Organic carbon data (TOC, $\delta^{13}C$, Total N, C:N) at Millville, NJ (Chapter Two). Table includes modified for core expansion depths (mcd). Samples from the core expansion are marked in quotes 204

Appendix 5. Trace elements ratios in in *Morozovella*, *Acarinina*, *Subbotina, Cibicidoides*, and *Anomalinoides* spp. at MAP 3A, Medford, NJ (Chapter Four) 205

LIST OF FIGURES

Fig. 2.1. Location map of the PETM sections on the New Jersey coastal plain: Wilson Lake, Ancora, Millville, and Bass River. Red circles indicate the New Jersey coreholes and blue circle shows an anchor point at Medford, NJ used for paleodepth reconstructions during Vincentown deposition. Black solid lines represent projection of sites onto a dip profile drawn through Medford outcrop and Bass River. Dashed lines indicate structural contours from Zapecza [1984] with depths to the top of the Campanian in meters (red) and feet (blue) (modified after Esmeray-Senlet et al. [2015]) 49

Fig. 2.2. Correlation of bulk carbonate $\delta^{13}C$ records between the New Jersey coastal plain ODP sites Wilson Lake Hole B [Wright and Schaller, 2013], Ancora [this study], Millville [this study], Bass River [Cramer et al., 1999; John et al., 2008] and open ocean ODP Site 690, the Weddell Sea [Bains et al., 1999]. Records are aligned on the CIE onset and correlated at the CIE "core" and recovery sections. Vertical scale is uniform to demonstrate different resolution of the CIE "core" and recovery intervals among the sites 50

Fig. 2.3. Compilation of records at Millville, NJ: cumulative grain size, % CaCO3, $\delta^{13}C$ and $\delta^{18}O$ (plotted in reverse order) of bulk carbonate, planktonic and benthic foraminifera. Bulk carbonate data are from this study and Wright and Schaller [2013]. Thermocline dwellers *Subbotina* spp. are in blue, surface dwellers *Morozovella* spp. and *Acarinina* spp. are in red and green, respectively. For benthic foraminifera, *Gavelinella beccariiformis* in black, *Anomalinoides acuta* in purple, and *Cibicidoides* spp. in brown. Wavy red lines represent sharp unconformable contacts and dashed red lines indicate gradational contacts between the formations. Arrow indicates the CIE onset. Depths are modified, corrected for core expansion. Both corrected and modified core depths are given in Table 2.S1. Mnsq – Manasquan Formation 51

Fig. 2.4. Monogeneric stable carbon isotopes records of foraminifera at Millville. Samples from smaller size fractions (150-212 and 212-250 μm) are outlined in black, solid lines represent corrected for the test size $\delta^{13}C$ values. The orange vertical bar indicates a stable interval of the CIE "core" from which the average CIE "core" $\delta^{13}C$ value was estimated 52

Fig. 2.5. Monogeneric stable oxygen isotopes records of foraminifera at Millville. Samples from smaller size fractions (150-212 and 212-250 μm) are outlined in black. The orange vertical bar indicates a stable interval of the CIE "core" from which the average CIE "core" $\delta^{18}O$ value was estimated 53

Fig. 2.6. Planktonic and benthic foraminifera cross plots of $\delta^{18}O$ versus $\delta^{13}C$ generated for the New Jersey coastal plain ODP sites Wilson Lake Hole A [Zachos et al., 2006], Ancora [Cramer and Kent, 2005; Babila, 2014], Millville [this study], and Bass River [Cramer et al., 1999; Zachos et al., 2007; John et al., 2008; Babila et al., 2016]. Bottom panels show surface to benthic foraminifera isotopic gradients

in the interval below the CIE onset and top panels illustrate those in the CIE "core" 54

Fig. 2.7. Hydrographic reconstruction of the New Jersey paleoshelf for the periods of pre-CIE (a) and CIE "core" deposition (b, c). Panels b and c illustrate two scenarios explaining different isotopic response in surface versus thermocline dwellers after the CIE onset: b – change in the water column structure; c – change in habitat of the surface dwellers. Red and blue lines represent $\delta^{18}O$ gradients drawn for each site with single genera average $\delta^{18}O$ values plotted on top. Foraminiferal $\delta^{18}O$ data are from: Wilson Lake Hole A [Zachos et al., 2006]; Ancora [Babila, 2014; Cramer and Kent, 2005]; Millville [this study]; and Bass River [Cramer et al., 1999; Zachos et al., 2007; John et al., 2008; Babila et al., 2016]. Paleoslope reconstruction is modified for the PETM after Esmeray-Senlet et al. [2015]. Plots on the right show thermal structure of the water column across the modern New Jersey shelf in June and October [Castelao et al., 2010] 55

Fig. 2.S1. Stable carbon and oxygen isotopes of planktonic and benthic foraminifera at Millville, NJ: top – monogeneric records compiled from single species samples indicated in the legend; bottom – single species cross plots of $\delta^{18}O$ vs. $\delta^{13}C$ for the pre-CIE, CIE "core", CIE recovery, and post-CIE intervals. Thermocline dwellers *Subbotina* spp. are in blue, surface dwellers *Morozovella* spp. and *Acarinina* spp. are in red and green, respectively. For benthic foraminifera, *Gavelinella beccariiformis* in black, *Anomalinoides acuta* in purple, and *Cibicidoides* spp. in brown. Samples from smaller size fractions of 150-212 and 212-250 μm are outlined in black. Carbon isotopic values from smaller specimens are corrected for the test size (See 2.4 "Methods" in the main text). Oxygen isotope records are plotted in reverse order. Depths are modified and corrected for core expansion 72

Fig. 2.S2. PETM carbon isotope records of planktonic and benthic foraminifera from New Jersey coastal plain sites correlated by the CIE onset: Wilson Lake Hole A [Zachos et al., 2006; Stassen et al., 2012]; Ancora [Cramer and Kent, 2005; Babila, 2014]; Millville [this study]; and Bass River [Cramer et al., 1999; Zachos et al., 2007; John et al., 2008; Stassen et al., 2012; Babila et al., 2016]. Arrow indicates the CIE onset. Benthic foraminifera: *Gavelinella beccariiformis* in black, *Anomalinoides acuta* in purple, *Cibicidoides* spp. in brown. Planktonic foraminifera: thermocline dwellers *Subbotina* spp. in blue, surface dwellers *Morozovella* spp. and *Acarinina* spp. in red and green, respectively 73

Fig. 3.S3. PETM oxygen isotope records (plotted in reverse) of planktonic and benthic foraminifera from New Jersey coastal plain sites correlated by the CIE onset: Wilson Lake Hole A [Zachos et al., 2006]; Ancora [Cramer and Kent, 2005; Babila, 2014]; Millville [this study]; and Bass River [Cramer et al., 1999; Zachos et al., 2007; John et al., 2008; Babila et al., 2016]. Arrow indicates the CIE onset. Benthic foraminifera: *Gavelinella beccariiformis* in black, *Anomalinoides acuta* in purple, *Cibicidoides* spp. in brown. Planktonic foraminifera: thermocline dwellers *Subbotina* spp. in blue, surface dwellers *Morozovella* spp. and *Acarinina* spp. in red and green, respectively 73

Fig. 3.1. Carbon (lower panel) and oxygen (upper panel) isotopic records of multispecimen samples of foraminifera at Millville, NJ: benthic *Cibicidoides* spp. (brown), *A. acuta* (purple), *G. beccariiformis* (gray); thermocline dwelling *Subbotina* spp. (blue); surface dwelling *Acarinina* spp. (green), *M. acuta* (red triangulars) and *M. aequa* (red diamonds). Samples contain spesimens from one size fraction (>250, 200-250, or 150-200 μm) with larger spesimens highlighted in darker shades and smaller spesimens in lighter. Isotopic values are given in Table 2.1 in Chapter Two. Data from Si and Aubry [2018] are plotted in black symbols 107

Fig. 3.2. Multiproxy records used for temperature reconstructions at Millville, NJ: $\delta^{18}O$ and Mg/Ca of surface dwelling (*Morozovella* spp. in red; *Acarinina* spp. in green) and thermocline dwelling (*Subbotina* spp. in blue) foraminifera and TEX_{86} expressed as GDGT ratio-1 (TEX^{L}_{86}) and GDGT ratio-2 (TEX^{H}_{86}) [Kim et al., 2010]. See fig. 3.1 for labels of planktonic foraminiferal $\delta^{18}O$ symbols 108

Fig. 3.3. TEX_{86}-derived temperature estimates at Millville, NJ. Calibration errors for TEX^{H}_{86} and TEX^{L}_{86} are ±2.5°C and ±4°C, respectively [Kim et al., 2010]. Lithology and bulk carbonate $\delta^{13}C$ record are from Makarova et al. [2017] and Wright and Schaller [2013] 109

Fig. 3.4. Temperature anomaly (Δ) at Millville, NJ estimated from $\Delta\delta^{18}O$ values of surface dwelling (*Morozovella* spp. in red; *Acarinina* spp. in green) and thermocline dwelling dwelling (*Subbotina* spp. in blue) foraminifera considering a 0.25‰/°C gradient [O'Neil et al., 1969] and TEX_{86} indices from Kim et al. [2010]. Calibration errors for TEX^{H}_{86} and TEX^{L}_{86} are ±2.5°C and ±4°C, respectively [Kim et al., 2010]. See fig. 3.1 for labels of planktonic foraminiferal $\delta^{18}O$ symbols 110

Fig. 3.5. Temperature anomaly (Δ) at Millville, NJ estimated from $\Delta\delta^{18}O$ (0.25‰/°C gradient; O'Neil et al. [1969]) and Mg/Ca values of thermocline dwelling *Subbotina* spp. and TEX_{86} indices from Kim et al. [2010]. Mg/Ca values calibrated to temperatures using Anand et al. [2003] multispecies equation (calibration error is ±1°C). Different colors for Mg/Ca symbols indicate separate analyses performed in May 2013 (light blue), October 2013 (blue), and June 2018 (black). Calibration errors for TEX^{H}_{86} and TEX^{L}_{86} are ±2.5°C and ±4°C, respectively [Kim et al., 2010]. See fig. 3.1 for labels of $\delta^{18}O$ symbols 111

Fig. 3.6. TEX^{H}_{86} (upper panel) and TEX^{L}_{86} (lower panel) calibrated temperature records from New Jersey coastal plain sites Medford MAP 3B, Wilson Lake Hole A, Millville, and Bass River aligned by the PETM/CIE onset. See fig. 2.1 in Chapter Two for the location map. TEX^{H}_{86}-derived records at updip Medford and Wilson Lake show ~7°C temperature increase associated with the PETM onset and downdip Millville and Bass River indicate less warming of 6°C. TEX^{H}_{86}-based estimates from all sites reveal temperature maximum at 36°C and a two-step warming with a temperature plateau at 33.5-34°C. TEX^{L}_{86} estimated temperatures are lower and indicated a larger temperature anomaly than TEX^{H}_{86} in each site.

Calibration errors for TEX^{H}_{86} and TEX^{L}_{86} are ±2.5°C and ±4°C, respectively [Kim et al., 2010] 112

Fig. 3.S1. Scanning electron microscopy (SEM) and optical photographs of planktonic foraminifera from clayey silts of the Marlboro Formation at Millville, NJ showing excellent preservation of tests. Scale bar is 100 μm 113

Fig. 3.S2. Mg/Ca of surface dwelling (*Morozovella* spp. in red; *Acarinina* spp. in green) and thermocline (*Subbotina* spp. in blue) dwelling foraminifera at Millville, NJ 114

Fig. 3.S3. Structures of isoprenoid glycerol dialkyl glycerol tetraethers (GDGTs) used for TEX^{H}_{86} and TEX^{L}_{86} indices and their calibrations to modern sea surface temperatures (SSTs) [Kim et al., 2010] 115

Fig. 3.S4. Carbon (lower panel) and oxygen (upper panel) isotopic records of multispecimen samples of foraminifera at Millville, NJ: benthic *Cibicidoides* spp. (brown), *A. acuta* (purple), *G. beccariiformis* (gray); thermocline dwelling *Subbotina* spp. (blue); surface dwelling *Acarinina* spp. (green), *M. acuta* (red triangulars) and *M. aequa* (red diamonds). Samples contain spesimens from one size fraction (>250, 200-250, or 150-200 μm) with larger spesimens highlighted in darker shades and smaller spesimens in lighter. Isotopic values are given in Table 2.1 in Chapter Two. Data from Si and Aubry [2018] are plotted in black symbols 116

Fig. 3.S5. Mg/Ca of surface dwelling (*Morozovella* spp. in red; *Acarinina* spp. in green) and thermocline (*Subbotina* spp. in blue) dwelling foraminifera at Ancora [Babila, 2014], Millville, and Bass River [Babila et al., 2016], New Jersey coastal plain sites 117

Fig. 3.S6. Relative distribution of GDGTs used in TEX^{H}_{86} calibration: GDGT-1 (m/z 1300), GDGT-2 (m/z 1298), GDGT-3 (m/z 1296), and crenarchaeol regio-isomer (1292) in Medford MAP 3B [Chapter Four], Millville, and Bass River [Sluijs et al., 2007]. Top panel shows relative distribution of each GDGT in terms of their fractions normalized to the sum of GDGT-1, GDGT-2, GDGT-3, and crenarchaeol regio-isomer. Fractions of GDGT-1, GDGT-2, GDGT-3, and crenarchaeol regio-isomer are plotted separately in lower panels. Note that TEX^{H}_{86} uses the following ratio: (GDGT-2 + GDGT-3 + crenarchaeol regio-isomer) / (GDGT1 + GDGT-2 + GDGT-3 + crenarchaeol regio-isomer). Fractional GDGT abundances show that crenarchaeol regio-isomer is most variable among sites and, therefore, is responsible for larger temeprature anomaly in proximal Medford MAP 3B versus distal Millville and Bass River 118

Fig. 3.S7. Relative distribution of GDGTs used in TEX^{L}_{86} calibration: GDGT-1 (m/z 1300), GDGT-2 (m/z 1298), and GDGT-3 (m/z 1296) in Medford MAP 3B [Chapter Four], Millville, and Bass River [Sluijs et al., 2007]. Top panel shows relative distribution of each GDGT in terms of their fractions normalized to the

sum of GDGT-1, GDGT-2 and GDGT-3. Fractions of GDGT-1 and GDGT-2 are plotted separately in lower panels. Note that TEX^{L}_{86} uses the following ratio: GDGT-2 / (GDGT1 + GDGT-2 + GDGT-3) shown on the bottom panel. Fractions of each lipid show that only GDGT-2 relative abundance is variable among sites and, therefore, is responsible for larger temeprature anomaly in proximal Medford MAP 3B versus distal Millville and Bass River 120

Fig. 4.1. Location map of the PETM sections on the New Jersey coastal plain: Medford, Wilson Lake, Ancora, Millville, and Bass River. Black solid lines represent projection of sites onto a dip profile drawn through Medford outcrop and Bass River [Makarova et al., 2017] 156

Fig. 4.2. Percent coarse fraction (>63 μm) records from MAP Sites 5A, 3A, and 3B, Medford, NJ 157

Fig. 4.3. Bulk sediment records (% $CaCO_3$, $\delta^{13}C$, $\delta^{18}O$; Podrecca [2018]) from MAP 3A and 3B cores, Medford, NJ 158

Fig. 4.4. Summary of the MAP 3A core from Medford, NJ: % coarse (>63 μm) fraction; lithological description; bulk sediment $\delta^{13}C$ with highlighted in blue low (<1%) $CaCO_3$ zone [Podrecca, 2018]; planktonic to benthic foraminifera relative abundance (P stands for planktonic foraminifera and B for benthic foraminifera); general description of planktonic and benthic foraminifera assemblages 159

Fig. 4.5. Bulk sediment [Podrecca, 2018], planktonic (*Acarinina* spp. in green), and benthtic foraminiferal (*Cibicidoides* spp. in brown; *Anomalinoides* spp. in blue; *A. acuta* in purple) $\delta^{13}C$ records confirming the CIE onset at the MAP 3A core from Medford, NJ. SS stands for *sensu stricto*. Oxygen isotopic records show delayed anomaly in *Acarinina* spp. and *Anomalinoides* spp. in regards to the CIE 160

Fig. 4.6. Foraminiferal abundances in the MAP 3A core from Medford, NJ: number of planktonic to benthic foraminifera from >300 μm, 250-300 μm, 212-250 μm, and 150-212 μm size fractions per gram dry sediment; P/B ratio in >300 μm, 250-300 μm, 212-250 μm, and 150-212 μm size fractions. Bulk sediment $\delta^{13}C$ with highlighted in blue low (<1%) $CaCO_3$ zone are from Podrecca [2018] 161

Fig. 4.7. Percent plankton in each fraction(>300 μm, 250-300 μm, 212-250 μm, and 150-212 μm) and total percent plankton in the MAP 3A core from Medford, NJ. Bulk sediment $\delta^{13}C$ with highlighted in blue low (<1%) $CaCO_3$ zone are from Podrecca [2018] 162

Fig. 4.8. Carbon and oxygen isotopic records from multi-specimen samples of foraminifera in the MAP 3A core from Medford, NJ. Bulk sediment $\delta^{13}C$ with highlighted in blue low (<1%) $CaCO_3$ zone are from Podrecca [2018] 163

Fig. 4.9. Carbon and oxygen isotopic records from single-specimen samples of foraminifera in the MAP 3A core from Medford, NJ. Bulk sediment $\delta^{13}C$ and $\delta^{18}O$ (pink lines) and % $CaCO_3$ (<1% $CaCO_3$ zone highlighted in blue) are from

Podrecca [2018]. See legend for foraminiferal symbols in Fig. 4.5. Lines indicate multi-specimen foraminiferal isotopic records 164

Fig. 4.10. Mg/Ca records of foraminifera in the MAP 3A core from Medford, NJ: top panels – all foraminifera; middle panels – benthic foraminifera; bottom panels – planktonic foraminifera. Temperature scale is given for a relative change in tempertature for each species 165

Fig. 4.11. I/Ca records of foraminifera in the MAP 3A core from Medford, NJ 166

Fig. 4.12. Trace elemental ratios of foraminifera in the MAP 3A core from Medford, NJ: Mn/Ca, Ba/Ca, Nd/Ca, U/Ca, Fe/Ca 167

Fig. 4.13. Bulk sediment records (% $CaCO_3$, $\delta^{13}C$; Podrecca [2018]) and TEX_{86}-derived temperature estimates from MAP 3B core, Medford, NJ. Calibration errors for TEX^H_{86} and TEX^L_{86} are ±2.5°C and ±4°C, respectively [Kim et al., 2010]. The CIE onset at the MAP 3B core is shaded in red with top level representing *sensu stricto* placement of the CIE onset 168

Fig. 4.S1. Medford Auger Project (MAP) holes location and cross section through the dip line with surface elevation, top and bottom of the Marlboro Formation, containing kaolinitic clay deposits of the PETM at Medford, NJ [Podrecca, 2018] 169

Fig. 4.S2. Percent coarse fraction (>63 μm) records from Medford (MAP Sites 3A and 3B), Wilson Lake A [Stassen et al., 2015], Millville [Makarova et al., 2017], and Bass River [John et al., 2008]. Units of transitional from Upper Paleocene Vincentown Formation to the Lower Eocene Marlboro Formation lithologies are shown in green 170

Fig. 4.S3. Clinoform depositional model showing a fluid mud reservoir source bypassing shallow zones and rapidly building foresets at the rollover point. Overlaying NJCP sections from Medford, Wilson Lake, Millville, and Bass River support variation in CIE preservation between sites [Podrecca, 2018] 171

Fig. 4.S4. Correlation of bulk sediment $\delta^{13}C$ records from Medford MAP 3A and 3B [Podrecca, 2018], Wilson Lake B [Wright and Schaller, 2013], Millville [Wright and Schaller, 2013; Makarova et al., 2017], and Bass River [Kent et al., 2003; John et al., 2008] New Jersey coastal plain cores leveled to the base of low (<1%) $CaCO_3$ zone (a) with the map of site locations (b) and New Jersey paleoshelf reconstruction during the latest Paleocene (c). Spherules counts per gram from Wilson Lake B and Millville are from Schaller et al. [2016] 172

Fig. 4.S5. Corelation of bulk sediment records (% $CaCO_3$, $\delta^{13}C$, $\delta^{18}O$; Podrecca [2018]) from MAP 3A and 3B cores, Medford, NJ based on drilling depths modified for core expansion 173

Fig. 4.S6. Scanning electron microscopy (SEM) and optical photographs of planktonic foraminifera from low carbonate (<1% $CaCO_3$) zone in MAP 3A core at Medford, NJ. Scale bar is 100 μm. Quotation marks indicate depths from core catcher .. 174

Fig. 4.S7. Scanning electron microscopy (SEM) and optical photographs of malformed tests of planktonic foraminifera with abnormal chamber morphology or abnormal additional chambers from MAP 3A core at Medford, NJ. Scale bar is 100 μm 177

Fig. 4.S8. Scanning electron microscopy (SEM) and optical photographs of benthic foraminifera with pyrite coatings and filling from MAP 3A core at Medford, NJ. Scale bar is 100 μm 178

Fig. 4.S9. Mg/Ca records of planktonic foraminifera (*Morozovella* spp. in red; *Acarinina* spp. in green; *Subbotina* spp. in blue) at Medford (MAP 3A), Ancora [Babila, 2014], Millville, and Bass River [Babila et al., 2016] New Jersey coastal plain sites during the PETM 179

Fig. 4.S10. Percent total organic carbon (TOC) at Bass River [John et al., 2008], Wilson Lake A [Zachos et al., 2006], and Millville [Kopp et al., 2009; this study] New Jersey coastal plain sites during the PETM 180

I CHAPTER ONE

Introduction to the dissertation

1.1 Introduction

Understanding past climate perturbations with a focus on time intervals of high temperatures and elevated CO_2 levels is important for evaluation of Earth's system response to rising greenhouse gas concentrations. The Paleocene-Eocene Thermal Maximum (PETM) represents one the largest global warmings of the Cenozoic that initiated in the beginning of the Eocene (~56 Ma) and lasted less than ~200 kyr based on various estimates [Dickens et al., 1997; Katz, et al., 1999; Röhl et al., 2007; Murphy et al., 2010]. The PETM was a rapid transient warming with a temperature rise of 4-9°C estimated by independent proxies in pelagic, shelf, and terrestrial sections [Dunkley Jones et al., 2013]. This warming was associated with a negative carbon isotope excursion (CIE) of ~2.5-7 ‰ found in marine and terrestrial realms that requires a massive input of light carbon into the Earth's system [McInerney and Wing, 2011]. However, the duration of the PETM onset and therefore causal mechanism(s) are not well constrained.

The large magnitude of the CIE and rapidity of the PETM onset (less than a few thousand years; Kirtland Turner [2018]) cannot be explained by carbon transfer through outgassing and weathering. The originally favored hypothesis is the injection of isotopically depleted carbon via methane hydrate dissociation [Dickens et al., 1995, 1997; Katz et al., 2001; Thomas et al., 2002]; however, this is being challenged currently by both sill intrusion or massive flood basalt volcanism in the North Atlantic [Svensen et al., 2004; Storey et al., 2007; Dickson et al., 2015; Gutjahr et al., 2017] and cometary impact

[Kent et al., 2003; Cramer and Kent, 2005; Kent et al., 2017] that was supported by recent discovery of microtektites and burned wood at the PETM onset sections from the U.S. North Atlantic margin [Schaller et al., 2016; Schaller and Fung, 2018]. Various studies also suggest alternative PETM triggers, such as: burning of peatlands and coal [Kurtz et al., 2003]; oxidation of organic-rich wetlands [Higgins and Schrag, 2006]; decomposition of soil organic carbon in thawing permafrost [DeConto et al., 2012]; and kimberlite pipes emplacement [Patterson and Francis, 2013].

Thorough paleoenvironmental reconstructions are vital to understanding triggers, mechanisms, and impacts of the PETM warming on the Earth's system. Reconstructions of past climate transitions require the use of proxies. As indirect measures of climate response, proxies need to be calibrated using modern conditions, including modern species and modern seawater. Thus, proxies are associated with larger uncertainties further back in time. One of the ways to reduce ambiguities in paleoclimate reconstructions is to apply multiple proxies. The focus of this dissertation is to apply a multiproxy approach to estimate temperatures, evaluate salinity variations, reconstruct water column structure, and decipher any environmental changes on the mid-Atlantic paleoshelf associated with the PETM onset. Strengths of my studies are: 1) different proxies record different aspects of the water column and 2) the shelf provides a bottom limit for biomarker components and chemical tracers eliminating the "deep ocean" signal (e.g., >200 m; Ingalls [2016]).

Most of the PETM records are from pelagic sites that have thin (less than 1 m) sections, recording low stable $\delta^{13}C$ values that correspond to the maximum warmth. Much thicker (up to 11 m) marine PETM sections are found along the U.S. mid-Atlantic

margin, New Jersey Coastal Plain (NJCP) [Makarova et al., 2017]. The Paleocene/Eocene (P/E) boundary on the NJCP is accompanied by a lithologic change from glauconitic sandy silts or silty sands to kaolinitic clays. In contrast to many deep sea records affected by dissolution, the clay lithology of the PETM sections from NJCP facilitates excellent preservation of foraminifera used for paleoenvironmental reconstructions. The proximal sections from the NJCP are also much more expanded than most marine records. This appears to be especially true for the PETM onset represented by continuous decreases in $\delta^{13}C$ values and gradual changes in lithology across the P/E boundary at the updip Medford and Wilson Lake locations. Thus, the P/E transitional sections from the NJCP allow reconstructions of the PETM at high resolution and application of multiple paleoproxies from well-reserved foraminiferal tests, sediments, and organic matter.

This thesis consists of three main chapters (Two, Three, and Four). Chapter Two of my dissertation was published in *Paleoceanography* [Makarova et al., 2017]. It represents a cumulative study of carbon and oxygen stable isotopes of foraminifera from four NJCP sites to understand the spatial and temporal hydrographic responses to the PETM on the New Jersey paleoshelf. I present new multi-specimen $\delta^{13}C$ and $\delta^{18}O$ records of surface (*Morozovella* and *Acarinina)* and thermocline dwelling (*Subbotina*) planktonic foraminifera and benthic foraminifera (*Gavelinella*, *Cibicidoides*, and *Anomalinoides*) from the Millville site (70-90 m paleowater depths). Comparisons of foraminiferal isotopic records along the shelf transection of four NJCP sections (Wilson Lake, Ancora, Millville, and Bass River) show similar responses in foraminiferal $\delta^{13}C$ and $\delta^{18}O$ values to the PETM among sites. Whereas all taxa recorded the CIE of a ~4 ‰

magnitude, thermocline dwelling and benthic foraminifera showed larger $\delta^{18}O$ decreases of 1.8 ‰ compared to those of only 1 ‰ in surface dwellers. I discuss in Chapter Two possible factors influencing foraminiferal isotopic values, such as symbiont loss, carbonate ion effect, acidification, and salinity, and propose two scenarios to explain the observed isotopic records in foraminifera. The first scenario posits a change in the water column structure to a more gradual thermocline structure. The second scenario suggests a change to a deeper habitat or colder season of calcification in the surface dwellers due to environmental stress associated with the PETM onset. I conclude that the similar $\delta^{13}C$ changes in all foraminifera across the shelf argue against migration of the surface dwelling taxa deeper into the thermocline, favoring either a change in water column structure or season of calcification.

Chapter Three carries on the discussion about the shift in calcification of surface dwelling taxa to colder seasons. Smaller $\delta^{18}O$ anomalies seen in surface dwellers from the PETM sections of NJCP sites are observed in other low-mid latitudinal locations, but not revealed in sections from high latitudes. Modern cultures studies [Bijma et al., 1990] have shown that planktonic foraminifera do not calcify at temperatures above ~33°C. Therefore, if sea surface temperatures (SSTs) in low-mid latitudes rose above 33°C during the PETM, then the season of calcification for surface dwelling taxa would have been affected. In Chapter Three, I compare the temperature estimates based on foraminiferal oxygen isotopic data from Millville, NJCP with temperature records derived from independent paleotemperature proxies: Mg/Ca ratio in planktonic foraminifera and the organic paleothermometer TEX_{86}. I also compare oxygen isotopic records of foraminifera from other low latitudinal marine locations to support the

seasonality shift in subtropical surface dwellers due to the extreme PETM warmth. This study suggests a more robust $\delta^{18}O$-derived temperature anomaly estimated from thermocline dwelling *Subbotina* spp. for low-mid latitudinal locations because surface dwellers *Morozovella* and *Acarinina* spp. might have not registered the full warming anomaly during the PETM.

The application of a multiproxy approach to evaluate the warming anomaly from the NJCP sites indicates that the paleoshelf warmed by 6-7°C during the PETM. TEX_{86} indicated similar SSTs to temperature records from $\delta^{18}O$ of thermocline dwelling *Subbotina* spp. suggesting either similar surface water and thermocline temperature variations or both proxies recording subsurface temperature. Similar temperature anomalies estimated from these proxies argue against major salinity variations on the middle shelf (at the Millville site location) associated with the PETM onset. Comparison of TEX_{86} with foraminiferal Mg/Ca and $\delta^{18}O$ data among NJCP sites reveals spatially similar warming anomalies in records from foraminiferal proxies, but an amplified warming anomaly in shallower, more proximal sites based on the TEX_{86}-derived temperature estimates. Using TEX_{86} values from modern shelf settings, I conclude that the larger warming in proximal sites Medford and Wilson Lake versus distal sites Millville and Bass River is attributed to other than temperature controls on lipid distributions in the nearshore environments, and that the TEX^{H}_{86} calibration [Kim et al., 2010] from distal sites provided more plausible temperature estimates reflecting a warming of 6°C on the New Jersey paleoshelf during the PETM.

Chapter Four explores lead/lag relationships between the CIE and environmental changes associated with the PETM using a multiproxy analysis of the PETM sections

from Medford, NJ, the most proximal site on the NJCP. The Medford cores recorded the most expanded PETM onset among NJCP sites with a continuous 3.5 ‰ $\delta^{13}C$ decrease in bulk sediment and foraminifera within a 1.65 ft (0.5 m) thick interval and a gradational lithologic change from glauconite-quartz silty sands to kaolinitic clays. Data from coarse fraction percent, carbonate content, and foraminiferal assemblages suggest a dramatic increase in sedimentation associated with rapid clay input. Well-preserved tests of foraminifera and an increase in percent plankton within the P/E transitional interval suggest that the drop in % $CaCO_3$ at the PETM onset represents dilution of carbonate rather than dissolution observed in deep ocean PETM sections.

The Medford cores also provided new insights on the mechanism of the PETM onset and changes in redox conditions on the New Jersey paleoshelf. High-resolution TEX_{86} temperature estimates showed no warming prior to the CIE onset at the expanded Medford section, refuting the precursor warming hypothesis suggested by the TEX_{86} record from more condensed PETM onset section at the distal Bass River site [Sluijs et al., 2007]. The novel paleoredox proxy utilizing foraminiferal I/Ca [Lu et al., 2010] and various trace elemental ratios measured in foraminiferal calcite showed development of dysoxic, but not fully anoxic conditions on the New Jersey paleoshelf during the PETM. Eutrophication suggested for shelf areas during the PETM [e.g., Crouch et al., 2003; Egger et al.., 2003; Gavrilov et al., 2003; John et al., 2008; Aleksandrova and Shcherbinina, 2011] is not evident from analyses of total organic carbon and foraminiferal trace elemental ratios.

Overall, my dissertation provides a cumulative view of hydrographic, ecological, and environmental variations on the mid-Atlantic continental margin during the PETM. It

discusses insights from proxies used for paleoclimate reconstructions, as well as their limitations and potential biases. Chapter Two of this work has been published in *Paleoceanography* [Makarova et al., 2017] and Chapters Three and Four are in preparation for publication.

1.2 References

Aleksandrova, G.N. and E.A. Shcherbinina (2011), Stratigraphy and Paleoenvironmental Interpretation of the Paleocene–Eocene Transition in the Eastern Crimea, Stratigraphy and Geological Correlation, 19(4), 424–449, doi:10.1134/S0869593811040022.

Bijma, J., W.W. Faber Jr., and C. Hemleben (1990), Temperature and salinity limits for growth and survival of some planktonic foraminifers in laboratory cultures, Journal of Foraminiferal Research, 20(2), 95–116.

Cramer, B.S. and D.V. Kent (2005), Bolide summer: The Paleocene/Eocene thermal maximum as a response to an extraterrestrial trigger, Palaeogeography, Palaeoclimatology, Palaeoecology, 224, 144–166.

Crouch, E.M., G.R. Dickens, H. Brinkhuis, M.-P. Aubry, C.J. Hollis, K.M. Rogers, and H. Visscher (2003), The *Apectodinium* acme and terrestrial discharge during the Paleocene–Eocene thermal maximum: new palynological, geochemical and calcareous nannoplankton observations at Tawanui, New Zealand, Palaeogeography, Palaeoclimatology, Palaeoecology, 194, 387–403.

DeConto, R.M., S. Galeotti, M. Pagani, D. Tracy, K. Schaefer, T. Zhang, D. Pollard, and D.J. Beerling (2012), Past extreme warming events linked to massive carbon release from thawing permafrost, Nature, 484, 87–91.

Dickens, G.R., J.R. O'Neil, D.K. Rea, and R.M. Owen (1995), Dissociation of oceanic methane hydrate as a cause of the carbon isotope excursion at the end of the Paleocene., Paleoceanography, 10(6), 965–971.

Dickens, G.R., M.M. Castillo, and J.C.G. Walker (1997), A blast of gas in the latest Paleocene: Simulating first-order effects of massive dissociation of oceanic methane hydrate, Geology, 25(3), 259–262.

Dickson, A.J., A.S. Cohen, A.L. Coe, M. Davies, E.A. Shcherbinina, Y.O. Gavrilov (2015), Evidence for weathering and volcanism during the PETM from Arctic Ocean and Peri-Tethys osmium isotope records, Palaeogeography, Palaeoclimatology, Palaeoecology, 438, 300–307.

Dunkley Jones, T., D.J. Lunt, D.N. Schmidt, A. Ridgwell, A. Sluijs, P.J. Valdes, and M. Maslin (2013), Climate model and proxy data constraints on ocean warming across the Paleocene-Eocene Thermal Maximum, Earth-Science Reviews, 125, 123–145, doi:10.1016/j.earscirev.2013.07.004.

Egger, H., J. Fenner, C. Heilmann-Clausen, F. Rögl, R.F. Sachsenhofer, and B. Schmitz (2003), Paleoproductivity of the northwestern Tethyan margin (Anthering Section, Austria) across the Paleocene-Eocene transition, in S.L. Wing et al., eds., Causes and consequences of globally warm climates in the early Paleogene: Geological Society of America Special Paper, 369, 133–146.

Gavrilov, Y.O., E.A. Shcherbinina, and H. Oberhänsli (2003), Paleocene-Eocene boundry events in the northeastern Peri-Tethys, Special Paper of the Geological Society of America, 369, 147–168, doi:10.1130/0-8137-2369-8.147.

Gutjahr, M., Andy Ridgwell, P.F. Sexton, E. Anagnostou, P.N. Pearson, H. Pälike, R.D. Norris, E. Thomas, and G.L. Foster (2017), Very large release of mostly volcanic carbon during the Palaeocene–Eocene Thermal Maximum, Nature, 548, 573–577, doi:10.1038/nature23646.

Higgins, J.A. and D.P. Schrag (2006), Beyond methane: Towards a theory for the Paleocene-Eocene Thermal Maximum, Earth and Planetary Science Letters, 245, 523–537.

Ingalls, A.E. (2016), Signal from the subsurface, Nature Geoscience, 9, 572–573

John, C.M., S.M. Bohaty, J.C. Zachos, A. Sluijs, S. Gibbs, H. Brinkhuis, and T.J. Bralower (2008), North American continental margin records of the Paleocene-Eocene thermal maximum: Implications for global carbon and hydrological cycling, Paleoceanography, 23, 1–20, doi:10.1029/2007PA001465.

Katz, M.E., D.K. Pak, G.R. Dickens, and K.G. Miller (1999), The Source and Fate of Massive Carbon Input During the Latest Paleocene Thermal Maximum, Science, 286, 1531–1533.

Katz, M.E., B.S. Cramer, G.S. Mountain, S. Katz, and K.G. Miller (2001), Uncorking the bottle: What triggered the Paleocene/Eocene thermal maximum methane release? Paleoceanography, 16(6), 549–562.

Kent, D.V., B.S. Cramer, L. Lanci, D. Wang, J.D. Wright, and R. Van der Voo (2003), A case for a comet impact trigger for the Paleocene/Eocene thermal maximum and carbon isotope excursion, Earth and Planetary Science Letters, 211, 13–26.

Kent, D.V., L. Lanci, H. Wang, and J.D. Wright (2017), Enhanced magnetization of the Marlboro Clay as a product of soil pyrogenesis at the Paleocene–Eocene boundary? Earth and Planetary Science Letters, 473, 303–312.

Kim, J.-H., J. van der Meer, S. Schouten, P. Helmke, V. Willmott, F. Sangiorgi, N. Koc, E.C. Hopmans, and J.S. Sinninghe Damsté (2010), New indices and calibrations derived from the distribution of crenarchaeal isoprenoid tetraether lipids: implications for past sea surface temperature reconstructions, Geochimica et Cosmochimica Acta, 74, 4639–4654.

Kirtland Turner, S. (2018), Constraints on the onset duration of the Paleocene–Eocene Thermal Maximum, Philosophical Transaction of Royal Society A, 376, 20170082, 1–16, http://dx.doi.org/10.1098/rsta.2017.0082.

Kurtz, A.C., L.R. Kump, M.A. Arthur, J.C. Zachos, and A. Paytan (2003), Early Cenozoic decoupling of the global carbon and sulfur cycles, Paleoceanography, 18(4), 1–14, doi:10.1029/2003PA000908.

Lu. Z., H.C. Jenkyns, and R.E.M. Rickaby (2010), Iodine to calcium ratios in marine carbonate as a paleo-redox proxy, Geology, 38(12), 1107–1110, doi:10.1130/G31145.1.

Makarova, M., J.D. Wright, K.G. Miller, T.L. Babila, Y. Rosenthal, and J.I. Park (2017), Hydrographic and ecologic implications of foraminiferal stable isotopic response across the U.S. mid-Atlantic continental shelf during the Paleocene-Eocene Thermal Maximum, Paleoceanography, 31, doi:10.1002/2016PA002985.

McInerney, F.A. and S.L. Wing (2011), The Paleocene-Eocene thermal maximum: a perturbation of carbon cycle, climate, and biosphere with implications for the future, Annual Review of Earth and Planetary Sciences, 39, 489–516.

Murphy, B.H., K.A. Farley, and J.C. Zachos (2010), An extraterrestrial ^{3}He-based timescale for the Paleocene-Eocene thermal maximum (PETM) from Walvis Ridge, IODP Site 1266, Geochimica et Cosmochimica Acta, 74, 5098–5108.

Patterson, M.V. and D. Francis (2013), Kimberlite eruptions as triggers for early Cenozoic hyperthermals, Geochemistry Geophysics Geosystems, 14(2), 448–456.

Röhl, U., T. Westerhold, T.J. Bralower, and J.C. Zachos (2007), On the duration of the Paleocene-Eocene thermal maximum (PETM), Geochemistry Geophysics Geosystems, 8(12), 1–13.

Schaller, M.F., M.K. Fung, J.D. Wright, M.E. Katz, and D.V. Kent (2016), Impact ejecta at the Paleocene-Eocene boundary, Science, 354(6309), 225–229, doi:10.1126/science.aaf5466.

Schaller, M.F. and M.K. Fung (2018), The extraterrestrial impact evidence at the Palaeocene–Eocene boundary and sequence of environmental change on the continental shelf, Philosophical Transaction of Royal Society A, 376, 20170081, 1–30, http://dx.doi.org/10.1098/rsta.2017.0081.

Sluijs, A., H. Brinkhuis, S. Schouten, S.M. Bohaty, C.M. John, J.C. Zachos, G.J. Reichart, J.S. Sinninghe Damsté, E.M. Crouch, and G.R. Dickens (2007), Environmental precursors to rapid light carbon injection at the Palaeocene/Eocene boundary, Nature, 450(7173), 1218–1221, doi:10.1038/nature06400.

Storey, M., R.A. Duncan, and C.C. Swisher III (2007), Paleocene-Eocene thermal maximum and the opening of the Northeast Atlantic, Science, 316, 587–589.

Svensen, H., S. Planke, A. Malthe-Sørenssen, B. Jamtveit, R. Myklebust, T. Rasmussen Eidem, and S.S. Rey (2004), Release of methane from a volcanic basin as a mechanism for initial Eocene global warming, Nature, 429, 542–545.

Thomas, D.J., J.C. Zachos, T.M. Bralower, E. Thomas, and S. Bohaty (2002), Warming the fuel for the fire: Evidence for the thermal dissociation of methane hydrate during the Paleocene-Eocene thermal maximum, Geology, 30(12), 1067–1070.

II CHAPTER TWO

Hydrographic and ecologic implications of foraminiferal stable isotopic response across the mid-Atlantic U.S. continental shelf during the Paleocene-Eocene Thermal Maximum

Maria Makarova1[1], James D. Wright[1,2], Kenneth G. Miller[1,2], Tali L. Babila[3,4], Yair Rosenthal[1,2,3], and Jill I. Park[1]

[1] Department of Earth and Planetary Sciences and Institute of Earth, Oceans, and Atmospheric Sciences, Rutgers, The State University of New Jersey, 610 Taylor Road, Piscataway, NJ 08854-8066

[2] Institute of Earth, Ocean, and Atmospheric Sciences, Rutgers, The State University of New Jersey, 71 Dudley Road, New Brunswick, NJ 08901-8525

[3] Department of Marine and Coastal Sciences, Rutgers, The State University of New Jersey, 71 Dudley Road, New Brunswick, NJ 08901-8525

[4] Department of Earth and Planetary Sciences, University of California Santa Cruz, 1156 High Street, Santa Cruz, CA 95064, USA

*Published in Paleoceanography Journal in January, 2017

Citation: Makarova, M., J. D. Wright, K. G. Miller, T. L. Babila, Y. Rosenthal, and J. I. Park (2017), Hydrographic and ecologic implications of foraminiferal stable isotopic response across the U.S. mid-Atlantic continental shelf during the Paleocene-Eocene Thermal Maximum, Paleoceanography, 32, doi:10.1002/2016PA002985.

2.1 Abstract

We present new $\delta^{13}C$ and $\delta^{18}O$ records of surface (*Morozovella* and *Acarinina)* and thermocline dwelling (*Subbotina*) planktonic foraminifera and benthic foraminifera (*Gavelinella*, *Cibicidoides*, and *Anomalinoides*) during the Paleocene-Eocene Thermal Maximum (PETM) from Millville, New Jersey and compare them with three other sites located along a paleoshelf transect from the U.S. mid-Atlantic coastal plain. Our analyses show different isotopic responses during the PETM in surface versus thermocline and benthic species. Whereas all taxa record a 3.6-4.0 ‰ $\delta^{13}C$ decrease associated with the carbon isotope excursion (CIE), thermocline dwellers and benthic foraminifera show larger $\delta^{18}O$ decreases compared to surface dwellers. We consider two scenarios that can explain the observed isotopic records: 1) a change in the water column structure; and 2) a change in habitat or calcification season of the surface dwellers due to environmental stress (e.g., warming, ocean acidification, surface freshening, and/or eutrophication). In the first scenario, persistent warming during the PETM would have propagated heat into deeper layers and created a more homogenous water column with a thicker warm mixed layer and deeper, more gradual thermocline. We attribute the hydrographic change to decreased meridional thermal gradients, consistent with models that predict polar amplification. The second scenario assumes that environmental change was greater in the mixed layer forcing surface dwellers to descend into thermocline waters as a refuge or restrict their calcification to the colder seasons. Though both scenarios are plausible, similar $\delta^{13}C$ responses recorded in surface, thermocline, and benthic foraminifera challenge mixed layer taxa migration.

2.2 Introduction

The Paleocene-Eocene Thermal Maximum (PETM) was an abrupt warming event initiated at the beginning of the Eocene (~56 Ma) and characterized by a global temperature increase of about 4-8°C [Kennett and Stott, 1991; Bralower et al., 1995; Thomas et al., 1999; Zachos et al., 2003; Tripati and Elderfield, 2004; Sluijs et al., 2006; Dunkley Jones et al., 2013]. The PETM is associated with the carbon isotope excursion (CIE) represented by a decrease in $\delta^{13}C$ values in marine (~2-3 ‰ in benthic and ~2.5-4 ‰ in planktonic foraminifera) [Kennett and Stott, 1991; Zachos et al., 2007; McInerney and Wing, 2011] and terrestrial (~2.5-7 ‰) [Koch et al., 1992; Wing et al., 2005; McInerney and Wing, 2011; Bowen et al., 2015] environments requiring a substantial addition of light carbon (^{12}C) into global reservoirs. The CIE can be subdivided into four stages: 1) the initiation of the $\delta^{13}C$ decrease termed the CIE onset [Röhl et al., 2007] that was used to correlate the Paleocene/Eocene (P/E) boundary stratotype at Dababiya, Egypt [Aubry et al., 2007]; 2) a sharp $\delta^{13}C$ decrease, the rapidity of which is contentious [cf., Cui et al., 2011; Wright and Schaller, 2013], though most studies estimate that the decrease occurred in several thousand years or less [e.g., Kennett and Stott, 1991; Bowen et al., 2015; Kirtland Turner and Ridgwell, 2016; Zeebe et al., 2016]; 3) a period of stable low carbon isotope values, termed the CIE "core" [Röhl et al., 2007; Stassen et al., 2012], the duration of which is uncertain, with astronomical estimates on the order of 40 kyr [Katz et al., 1999] to 80 kyr [Röhl et al., 2007] and ^{3}He-based chronology of ~135 kyr [Murphy et al., 2010]; and 4) an exponential recovery period to near pre-CIE values of ~80 kyr [Murphy et al., 2010] to ~120-140 kyr [Dickens et al., 1997; Katz, et al., 1999; Röhl et al., 2007]. The majority of PETM foraminiferal isotope records are from open

ocean cores that have thinner, lower resolution CIE "core" intervals of ~1 m or less [e.g., Kennett and Stott, 1991; Bralower et al., 1995; Thomas et al., 1999; Thomas et al., 2002; Zachos et al., 2003; Hollis et al., 2015]. The CIE onset and "core" in deep-sea records are generally truncated owing to the corrosive conditions in bottom waters at the onset of the PETM and therefore dissolution of calcium carbonate sediments on the seafloor [Zachos et al., 2005; Bralower et al., 2014].

Stratigraphically more complete in regard to the CIE onset and "core" and much thicker (up to ~11 m) marine PETM sections are found along the New Jersey paleoshelf (Figs 2.1 and 2.2) [Cramer et al., 1999; Zachos et al., 2006; John et al., 2008; Harris et al., 2010; Wright and Schaller, 2013]. An advantage of the New Jersey paleoshelf is its location on a passive margin with relatively simple tectonics that allows paleodepth reconstructions and higher temporal resolution due to high sedimentation rates (>10 m deposited during the "core", requiring rates >20 cm/kyr using astronomical time scales). The P/E boundary in New Jersey is accompanied by a lithologic change from sandy silts of the underlying Vincentown Formation to clayey silts of the overlying Marlboro Formation (Fig. 2.3) [Gibson et al., 1993; Cramer et al., 1999; Sugarman et al., 2005; Kopp et al., 2009; Lombardi, 2013]. The clayey-silt-rich lithology of the Marlboro Formation acts as an impermeable barrier to fluid interaction with carbonate sediments providing excellent preservation of foraminifera as seen in other clay-rich marine sections [e.g., Pearson et al., 2001; Sexton et al., 2006]. Planktonic foraminifera from the underlying sandier Vincentown Formation are less well preserved [Zachos et al., 2006; Babila et al., 2016].

The aim of this study is to understand the spatial and temporal hydrographic response on the continental shelf to climate change during the PETM. The hydrography along shelf is dynamic as physical processes are governed by the interplay between land and open ocean interactions, including storms, coastal currents, and freshwater inputs [Gong et al., 2010]. An approach to resolve regional from global isotopic marine trends is to construct a cross shelf transect with sites that range in coastal proximity and environmental influence. Here, we sampled the PETM in a shelf transect of four cores drilled as part of the New Jersey Ocean Drilling Program (ODP) Leg 174AX: Wilson Lake (Holes A and B), Ancora, Millville, and Bass River, with Wilson Lake being the most nearshore and Bass River being the furthest offshore (Fig. 2.1) [Miller et al., 1998; Miller at el., 1999; Sugarman et al., 2005].

Stable isotope studies of planktonic (surface and deep dwelling) and benthic foraminifera from expanded shelf records provide insights into hydrographic changes in the mixed layer versus thermocline and deeper layers during the PETM. Though previous studies have provided evidence for an enhanced hydrological cycle on the U.S. mid-Atlantic shelf [e.g., Kopp et al., 2009; Stassen et al., 2012; 2015], we currently lack a comprehensive reconstruction of cross shelf hydrography. Here, we present new stable isotope ($\delta^{13}C$ and $\delta^{18}O$) records of multiple taxa from Millville, combining them with previously published data from Wilson Lake, Ancora, and Bass River [Cramer et al., 1999; Cramer and Kent, 2005; Zachos et al., 2006; Zachos et al., 2007; John et al., 2008; Stassen et al., 2012; Babila, 2014; Babila et al., 2016]. We analyzed surface mixed layer dwelling foraminiferal species in two genera (*Morozovella* and *Acarinina*), thermocline dwelling foraminiferal species of the genus *Subbotina*, and benthic foraminiferal species

of *Cibicidoides*, *Anomalinoides*, and *Gavelinella*. We employ the fact that planktonic foraminifera occupy different habitats to reconstruct $\delta^{13}C$ and $\delta^{18}O$ depth profiles [e.g., Fairbanks et al., 1982; Boersma et al., 1987; Pearson et al., 1993; Bralower et al., 1995; Lu and Keller, 1996; Coxall et al., 2000; Pearson et al., 2001]. We compile vertical isotope profiles from New Jersey cores to reconstruct the water column structure along the continental shelf. The strength of our reconstructions is the spatial coverage afforded by a cross shelf transect and temporal resolution allowed by relatively high sedimentation rates on the New Jersey paleoshelf minimizing the effects of bioturbation.

2.3 ODP Leg 174AX Millville site

ODP Leg 174AX Millville core recovered the Vincentown, Marlboro, and Manasquan Formations (257.55-280.33 m) that span the Paleocene/Eocene boundary (Fig. 2.3). The Vincentown Formation is a micaceous, glauconitic, sandy silt at Millville. The contact between the Vincentown and Marlboro Formations occurs within a 0.6 ft-transition zone with decreasing upwards glauconite and coarse fraction content. Clayey silts (mean grain size 8 μm) of the Marlboro Formation comprise an expanded CIE "core" (10 m thick) at Millville. The CIE recovery interval (5.5 m thick) captures a lithologic transition from the Marlboro Formation to coarser informal units referred to as A and B here (discussed in section 2.12 "Supporting information"). The post-CIE section consists of glauconitic, carbonate-rich sandy silts of the Manasquan Formation overlying unit B above an unconformity at 258.09 m. For more information on lithostratigraphy and paleowater depth estimates see section 2.12 "Supporting information".

The Millville site provides advantages over other New Jersey coastal plain sites. It has higher sedimentation rates and temporal resolution than further offshore Bass River, but it is still deep enough to sample the water column from the mixed layer to thermocline and colder bottom waters that is missing in the upper Paleocene sections of the updip Ancora and Wilson Lake cores. Deposition at Millville was below storm wave base in the middle neritic zone allowing reconstruction of the full range of foraminiferal isotopic gradients distributed throughout the water column. The Millville core recovered sufficient well-preserved pre-CIE foraminifera (273.77-275.40 m) used to establish isotopic changes across the CIE onset, although there is a thin low carbonate interval (<1%; 273.38-273.77 m) above the CIE onset [this study; Wright and Schaller, 2013] with no foraminifera (Fig. 2.3). The sharp $\delta^{13}C$ decrease at Millville appears within the Vincentown/Marlboro transitional interval at 273.77-273.95 m. In comparison, the updip Wilson Lake and Ancora cores also record gradational lithologic transitions into the PETM, but resolution of the isotopic records is limited because there are insufficient planktonic foraminifera for a full suite of geochemical analyses within the upper Paleocene [Zachos et al., 2006; Babila, 2014]. Conversely, the uppermost Paleocene section at the deepest water Bass River core recovered the highest foraminiferal abundances [Zachos et al., 2007; John et al., 2008; Babila et al., 2016]; however, the CIE initiation at Bass River appears to be truncated [John et al., 2008; Stassen et al., 2012], possibly yielding incomplete records. Thus, Millville is located in the ideal setting to contain more continuous lithologic and foraminifera-rich marine sediment archive to generate detailed stable isotope records of the PETM from shelf.

2.4 Methods

2.4.1 Analyses

Core samples were disaggregated in a sodium metaphosphate solution (5.5 g of sodium metaphosphate per liter) to deflocculate clays and then washed through a 63 μm sieve to separate the fine fraction (<63 μm). The >63 μm fraction was dried overnight in a 50°C oven and weighed dry to compute the percentage of coarse sediment. Subsamples for percent calcium carbonate (% $CaCO_3$) and stable isotope ($\delta^{13}C$ and $\delta^{18}O$) measurements of bulk sediment were dried overnight in a 50°C oven and homogenized using a mortar and pestle.

For stable isotope analysis of planktonic foraminifera, specimens of *Morozovella* (*M. aequa, M. acuta, M. subbotinae, M. velascoensis*), *Acarinina* (*A. soldadoensis, A. esnehensis, A. coalingensis, A. angulosa*), and *Subbotina* (*S. roesnaesensis*, *S. velascoensis, S. triangularis, S. hornibrooki*) were picked mainly from the >250 μm size fraction using the taxonomy of Olsson et al. [1999] and Pearson et al. [2006]. For stable isotope analysis of benthic foraminifera, specimens of *Gavelinella beccariiformis*, *Anomalinoides acuta*, and *Cibicidoides* (*C. alleni, C. howelli, C. succedens*) were picked mainly from the >250 μm size fraction using the taxonomy of Cushman [1951] and Berggren and Aubert [1975]. To avoid species bias, most of the samples analyzed consisted of single species of one size fraction (Table 1). However, uneven distribution of single species throughout the section precluded compilation of continuous monospecific records compelling us to present the data by genera. Comparison of monospecific multi-specimen analyses at Millville (Table 1 and Fig. 2.S1) and elsewhere [e.g., Pearson et al.,

1993; Bralower et al., 1995; Babila et al., 2016] justifies compilation of monogeneric records.

Stable isotope analyses of foraminifera and bulk sediment were conducted on a Micromass Optima Mass Spectrometer with an attached multi-prep device. Carbonate samples were reacted in 100% phosphoric acid (H_3PO_4) at 90°C for 15 minutes and the evolved CO_2 gas was collected in a liquid nitrogen cold finger. Ratios are reported in standard delta notation in parts per thousand (per mil, ‰) $\delta = [(R_{sample}/R_{standard}) - 1] \times 1000$ where $R = {}^{13}C/{}^{12}C$ or ${}^{18}O/{}^{16}O$, relative to Vienna-Pee Dee Belemnite ($\delta^{13}C_{VPDB}$ and $\delta^{18}O_{VPDB}$). One-sigma analytical errors based on analyses of an internal laboratory reference material (~8 standards for every 24 samples) are ±0.05 ‰ and ±0.08 ‰ for $\delta^{13}C$ and $\delta^{18}O$, respectively.

Percent carbonate values were determined by converting the transducer reading for each sample analysis to a mass of $CaCO_3$ using an empirically derived calibration based on sample weight and transducer readings.

Depths of lithologic boundaries and samples at Millville reported here are modified for core expansion by adjusting the core recovery length to a 10 ft (~3 m) interval per run [Sugarman et al., 2005]. The true core depths of analyzed samples are given in Table 1.

2.4.2 Correction for test size

Most of the samples analyzed from the section below the CIE onset were picked from a smaller size fraction of 150-200 μm due to the lack of larger specimens in this interval. We applied a $\delta^{13}C$ correction for test size to allow comparison of carbon isotopic values from the pre-CIE samples that contain smaller specimens to the rest of the

Millville section. *Morozovella* and *Acarinina* are considered obligate symbiont-bearing surface dwellers with well-established positive $\delta^{13}C$ to test size correlation [e.g., Pearson et al., 1993; D'Hondt et al., 1994; Norris, 1996; Quillévéré et al., 2001]. We applied a 1‰ correction in $\delta^{13}C$ per 100 μm test size change that was previously quantified for *Morozovella* and *Acarinina* [e.g., Norris, 1996; Tripati and Elderfield, 2004; Wade et al., 2008; Birch et al., 2012]. Asymbiotic thermocline dwelling *Subbotina* also exhibit a test size-dependent $\delta^{13}C$ offset; however, this effect is likely due to increased kinetic fractionation observed in almost all foraminifera <150 μm [D'Hondt and Zachos, 1993; Bornemann and Norris, 2007; Birch et al., 2012]. We measured $\delta^{13}C$ in *Subbotina roesnaesensis* from small (150-212 μm) and large (250-300 μm) size fractions at Wilson Lake Hole B and detected a consistent offset of 0.41 ± 0.05 ‰ (n=4) between small and large specimens (Table 2.S2). Bornemann and Norris [2007] showed a similar change of 0.3-0.5 ‰ in $\delta^{13}C$ per test size due to higher metabolic activity in smaller foraminifera. Accordingly, we applied a 0.4 ‰ correction in $\delta^{13}C$ for small (150-212 μm size fraction) specimens of *Subbotina* at Millville. Measured and corrected for test size $\delta^{13}C$ values in all analyzed planktonic foraminifera are given at Table 1. These corrections only apply to $\delta^{13}C$ data because previous studies of test size effects on oxygen isotopic values indicated no consistent change in $\delta^{18}O$ with foraminiferal test size variation [e.g., Norris et al., 1996; Wade et al., 2008; Birch et al., 2012]. Similarly, benthic foraminiferal vital effects can be minimized by measurements of monospecific samples from the larger size fraction [Katz et al., 2010].

2.4.3 Planktonic foraminiferal depth habitats

We used $\delta^{18}O$ as a relative indicator of ocean temperature to estimate a depth ranking of planktonic foraminifera, subdividing them into surface (mixed layer) and deep (thermocline) dwellers. The $\delta^{18}O_{calcite}$ is controlled in part by the temperature of the surrounding seawater from which the foraminiferal test is precipitated [*Epstein et al.*, 1953] and thus is used to constrain the temperature of habitats occupied by extinct planktonic foraminifera [e.g., Emiliani, 1954; Boersma et al., 1987; Pearson et al., 1993, 2001; Coxall et al., 2000]. Most studies assume that the stable isotopic differences reflect calcification at different depths. Accordingly, high $\delta^{18}O$ values of *Subbotina* spp. reflect calcification in colder thermocline waters, whereas lower $\delta^{18}O$ values of *Morozovella* spp. and *Acarinina* spp. indicate warmer temperatures in the surface mixed layer. Moreover, measurements of $\delta^{11}B$ in foraminiferal tests that reflect seawater pH also support this depth habitat ranking [Pearson and Palmer, 1999; Anagnostou et al., 2016]. However, generic differences in $\delta^{18}O$ values could reflect seasonal differences, as they do in modern assemblages [e.g., Bé, 1960; Curry et al., 1983; Thunell et al., 1983; Deuser and Ross, 1989; Ravelo and Fairbanks, 1992]. In the mid- to high-latitudes, seasonal variability in light and other environmental properties control the "blooms" of different species, and these seasonal variations in surface temperature and nutrients can mimic mean annual vertical conditions. Since vertical temperature gradients that develop in the spring and summer to a large part reflect the seasonal temperature changes in surface water, we discuss isotopic gradients between them as surface to thermocline differences.

Morozovella spp. and *Acarinina* spp. record higher $\delta^{13}C$ values relative to *Subbotina* spp. mirroring typical vertical nutrient profiles [e.g., Boersma et al., 1987;

Pearson et al., 1993; Bralower et al., 1995; Lu and Keller, 1996; Coxall et al., 2000]. Near complete removal of nutrients by biological productivity increases dissolved inorganic carbon (DIC) $\delta^{13}C$ values in the surface mixed layer. Organic matter remineralization occurs within the seasonal thermocline on the continental shelf in the lower photic zone (25-50 m) [Fairbanks and Wiebe, 1980; Glenn et al., 2008]. The net effect results in higher $\delta^{13}C$ values in *Morozovella* spp. and *Acarinina* spp. and lower $\delta^{13}C$ values of *Subbotina* spp. We note that seasonal blooms would produce similar stable isotope patterns as described versus depth. Such isotopic relationships between *Morozovella*, *Acarinina*, and *Subbotina* are also reported from PETM sections at New Jersey coastal plain sites Wilson Lake Hole A, Ancora, and Bass River [Zachos et al., 2006; Zachos et al., 2007; John et al., 2008; Babila, 2014; Babila et al., 2016], as well as from open ocean sites [e.g., Kennett and Stott, 1991; Bralower et al., 1995; Lu and Keller, 1996; Thomas et al., 2002; Tripati and Elderfield, 2004; Hollis et al., 2015].

2.5 Results

2.5.1 Millville foraminiferal isotopic records

We recognize the CIE onset at Millville by a sharp decrease in bulk $\delta^{13}C$ values and by a drop in percent carbonate at 273.77 m (Figs. 2.2 and 2.3), delineated in detailed bulk $\delta^{13}C$ records by Wright and Schaller [2013]. This decrease is recognized not only by its large amplitude, but also by biostratigraphic data that clearly put it at the P/E boundary [Sugarman et al., 2005]. Using the bulk $\delta^{13}C$ record [this study and Wright and Schaller, 2013] supported by our foraminiferal $\delta^{13}C$ data, the section has been divided into four

intervals: 1) pre-CIE; 2) the CIE "core"; 3) CIE recovery during which isotopic values returned to pre-CIE isotopic levels; and 4) post-CIE (Fig. 2.S1).

Our analyses show specific isotopic responses to the PETM in surface versus thermocline and benthic species. We define changes in $\delta^{13}C$ ($\Delta\delta^{13}C$) and $\delta^{18}O$ ($\Delta\delta^{18}O$) as differences between the average pre-CIE value and average value from the stable interval of the CIE "core" indicated by vertical bars on Figs. 2.4 and 2.5. Most taxa show $\Delta\delta^{13}C$ of -4 ‰ following the CIE initiation with slightly lower *Subbotina* spp. $\Delta\delta^{13}C$ of -3.6 ‰ (Fig. 2.4). Changes in $\delta^{18}O$ values vary among foraminifera: $\Delta\delta^{18}O$ in surface dwellers *Morozovella* spp. and *Acarinina* spp. are -1 ‰, whereas *Subbotina* spp. and benthic taxa show a larger $\Delta\delta^{18}O$ of -1.8 ‰ (Fig. 2.5). The isotopic response of *Morozovella* spp. should be interpreted cautiously because of the limited data in the pre-CIE interval (six measurements within 60 cm below the CIE onset). However, we note that the pre-CIE $\delta^{13}C$ and $\delta^{18}O$ values in *Morozovella* spp. at Bass River [Zachos et al., 2007; John et al., 2008; Babila et al., 2016] are similar to those at Millville, thus validating the Millville pre-CIE record (Figs. 2.6, 2.S2, and 2.S3). The same is true for the benthic pre-CIE isotopic records.

To compare the isotopic responses of foraminifera across the PETM section at Millville, we present cross plots of $\delta^{18}O$ versus $\delta^{13}C$ for intervals representing pre-CIE, CIE "core", CIE recovery, and post-CIE (Fig. 2.S1). Below the CIE onset, the carbon isotopic gradient between surface and benthic species is ~3.0-3.5 ‰ and the oxygen isotopic gradient is ~1.75 ‰. *Morozovella* spp. have high $\delta^{13}C$ and low $\delta^{18}O$ values indicating calcification in shallowest water column, *Subbotina* spp. have low $\delta^{13}C$ and high $\delta^{18}O$ and are deeper dwellers, and *Acarinina* spp. have isotopic values in between

(however, closer to those of *Morozovella* spp.). Benthic species of *Cibicidoides* record bottom water conditions and *G. beccariiformis* show the lowest $\delta^{13}C$ and highest $\delta^{18}O$ implying an infaunal habitat as suggested previously [e.g., Katz et al., 2010]. We exclude *G. beccariiformis* from our interpretations of surface to bottom isotopic gradients because it is only found in the uppermost Paleocene (pre-CIE interval) and has an infaunal habitat.

In the CIE "core", the surface to thermocline to bottom $\delta^{13}C$ gradient is similar to the pre-CIE, whereas the vertical $\delta^{18}O$ gradient decreases to ~1 ‰. *Morozovella* spp. and *Acarinina* spp. record similar $\delta^{13}C$ values and both are higher than thermocline dwelling *Subbotina* spp. and benthic foraminifera. *Morozovella* spp. continues to record the lowest $\delta^{18}O$ values, though *Acarinina* spp. are similar to $\delta^{18}O$ values in *Subbotina* spp. and benthic species of *Cibicidoides* and *A. acuta*. Post-CIE values of all taxa are similar to the pre-CIE values, with a return occurring through the recovery phase (Fig. 2.S1). Both the recovery and post-CIE intervals record reestablished surface to thermocline isotopic gradients with *Acarinina* spp. $\delta^{18}O$ values identical to those of *Morozovella* spp. (Fig. 2.S1).

2.5.2 Foraminiferal isotopic records from the New Jersey paleoshelf

Water column gradients on the New Jersey paleoshelf were reconstructed using foraminiferal $\delta^{13}C$ and $\delta^{18}O$ to assess changes in hydrography and organic carbon cycling that may be associated with climate perturbation during the PETM (Figs. 2.1, 2.6, 2.S2, and 2.S3). We use previously reported data from Bass River (~12 km seaward) [Cramer et al., 1999; Zachos et al., 2007; John et al., 2008; Babila et al., 2016], Ancora (~16 km landward) [Cramer and Kent, 2005; Babila, 2014], and Wilson Lake Hole A (~23 km

landward) [Zachos et al., 2006] sites to summarize foraminiferal isotopic data in a series of cross plots representing intervals of the pre-CIE and CIE "core" deposition (Fig. 2.6).

One concern about merging our datasets with previous published records is the difference in single versus multiple species analyses. Millville and Bass River are the only cores with a complete surface, thermocline, and benthic assemblage of foraminifera allowing reconstruction of $\delta^{13}C$ and $\delta^{18}O$ gradients below the CIE onset. Measurements of surface dwellers *Morozovella* spp. and *Acarinina* spp. below the CIE onset at Bass River were mostly done on single specimens [Zachos et al., 2007] yielding higher variability in $\delta^{13}C$ and $\delta^{18}O$ values which likely reflects a seasonal signal and a range of actual environmental conditions. Isotopic measurements performed on multiple specimens at Millville exhibit less scatter and show a few intermediate $\delta^{13}C$ and $\delta^{18}O$ values across the CIE onset instead of bimodal isotopic distribution observed at Bass River (Figs. 2.S2 and 2.S3). Specifically, most of intermediate values at Millville occur below the CIE onset within the Vincentown/Marlboro transitional interval and likely represent mixing of pre-CIE and CIE populations due to bioturbation/reworking (Figs. 2.3 and 2.4).

Considering an average of the single specimen data at Bass River, the carbon isotopic gradient between surface dwellers and benthic foraminifera below the CIE onset is ~3.0-3.5 ‰, with *Acarinina* spp. falling between *Morozovella* spp. and *Subbotina* spp. (Figs. 2.6 and 2.S2). In the CIE "core", the $\delta^{13}C$ surface to bottom gradients among all sites along the shelf remain the same value of ~3.0-3.5 ‰ (Figs. 2.6 and 2.S2). Through the entire CIE "core", surface dwellers *Morozovella* spp. and *Acarinina* spp. record similar $\delta^{13}C$ values, with *Morozovella* spp. being slightly more positive (Figs. 2.6 and

2.S2). The $\delta^{13}C$ vertical gradients derived from the Paleocene-Eocene foraminifera are consistent with $\delta^{13}C$ gradients previously reported for the Cretaceous-Eocene warm ocean at various locations [Pearson et al., 2001; Sexton et al., 2006; John et al., 2013]. The observed $\delta^{13}C$ gradients are much greater than $\delta^{13}C$ vertical gradients in the modern ocean (<2 ‰) and have been explained as evidence for more efficient biological pump in greenhouse worlds [Hilting et al., 2008; John et al., 2013].

All New Jersey cores show reductions in $\delta^{18}O$ vertical gradients in the CIE "core" compared to below the CIE onset (Figs 2.6 and 2.S3). Below the CIE, the $\delta^{18}O$ gradient between *Morozovella* spp. and *Cibicidoides* spp. is ~1.75 ‰ based on records from Millville and Bass River (Figs. 2.6 and 2.S3). In the CIE "core", it decreases to ~1 ‰ in all four cores (Figs. 2.6 and 2.S3), being especially reduced in the lowest part of the "core" (Fig. 2.S3). *Acarinina* spp. display a change in the relative position in the surface to thermocline $\delta^{18}O$ gradient. Below the CIE onset, *Acarinina* spp. record $\delta^{18}O$ values that are between *Morozovella* spp. and *Subbotina* spp. (Figs. 2.6 and 2.S3). Above the CIE onset, *Acarinina* spp. show $\delta^{18}O$ values similar to those in *Subbotina* spp. at Bass River and Millville, and even lower than in *Subbotina* spp. at more proximal sites Wilson Lake Hole A and Ancora (Figs. 2.6 and 2.S3). In the CIE recovery, *Acarinina* spp. $\delta^{18}O$ values sharply decrease by ~ 0.75 ‰ towards values similar to *Morozovella* spp. (Fig. 2.S3). This pattern in the $\delta^{18}O$ record of *Acarinina* spp. is recognized in the PETM sections of Millville and Bass River; the pattern is not seen at Wilson Lake Hole A and Ancora due to truncation of the recovery interval of the PETM section at these sites (Fig. 2.S3). This shift in *Acarinina* spp. $\delta^{18}O$ can be used as another characteristic of the

recovery onset accompanying the returning trend in stable isotopes among all genera to pre-CIE isotopic levels.

2.6 Discussion

2.6.1 Environmental and biotic controls on stable isotope records of foraminifera

We examine two scenarios to explain different isotopic responses recorded by foraminifera in the PETM shelf records. The first makes a standard paleoceanographic assumption that ascribes isotopic differences to depth habitats of the different taxa (i.e., surface-mixed layer versus thermocline dwellers versus benthic foraminifera). Implicit in this assumption is that the planktonic foraminiferal values reflect mean annual conditions. Therefore, changes in the differences among the different taxa must reflect reorganization of the hydrographic column. The second scenario allows for a change in habitat due to an environmental perturbation, which can be accomplished by changes in either the season of planktonic foraminifera calcification or the depth at which they calcify. This scenario more accurately reflects the modern foraminiferal populations in the mid-to-high latitudes where a succession of species grows throughout the spring bloom and into the summer [e.g., Bé, 1982; Reynolds and Thunell, 1984]. We also discuss the potential influences of symbiont loss and carbonate ion effect on foraminiferal stable isotope records section 2.12 “Supporting information”.

We reconstruct the New Jersey paleoslope following Esmeray-Senlet et al. [2015] for four sites: Wilson Lake, Ancora, Millville, and Bass River (Fig. 2.7). The bottom panel demonstrates the hydrography of the New Jersey paleoshelf prior the CIE onset (Fig. 2.7a), whereas the two other panels illustrate hydrographic conditions after the CIE

onset each representing the proposed mechanisms (Figs. 2.7b and 2.7c). To characterize paleoshelf hydrography, we plot $\delta^{18}O$ gradients in the water column for all sites based on average $\delta^{18}O$ values of *Morozovella* spp., *Acarinina* spp., *Subbotina* spp., *Cibicidoides* spp., and *A. acuta*. Small insets on the right indicate the water column on the modern New Jersey shelf after Castelao et al. [2010] with the seasonal thermal structure and thus $\delta^{18}O$ gradients in June and October that we used as analogs (Fig. 2.7).

Based on the different $\delta^{18}O$ changes recorded among the foraminiferal taxa, we suggest that the thermocline deepened on the shelf after the CIE onset, responding to warming (Scenario 1; Fig. 2.7b). Under this scenario, the surface-mixed taxa (*Morozovella* and *Acaranina*) record the mean surface temperature change of ~5°C ($\Delta\delta^{18}O$ = -1 ‰) with greater warming in the thermocline and benthic taxa of 8 to 9°C ($\Delta\delta^{18}O$ = -1.75 ‰). Persistent warming during the PETM would propagate heat into deeper layers and create a more homogenous water column with a thicker warm mixed layer and a deeper, more gradual thermocline. This is similar in nature to hydrographic changes observed on the modern New Jersey shelf with a thinner mixed layer in summer and a thicker mixed layer with a deeper and more gradual seasonal thermocline in fall (Fig. 2.7 insets). Today, the surface ocean stores heat for the entire summer resulting in a strong seasonal thermocline that breaks down to a more homogenous water column structure in the fall as a result of cooling and increased storm activity [Castelao et al., 2010]. Assuming a relatively constant depth habitat of planktonic foraminifera, a more gradual thermocline during the CIE "core" would explain such different $\delta^{18}O$ responses in surface dwellers versus thermocline dwelling and benthic foraminifera (Fig. 2.7b).

A change in the water column structure during the PETM is a plausible mechanism to explain isotopic trends in planktonic foraminifera observed on the shelf. A global temperature rise of 4-8°C [e.g., Dunkley Jones et al., 2013] and a possible increase in mixing and storm activity due to an enhanced tropical heat and moisture transport during the PETM [e.g., Caballero and Langen, 2005; Pagani et al., 2006; Carmichael et al., 2016] would produce a deeper, more gradual thermocline. However, a few centuries to thousands of years after the initial warming, establishment of equilibrium conditions would require restoration of the thermocline structure similar to the pre-CIE. Sustainability of hydrographic changes during the CIE would require either a freshwater input initiating stratification [*Stassen et al.*, 2015] or a decrease in the meridional thermal gradient that would have caused more warming in thermocline waters globally. Proxy data for the sea surface [e.g., Sluijs et al., 2006; Bijl et al., 2009; Sluijs et al., 2011; Frieling et al., 2014] and mean air [Weijers et al., 2007] temperatures indicate amplified warming in the Arctic region and the Southern Ocean suggesting strongly reduced meridional temperature gradient during the PETM. Furthermore, model simulations for the Eocene period of global warmth also predict polar amplification where higher latitudes experience greater warming than low latitudes [Huber and Caballero, 2003; Huber and Caballero, 2011; Lunt et al., 2012]. Suggested polar amplification would have caused reorganization of the thermocline globally until meridional temperature gradient restored to the pre-CIE state. The reduced to 1 ‰ $\delta^{18}O$ vertical gradient during the PETM, i.e. decreased thermal gradient on the paleoshelf, is consistent with a reduced meridional thermal gradient and polar amplification.

The second scenario considers that planktonic foraminifera may have responded differently to environmental perturbations associated with the PETM onset by changing their depth habitat and/or season of dominant calcification. Surface dwellers (*Morozovella* and *Acarinina* spp.) may have migrated out of the surface mixed layer due to inhospitable conditions (e.g., high temperature, lower salinity, intense acidification) (Scenario 2; Fig. 2.7c). In this scenario, the mixed layer in contact with the PETM atmosphere was too warm, fresh, or corrosive, forcing surface dwellers to descend into cooler, saltier, and possibly more buffered thermocline waters. Both of the surface mixed taxa either descended deeper in the water column or "bloomed" earlier in the season, thus *Morozovella* spp. and *Acarinina* spp. $\delta^{18}O$ values record the PETM warming minus the change in habitat cooling (Fig. 2.7c). Accordingly, $\delta^{13}C$ values would reflect the whole ocean reservoir decrease plus a change in habitat. It is, however, possible that the variable isotopic responses also reflect a shift in bloom seasons and not just depth migration. Furthermore, one could interpret the $\delta^{13}C$ in terms of warm, nutrient depleted water during the summer months (e.g., *Morozovella*) and lower $\delta^{13}C$ associated with spring upwelling (e.g., *Subbotina*).

To test the idea that acidification was the environmental driver for the depth migration of planktonic foraminifera, we use estimates of surface ocean acidification from recent boron based proxy records [Penman et al., 2014; Babila et al., 2016]. Studies from both the North Pacific [Penman et al., 2014] and paleoshelf of New Jersey [Babila et al., 2016] show a decrease of ~0.3-0.4 pH units in both surface and thermocline waters. If acidification is a possible environmental stress to planktonic foraminifera it seems unlikely that migration to more corrosive thermocline waters would occur. Conversely,

B/Ca and $\delta^{18}O$ records of surface dwelling *Acarinina* spp. and thermocline dwelling *Subbotina* spp. indicate similar pH and $\delta^{18}O$ values, respectively, recorded by these taxa after the CIE onset (Figs. 2.3, 2.6, and 2.S3). This means that *Acarinina* spp. might have occupied the same niche in the water column as *Subbotina* spp. during the "CIE" core phase and then possibly migrated back to the mixed layer during the recovery phase.

Another possible reason for surface dwellers migration deeper into the water column could be due to the freshening of the mixed layer. Though individual species of foraminifera can tolerate and reproduce in cultures in salinities as low as 20 psu and over 40 psu [Bijma et al., 1990; Spindler, 1996], robust assemblages of planktonic foraminifera are restricted to salinities greater than 30 psu [Bé and Tolderland, 1971; Bijma et al., 1990]. Similarly, though r-selected coccolithophroidae such as Emiliani huxleyi tolerate nearshore, low salinity environments [e.g., Fisher and Honjo, 1989], diverse nannoplankton assemblages such as those found in Wilson Lake [Gibbs et al., 2006a], Millville, and Bass River [Kahn and Aubry, 2004; Harris, 2010] are restricted to normal marine salinities (e.g., >32 psu) [Menschel et al., 2016].

An enhanced hydrological cycle during the PETM [e.g., Pagani et al., 2006; Kopp et al., 2009] would have triggered greater river discharge and resulted in formation of a freshwater lens at the sea surface. Previous studies have suggested a modest freshening (up to 3-4 psu) of surface waters on New Jersey paleoshelf during the PETM [Zachos et al., 2006], though this result requires verification due to sparse pre-CIE isotopic data and will be subject of the subsequent study [Makarova et al., 2013]. A low salinity anomaly associated with a freshwater lens at the top would be inhospitable pushing the mixed layer dwellers deeper into the water column. Following Kopp et al.'s [2009] suggestion

of an Appalachian Amazon development on the mid-Atlantic shelf, we use the modern Amazon salinity variability on the shelf as an analog. The Amazon plume extends up to 80-250 km offshore and causes sea surface salinities (SSS) in the upper 5-10 m water column to drop below 33 psu [Lentz and Limeburner, 1995; Geyer et al., 1996]. A smaller scale river system would probably not lower SSS as much and as far offshore as the Amazon-type river system. For example, Hudson River runoff lowers SSS in the upper 10-15 m by only 1 unit psu during spring and summer [Castelao et al., 2010]. Nevertheless, even in the heart of the modern Amazon low salinity lens, effects on the shelf in water depths greater than 20 m (100 km from shore) are limited to the top few meters [Lentz and Limeburner, 1995], allowing us to reject the hypothesis that surface dwellers were forced by fresh water into the thermocline.

Development of the river-dominated drainage system on the mid-Atlantic shelf during the PETM might have affected bottom salinities as well. Powars and Edwards [2015] suggest that the Marlboro Formation represents delta front turbidites and/or wave enhanced sediment gravity flows. Similarly, most of fine sediments deposited on the Amazon shelf are transported at the bottom in form of fluid mud [Lentz and Limeburner, 1995; Geyer et al., 1996]. Fluid muds decrease near bottom salinities to 28-30 psu within the lower 2-3 m of the water the column on the Amazon shelf, but they do not affect bottom salinity at deeper than 20 m isobaths where the shelf deep waters are constant at normal marine salinities [Lentz and Limeburner, 1995; Geyer et al., 1996]. Therefore, bottom gravity flows of mud on the mid-Atlantic shelf during the PETM would not have affected bottom salinity nor would they have created a larger $\delta^{18}O$ decrease in benthic foraminifera across the CIE onset. Moreover, analyses of benthic foraminiferal

assemblages from the New Jersey paleoshelf show abundant benthic foraminifera in the CIE "core" despite the turnover across the P/E boundary [Cramer et al., 1999; Harris et al., 2010; Stassen et al., 2012]. A detailed recent study by Stassen et al. [2015] indicates an overall decrease in benthic foraminiferal abundances and prevalence of stress-tolerant taxa after the CIE onset suggesting water column stratification and oxygen depletion and eutrophication of the bottom waters. Based on benthic foraminiferal biofacies that indicate a response to productivity and oxygen levels, we conclude that gravity flows did not stress benthic assemblage by freshening (i.e., not affecting $\delta^{18}O$) or by changing the clarity of bottom seawater.

Though we cannot exclude Scenario 2, the similar $\delta^{13}C$ changes in all foraminifera across the shelf argues against a change in depth habitats unless there was a change in bloom season. If the surface dwellers were forced out of the mixed layer, they would record lower $\delta^{13}C$ values resulting in reduced $\delta^{13}C$ surface to bottom gradient. Instead, our stable isotopes records show a similar (3.6-4.0 ‰) magnitude of CIE among all taxa, challenging the migration scenario (Figs. 2.4 and 2.S2). Maintenance of the same $\delta^{13}C$ vertical gradient between surface dwellers and deep/benthic foraminifera suggests no major change in organic matter cycling on the shelf through the CIE and that foraminifera maintained their vertical habitat distribution with a weakened thermocline structure or change the season of calcification.

Scenario 2 could still be valid if there was change in bloom season. Extremely high-summer SSTs could have precluded calcification of surface dwellers during the summer months and restricted calcification to the cooler times of the year. Thus, the reduced $\Delta\delta^{18}O$ reflects the inability of the surface dwelling foraminifera to calcify in

summer, hence, shifting the population to cooler temperatures and higher $\delta^{18}O$ values, though they continued to calcify in nutrient depleted surface waters explaining the similar $\delta^{13}C$ changes. In this scenario, the true temperature change on the paleoshelf was on the order of 8 to 9°C (recorded by the thermocline and benthic taxa). In the modern ocean, 33°C is an upper limit on planktonic foraminiferal calcification [Bijma et al., 1990]. Given these constraints, it is not expected that surface dwelling planktonic foraminifera would be able to calcify in the warmest parts of the year if temperature change in coast surface waters was on the order of 8-9°C, exceeding temperatures of 33°C [Zachos et al., 2006; Sluijs et al., 2007; Makarova et al., 2013].

A 8-9°C warming during the PETM on shelf is higher than observed for open ocean low-mid latitude sites [e.g., Bralower et al., 1995; Zachos et al., 2003; Tripati and Elderfield, 2004; Hollis et al., 2015]. We note that in coastal regions, the proximity to land and the shallow water depths produce larger seasonal changes in temperature relative to the open ocean. CLIMAP (1976; 1981) also demonstrated that coastal regions recorded larger temperature changes relative to the open ocean under different climate conditions. The paleoshelf setting allows us to distinguish between different scenarios. However, the observation that planktonic foraminifera on the shelf may have had a similar upper temperature limit (<33°C) means that planktonic foraminifera in tropical and subtropical ocean must have responded in kind and did not record the full range of SST warming due to their temperature limits during the PETM.

2.6.2. Environmental response of other plankton

The biotic and ecological responses of other groups of planktonic organisms, calcareous nannofossils and dinoflagellates, provide useful insights to planktonic

foraminiferal responses. Studies of calcareous nannofossils from various locations, both open ocean and shelf, have suggested significant shifts in assemblages associated with global turnover [e.g., Bralower et al., 2002; Tremolada and Bralower, 2004; Gibbs et al., 2006a; Bown and Pearson, 2009; Self-Trail et al., 2012]. Gibbs et al. [2006b] noted the co-occurrence of fragile and heavily calcified forms of coccolithophorids in PETM sections suggesting no crash of calcification in the upper water column. Despite surface ocean acidification associated with the PETM onset [Penman et al., 2014; Babila et al., 2016], most studies agree that acidification did not affect production of calcareous nannofossils, but rather elevated temperature and/or nutrients did [e.g., Bralower et al., 2002; Tremolada and Bralower, 2004; Gibbs et al., 2006a; Bown and Pearson, 2009; Gibbs et al., 2010; Self-Trail et al., 2012]. In contrast to the nutrient-depleted, thermally stratified open ocean gyres, shelf areas show increased productivity [Bralower et al., 2002; Gibbs et al., 2006a; Self-Trail et al., 2012] that is also supported by elevated Sr/Ca ratios in coccolithophores [Stoll et al., 2007]. Whereas some species on the shelf adapted to warm-water, eutrophic conditions in the upper water column [e.g., Self-Trail et al., 2012], malformed ecophenotypes of the excursion taxa *Discoaster* and *Rhomboaster* [Aubry, 1998; Kahn and Aubry, 2004] might have migrated lower in the photic zone near the nutricline. Bralower and Self-Trail [2016] suggested that migration of the excursion species into a deeper habitat with lower carbonate saturation levels due to remineralization of organic matter resulted in their malformation. They also proposed that *Discoaster* spp. occupied a deeper habitat near the nutricline as a result of the expansion of a lower photic zone niche caused by warming and increased stratification, whereas normal calcareous nannoplankton assemblages characterized the upper photic zone.

Similar to the perturbations observed in calcareous nannofossil assemblages, records of dinoflagellate cysts document abrupt, global biotic changes across the PETM [e.g., Powell et al., 1996; Bujak and Brinkhuis, 1998; Crouch et al., 2001; Crouch et al., 2003; Iakovleva et al., 2001; Sluijs et al., 2006; Sluijs et al., 2007; Sluijs and Brinkhuis, 2009]. The most prominent response associated with the PETM/CIE is the rapid, synchronous onset of the *Apectodinium*-dominated assemblages (acme) observed ubiquitously [e.g., Bujak and Brinkhuis, 1998; Crouch et al., 2001; Sluijs and Brinkhuis, 2009]. Most studies suggest that the increase in *Apectodinium* abundances is associated with significantly higher sea surface temperatures (SSTs) and increased surface-water productivity (eutrophication) [Bujak and Brinkhuis, 1998; Sluijs and Brinkhuis, 2009]. However, dinocyst distribution from the New Jersey paleoshelf may also indicate low salinity and/or changes in water column stratification affecting *Apectodinium* abundances [Sluijs et al., 2007; Sluijs and Brinkhuis, 2009]. As we show here, both planktonic foraminiferal and nannofossil assemblages suggest a limited change in salinity, but do suggest a change in water column stratification and chemistry, consistent with the dinoflagellate response.

Overall, studies of calcareous nannofossils and dinoflagellates suggest that elevated temperatures, increased productivity, and water column stratification influenced phytoplankton abundances in the coastal regions during the PETM. Some species went into the deep photic zone as refuge to escape stressful conditions in the surface ocean and some formed extreme morphotypes as adaptation to harsh environments. Surface dwelling foraminifera *Morozovella* and *Acarinina* also developed excursion taxa that presumably occupied a deep habitat during the PETM [Kelly et al., 1998]. However, the

species of *Morozovella* and *Acarinina* reported here are not the excursion foraminifera and planktonic foraminiferal excursion taxa, though present, are not dominant. The proposed migration of the surface dwellers into a deeper habitat (Scenario 2) should require their ability to tolerate the twilight zone. Sufficient light level might be critical since both *Morozovella* and *Acarinina* are symbiont-bearing genera that maintained photosynthetic symbionts during the PETM (see discussion of bleaching in section 2.12 "Supporting information").

2.7 Conclusions

We present new stable isotopic data from planktonic and benthic foraminifera at Millville, NJ and compare these data to other New Jersey coastal plain cores. Our comparisons show a similar isotopic response in foraminifera across the CIE onset on the mid-Atlantic shelf: a ~4 ‰ decrease in $\delta^{13}C$ values in all taxa and a larger $\Delta\delta^{18}O$ in thermocline dwelling and benthic foraminifera than in surface dwellers. Such isotopic responses are also expressed in constant $\delta^{13}C$ and reduced $\delta^{18}O$ vertical gradients between surface, thermocline dwelling and benthic foraminifera in the CIE "core". To explain this we propose two scenarios. Scenario 1 posits a change in water column structure: surface and thermocline dwellers kept the same depth in the water column, but they record the signal of a thicker warm mixed layer and a deeper, more gradual thermocline. Scenario 2 posits a change in the habitat of the surface dwellers due to environmental stress in the mixed layer or a shift to a cooler calcification season. In the first scenario, amplified warming in the thermocline waters sustained during the CIE "core" stage resulted from a reduction in the meridional thermal gradient. We eliminate

changing pH and salinity as major environmental stressors, but others such as temperature and nutrient level might have affected surface dwellers to change their depth habitat or calcification season. Though we cannot exclude Scenario 2, the similar $\delta^{13}C$ changes in all foraminifera across the shelf argues against migration of the surface dwelling taxa deeper into the thermocline.

2.8 Acknowledgments

This research was supported by ExxonMobil Russian Scholarship and excellence fellowship for doctoral research from the Graduate School New Brunswick, Rutgers University awarded to M. Makarova. T. Babila acknowledges support by the National Science Foundation (NSF OISE-1107787), Schlanger Ocean Drilling Fellowship, and Joanna Resig Foraminiferal Research Fellowship. M. Makarova and J. Park thank Summer Aresty Program for support of benthic foraminiferal analysis. We are grateful to R.K. Olsson for advice on foraminiferal taxonomy and J.V. Browning for comments. We thank R.A. Mortlock and N. Abdul for help with stable isotope analyses and P. Darias for assistance in sample preparation. Samples were provided by International Ocean Discovery Program Rutgers Core Repository supported by NSF grant OCE14-63759 (to K. Miller). We thank H. Pälike and two anonymous reviewers for their reviews and improvement of this manuscript.

2.9 References

Anagnostou, E., E.H. John, K.M. Edgar, G.L. Foster, A. Ridgwell, G.N. Inglis, R.D. Pancost, D. J. Lunt, and P. N. Pearson (2016), Changing atmospheric CO_2 concentration was the primary driver of early Cenozoic climate, Nature 533(7603), 380–384, doi:10.1038/nature17423.

Aubry, M.-P. (1998), Early Paleogene calcareous nannoplankton evolution: A tale of climatic amelioration in M.-P. Aubry, S.G. Lucas, and W.A. Berggren, eds., Late Paleocene-Early Eocene Climatic and Biotic Events in the Marine and Terrestrial Records, Columbia University Press, New York, 158–203.

Aubry, M.-P., K. Ouda, C. Dupuis, W.A. Berggren, J.A. Van Couvering, and the Members of the Working Group on the Paleocene/Eocene Boundary (2007), The Global Standard Stratotype-section and Point (GSSP) for the base of the Eocene Series in the Dababiya section (Egypt), Episodes, 30(4), 271–286.

Babila, T.L. (2014), Boron/calcium in planktonic foraminifera: proxy development and application to the Paleocene-Eocene boundary, Ph.D. Thesis, Rutgers University, 140 p.

Babila, T.L., Y. Rosenthal, J.D. Wright, and K.G. Miller (2016), A continental shelf perspective of ocean acidification and temperature evolution during the Paleocene-Eocene Thermal Maximum, Geology, 44(4), 275–278, doi:10.1130/G37522.1.

Bains, S., R.M. Corfield, and R.D. Norris (1999), Mechanisms of climate warming at the end of the Paleocene, Science, 285, 724–727.

Bé, A.W.H. (1960), Ecology of recent planktonic foraminifera: Part 2 – Bathymetric and seasonal distributions in the Sargasso Sea off Bermuda, Micropaleontology, 6(4), 373–392.

Bé, A.W.H. (1982), Biology of planktonic foraminifera, in M.A. Buzas, B.K. Sen Gupta, and T. W. Broadhead, eds. Foraminifera: notes for a short course University of Tennessee Studies in Geology, 6, 51–89.

Bé, A.W.H. and D.S. Tolderlund (1971), Distribution and ecology of living planktonic foraminifera in surface waters of the Atlantic and Indian Oceans, The Micropaleontology of Oceans, 105–149.

Berggren, W.A. and J. Aubert (1975), Paleocene Benthonic Foraminiferal Biostratigraphy, Paleobiogeography and Paleoecology of Atlantic-Tethyan Regions: Midway-Type Fauna, Palaeogeography, Paleoclimatology, Palaeoecology, 18, 73–192.

Bijl, P.K., S. Schouten, A. Sluijs, G.-J. Reichart, J.C. Zachos, and H. Brinkhuis (2009), Early Palaeogene temperature evolution of the southwest Pacific Ocean, Nature, 461, 776–779, doi:10.1038/nature08399.

Bijma, J., W.W. Faber Jr., and C. Hemleben (1990), Temperature and salinity limits for growth and survival of some planktonic foraminifers in laboratory cultures, Journal of Foraminiferal Research, 20(2), 95–116.

Birch, H.S., H.K. Coxall, and P.N. Pearson (2012), Evolutionary ecology of Early Paleocene planktonic foraminifera: size, depth habitat and symbiosis, Paleobiology, 38(3), 374–390.

Boersma, A., I. Premoli Silva, and N.J. Shackleton (1987), Atlantic Eocene planktonic foraminiferal paleohydrographic indicators and stable isotope paleoceanography, Paleoceanography, 2(3), 287–331.

Bornemann, A. and R.D. Norris (2007), Size-related stable isotope changes in Late Cretaceous planktic foraminifera: implications for paleoecology and photosymbiosis, Marine Micropaleontology, 65, 32–42.

Bowen, G.J., B.J. Maibauer, M.J. Kraus, U. Röhl, T. Westerhold, A. Steimke, P.D. Gingerich, S.L.Wing, and W.C. Clyde (2015), Two massive, rapid releases of carbon during the onset of the Palaeocene–Eocene thermal maximum, Nature Geoscience 8, 44–47, doi:10.1038/NGEO2316.

Bown, P. and P. Pearson (2009), Calcareous plankton evolution and the Paleocene/Eocene thermal maximum event: new evidence from Tanzania, Marine Micropaleontology, 71, 60–70, doi: 10.1016/j.marmicro.2009.01.005.

Bralower, T. (2002), Evidence for surface water oligotrophy during the Paleocene-Eocene thermal maximum: Nannofossil assemblage data from Ocean Drilling Program Site 690, Maud Rise, Weddell Sea, Paleoceanography, 17, 1023, doi: 10.1029/2001PA000662.

Bralower T.J. and J.M. Self-Trail (2016), Nannoplankton malformation during the Paleocene-Eocene Thermal Maximum and its paleoecological and paleoceangraphic significance, Paleoceanography, doi:10.1002/2016PA002980.

Bralower, T.J., J.C. Zachos, E. Thomas, M. Parrow, C.K. Paull, D.C. Kelly, I. Premoli Silva, W.V. Sliter, and K.C. Lohmann (1995), Late Paleocene to Eocene paleoceanography of the equatorial Pacific Ocean: stable isotopes recorded at Ocean Drilling Program Site 865, Allison Guyot, Paleoceanography, 10, 841–865.

Bralower, T.J., D.C. Kelly, S. Gibbs, K. Farley, L. Eccles, T.L. Lindemann, and G.J. Smith (2014), Impact of dissolution on the sedimentary record of the Paleocene–Eocene thermal maximum, Earth and Planetary Science Letters, 401, 70–82, doi:10.1016/j.epsl.2014.05.055.

Browning, J.V., K.G. Miller, and R.K. Olsson (1997), Lower to middle Eocene benthic foraminiferal biofacies, lithostratigraphic units, and their relationship to sequences, New Jersey Coastal Plain, in K.G. Miller and S.W. Snyder, eds., Proceedings of the Ocean Drilling Program, Scientific results, Vol. 150X: College Station, Texas, Ocean Drilling Program, 207–228.

Bujak, J.P. and H. Brinkhuis (1998), Global warming and dinocyct changes across the Paleocene-Eocene epoch boundary in M.-P. Aubry, S. G. Lucas, and W. A. Berggren, eds., Late Paleocene-Early Eocene Climatic and Biotic Events in the Marine and Terrestrial Records, Columbia University Press, New York, 277–295.

Caballero, R. and P.L. Langen (2005), The dynamic range of poleward energy transport in an atmospheric general circulation model, Geophysical Research Letters, 32, L02705, doi:10.1029/2004GL021581.

Carmichael, M.J., D.J. Lunt, M.Huber, M. Heinemann, J. Kiehl, A. LeGrande, C.A. Loptson, C.D. Roberts, N. Sagoo, C. Shields, P.J. Valdes, A. Winguth, C. Winguth, and R.D. Pancost (2016), A model–model and data–model comparison for the early Eocene hydrological cycle, Climate of the Past, 12, 455–481, doi:10.5194/cp-12-455-2016.

Castelao, R., S. Glenn, and O. Schofield (2010), Temperature, salinity, and density variability in the central Middle Atlantic Bight, Journal of Geophysical Research, 115, 1–14, doi:10.1029/2009JC006082.

CLIMAP Project Members (1976), The surface of the ice-age earth, Science (New York, NY), 191(4232), 1131.

CLIMAP Project Members (1981), Seasonal reconstructions of the Earth's surface at the Last Glacial Maximum, Geological Society of America.

Cramer, B.S. and D.V. Kent (2005), Bolide summer: The Paleocene/Eocene thermal maximum as a response to an extraterrestrial trigger, Palaeogeography, Palaeoclimatology, Palaeoecology, 224, 144–166.

Cramer, B.S., M.-P. Aubry, K.G. Miller, R.K. Olsson, J.D. Wright, and D.V. Kent (1999), An exceptional chronologic, isotopic, and clay mineralogic record at the latest Paleocene thermal maximum, Bass River, NJ, ODP 174AX, Bulletin de la Société géologique de France, 170(6), 883–897.

Coxall, H.K., P.N. Pearson, N.J. Shackleton, and M.A. Hall (2000), Hantkeninid depth adaptation: An evolving life strategy in a changing ocean, Geology, 28(1), 87–90.

Crouch, E.M., C. Heilmann-Clausen, H. Brinkhuis, H.E.G. Morgans, K.M. Rogers, H. Egger, and B. Schmitz (2001), Global dinoflagellate event associated with the late Paleocene thermal maximum, Geology, 29(4), 315–318.

Crouch, E.M., G.R. Dickens, H. Brinkhuis, M.-P. Aubry, C.J. Hollis, K.M. Rogers, and H. Visscher (2003), The *Apectodinium* acme and terrestrial discharge during the Paleocene-Eocene thermal maximum: new palynological, geochemical and calcareous nannoplankton observations at Tawanui, New Zealand, Palaeogeography, Palaeoclimatology, Palaeoecology, 194, 387–403.

Cui, Y., L.R. Kump, A.J. Ridgwell, A.J. Charles, C.K. Junium, A.F. Diefendorf, K.H. Freeman, N.M. Urban, and I.C. Harding (2011), Slow release of fossil carbon during the Palaeocene–Eocene Thermal Maximum, Nature Geoscience, 4, 481–485, doi:10.1038/NGEO1179.

Curry, W.B., R.C. Thunell, and S. Honjo (1983), Seasonal changes in the isotopic composition of planktonic foraminifera collected in Panama Basin sediment traps, Earth and Planetary Science Letters, 64, 33–43.

Cushman, J.A. (1951), Paleocene Foraminifera of the Gulf Coastal Region of the United States and Adjacent Areas, Geological Survey Professional Paper 232, United States Government Printing Office, 1–75.

Deuser, W.G. and E.H. Ross (1989), Seasonally abundant planktonic foraminifera of the Sargasso Sea: succession, deep-water fluxes, isotopic compositions, and paleoceanographic implications, Journal of Foraminiferal Research, 19(4), 268–293.

D'Hondt, S. and J.C. Zachos (1993), On stable isotopic variation and earliest Paleocene planktonic foraminifera, Paleoceanography, 8(4), 527–547.

D'Hondt, S., J.C. Zachos, and G. Schultz (1994), Stable isotopic signals and photosymbiosis in late Paleocene planktic foraminifera, Paleobiology, 20, 391–406.

Dickens, G.R., M.M. Castillo, and J.C.G. Walker (1997), A blast of gas in the latest Paleocene: Simulating first-order effects of massive dissociation of oceanic methane hydrate, Geology, 25(3), 259–262.

Dunkley Jones, T., D.J. Lunt, D.N. Schmidt, A. Ridgwell, A. Sluijs, P.J. Valdes, and M. Maslin (2013), Climate model and proxy data constraints on ocean warming across the Paleocene-Eocene Thermal Maximum, Earth-Science Reviews, 125, 123–145, doi:10.1016/j.earscirev.2013.07.004.

Emiliani, C. (1954), Depth habitats of some species of pelagic Foraminifera as indicated by oxygen isotope ratios, American Journal of Science, 252(3), 149–158, doi:10.2475/ajs.252.3.149.

Epstein, S., R. Buchsbaum, H. Lowenstam, and H. Urey (1953), Revised carbonate-water isotopic temperature scale, Geological Society of America Bulletin, 64(11), 1315–1325.

Esmeray-Senlet, S., J.D. Wright, R.K. Olsson, K.G. Miller, J.V. Browning, and T.M. Quan (2015), Evidence for reduced export productivity following the Cretaceous/Paleogene mass extinction, Paleoceanography, 30, 1–21, doi:10.1002/2014PA002724.

Fairbanks, R.G. (1982), The origin of continental shelf and slope water in the New York Bight and Gulf of Maine: Evidence from $H_2{}^{18}O/H_2{}^{16}O$ ratio measurements, Journal of Geophysical Research, 87(C8), 5796–5808.

Fairbanks, R.G. and P.H. Wiebe (1980), Foraminifera and chlorophyll maximum: Vertical distribution, seasonal succession, and paleoceanographic significance, Science, 209, 1524–1526.

Fairbanks, R.G., M. Sverdlove, R. Free, P.H. Wiebe, and A.W.H. Bé (1982), Vertical distribution and isotopic fractionation of living planktonic foraminifera in the Panama Basin, Nature, 298, 841–844.

Fisher, N.S. and S. Honjo (1989), Intraspecific differences in temperature and salinity responses in the coccolithophore Emiliania huxleyi, Biological Oceanography, 6(3-4), 355–361.

Frieling, J., A.I. Iakovleva, G.J. Reichart, G.N. Aleksandrova, Z.N. Gnibidenko, S. Schouten, and A. Sluijs (2014), Paleocene–Eocene warming and biotic response in the epicontinental West Siberian Sea, Geology, 42(9), 767-770, doi:10.1130/G35724.1.

John, C.M., S.M. Bohaty, J.C. Zachos, A. Sluijs, S. Gibbs, H. Brinkhuis, and T.J. Bralower (2008), North American continental margin records of the Paleocene-Eocene thermal maximum: Implications for global carbon and hydrological cycling, Paleoceanography, 23, 1–20, doi:10.1029/2007PA001465.

John, E.H, P.N. Pearson, H.K. Coxall, H. Birch, B.S. Wade, and G.L. Foster (2013), Warm ocean processes and carbon cycling in the Eocene, Philosophical Transitions of the Royal Society A, 371, 1–20, doi:10.1098/rsta.2013.0099.

Geyer, W.R., R.C. Beardsley, S.J. Lentz, J. Candela, R. Limeburner, W.E. Johns, B.M. Castro, and I.D. Soares (1996), Physical oceanography of the Amazon shelf, Continental Shelf Research, 16(5/6), 575–616.

Gibbs, S.J., T.J. Bralower, P.R. Bown, J.C. Zachos, and L.M. Bybell (2006a), Shelf and open-ocean calcareous phytoplankton assemblages across the Paleocene-Eocene Thermal Maximum: Implications for global productivity gradients, Geology, 34(4), 233, doi:10.1130/g22381.1.

Gibbs, S.J., P.R. Bown, J.A. Sessa, T.J. Bralower, and P.A. Wilson (2006b), Nannoplankton extinction and origination across the Paleocene-Eocene Thermal Maximum, Science, 314(5806), 1770–1773, doi:10.1126/science.1133902.

Gibbs, S.J., H.M. Stoll, P.R. Bown, and T.J. Bralower (2010), Ocean acidification and surface water carbonate production across the Paleocene–Eocene thermal maximum, Earth and Planetary Science Letters, 295, 583–592, doi:10.1016/j.epsl.2010.04.044.

Gibson, T.G., L.M. Bybell, and J.P. Owens (1993), Latest Paleocene lithologic and biotic events in neritic deposits of southwestern New Jersey, Paleoceanography, 8(4), 495–514.

Glenn, S.M., C. Jones, M. Twardowski, L. Bowers, J. Kerfoot, D. Webb, and O. Schofield (2008), Glider observations of sediment resuspension in a Middle Atlantic Bight fall transition storm, Limnology and Oceanography, 53, 2180–2196.

Gong, D., J.T. Kohut, and S.M. Glenn (2010), Seasonal climatology of wind-driven circulation on the New Jersey Shelf, Journal of Geophysical Research, 115, C04006, C04006, doi:10.1029/2009JC005520.

Harris, A.D. (2010), Integrated sequence stratigraphy of the Paleocene-lowermost Eocene, New Jersey coastal plain: Implications for eustatic and paleoceanographic change, Ph.D. Thesis, Rutgers University, 183 p.

Harris, A.D., K.G. Miller, J.V. Browning, P.J. Sugarman, R.K. Olsson, B.S. Cramer, and J.D. Wright (2010), Integrated stratigraphic studies of Paleocene-lowermost Eocene sequences, New Jersey Coastal Plain: Evidence for glacioeustatic control, Paleoceanography, 25, 1–18, doi:10.1029/2009PA001800.

Hilting, A.K., L.R. Kump, and T.J. Bralower (2008), Variations in the oceanic vertical carbon isotope gradient and their implications for the Paleocene-Eocene biological pump, Paleoceanography, 23, 1–15, doi:10.1029/2007PA001458.

Hollis, C.J., B.R. Hines, K. Littler, V. Villasante-Marcos, D.K. Kulhanek, C.P. Strong, J.C. Zachos, S.M. Eggins, L. Northcote, and A. Phillips (2015), Onset of the Paleocene–Eocene Thermal Maximum in the southern Pacific Ocean (DSDP Site 277, Campbell Plateau), Climate of the Past Discussions, 11, 243–278, doi:10.5194/cpd-11-243-2015.

Hönisch B., A. Ridgwell, D.N. Schmidt, E. Thomas, S.J. Gibbs, A. Sluijs, R. Zeebe, L. Kump, R.C. Martindale, S.E. Greene, W. Kiessling, J. Ries, J.C. Zachos, D.L. Royer, S. Barker, T.M. Marchitto Jr., R. Moyer, C. Pelejero, P. Ziveri, G.L. Foster, and B. Williams (2012), The Geological Record of Ocean Acidification, Science, 334, 1058–1063.

Huber, M. and R. Caballero (2003), Eocene El Niño: Evidence for Robust Tropical Dynamics in the “Hothouse”, Science, 299, 877–881, doi:10.1126/science.1078766.

Huber, M. and R. Caballero (2011), The early Eocene equable climate problem revisited, Climate of the Past, 7, 603–633, doi:10.5194/cp-7-603-2011.

Iakovleva, A.I., H. Brinkhuis, and C. Cavagnetto (2001), Late Palaeocene-Early Eocene dinoflagellate cysts from the Turgay Strait, Kazakhstan; correlations across ancient seaways, Palaeogeography, Palaeoclimatology, Palaeoecology, 172, 243–268.

Kahn, A. and M.-P. Aubry (2004), Provincialism associated with the Paleocene/Eocene thermal maximum: temporal constraint, Marine Micropaleontology, 52, 117–131, doi:10.1016/j.marmicro.2004.04.003.

Katz, M.E., D.K. Pak, G.R. Dickens, and K.G. Miller (1999), The Source and Fate of Massive Carbon Input During the Latest Paleocene Thermal Maximum, Science, 286, 1531–1533.

Katz, M.E., B.S. Cramer, A, Franzese, B. Hönisch, K.G. Miller, Y. Rosenthal, and J.D. Wright (2010), Traditional and emerging geochemical proxies in foraminifera, Journal of Foraminiferal Research, 40(2), 165–192, doi:10.2113/gsjfr.40.2.165.

Kelly, D.C., T.J. Bralower, and J.C. Zachos (1998), Evolutionary consequences of the latest Paleocene thermal maximum for tropical planktonic foraminifera, Palaeogeography, Palaeoclimatology, Palaeoecology, 141, 139-161.

Kennett, J.P. and L.D. Stott (1991), Abrupt deep-sea warming, palaeoceanographic changes and benthic extinctions at the end of the Palaeocene, Nature, 353, 225–229.

Kent, D.V., B.S. Cramer, L. Lanci, D. Wang, J.D. Wright, and R. Van der Voo (2003), A case for a comet impact trigger for the Paleocene/Eocene thermal maximum and carbon isotope excursion, Earth and Planetary Science Letters, 211, 13–26.

Kirtland Turner, S. and A. Ridgwell (2016), Development of a novel empirical framework for interpreting geological carbon isotope excursions, with implications for the rate of carbon injection across the PETM, Earth and Planetary Science Letters, 435, 1–13, doi:10.1016/j.epsl.2015.11.027.

Koch, P.L., J.C. Zachos, and P.D. Gingerich (1992), Correlation between isotope records in marine and continental carbon reservoirs near the Palaeocene/Eocene boundary, Nature, 358, 319–322.

Kopp, R.E., D. Schumann, T.D. Raub, D.S. Powars, L.V. Godfrey, N.L. Swanson-Hysell, A.C. Maloof, and H. Vali (2009), An Appalachian Amazon? Magnetofossil evidence for the development of a tropical river-like system in the mid-Atlantic United States during the Paleocene-Eocene thermal maximum, Paleoceanography, 24, 1–17, doi:10.1029/2009PA001783.

Lentz, S.J. and R. Limeburner (1995), The Amazon River Plume during AMASSEDS: Spatial characteristics and salinity variability, Journal of Geophysical Research, 100(2), 2355–2375.

Lombardi, C.J. (2013), Lithostratigraphy and clay mineralogy of Paleocene-Eocene thermal maximum sediments at Wilson Lake, NJ, M.S. Thesis, Rutgers University, 94 p.

Lu, G. and G. Keller (1996), Separating ecological assemblages using stable isotope signals: late Paleocene to early Eocene planktonic foraminifera, DSDP Site 577, Journal of Foraminiferal Research, 26(2), 103–112.

Lunt, D.J., T. Dunkley Jones, M. Heinemann, M. Huber, A. LeGrande, A. Winguth, C. Loptson, J. Marotzke, C.D. Roberts, J. Tindall, P. Valdes, and C. Winguth (2012), A model–data comparison for a multi-model ensemble of early Eocene atmosphere-ocean simulations: EoMIP, Climate of the Past, 8, 1717–1736, doi:10.5194/cp-8-1717-2012.

Makarova, M., K.G. Miller, J.D. Wright, Y. Rosenthal, T. Babila, and J.V. Browning (2013), Paleoenvironmental changes associated with the PETM, Millville (ODP Leg 174AX), New Jersey coastal plain, American Geophysical Union, Fall Meeting 2013, abstract #PP23B-1971.

McInerney, F.A. and S.L. Wing (2011), The Paleocene-Eocene thermal maximum: a perturbation of carbon cycle, climate, and biosphere with implications for the future, Annual Review of Earth and Planetary Sciences, 39, 489–516.

Menschel, E., H.E. González, and R. Giesecke (2016), Coastal-oceanic distribution gradient of coccolithophores and their role in the carbonate flux of the upwelling system off Concepción, Chile (36° S), Journal of Plankton Research, 38(4), 798–817, doi:10.1093/plankt/fbw037.

Miller, K.G., P.J. Sugarman, J.V. Browning, R.K. Olsson, S.F. Pekar, T.J. Reilly, B.S. Cramer, M.-P. Aubry, R.P. Lawrence, J. Curran, M. Stewart, J.M. Metzger, J. Uptegrove, D. Bukry, L.H. Burckle, J.D. Wright, M.D. Feigenson, G.J. Brenner, and R.F. Dalton (1998), Bass River Site, in K.G. Miller, P.J. Sugarman, J.V. Browning et al., eds., Proceedings of the Ocean Drilling Program, Initial reports, Volume 174AX: College Station, TX, Ocean Drilling Program, 5–43.

Miller, K.G., P.J. Sugarman, J.V. Browning, B.S. Cramer, R.K. Olsson, L. de Romero, M.-P. Aubry, S.F. Pekar, M.D. Georgescu, K.T. Metzger, D.H. Monteverde, E.S. Skinner, J. Uptegrove, L.G. Mullikin, F.L. Muller, M.D. Feigenson, T.J. Reilly, C.J. Brenner, and D. Queen (1999), Ancora Site, in K.G. Miller, P.J. Sugarman, J.V. Browning et al., eds., Proceedings of the Ocean Drilling Program, Initial Reports, Volume 174AX (supplement): College Station, TX, Ocean Drilling Program, 1–65.

Murphy, B.H., K.A. Farley, and J.C. Zachos (2010), An extraterrestrial ^{3}He-based timescale for the Paleocene-Eocene thermal maximum (PETM) from Walvis Ridge, IODP Site 1266, Geochimica et Cosmochimica Acta, 74, 5098–5108.

Norris, R.D. (1996), Symbiosis as an evolutionary innovation in the radiation of Paleocene planktic foraminifera, Paleobiology, 22, 461–480.

Olsson, R.K., and E.E. Nyong (1984), A paleoslope model for Campanian-lower Maestrichtian foraminifera of New Jersey and Delaware, Journal of Foraminiferal Research, 14, 50–68.

Olsson, R.K., C. Hemleben, W.A. Berggren, and B.T. Huber eds. (1999), Atlas of Paleocene planktonic foraminifera, Smithsonian contributions to paleobiology, 85, Smithsonian Institution Press, Washington D.C., 252 p.

Pagani, M., N. Pedentchouk, M. Huber, A. Sluijs, S. Schouten, H. Brinkhuis, J.S.

Sinninghe Damsté, G.R. Dickens, and the Expedition 302 Scientists (2006), Arctic hydrology during global warming at the Palaeocene/Eocene thermal maximum, Nature, 442, 671–675.

Pearson, P.N. and M.R. Palmer (1999), Middle Eocene Seawater pH and Atmospheric Carbon Dioxide Concentrations, Science, 284, 1824–1826, doi:10.1126/science.284.5421.1824.

Pearson, P.N., N.J. Shackleton, and M.A. Hall (1993), Stable isotope paleoecology of middle Eocene planktonic foraminifera and multispecies isotope stratigraphy, DSDP Site 523, South Atlantic, Journal of Foraminiferal Research, 23, 123–140.

Pearson, P.N., P.W. Ditchfield, J. Singano, K.G. Harcourt-Brown, C.J. Nicholas, R.K. Olsson, N.J. Shackleton, and M.A. Hall (2001), Warm tropical sea surface temperatures in the Late Cretaceous and Eocene epochs, Nature, 413, 481–487.

Pearson, P.N., R.K. Olsson, B.T. Huber, C. Hemleben, and W.A. Berggren eds. (2006), Atlas of Eocene planktonic foraminifera, Cushman Foundation for foraminiferal research special publications, 41, 513 p.

Penman, D.E., B. Hönisch, R.E. Zeebe, E. Thomas, and J.C. Zachos (2014), Rapid and sustained surface ocean acidification during the Paleocene-Eocene Thermal Maximum, Paleoceanography, 29, 357–369, doi:10.1002/2014PA002621.

Powars, D.S. and L.E. Edwards (2015), Paleocene-Eocene thermal maximum lithofacies across the mid-Atlantic coastal plain: sedimentalogical analysis of 100's of stacked turbidite packages, Abstract, 2015 GSA Annual Meeting in Baltimore, Maryland, USA (1-4 November 2015), Paper No. 247-10.

Powell, A.J., H. Brinkhuis, and J.P. Bujak (1996), Upper Paleocene - Lower Eocene dinoflagellate cyst sequence biostratigraphy of southeast England, in R.W.O.B. Knox, R.M. Corfield, and R.S. Dunay, eds., Correlation of the Early Paleogene in Northwest Europe, Geological Society Special Publication, 101, 145–183.

Ravelo, A.C. and R.G. Fairbanks (1992), Oxygen isotopic composition of multiple species of planktonic foraminifera: recorders of the modern photic zone temperature gradient, Paleoceanography, 7(6), 815–831.

Reynolds, L., and R.C. Thunell (1985), Seasonal succession of planktonic foraminifera in the subpolar North Pacific, The Journal of Foraminiferal Research, 15(4), 282–301.

Röhl, U., T. Westerhold, T.J. Bralower, and J.C. Zachos (2007), On the duration of the Paleocene-Eocene thermal maximum (PETM), Geochemistry Geophysics Geosystems, 8(12), 1–13.

Quillévéré, F., R.D. Norris, I. Moussa, and W.A. Berggren (2001), Role of photosymbiosis and biogeography in the diversification of early Paleogene acarininids (planktonic foraminifera), Paleobiology, 27, 311–326.

Self-Trail, J.M., D.S. Powars, D.K. Watkins, and G.A. Wandless (2012), Calcareous nannofossil assemblage changes across the Paleocene–Eocene Thermal Maximum: Evidence from a shelf setting, Marine Micropaleontology, 92-93, 61–80, doi: 10.1016/j.marmicro.2012.05.003.

Sexton, P.F., P.A. Wilson, and P.N. Pearson (2006), Microstructural and geochemical perspectives on planktic foraminiferal preservation: "Glassy" versus "Frosty",

Geochemistry Geophysics Geosystems, 7, Q12P19, 1–29, doi:10.1029/2006GC001291.

Sluijs, A. and H. Brinkhuis (2009), A dynamic climate and ecosystem state during the Paleocene-Eocene Thermal Maximum: inferences from dinoflagellate cyst assemblages on the New Jersey Shelf, Biogeosciences, 6, 1755–1781.

Sluijs, A., S. Schouten, M. Pagani, M. Woltering, H. Brinkhuis, J.S. Sinninghe Damsté, G.R. Dickens, M. Huber, G.-J. Reichart, R. Stein, J. Matthiessen, L.J. Lourens, N. Pedentchouk, J. Backman, K. Moran, and the Expedition 302 Scientists (2006), Subtropical Arctic Ocean temperatures during the Palaeocene/Eocene thermal maximum, Nature, 441, 610–613.

Sluijs, A., H. Brinkhuis, S. Schouten, S.M. Bohaty, C.M. John, J.C. Zachos, G.J. Reichart, J.S. Sinninghe Damsté, E.M. Crouch, and G.R. Dickens (2007), Environmental precursors to rapid light carbon injection at the Palaeocene/Eocene boundary, Nature, 450(7173), 1218–1221, doi: 10.1038/nature06400.

Sluijs, A., P.K. Bijl, S. Schouten, U. Röhl, G.-J. Reichart, and H. Brinkhuis (2011), Southern ocean warming, sea level and hydrological change during the Paleocene-Eocene thermal maximum, Climate of the Past, 7, 47–61, doi:10.5194/cp-7-47-2011.

Spindler, M. (1996), On the salinity tolerance of the planktonic foraminifera Neogloboquadrina pachyderma from Antarctic sea ice, Proceedings of the NIPR Symposium on Polar Biology, 9, 85–91.

Stassen, P., E. Thomas, and R.P. Speijer (2012), Integrated stratigraphy of the Paleocene-Eocene thermal maximum in the New Jersey Coastal Plain: Toward understanding the effects of global warming in a shelf environment, Paleoceanography, 27, 1–17, doi:10.1029/2012PA002323.

Stassen, P., E. Thomas, and R.P. Speijer (2015), Paleocene–Eocene Thermal Maximum environmental change in the New Jersey Coastal Plain: benthic foraminiferal biotic events, Marine Micropaleontology, 115, 1–23, doi:10.1016/j.marmicro.2014.12.001.

Stoll, H.M., N. Shimizu, D. Archer, and P. Ziveri (2007), Coccolithophore productivity response to greenhouse event of the Paleocene–Eocene thermal maximum, Earth and Planetary Science Letters, 258, 192–206, doi:10.1016/j.epsl.2007.03.037.

Sugarman, P.J., K.G. Miller, J.V. Browning, M.-P. Aubry, G.J. Brenner, G. Cobbs III, L. de Romero, M.D. Feigenson, A. Harris, M.E. Katz, A. Kulpecz, P.P. McLaughlin Jr., S. Misintseva, D.H. Monteverde, R.K. Olsson, L. Patrick, S.J. Pekar, and J. Uptegrove (2005), Millville site, in K.G. Miller, P.J. Sugarman, J.V. Browning et al., eds., Proceedings of the Ocean Drilling Program, Scientific results, Vol. 174AX (supplement): College Station, Texas, Ocean Drilling Program, 1–95.

Sugarman, P.J., K.G. Miller, J.V. Browning, M.-P. Aubry, G.J. Brenner, D. Bukry, B. Butari, M.D. Feigenson, A.A. Kulpecz, P.P. McLaughlin Jr., S. Mizintseva, D.H. Monteverde, R.K. Olsson, A. Pusz, H. Rancan, J. Tomlinson, J. Uptegrove, and C.C. Velez (2010), Medford Site, in K.G. Miller, P.J. Sugarman, J.V. Browning et al., eds., Proceedings of the Ocean Drilling Program, Initial reports, Vol. 174AX (supplement): College Station, TX, 1–93.

Thomas, D.J., T.J. Bralower, and J.C. Zachos (1999), New evidence for subtropical warming during the late Paleocene thermal maximum: Stable isotopes from Deep Sea Drilling Project Site 527, Walvis Ridge, Paleoceanography, 14(5), 561–570.

Thomas, D.J., J.C. Zachos, T.M. Bralower, E. Thomas, and S. Bohaty (2002), Warming the fuel for the fire: Evidence for the thermal dissociation of methane hydrate during the Paleocene-Eocene thermal maximum, Geology, 30(12), 1067–1070.

Thunell, R.C., W.B. Curry, and S. Honjo (1983), Seasonal variations in the flux of planktonic foraminifera: time series sediment trap results from the Panama Basin, Earth and Planetary Science Letters, 64, 44–55.

Tremolada, F. and T.J. Bralower (2004), Nannofossil assemblage fluctuations during the Paleocene–Eocene Thermal Maximum at Sites 213 (Indian Ocean) and 401 (North Atlantic Ocean): palaeoceanographic implications, Marine Micropaleontology, 52, 107–116, doi:10.1016/j.marmicro.2004.04.002.

Tripati, A.K. and H. Elderfield (2004), Abrupt hydrographic changes in the equatorial Pacific and subtropical Atlantic from foraminiferal Mg/Ca indicate greenhouse origin for the thermal maximum at the Paleocene-Eocene Boundary, Geochemistry Geophysics Geosystems, 5(2), 1–11, doi:10.1029/2003GC000631.

Wade, B.S., N. Al-Sabouni, C. Hemleben, and D. Kroon (2008), Symbiont bleaching in fossil planktonic foraminifera, Evolutionary Ecology, 22, 253–265, doi:10.1007/s10682-007-9176-6.

Weijers, J.W.H., S. Schouten, A. Sluijs, H. Brinkhuis, and J.S. Sinninghe Damsté (2007), Warm arctic continents during the Palaeocene–Eocene thermal maximum, Earth and Planetary Science Letters, 261, 230–238, doi:10.1016/j.epsl.2007.06.033.

Wing, S.L., G.J. Harrington, F.A. Smith, J.I. Bloch, D.M. Boyer, and K.H. Freeman (2005), Transient floral change and rapid global warming at the Paleocene-Eocene boundary, Science, 310, 993–996.

Wright, J.D. and M.F. Schaller (2013), Evidence for a rapid release of carbon at the Paleocene-Eocene thermal maximum, Proceedings of the National Academy of Sciences of the United States of America, 110(40), 15908–15913.

Zachos, J.C., M.W. Wara, S.M. Bohaty, M.L. Delaney, M. Rose-Petrizzo, A. Brill, T.J. Bralower, and I. Premoli-Silva (2003), A transient rise in tropical sea surface temperature during the Paleocene-Eocene thermal maximum, Science, 302, 1551–1554.

Zachos, J.C., U. Röhl, S.A. Schellenberg, A. Sluijs, D.A. Hodell, D.C. Kelly, E. Thomas, M. Nicolo, I. Raffi, L.J. Lourens, H. McCarren, and D. Kroon (2005), Rapid Acidification of the Ocean During the Paleocene-Eocene Thermal Maximum, Science, 308, 1611–1615, doi:10.1126/science.1109004.

Zachos, J.C., S. Schouten, S. Bohaty, T. Quattlebaum, A. Sluijs, H. Brinkhuis, S.J. Gibbs, and T.J. Bralower (2006), Extreme warming of mid-latitude coastal ocean during the Paleocene-Eocene Thermal Maximum: Inferences from TEX_{86} and isotope data, Geology, 34(9), 737–740.

Zachos, J.C., S.M. Bohaty, C.M. John, H. McCarren, D.C. Kelly, and T. Nielsen (2007), The Palaeocene–Eocene carbon isotope excursion: constraints from individual

shell planktonic foraminifer records, Philosophical Transitions of the Royal Society A, 365, 1829–1842, doi:10.1098/rsta.2007.2045.

Zeebe, R.E., A. Ridgwell, and J.C. Zachos (2016), Anthropogenic carbon release rate unprecedented during the past 66 million years, Nature Geoscience, 9, 325–329, doi:10.1038/ngeo2681.

2.10 Figures

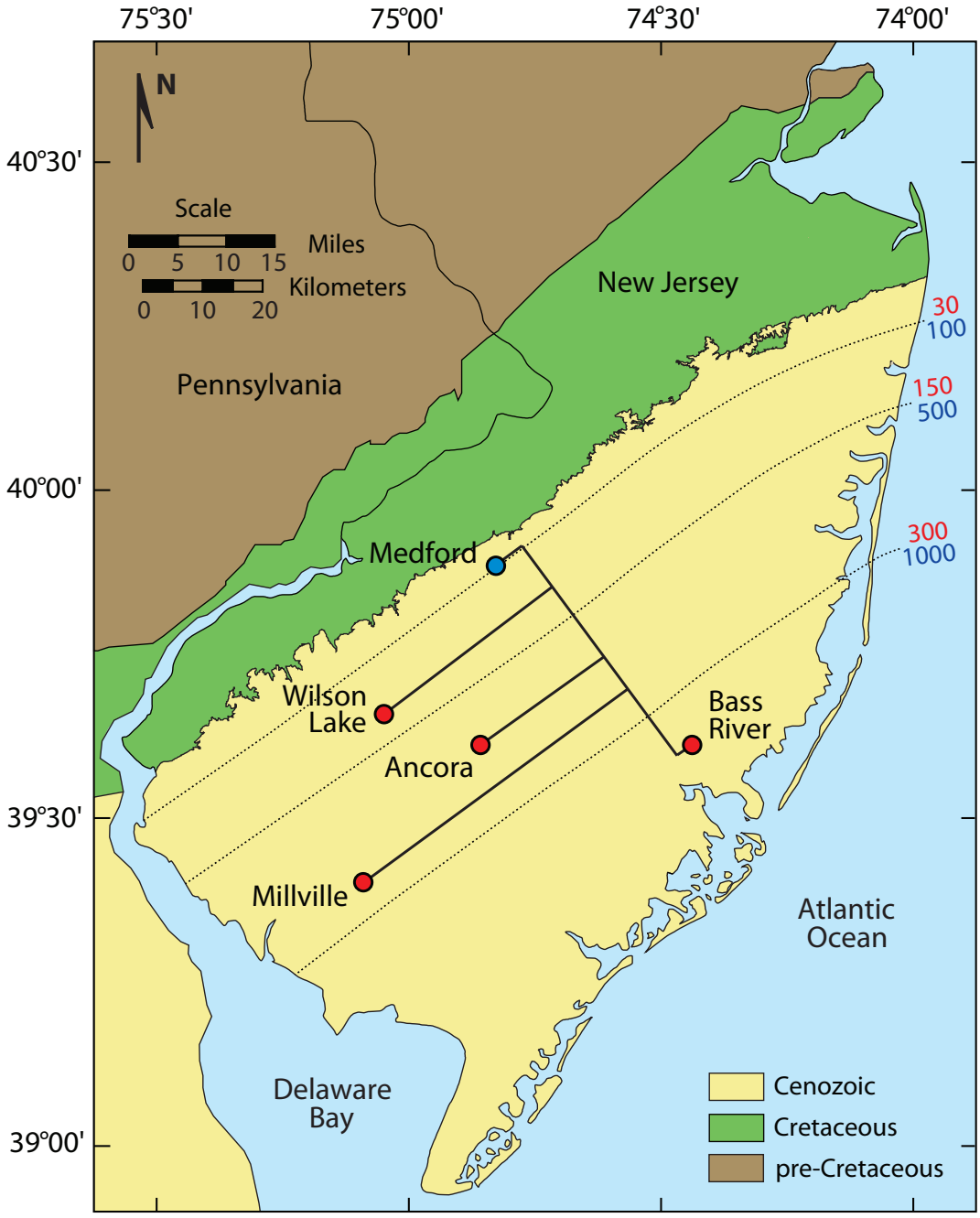

Fig. 2.1. Location map of the PETM sections on the New Jersey coastal plain: Wilson Lake, Ancora, Millville, and Bass River. Red circles indicate the New Jersey coreholes and blue circle shows an anchor point at Medford, NJ used for paleodepth reconstructions during Vincentown deposition. Black solid lines represent projection of sites onto a dip profile drawn through Medford outcrop and Bass River. Dashed lines indicate structural contours from Zapecza [1984] with depths to the top of the Campanian in meters (red) and feet (blue) (modified after Esmeray-Senlet et al. [2015]).

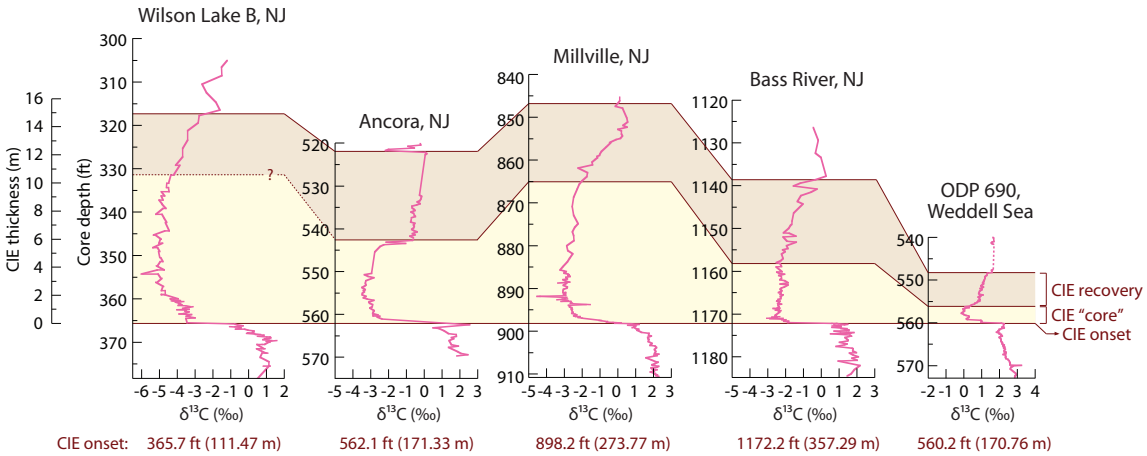

Fig. 2.2. Correlation of bulk carbonate $\delta^{13}C$ records between the New Jersey coastal plain ODP sites Wilson Lake Hole B [Wright and Schaller, 2013], Ancora [this study], Millville [this study], Bass River [Cramer et al., 1999; John et al., 2008] and open ocean ODP Site 690, the Weddell Sea [Bains et al., 1999]. Records are aligned on the CIE onset and correlated at the CIE "core" and recovery sections. Vertical scale is uniform to demonstrate different resolution of the CIE "core" and recovery intervals among the sites.

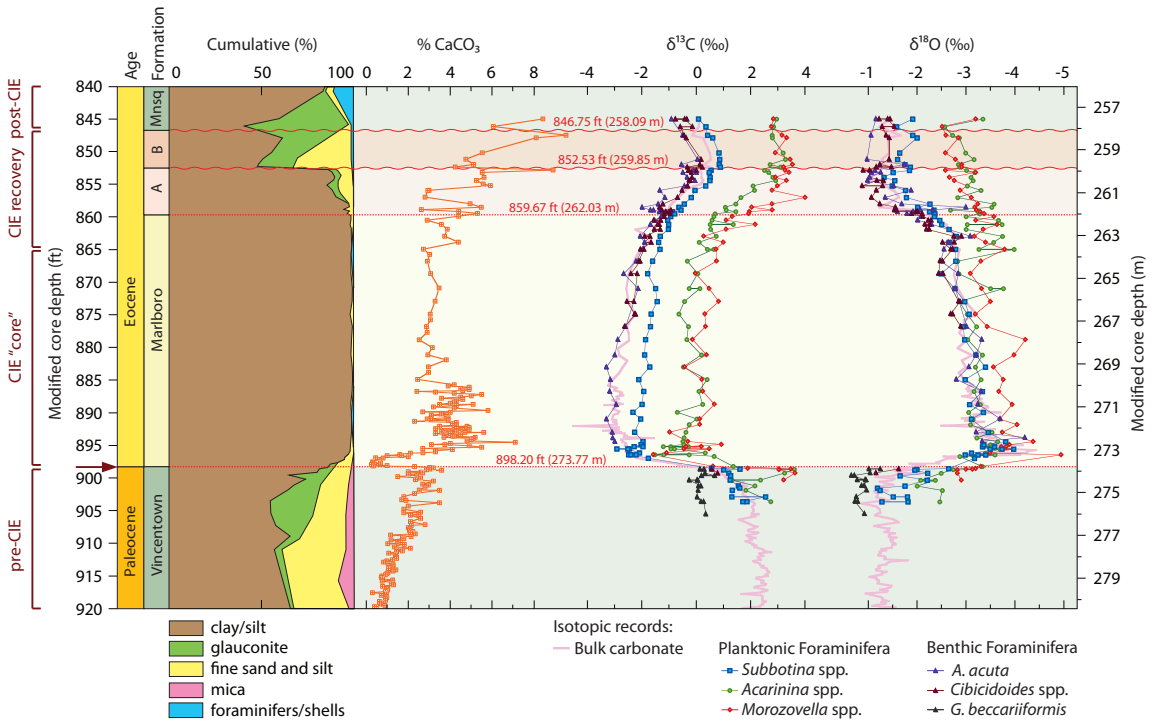

Fig. 2.3. Compilation of records at Millville, NJ: cumulative grain size, % CaCO3, $\delta^{13}C$ and $\delta^{18}O$ (plotted in reverse order) of bulk carbonate, planktonic and benthic foraminifera. Bulk carbonate data are from this study and Wright and Schaller [2013]. Thermocline dwellers *Subbotina* spp. are in blue, surface dwellers *Morozovella* spp. and *Acarinina* spp. are in red and green, respectively. For benthic foraminifera, *Gavelinella beccariiformis* in black, *Anomalinoides acuta* in purple, and *Cibicidoides* spp. in brown. Wavy red lines represent sharp unconformable contacts and dashed red lines indicate gradational contacts between the formations. Arrow indicates the CIE onset. Depths are modified, corrected for core expansion. Both corrected and modified core depths are given in Table 2.S1. Mnsq – Manasquan Formation.

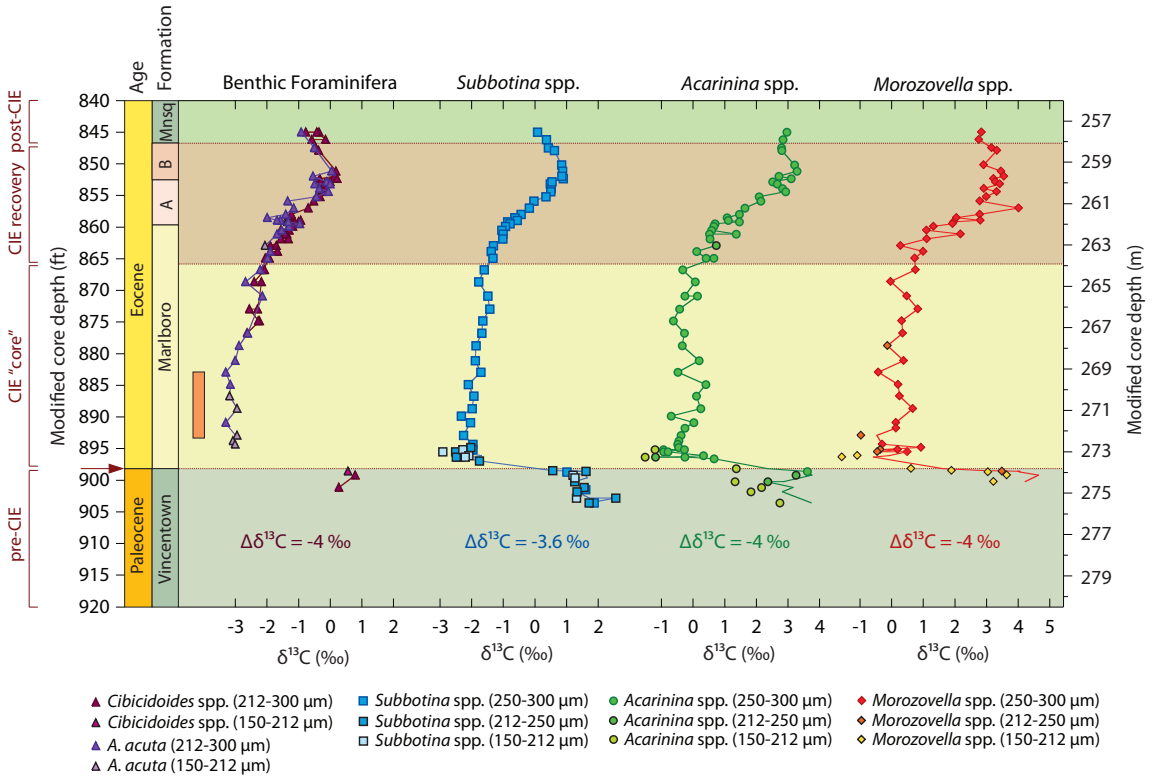

Fig. 2.4. Monogeneric stable carbon isotopes records of foraminifera at Millville. Samples from smaller size fractions (150-212 and 212-250 µm) are outlined in black, solid lines represent corrected for the test size $\delta^{13}C$ values. The orange vertical bar indicates a stable interval of the CIE "core" from which the average CIE "core" $\delta^{13}C$ value was estimated.

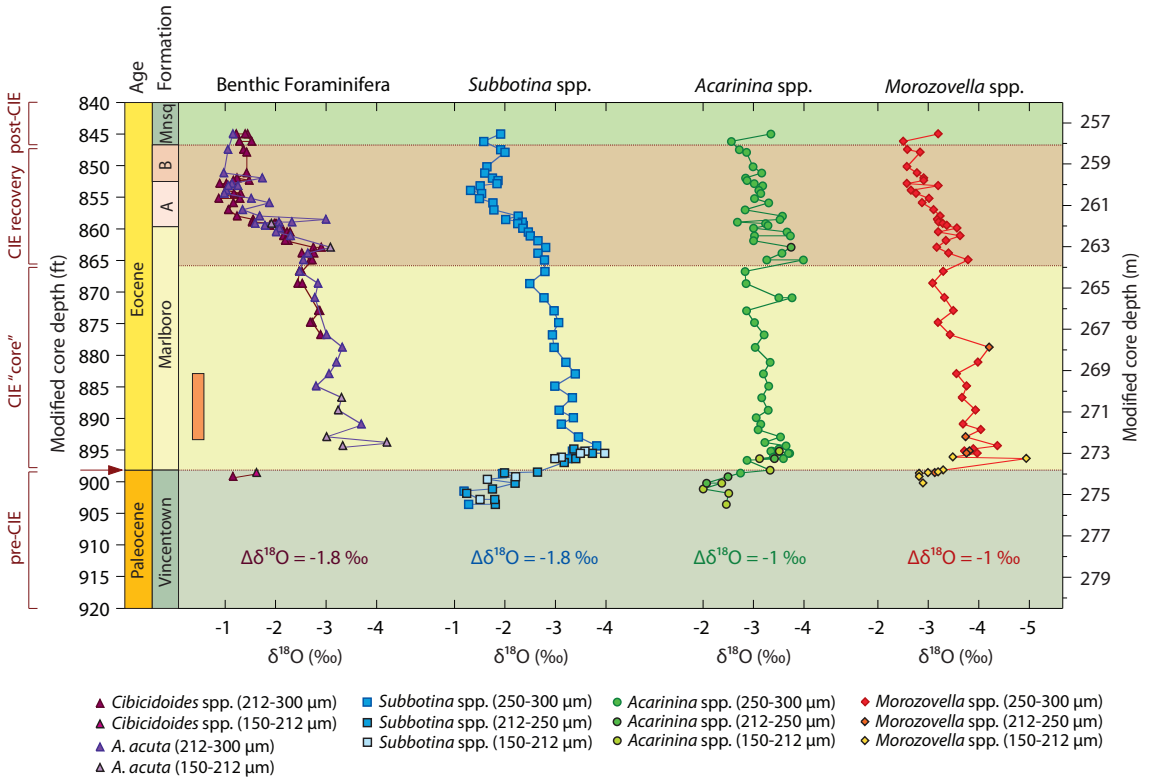

Fig. 2.5. Monogeneric stable oxygen isotopes records of foraminifera at Millville. Samples from smaller size fractions (150-212 and 212-250 µm) are outlined in black. The orange vertical bar indicates a stable interval of the CIE "core" from which the average CIE "core" $\delta^{18}O$ value was estimated.

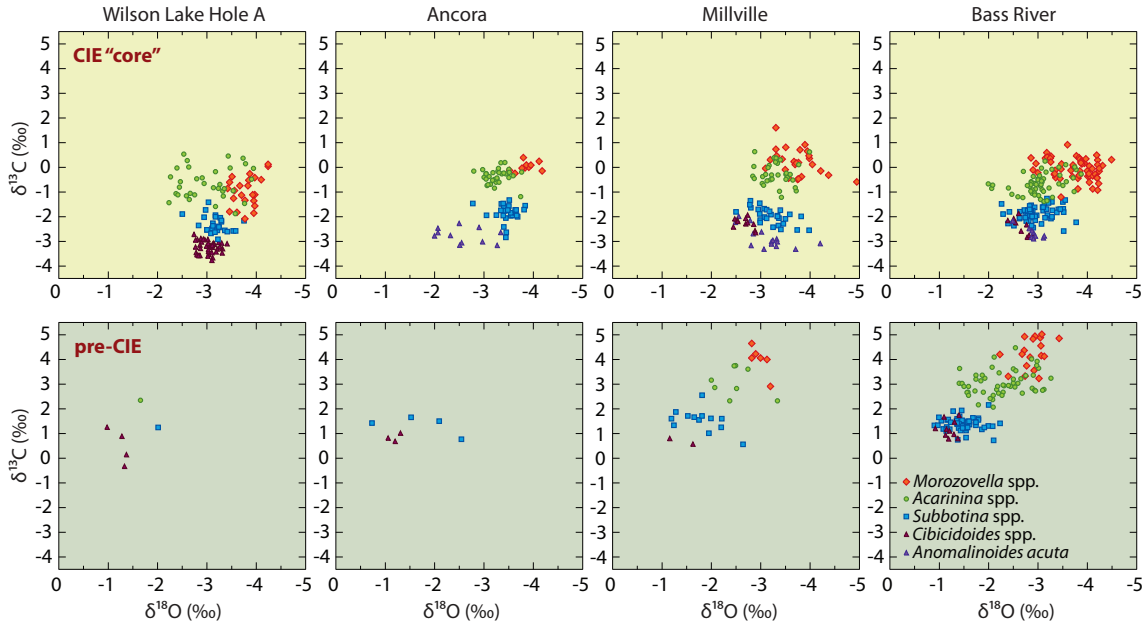

Fig. 2.6. Planktonic and benthic foraminifera cross plots of $\delta^{18}O$ versus $\delta^{13}C$ generated for the New Jersey coastal plain ODP sites Wilson Lake Hole A [Zachos et al., 2006], Ancora [Cramer and Kent, 2005; Babila, 2014], Millville [this study], and Bass River [Cramer et al., 1999; Zachos et al., 2007; John et al., 2008; Babila et al., 2016]. Bottom panels show surface to benthic foraminifera isotopic gradients in the interval below the CIE onset and top panels illustrate those in the CIE "core".

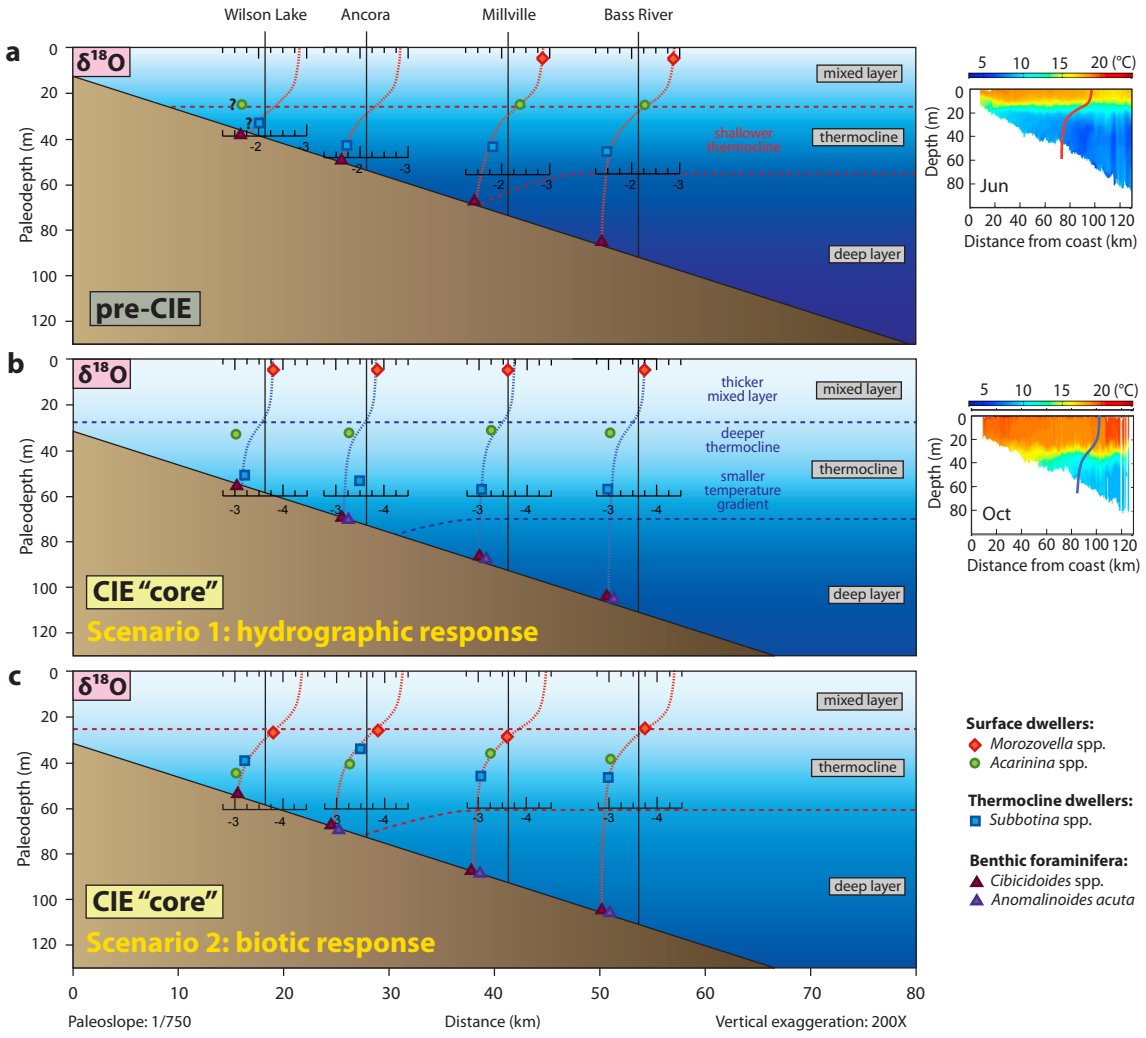

Fig. 2.7. Hydrographic reconstruction of the New Jersey paleoshelf for the periods of pre-CIE (a) and CIE "core" deposition (b, c). Panels b and c illustrate two scenarios explaining different isotopic response in surface versus thermocline dwellers after the CIE onset: b – change in the water column structure; c – change in habitat of the surface dwellers. Red and blue lines represent $\delta^{18}O$ gradients drawn for each site with single genera average $\delta^{18}O$ values plotted on top. Foraminiferal $\delta^{18}O$ data are from: Wilson Lake Hole A [Zachos et al., 2006]; Ancora [Babila, 2014; Cramer and Kent, 2005]; Millville [this study]; and Bass River [Cramer et al., 1999; Zachos et al., 2007; John et al., 2008; Babila et al., 2016]. Paleoslope reconstruction is modified for the PETM after Esmeray-Senlet et al. [2015]. Plots on the right show thermal structure of the water column across the modern New Jersey shelf in June and October [Castelao et al., 2010].

2.11 Tables

Table 2.1. Measured stable isotopic values of planktonic and benthic foraminifera at Millville, NJ. Table includes modified for core expansion depths (mcd) and corrected for test size $\delta^{13}C$ values. Samples from the core expansion are marked in quotes.

Depth interval (ft)		Mean depth (ft)	Mcd (ft)	Mcd (m)	Species	Size (μm)	#	$\delta^{13}C$ PDB (‰)	$\delta^{13}C$ PDB corr. (‰)	$\delta^{18}O$ PDB (‰)
bottom	top									
844.92	845.02	844.97	844.97	257.55	*M. aequa*	250-300	10	2.84		-3.20
846.10	846.20	846.15	846.15	257.91	*M. aequa*	250-300	9	2.76		-2.51
847.40	847.50	847.45	847.45	258.30	*M. aequa*	250-300	10	3.16		-2.59
847.82	847.90	847.86	847.86	258.43	*M. aequa*	250-300	10	3.33		-2.84
850.10	850.20	850.15	850.15	259.13	*M. aequa*	250-300	8	2.91		-2.58
851.10	851.20	851.15	851.14	259.43	*M. aequa*	250-300	10	3.46		-2.78
851.90	852.00	851.95	851.93	259.67	*M. aequa*	250-300	10	3.55		-2.91
852.30	852.40	852.35	852.33	259.79	*M. aequa*	250-300	10	3.22		-2.91
852.80	852.90	852.85	852.82	259.94	*M. aequa*	250-300	10	3.27		-2.58
853.14	853.26	853.20	853.17	260.05	*M. aequa*	250-300	10	3.42		-3.20
853.90	853.96	853.93	853.89	260.27	*M. aequa*	250-300	10	2.92		-2.66
854.38	854.48	854.43	854.39	260.42	*M. aequa*	250-300	10	3.32		-2.76
855.20	855.30	855.25	855.20	260.66	*M. aequa*	250-300	10	2.99		-3.02
855.90	856.00	855.95	855.89	260.88	*M. aequa*	250-300	10	2.79		-2.88
857.00	857.10	857.05	856.98	261.21	*M. aequa*	> 250	5	4.01		-3.11
858.00	858.10	858.05	857.97	261.51	*M. aequa*	> 250	6	2.79		-3.24
858.56	858.61	858.59	858.50	261.67	*M. aequa*	> 250	6	2.05		-3.18
858.92	859.07	859.00	858.91	261.79	*M. aequa*	> 250	5	2.80		-3.21
859.21	859.27	859.24	859.15	261.87	*M. aequa*	> 250	6	1.96		-3.29
859.53	859.58	859.56	859.46	261.96	*M. aequa*	> 250	6	1.93		-3.37
859.95	860.00	859.98	859.88	262.09	*M. aequa*	> 250	6	1.33		-3.57
860.47	860.55	860.51	860.49	262.28	*M. aequa*	> 250	6	1.10		-3.20
861.10	861.20	861.15	861.10	262.46	*M. aequa*	> 250	5	2.18		-3.63
861.90	862.00	861.95	861.86	262.69	*M. aequa*	> 250	6	1.11		-3.35
863.00	863.15	863.08	862.93	263.02	*M. aequa*	225-275	5	0.28		-3.17
864.00	864.10	864.05	863.86	263.30	*M. aequa*	> 250	6	1.00		-3.40
865.10	865.18	865.14	864.90	263.62	*M. aequa*	> 250	5	0.73		-3.79
867.00	867.15	867.08	866.74	264.18	*M. aequa*	> 250	4	0.75		-3.30
869.00	869.10	869.05	868.62	264.76	*M. aequa, 1 subbotinae*	> 250	7	-0.03		-3.09
870.88	871.00	870.94	870.90	265.45	*M. aequa*	> 250	5	0.48		-3.32
873.02	873.13	873.08	872.94	266.07	*M. aequa*	> 250	6	0.83		-3.50

875.00	875.10	875.05	874.83	266.65	*M. aequa*	225	7	0.32		-3.19
876.95	877.16	877.06	876.75	267.23	*M. aequa*	> 250	5	0.35		-3.43
879.07	879.20	879.14	878.74	267.84	*M. acuta*	200-225	7	-0.13		-4.21
881.10	881.20	881.15	881.09	268.56	*M. acuta*	250	6	0.38		-3.98
883.05	883.16	883.11	882.94	269.12	*M. acuta/velascoensis*	200-300	7	-0.42		-3.56
885.06	885.17	885.12	884.85	269.70	*M. acuta*	250-300	6	0.21		-3.76
886.99	887.10	887.05	886.68	270.26	*M. acuta*	250-300	7	0.25		-3.67
889.08	889.20	889.14	888.66	270.86	*M. acuta*	250-300	8	0.67		-3.94
890.90	891.02	890.96	890.90	271.55	*M. acuta*	250-300	8	0.13		-3.69
891.83	891.95	891.89	891.77	271.81	*M. acuta*	250-300	7	0.13		-4.04
893.04	893.16	893.10	892.91	272.16	*M. acuta*	200	8	-0.97	-0.47	-3.74
894.60	894.65	894.63	894.34	272.60	*M. acuta*	250-300	8	-0.30		-4.37
895.09	895.19	895.14	894.83	272.74	*M. acuta*	> 250	9	0.93		-3.89
895.46	895.50	895.48	895.15	272.84	*M. acuta*	210-250	8	-0.36		-3.82
895.46	895.50	895.48	895.15	272.84	*M. acuta*	250-300	7	0.19		-3.72
895.84	895.89	895.87	895.51	272.95	*M. acuta*	210-250	14	-0.45		-3.76
895.84	895.89	895.87	895.51	272.95	*M. acuta*	250-300	8	0.49		-3.97
896.44	896.54	896.49	896.09	273.13	*M. acuta*	150-175	10	-1.08	-0.08	-3.49
896.75	896.80	896.78	896.36	273.21	*M. acuta*	150-210	9	-1.57	-0.57	-4.94
898.64	898.74	898.69	898.16	273.76	*M. aequa*	175-200	4	0.62	1.62	-3.30
898.94	899.09	899.02	898.46	273.85	*M. acuta*	150-175	6	1.90	2.90	-3.20
899.05	899.20	899.13	898.57	273.88	*M. aequa*	5x150, 1x225	6	3.05	4.05	-3.00
899.05	899.20	899.13	898.57	273.88	*M. acuta*	200	6	3.49	3.99	-3.13
899.20	899.31	899.26	898.69	273.92	*M. aequa*	150-175	3	3.05	4.05	-2.82
899.73	899.82	899.78	899.18	274.07	*M. aequa*	150-200	4	3.64	4.64	-2.82
900.18	900.30	900.24	900.23	274.39	*M. aequa*	6x175, 1x225	7	3.22	4.22	-2.90
844.92	845.02	844.97	844.97	257.55	*A. soldadoensis*	250-300	10	2.96		-3.34
846.10	846.20	846.15	846.15	257.91	*A. soldadoensis*	250-300	10	2.84		-2.56
847.40	847.50	847.45	847.45	258.30	*A. soldadoensis*	250-300	10	2.79		-2.72
847.82	847.90	847.86	847.86	258.43	*A. soldadoensis*	250-300	10	2.80		-2.86
850.10	850.20	850.15	850.15	259.13	*A. soldadoensis*	250-300	10	3.20		-2.99
851.10	851.20	851.15	851.14	259.43	*A. soldadoensis*	250-300	10	3.28		-3.16
851.90	852.00	851.95	851.93	259.67	*A. soldadoensis*	250-300	8	2.71		-2.84
852.30	852.40	852.35	852.33	259.79	*A. soldadoensis*	250-300	10	3.10		-2.87
852.80	852.90	852.85	852.82	259.94	*A. soldadoensis*	250-300	10	2.51		-3.01
853.14	853.26	853.20	853.17	260.05	*A. soldadoensis*	250-300	10	2.66		-3.18
853.90	853.96	853.93	853.89	260.27	*A. soldadoensis*	250-300	10	2.82		-3.10
854.38	854.48	854.43	854.39	260.42	*A. soldadoensis*	250-300	10	2.92		-3.14
855.20	855.30	855.25	855.20	260.66	*A. soldadoensis*	250-300	10	2.09		-3.02
855.90	856.00	855.95	855.89	260.88	*A. soldadoensis*	250-300	10	2.14		-3.30

857.00	857.10	857.05	856.98	261.21	*A. esnehensis*	>250	6	1.64		-2.83
858.00	858.10	858.05	857.97	261.51	*A. soldadoensis*	>250	10	1.46		-3.57
858.56	858.61	858.59	858.50	261.67	*A. soldadoensis*	>250	7	1.07		-3.52
858.92	859.07	859.00	858.91	261.79	*A. esnehensis*	>250	7	1.11		-2.68
859.21	859.27	859.24	859.15	261.87	*A. soldadoensis*	>250	8	1.46		-3.24
859.53	859.58	859.56	859.46	261.96	*A. soldadoensis*	>250	8	0.69		-3.28
859.95	860.00	859.98	859.88	262.09	*A. soldadoensis*	>250	8	0.65		-3.00
860.47	860.55	860.51	860.49	262.28	*A. soldadoensis*	>250	8	0.58		-3.66
861.10	861.20	861.15	861.10	262.46	*A. esnehensis*	>250	6	1.36		-3.73
861.10	861.20	861.15	861.10	262.46	*A. soldadoensis/angulosa*	>250	6	0.51		-3.02
861.90	862.00	861.95	861.86	262.69	*A. soldadoensis*	>250	7	0.53		-3.00
863.00	863.10	863.05	862.90	263.01	*A. esnehensis*	200-250	7	0.73		-3.74
864.00	864.10	864.05	863.86	263.30	*A. soldadoensis*	>250	7	0.11		-3.56
865.10	865.18	865.14	864.90	263.62	*A. esnehensis*	>250	7	0.41		-3.26
865.10	865.18	865.14	864.90	263.62	*A. soldadoensis/angulosa /esnehensis/coalingens is*	>250	5	0.65		-3.98
867.00	867.15	867.08	866.74	264.18	*A. esnehensis*	>250	7	-0.33		-2.83
869.00	869.15	869.08	868.64	264.76	*A. esnehensis*	>250	6	0.06		-2.85
870.88	871.00	870.94	870.90	265.45	*A. esnehensis*	>250	3	-0.26		-3.50
870.88	871.00	870.94	870.90	265.46	*A. coalingensis/esnehensi s*	>250	6	0.13		-3.76
873.02	873.13	873.08	872.94	266.11	*A. esnehensis*	>250	7	-0.43		-2.86
875.00	875.10	875.05	874.83	266.72	*A. esnehensis*	>250	5	-0.63		-3.02
876.95	877.16	877.06	876.75	267.33	*A. esnehensis*	>250	6	-0.28		-3.21
879.07	879.20	879.14	878.74	267.96	*A. esnehensis*	>250	6	-0.35		-3.03
881.10	881.20	881.15	881.09	268.57	*A. soldadoensis*	>250	5	0.19		-3.33
883.05	883.16	883.11	882.94	269.17	*A. soldadoensis*	>250	5	-0.48		-3.19
885.06	885.17	885.12	884.85	269.78	*A. soldadoensis*	>250	5	0.40		-3.30
886.99	887.10	887.05	886.68	270.37	*A. soldadoensis*	>250	5	0.10		-3.16
889.08	889.20	889.14	888.66	271.01	*A. soldadoensis*	>250	5	0.24		-3.29
"890.3 5"	"890.4 5"	890.40	889.86	271.23	*A. soldadoensis*	250-300	10	-0.70		-3.05
890.90	891.02	890.96	890.90	271.56	*A. soldadoensis*	>250	5	0.02		-3.14
891.83	891.95	891.89	891.77	271.81	*A. soldadoensis*	250-300	10	-0.26		-3.09
893.04	893.16	893.10	892.91	272.22	*A. soldadoensis*	>250	5	-0.38		-3.53
894.00	894.06	894.03	893.78	272.43	*A. soldadoensis*	250-300	9	-0.45		-3.22
894.60	894.65	894.63	894.34	272.60	*A. soldadoensis*	250-300	9	-0.49		-3.64
895.09	895.19	895.14	894.83	272.74	*A. soldadoensis*	225-275	6	-0.46		-3.50
895.46	895.50	895.48	895.15	272.84	*A. soldadoensis*	150-210	16	-1.21	-0.21	-3.51
895.46	895.50	895.48	895.15	272.84	*A. soldadoensis*	210-250	9	-0.94		-3.37
895.46	895.50	895.48	895.15	272.84	*A. soldadoensis*	250-300	6	-0.28		-3.34

895.84	895.89	895.87	895.51	272.95	*A. soldadoensis*	210-250	7	-0.93		-3.71
895.84	895.89	895.87	895.51	272.95	*A. soldadoensis (esnehensis?)*	250-300	6	-0.80		-3.69
896.44	896.54	896.49	896.09	273.25	*A. esnehensis*	>250	7	0.33		-3.39
896.75	896.80	896.78	896.36	273.21	*A. soldadoensis*	150-210	9	-1.52	-0.52	-3.12
896.75	896.80	896.78	896.36	273.21	*A. soldadoensis*	210-250	12 ?	-1.19		-3.41
896.75	896.80	896.78	896.36	273.21	*A. soldadoensis*	250-300	4	-0.26		-3.59
896.98	897.11	897.05	896.62	273.42	*A. soldadoensis*	>250	3	0.66		-2.87
898.64	898.74	898.69	898.16	273.76	*A. primitiva/soldadoensis*	175	2	1.36	2.36	-3.33
899.05	899.31	899.18	898.62	274.07	*A. soldadoensis*	>250	4	3.61		-2.74
899.73	899.82	899.78	899.18	274.07	*A. coalingensis*	200-225	3	3.25	3.75	-2.49
900.18	900.30	900.24	900.23	274.39	*A. coalingensis*	200	5	2.36	2.86	-2.07
900.18	900.30	900.24	900.23	274.39	*A. coalingensis*	150	4	1.32	2.32	-2.37
901.12	901.3	901.21	901.15	274.67	*A. coalingensis, soldadoensis*	150	7	2.16	3.16	-2.00
901.87	902.00	901.94	901.84	274.88	*A. coalingensis, soldadoensis*	150	4	1.82	2.82	-2.51
903.67	903.80	903.74	903.56	275.40	*A. coalingensis, soldadoensis*	3x150, 1x200	4	2.74	3.74	-2.46
844.92	845.02	844.97	844.97	257.55	*S. roesnaesensis*	250-300	10	0.08		-1.91
846.10	846.20	846.15	846.15	257.91	*S. roesnaesensis*	250-300	10	0.36		-1.58
847.40	847.50	847.45	847.45	258.30	*S. roesnaesensis*	250-300	10	0.42		-1.91
847.82	847.90	847.86	847.86	258.43	*S. roesnaesensis*	250-300	10	0.61		-2.00
850.10	850.20	850.15	850.15	259.13	*S. roesnaesensis*	250-300	10	0.84		-1.64
851.10	851.20	851.15	851.14	259.43	*S. roesnaesensis*	250-300	10	0.87		-1.60
851.90	852.00	851.95	851.93	259.67	*S. roesnaesensis*	250-300	9	0.85		-1.75
852.30	852.40	852.35	852.33	259.79	*S. roesnaesensis*	250-300	10	0.89		-1.86
852.80	852.90	852.85	852.82	259.94	*S. roesnaesensis*	250-300	10	0.54		-1.84
853.14	853.26	853.20	853.17	260.05	*S. roesnaesensis*	250-300	10	0.48		-1.51
853.90	853.96	853.93	853.89	260.27	*S. roesnaesensis*	250-300	10	0.51		-1.32
854.38	854.48	854.43	854.39	260.42	*S. roesnaesensis*	250-300	10	0.50		-1.54
855.20	855.30	855.25	855.20	260.66	*S. roesnaesensis*	250-300	10	0.35		-1.49
855.90	856.00	855.95	855.89	260.88	*S. roesnaesensis*	250-300	10	-0.04		-1.76
857.00	857.10	857.05	856.98	261.21	*S. roesnaesensis*	>250	10	-0.18		-1.78
858.00	858.10	858.05	857.97	261.51	*S. roesnaesensis*	>250	10	-0.44		-2.26
858.56	858.61	858.59	858.50	261.67	*S. roesnaesensis*	>250	10	-0.64		-2.01
858.92	859.07	859.00	858.91	261.79	*S. roesnaesensis*	>250	10	-0.56		-2.34
859.21	859.27	859.24	859.15	261.87	*S. roesnaesensis*	>250	10	-0.87		-2.25
859.53	859.58	859.56	859.46	261.96	*S. roesnaesensis*	>250	10	-0.79		-2.36
859.95	860.00	859.98	859.88	262.09	*S. roesnaesensis*	>250	10	-0.94		-2.35
860.47	860.55	860.51	860.49	262.28	*S. roesnaesensis*	>250	10	-1.05		-2.46
861.10	861.20	861.15	861.10	262.46	*S. roesnaesensis*	>250	10	-1.01		-2.50
861.90	862.00	861.95	861.86	262.69	*S. roesnaesensis*	>250	10	-1.02		-2.65

863.00	863.15	863.08	862.93	263.02	*S. roesnaesensis*	>250	10	-1.32		-2.80
864.00	864.10	864.05	863.86	263.30	*S. roesnaesensis*	>250	10	-1.38		-2.65
865.10	865.18	865.14	864.90	263.62	*S. roesnaesensis*	>250	10	-1.33		-2.78
867.00	867.15	867.08	866.74	264.18	*S. roesnaesensis*	>250	10	-1.61		-2.79
869.00	869.15	869.08	868.64	264.76	*S. roesnaesensis*	>250	10	-1.78		-2.49
870.88	871.00	870.94	870.90	265.45	*S. roesnaesensis*	>250	10	-1.49		-2.77
873.02	873.13	873.08	872.94	266.07	*S. roesnaesensis*	>250	10	-1.43		-2.97
875.00	875.10	875.05	874.83	266.65	*S. roesnaesensis*	>250	8	-1.65		-3.06
876.95	877.16	877.06	876.75	267.23	*S. roesnaesensis*	>250	10	-1.68		-2.94
879.07	879.20	879.14	878.74	267.84	*S. roesnaesensis*	>250	10	-1.86		-2.97
881.10	881.20	881.15	881.09	268.56	*S. roesnaesensis*	>250	10	-1.89		-3.20
883.05	883.16	883.11	882.94	269.12	*S. roesnaesensis*	>250	10	-1.71		-3.39
885.06	885.17	885.12	884.85	269.70	*S. roesnaesensis*	>250	10	-2.11		-2.98
886.99	887.10	887.05	886.68	270.26	*S. roesnaesensis*	>250	10	-1.93		-3.33
889.08	889.20	889.14	888.66	270.86	*S. roesnaesensis*	>250	10	-1.99		-3.07
"890.35"	"890.45"	890.40	889.86	271.23	*S. roesnaesensis*	250-300	10	-2.33		-3.35
890.90	891.02	890.96	890.90	271.55	*S. roesnaesensis*	>250	10	-2.04		-3.11
893.04	893.16	893.10	892.91	272.16	*S. triangularis*	250	7	-2.26		-3.45
894.60	894.65	894.63	894.34	272.60	*S. roesnaesensis*	250-300	8	-1.96		-3.81
895.09	895.19	895.14	894.83	272.74	*S. roesnaesensis*	200-225	7	-2.03		-3.36
895.46	895.50	895.48	895.15	272.84	*S. roesnaesensis*	150-210	13	-2.28	-1.88	-3.58
895.46	895.50	895.48	895.15	272.84	*S. roesnaesensis*	210-250	11	-1.96		-3.33
895.84	895.89	895.87	895.51	272.95	*S. spp.*	150-210	12	-2.46	-2.06	-3.49
895.84	895.89	895.87	895.51	272.95	*S. spp.*	150-210	13	-2.92	-2.52	-3.97
895.84	895.89	895.87	895.51	272.95	*S. roesnaesensis*	210-250	8	-2.51		-3.73
896.44	896.54	896.49	896.09	273.13	*S. roesnaesensis, 2 hornibrooki*	150-175	10	-2.09	-1.69	-3.11
896.75	896.80	896.78	896.36	273.21	*S. spp.*	150-210	12	-2.21		-2.98
896.75	896.80	896.78	896.36	273.21	*S. spp.*	210-150	12	-2.49		-3.40
896.75	896.80	896.78	896.36	273.21	*S. spp.*	250-300	3	-2.40		-3.24
897.31	897.43	897.37	896.92	273.38	*S. roesnaesensis*	200	2	-1.76		-3.17
898.94	899.09	899.02	898.46	273.85	*S. roesnaesensis, velascoensis, triangularis*	200	4	0.56		-2.64
899.05	899.20	899.13	898.57	273.88	*S. velascoensis*	225	6	1.61		-1.99
899.20	899.31	899.26	898.69	273.92	*S. roesnaesensis*	>250	5	1.01		-1.95
899.73	899.82	899.78	899.18	274.07	*S. velascoensis*	150	6	1.20	1.60	-2.21
"900.16	900.29"	900.23	899.60	274.20	*S. velascoensis*	150-200	5	1.26	1.66	-1.65
900.18	900.3	900.24	900.23	274.39	*S. velascoensis*	200-225	6	1.25		-2.20
901.12	901.3	901.21	901.15	274.67	*S. velascoensis*	200	6	1.55		-1.75
901.12	902.00	901.56	901.49	274.77	*S. roesnaesensis*	250	4	1.60		-1.19
901.87	902.00	901.94	901.84	274.88	*S. velascoensis*	200	6	1.33		-1.24

902.90	903.01	902.96	902.81	275.18	*S. spp.*	150-210	8	1.31	1.71	-1.51
902.90	903.01	902.96	902.81	275.18	*S. spp.*	210-250	2	2.55		-1.80
903.67	903.80	903.74	903.56	275.40	*S. velascoensis*	200	5	1.71		-1.81
903.67	903.80	903.74	903.56	275.40	*S. triangularis*	>250	3	1.87		-1.28
899.05	899.20	899.13	898.57	273.88	*G. beccariiformis parvula*	212-250	4	0.13		-1.25
899.05	899.20	899.13	898.57	273.88	*G. beccariiformis parvula*	150-212	11	0.29		-1.02
899.73	899.82	899.78	899.18	274.07	*G. beccariiformis parvula*	150-212	10	0.32		-1.04
900.16	900.29 "	900.23	899.60	274.20	*G. beccariiformis beccariiformis*	250-300	3	0.68		-0.72
900.16	900.29 "	900.23	899.60	274.20	*G. beccariiformis parvula*	150-212	7	0.20		-0.66
900.18	900.3	900.24	900.23	274.39	*G. beccariiformis, 2 parvula, 3 beccariiformis*	250-300	5	0.03		-0.94
900.18	900.3	900.24	900.23	274.39	*G. beccariiformis 2 parvula, 1 beccariiformis*	212-250	3	0.06		-0.78
900.18	900.3	900.24	900.23	274.39	*G. beccariiformis parvula*	150-212	10	-0.26		-0.96
901.12	901.3	901.21	901.15	274.67	*G. beccariiformis parvula*	212-250	2	0.17		-0.92
901.12	901.3	901.21	901.15	274.67	*G. beccariiformis parvula*	150-212	10	0.08		-0.87
901.87	902.00	901.94	901.84	274.88	*G. beccariiformis parvula*	150-212	10	0.07		-0.97
902.90	903.10	903.00	902.86	275.19	*G. beccariiformis parvula*	150-212	7	0.03		-0.76
903.67	903.80	903.74	903.56	275.40	*G. beccariiformis parvula*	212-250	2	0.18		-0.79
903.67	903.80	903.74	903.56	275.40	*G. beccariiformis parvula*	150-212	8	0.27		-0.73
905.66	905.74	905.70	905.43	275.97	*G. beccariiformis parvula*	150-212	4	0.35		-0.93
844.92	845.02	844.97	844.97	257.55	*A. acuta*	212-250	5	-0.91		-1.16
847.40	847.50	847.45	847.45	258.30	*A. acuta*	250-300	3	-0.50		-1.06
851.10	851.20	851.15	851.14	259.43	*A. acuta*	212-250	4	0.05		-0.98
851.90	852.00	851.95	851.93	259.67	*A. acuta*	250-300	4	-0.54		-1.74
852.80	852.90	852.85	852.82	259.94	*A. acuta*	250-300	3	-0.10		-1.14
853.14	853.26	853.20	853.17	260.05	*A. acuta*	250-300	3	0.00		-1.07
853.14	853.26	853.20	853.17	260.05	*A. acuta*	250-300	3	-0.49		-1.26
853.90	853.96	853.93	853.89	260.27	*A. acuta*	212-250	5	-0.34		-1.03
854.38	854.48	854.43	854.39	260.42	*A. acuta*	250-300	5	-0.05		-0.99
855.20	855.30	855.25	855.20	260.66	*A. acuta*	250-300	5	-0.43		-1.52
855.90	856.00	855.95	855.89	260.88	*A. acuta*	212-250	5	-1.34		-1.88
857.00	857.10	857.05	856.98	261.21	*A. acuta*	250-300	5	-1.15		-1.35
858.00	858.10	858.05	857.97	261.51	*A. acuta*	250-300	6	-1.40		-1.69
858.56	858.61	858.59	858.50	261.67	*A. acuta*	212-250	6	-1.99		-3.00
858.92	859.07	859.00	858.91	261.79	*A. acuta*	250-300	4	-1.68		-2.33
858.92	859.07	859.00	858.91	261.79	*A. acuta*	212-250	10	-1.57		-2.07
859.21	859.27	859.24	859.15	261.87	*A. acuta*	250-300	4	-1.32		-1.60
859.21	859.27	859.24	859.15	261.87	*A. acuta*	150-212	10	-1.36		-1.92

859.53	859.58	859.56	859.46	261.96	*A. acuta*	250-300	3	-0.96	-1.79
859.95	860.00	859.98	859.88	262.09	*A. acuta*	212-250	3	-1.29	-2.08
860.47	860.55	860.51	860.49	262.28	*A. acuta*	250-300	3	-1.53	-2.01
861.10	861.20	861.15	861.10	262.46	*A. acuta*	212-250	10	-1.68	-2.30
863.00	863.15	863.08	862.93	263.02	*A. acuta*	150-212	16	-2.06	-3.09
864.00	864.10	864.05	863.86	263.30	*A. acuta*	212-250	6	-1.89	-2.64
865.10	865.18	865.14	864.90	263.62	*A. acuta*	212-250	6	-1.97	-2.55
867.00	867.15	867.08	866.74	264.18	*A. acuta*	212-250	5	-2.21	-2.48
869.00	869.15	869.08	868.64	264.76	*A. acuta*	212-250	6	-2.67	-2.84
870.88	871.00	870.94	870.90	265.45	*A. acuta*	212-250	3	-2.14	-2.78
876.95	877.16	877.06	876.75	267.23	*A. acuta*	212-250	8	-2.60	-3.01
879.07	879.20	879.14	878.74	267.84	*A. acuta*	212-250	8	-2.88	-3.32
881.10	881.20	881.15	881.09	268.56	*A. acuta*	212-250	10	-3.00	-3.21
883.05	883.16	883.11	882.94	269.12	*A. acuta*	212-250	3	-3.30	-3.06
885.06	885.17	885.12	884.85	269.70	*A. acuta*	212-250	8	-3.15	-2.80
886.99	887.10	887.05	886.68	270.26	*A. acuta*	150-212	24	-3.18	-3.31
889.08	889.20	889.14	888.66	270.86	*A. acuta*	150-212	13	-2.94	-3.24
890.90	891.02	890.96	890.90	271.55	*A. acuta*	212-250	6	-3.30	-3.70
890.90	891.02	890.96	890.90	271.55	*A. acuta*	212-250	6	-3.30	-3.70
893.04	893.16	893.10	892.91	272.16	*A. acuta*	150-212	4	-3.09	-3.21
894.00	894.06	894.03	893.78	272.43	*A. acuta*	150-212	11	-3.07	-4.20
894.60	894.65	894.63	894.34	272.60	*A. acuta*	150-212	26	-3.00	-3.33
844.92	845.02	844.97	844.97	257.55	*C. succendens*	250-300	9	-0.35	-1.23
844.92	845.02	844.97	844.97	257.55	*C. alleni*	250-300	8	-0.77	-1.45
844.92	845.02	844.97	844.97	257.55	*C. howelli*	250-300	6	-0.42	-1.40
846.10	846.20	846.15	846.15	257.91	*C. succendens*	250-300	5	-0.14	-1.53
846.10	846.20	846.15	846.15	257.91	*C. alleni*	250-300	10	-0.58	-1.29
847.40	847.50	847.45	847.45	258.30	*C. alleni*	250-300	10	-0.45	-1.37
847.82	847.90	847.86	847.86	258.43	*C. alleni*	250-300	10	-0.37	-1.43
851.10	851.20	851.15	851.14	259.43	*C. howelli*	250-300	6	0.18	-1.43
851.90	852.00	851.95	851.93	259.67	*C. alleni*	250-300	4	0.13	-1.24
852.30	852.40	852.35	852.33	259.79	*C. alleni*	250-300	9	-0.33	-1.48
852.30	852.40	852.35	852.33	259.79	*C. howelli*	250-300	9	0.22	-1.17
852.80	852.90	852.85	852.82	259.94	*C. alleni*	250-300	8	-0.29	-1.03
852.80	852.90	852.85	852.82	259.94	*C. howelli*	250-300	5	0.00	-0.90
853.14	853.26	853.20	853.17	260.05	*C. alleni*	250-300	5	-0.18	-1.06
853.90	853.96	853.93	853.89	260.27	*C. alleni*	250-300	7	-0.15	-1.02
854.38	854.48	854.43	854.39	260.42	*C. alleni*	250-300	4	-0.27	-1.31
854.38	854.48	854.43	854.39	260.42	*C. howelli*	250-300	7	-0.22	-1.18
855.20	855.30	855.25	855.20	260.66	*C. alleni*	250-300	8	-0.31	-0.88

855.20	855.30	855.25	855.20	260.66	*C. howelli*	250-300	10	-0.32	-1.30
855.90	856.00	855.95	855.89	260.88	*C. alleni*	250-300	6	-0.52	-1.17
857.00	857.10	857.05	856.98	261.21	*C. howelli*	250-300	7	-0.69	-1.07
858.00	858.10	858.05	857.97	261.51	*C. alleni*	250-300	9	-1.23	-1.24
858.56	858.61	858.59	858.50	261.67	*C. alleni*	250-300	6	-1.35	-1.56
858.92	859.07	859.00	858.91	261.79	*C. alleni*	250-300	9	-1.26	-1.54
858.92	859.07	859.00	858.91	261.79	*C. howelli*	250-300	3	-0.93	-1.58
859.21	859.27	859.24	859.15	261.87	*C. alleni*	250-300	7	-1.12	-2.01
859.21	859.27	859.24	859.15	261.87	*C. howelli*	250-300	7	-1.00	-1.98
859.53	859.58	859.56	859.46	261.96	*C. alleni*	250-300	8	-1.18	-2.11
859.53	859.58	859.56	859.46	261.96	*C. howelli*	250-300	9	-0.97	-1.89
859.95	860.00	859.98	859.88	262.09	*C. alleni*	250-300	6	-1.31	-2.12
859.95	860.00	859.98	859.88	262.09	*C. howelli*	250-300	6	-1.18	-2.12
860.47	860.55	860.51	860.49	262.28	*C. alleni*	250-300	6	-1.56	-2.29
860.47	860.55	860.51	860.49	262.28	*C. howelli*	250-300	6	-1.30	-2.23
861.10	861.20	861.15	861.10	262.46	*C. alleni*	250-300	8	-1.36	-2.16
861.10	861.20	861.15	861.10	262.46	*C. howelli*	250-300	8	-1.42	-2.26
861.90	862.00	861.95	861.86	262.69	*C. alleni*	250-300	8	-1.55	-2.25
861.90	862.00	861.95	861.86	262.69	*C. howelli*	250-300	8	-1.32	-2.19
863.00	863.15	863.08	862.93	263.02	*C. alleni*	250-300	5	-1.89	-2.75
863.00	863.15	863.08	862.93	263.02	*C. howelli*	250-300	7	-1.70	-2.91
864.00	864.10	864.05	863.86	263.30	*C. alleni*	250-300	8	-1.89	-2.76
864.00	864.10	864.05	863.86	263.30	*C. howelli*	250-300	8	-1.66	-2.52
865.10	865.18	865.14	864.90	263.62	*C. alleni*	250-300	6	-2.05	-2.69
865.10	865.18	865.14	864.90	263.62	*C. howelli*	250-300	8	-1.92	-2.73
867.00	867.15	867.08	866.74	264.18	*C. alleni*	250-300	6	-2.12	-2.52
867.00	867.15	867.08	866.74	264.18	*C. howelli*	250-300	6	-2.07	-2.47
869.00	869.15	869.08	868.64	264.76	*C. alleni*	250-300	5	-2.40	-2.44
869.00	869.15	869.08	868.64	264.76	*C. howelli*	250-300	6	-2.17	-2.53
873.02	873.13	873.08	872.94	266.07	*C. alleni*	250-300	5	-2.29	-2.85
873.02	873.13	873.08	872.94	266.07	*C. alleni*	212-250	7	-2.55	-2.88
875.00	875.10	875.05	874.83	266.65	*C. alleni*	250-300	7	-2.27	-2.69
875.00	875.10	875.05	874.83	266.65	*C. alleni*	212-250	6	-2.23	-2.73
876.95	877.16	877.06	876.75	267.23	*C. alleni*	250-300	6	-2.63	-2.89
899.05	899.20	899.13	898.57	273.88	*C. succendens*	150-212	6	0.56	-1.63
899.73	899.82	899.78	899.18	274.07	*C. succendens*	212-250	6	0.79	-1.16
901.12	901.3	901.21	901.15	274.67	*C. succendens*	212-250	3	0.27	-3.43

2.12 Supporting information

2.12.1 Introduction

Supporting information includes a chapter on geological setting that describes paleowater depth reconstructions in the U.S. mid-Atlantic margin during the Paleocene-Eocene Thermal Maximum (PETM) and gives a lithologic description of the ODP Leg 174AX Millville core. Table 2.S1 shows paleowater depths during Vincentown deposition estimated for four New Jersey coastal pain sites with best estimates assuming the 1:750 paleoslope gradient. Additionally, we review here symbiont loss and carbonate ion effect that can bias foraminiferal isotopic values. Supporting information also provides detailed information on the stable isotopic data of individual species of planktonic foraminifera that were used to compile monogeneric records of *Morozovella*, *Acarinina*, *Subbotina*, *Anomalinoides*, *Cibicidoides*, and *Gavelinella* at Millville (Table 1 and Fig. 2.S1). Table 1 has measured $\delta^{13}C$ and $\delta^{18}O$ values for each sample with true core depth and depth adjusted for core expansion. It also includes information on analyzed foraminifera: species names, number of specimens per sample, and size fraction. Fig. 2.S1 shows $\delta^{13}C$ and $\delta^{18}O$ records with highlighted in black specimens from smaller size fractions (150-212 and 212-250 μm) to which we applied the $\delta^{13}C$ correction for test size. Table 1 includes corrected for test size $\delta^{13}C$ values. Table 2.S2 provides additional carbon isotopic measurements of *Subbotina roesnaesensis* from Wilson Lake Hole B, NJ that were used to determine the vital effect corrections on $\delta^{13}C$ in *Subbotina*. Figs. 2.S2 and 2.S3 show correlation of stable carbon and oxygen isotopic records of *Morozovella*, *Acarinina*, and *Subbotina* between four New Jersey coastal plain cores: Wilson Lake Hole A, Ancora, Millvile, and Bass River (see figure captions for data references). The

correlation was based on the carbon isotope excursion (CIE) stages: pre-CIE, CIE "core", CIE partial recovery, and post-CIE. The order of isotopic records from left to right resembles relative position of coreholes along the New Jersey paleoshelf deepening to the right (Fig. 2.7 in the main text).

2.12.2 Geological Setting

2.12.2.1 New Jersey paleoshelf during the PETM

The New Jersey coastal plain is located in the northern part of the Salisbury Embayment [Gibson et al., 1993] with Paleogene paleolatitudes of ~35-40 °N [Müller et al., 2008]. During the PETM, deposition across the embayment occurred in neritic depths of ~30-100+ m [Harris et al., 2010; Stassen et al., 2015] with a lithology change from micaceous sandy silts of the Vincentown Formation below to kaolinitic clayey silts (mean grain size 8 μm) of the Marlboro Formation above [Gibson et al., 1993; Cramer et al., 1999; Sugarman et al., 2005; Kopp et al., 2009; Lombardi, 2013]. We estimate paleowater depths in the Vincentown Formation on the New Jersey paleoshelf following a similar method used by Esmeray-Senlet et al. [2015]. The New Jersey coastal plain sites were projected using structural contours [Zapecza, 1984] of the top of the Campanian (~72 Ma) onto a dip profile drawn through Medford outcrop and Bass River site (Fig. 2.1 in the main text). Based on estimates from two dimensional backstripping of Steckler et al. [1999] accounting for the effects of compaction, loading, and thermal subsidence, Esmeray-Senlet et al. [2015] noted that the paleoslope gradient could have varied from 1:500 to 1:1000, and used 1:750 as the best estimate. To compute paleowater depths for the Vincentown Formation in the New Jersey coastal plain sites, we use the updip section at Medford, NJ as an anchor point. The Vincentown Formation at Medford contains

sandy silts with wispy cross laminations interpreted as having been deposited in inner neritic, lower shoreface (~25 ± 5 m water depth) environments near storm wave base [Sugarman et al., 2005]. Using possible end-member assumptions of the paleoslope gradient, errors in the anchor point, and site projections to a dip profile (±5 m in the relative placement), the paleowater depth at the deepest and least constrained Bass River site is ~90 ± 20 m for the Vincentown Formation and ~70 ± 20 m at Millville (Table 2.S1). Our water depths are distinctly shallower than recent faunal estimates by Stassen et al. [2015] who inferred ~100-110 m paleowater depths for the Vincentown Formation at Wilson Lake and ~140-150 m at Bass River, even though sedimentary structures and benthic foraminifera [Harris et al., 2010] indicate that the Vincentown Formation was deposited above wave base at the updip sites. Paleowater depths during Marlboro deposition are less certain and appear to be deeper by 20-30 m [Stassen et al., 2015 and references therein] to 60 m [Harris et al., 2010], but the apparent change in water depth is based on application of standard biozonations to the non-analog conditions during the PETM. For this paper, we use ~20 m deeper paleowater depths for the Marlboro Formation than those of the Vincentown Formation.

2.12.2.2 ODP Leg 174AX Millville site: lithologic description

ODP Leg 174AX Millville core recovered the Vincentown, Marlboro, and Manasquan Formations (257.55-280.33 m) that span the Paleocene/Eocene boundary (Fig. 2.3 in the main text). The Vincentown Formation is a micaceous, glauconitic, sandy silt at Millville. The contact between the Vincentown and Marlboro Formations occurs within a 0.6 ft-transition zone with decreasing upwards glauconite and coarse fraction content. Clayey silts (mean grain size 8 μm) of the Marlboro Formation comprise an

expanded CIE "core" (10 m thick) at Millville. The CIE recovery interval (5.5 m thick) captures a lithologic transition from the Marlboro Formation to coarser informal units referred to as A and B here. Unit A is a slightly sandier facies of the Marlboro Formation that has not been sampled at other sites except possibly Ancora. Unit B is sandy silty clay to clayey silt more typical of the underlying Vincentown Formation and originally identified as such [Sugarman et al., 2005]; we assume that unit B marks the end of the CIE recovery based on decreasing trends in $\delta^{13}C$ records of bulk carbonate and planktonic foraminifera observed in the upper part of this unit (Fig. 2.3 in the main text). There is an unconformity between units A and B at 259.85 m, but the contact of unit A with the underlying Marlboro Formation is gradational and appears conformable. The post-CIE section consists of glauconitic, carbonate-rich sandy silts of the Manasquan Formation overlying unit B above an unconformity at 258.09 m.

2.12.3 Symbiont loss and carbonate ion effect in foraminiferal stable isotopes

We review here possible vital effects that can bias their isotopic signal. Symbiont activity decreases ^{12}C concentration inside hosting planktonic foraminifera and causes higher $\delta^{13}C$ values in foraminiferal tests [e.g., D'Hondt and Zachos, 1993; D'Hondt et al., 1994; Norris, 1996]. The loss of symbionts (or bleaching) in symbiont-bearing surface dwelling *Morozovella* and *Acarinina* could have produced a CIE of a larger magnitude than in symbiont barren thermocline dwelling *Subbotina*. The loss of symbionts can be detected by the disappearance of the $\delta^{13}C$-test size gradients in symbiont-bearing species, because foraminifera with larger tests can host more symbionts and thus have higher $\delta^{13}C$ than foraminifera with smaller tests [Wade et al., 2008; Edgar, 2013]. The $\delta^{13}C$-test size gradients in *Morozovella* spp. and *Acarinina* spp. from subtropical Atlantic sections are

maintained during the PETM [e.g., Tripati and Elderfield, 2004; Babila et al., 2016]. This suggests no symbiont loss in *Morozovella* spp. and *Acarinina* spp. precluding bleaching effect on their $\delta^{13}C$ magnitudes. Therefore, the similar decrease in $\delta^{13}C$ observed in all taxa across the CIE onset represents signal unbiased by vital effects.

Laboratory living culture and field experiments supported by results of numerical diffusion-reaction modeling show that an increase in seawater carbonate ion concentration [CO_3^{2-}] lowers both $\delta^{13}C$ and $\delta^{18}O$ values of planktonic foraminiferal calcite [e.g., Spero et al., 1997; Zeebe et al., 1999; Russell and Spero, 2000]. These relationships are usually referred as a carbonate ion effect or pH effect [Spero et al., 1997; Uchikawa and Zeebe, 2010]. Based on B/Ca analyses performed on the New Jersey Bass River core, Babila et al. [2016] estimated a 0.4 ± 0.2 pH units decrease in the mixed layer recorded by *Acarinina* spp. and 0.35 ± 0.15 pH units drop in the thermocline recorded by *Subbotina* spp. across the CIE onset. Use of the $\Delta\delta^{18}O/\Delta pH$ slope from Uchikawa and Zeebe [2010] and a 0.1 pH units offset recorded between *Acarinina* spp. and *Subbotina* spp. from Babila et al. [2016] would account for a minor difference between their $\Delta\delta^{18}O$ across the CIE onset, significantly smaller than the observed difference (Fig. 2.5). Furthermore, laboratory and field experiments on living planktonic foraminifera indicate that the carbonate ion effect is species specific [Spero et al., 1997; Russell and Spero, 2000]. However, assuming an enhanced pH effect in asymbiotic foraminifera, a decrease in alkalinity certainly cannot account for different oxygen isotopic responses. Thus, we exclude bleaching and a change in seawater [CO_3^{2-}] (due to pH) as likely side effects.

2.13.4 References

Babila, T.L. (2014), Boron/calcium in planktonic foraminifera: proxy development and application to the Paleocene-Eocene boundary, Ph.D. Thesis, Rutgers University, 140 p.

Babila, T.L., Y. Rosenthal, J.D. Wright, and K.G. Miller (2016), A continental shelf perspective of ocean acidification and temperature evolution during the Paleocene-Eocene Thermal Maximum, Geology, 44(4), 275–278, doi:10.1130/G37522.1.

Cramer, B.S. and D.V. Kent (2005), Bolide summer: The Paleocene/Eocene thermal maximum as a response to an extraterrestrial trigger, Palaeogeography, Palaeoclimatology, Palaeoecology, 224, 144–166.

Cramer, B.S., M.-P. Aubry, K.G. Miller, R.K. Olsson, J.D. Wright, and D.V. Kent (1999), An exceptional chronologic, isotopic, and clay mineralogic record at the latest Paleocene thermal maximum, Bass River, NJ, ODP 174AX, Bulletin de la Société géologique de France, 170(6), 883–897.

D'Hondt, S. and J.C. Zachos (1993), On stable isotopic variation and earliest Paleocene planktonic foraminifera, Paleoceanography, 8(4), 527–547.

D'Hondt, S., J.C. Zachos, and G. Schultz (1994), Stable isotopic signals and photosymbiosis in late Paleocene planktic foraminifera, Paleobiology, 20, 391–406.

Edgar, K.M., S.M. Bohaty, S.J. Gibbs, P.F. Sexton, R.D. Norris, and P.A. Wilson (2012), Symbiont 'bleaching' in planktic foraminifera during the middle Eocene climatic optimum, Geology, 41(1), 15–18, doi:10.1130/G33388.1.

Esmeray-Senlet, S., J.D. Wright, R.K. Olsson, K.G. Miller, J.V. Browning, and T.M. Quan (2015), Evidence for reduced export productivity following the Cretaceous/Paleogene mass extinction, Paleoceanography, 30, 1–21, doi:10.1002/2014PA002724.

Gibson, T.G., L.M. Bybell, and J.P. Owens (1993), Latest Paleocene lithologic and biotic events in neritic deposits of southwestern New Jersey, Paleoceanography, 8(4), 495–514.

Harris, A.D., K.G. Miller, J.V. Browning, P.J. Sugarman, R.K. Olsson, B.S. Cramer, and J.D. Wright (2010), Integrated stratigraphic studies of Paleocene-lowermost Eocene sequences, New Jersey Coastal Plain: Evidence for glacioeustatic control, Paleoceanography, 25, 1–18, doi:10.1029/2009PA001800.

John, C.M., S.M. Bohaty, J.C. Zachos, A. Sluijs, S. Gibbs, H. Brinkhuis, and T.J. Bralower (2008), North American continental margin records of the Paleocene-Eocene thermal maximum: Implications for global carbon and hydrological cycling, Paleoceanography, 23, 1–20, doi:10.1029/2007PA001465.

Kopp, R.E., D. Schumann, T.D. Raub, D.S. Powars, L.V. Godfrey, N.L. Swanson-Hysell, A.C. Maloof, and H. Vali (2009), An Appalachian Amazon? Magnetofossil evidence for the development of a tropical river-like system in the mid-Atlantic United States during the Paleocene-Eocene thermal maximum, Paleoceanography, 24, 1–17, doi:10.1029/2009PA001783.

Lombardi, C.J. (2013), Lithostratigraphy and clay mineralogy of Paleocene-Eocene thermal maximum sediments at Wilson Lake, NJ, M.S. Thesis, Rutgers University, 94 p.

Müller, R.D., M. Sdrolias, C. Gaina, B. Steinberger, and C. Heine (2008), Long-term sea-level fluctuations driven by ocean basin dynamics, Science, 319, 1357–1362, doi:10.1126/science.1151540.

Norris, R.D. (1996), Symbiosis as an evolutionary innovation in the radiation of Paleocene planktic foraminifera, Paleobiology, 22, 461–480.

Russell, A.D. and H.J. Spero (2000), Field examination of the oceanic carbonate ion effect on stable isotopes in planktonic foraminifera, Paleoceanography, 15(1), 43–52.

Spero, H.J., J. Bijima, D.W. Lea, and B.E. Bemis (1997), Effect of seawater carbonate concentration on foraminiferal carbon and oxygen isotopes, Nature, 390, 497–500, doi:10.1038/37333.

Stassen, P., E. Thomas, and R.P. Speijer (2012), Integrated stratigraphy of the Paleocene-Eocene thermal maximum in the New Jersey Coastal Plain: Toward understanding the effects of global warming in a shelf environment, Paleoceanography, 27, 1–17, doi:10.1029/2012PA002323.

Stassen, P., E. Thomas, and R.P. Speijer (2015), Paleocene–Eocene Thermal Maximum environmental change in the New Jersey Coastal Plain: benthic foraminiferal biotic events, Marine Micropaleontology, 115, 1–23, doi:10.1016/j.marmicro.2014.12.001.

Steckler, M.S., G.S. Mountain, K.G. Miller, and N. Christie-Blick (1999), Reconstruction of Tertiary progradation and clinoform development on the New Jersey passive margin by 2-D backstripping, Marine Geology, 154, 399–420.

Sugarman, P.J., K.G. Miller, J.V. Browning, M.-P. Aubry, G.J. Brenner, G. Cobbs III, L. de Romero, M.D. Feigenson, A. Harris, M.E. Katz, A. Kulpecz, P.P. McLaughlin Jr., S. Misintseva, D.H. Monteverde, R.K. Olsson, L. Patrick, S.J. Pekar, and J. Uptegrove (2005), Millville site, in K.G. Miller, P.J. Sugarman, J.V. Browning et al., eds., Proceedings of the Ocean Drilling Program, Scientific results, Vol. 174AX (supplement): College Station, Texas, Ocean Drilling Program, 1–95.

Tripati, A.K. and H. Elderfield (2004), Abrupt hydrographic changes in the equatorial Pacific and subtropical Atlantic from foraminiferal Mg/Ca indicate greenhouse origin for the thermal maximum at the Paleocene-Eocene Boundary, Geochemistry Geophysics Geosystems, 5(2), 1–11, doi:10.1029/2003GC000631.

Uchikawa, J. and R.E. Zeebe (2010), Examining possible effects of seawater pH decline on foraminiferal stable isotopes during the Paleocene-Eocene Thermal Maximum, Paleoceanography, 25, 1–14, doi:10.1029/2009PA001864.

Wade, B.S., N. Al-Sabouni, C. Hemleben, and D. Kroon (2008), Symbiont bleaching in fossil planktonic foraminifera, Evolutionary Ecology, 22, 253–265, doi:10.1007/s10682-007-9176-6.

Zachos, J.C., S. Schouten, S. Bohaty, T. Quattlebaum, A. Sluijs, H. Brinkhuis, S.J. Gibbs, and T.J. Bralower (2006), Extreme warming of mid-latitude coastal ocean during

the Paleocene-Eocene Thermal Maximum: Inferences from TEX_{86} and isotope data, Geology, 34(9), 737–740.

Zachos, J.C., S.M. Bohaty, C.M. John, H. McCarren, D.C. Kelly, and T. Nielsen (2007), The Palaeocene–Eocene carbon isotope excursion: constraints from individual shell planktonic foraminifer records, Philosophical Transitions of the Royal Society A, 365, 1829–1842, doi:10.1098/rsta.2007.2045.

Zapecza, O.S. (1984), Hydrogeologic framework of the New Jersey coastal plain, U.S. Geological Survey Open File Reports, 84(730), 1–61.

Zeebe, R.E., J. Bijma, and D.A. Wolf-Gladrow (1999), A diffusion-reaction model of carbon isotope fractionation in foraminifera, Marine Chemistry, 64, 199–227.

2.12.5 Supporting figures and tables

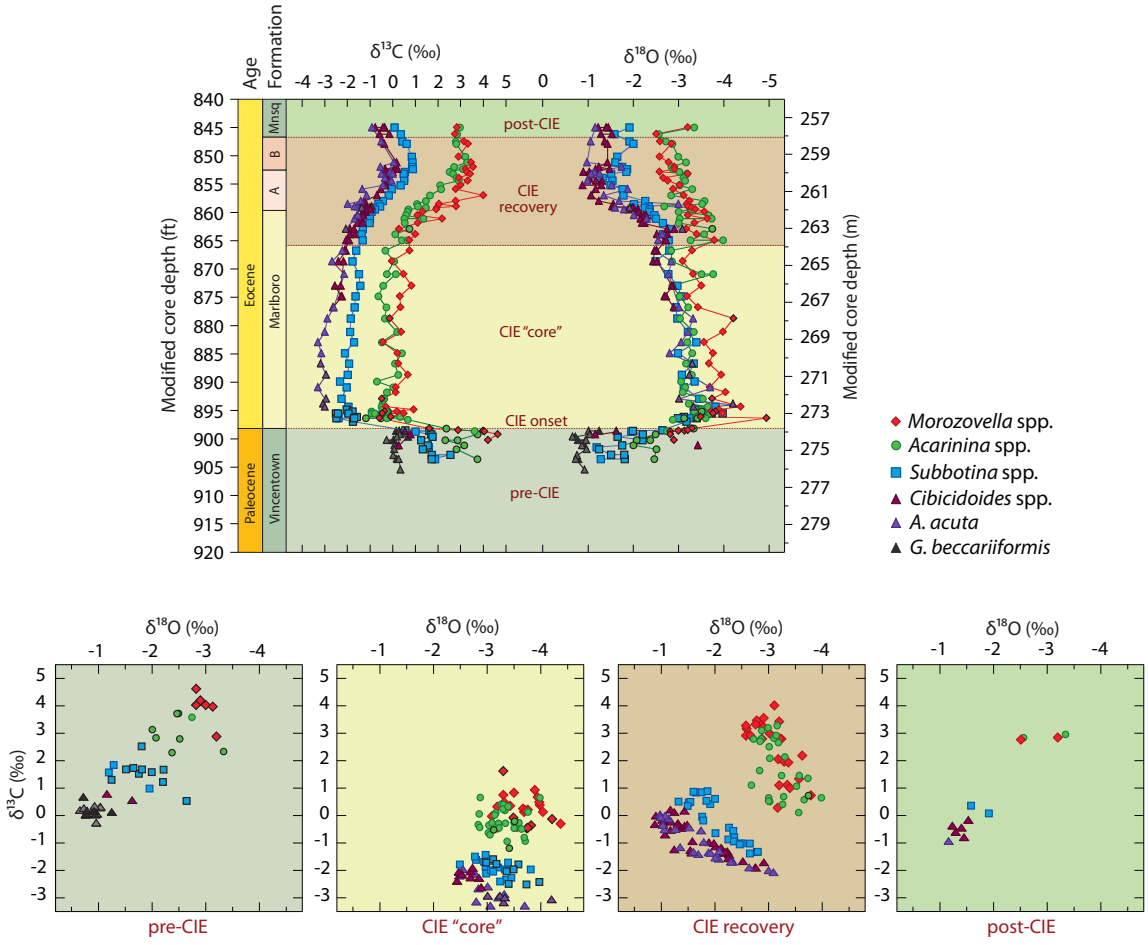

Fig. 2.S1. Stable carbon and oxygen isotopes of planktonic and benthic foraminifera at Millville, NJ: top – monogeneric records compiled from single species samples indicated in the legend; bottom – single species cross plots of $\delta^{18}O$ vs. $\delta^{13}C$ for the pre-CIE, CIE "core", CIE recovery, and post-CIE intervals. Thermocline dwellers *Subbotina* spp. are in blue, surface dwellers *Morozovella* spp. and *Acarinina* spp. are in red and green, respectively. For benthic foraminifera, *Gavelinella beccariiformis* in black, *Anomalinoides acuta* in purple, and *Cibicidoides* spp. in brown. Samples from smaller size fractions of 150-212 and 212-250 μm are outlined in black. Carbon isotopic values from smaller specimens are corrected for the test size (See 2.4 "Methods" in the main text). Oxygen isotope records are plotted in reverse order. Depths are modified and corrected for core expansion.

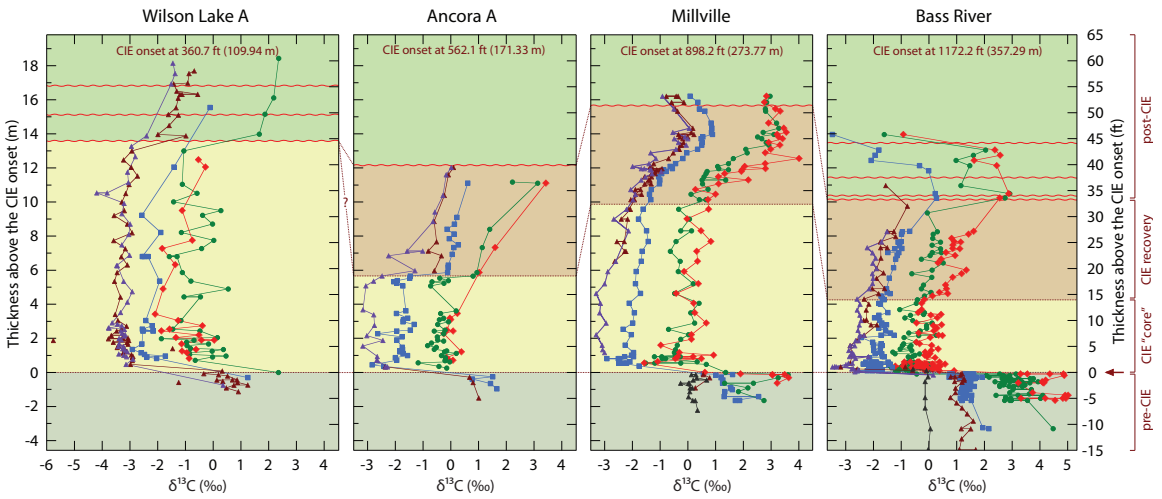

Fig. 2.S2. PETM carbon isotope records of planktonic and benthic foraminifera from New Jersey coastal plain sites correlated by the CIE onset: Wilson Lake Hole A [Zachos et al., 2006; Stassen et al., 2012]; Ancora [Cramer and Kent, 2005; Babila, 2014]; Millville [this study]; and Bass River [Cramer et al., 1999; Zachos et al., 2007; John et al., 2008; Stassen et al., 2012; Babila et al., 2016]. Arrow indicates the CIE onset. Benthic foraminifera: *Gavelinella beccariiformis* in black, *Anomalinoides acuta* in purple, *Cibicidoides* spp. in brown. Planktonic foraminifera: thermocline dwellers *Subbotina* spp. in blue, surface dwellers *Morozovella* spp. and *Acarinina* spp. in red and green, respectively.

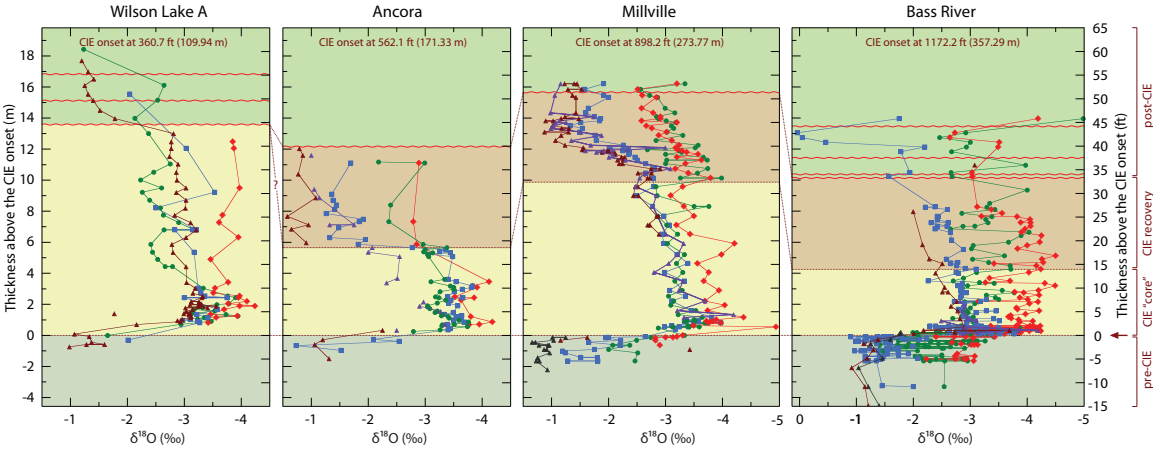

Fig. 2.S3. PETM oxygen isotope records (plotted in reverse) of planktonic and benthic foraminifera from New Jersey coastal plain sites correlated by the CIE onset: Wilson Lake Hole A [Zachos et al., 2006]; Ancora [Cramer and Kent, 2005; Babila, 2014]; Millville [this study]; and Bass River [Cramer et al., 1999; Zachos et al., 2007; John et al., 2008; Babila et al., 2016]. Arrow indicates the CIE onset. Benthic foraminifera: *Gavelinella beccariiformis* in black, *Anomalinoides acuta* in purple, *Cibicidoides* spp. in brown. Planktonic foraminifera: thermocline dwellers *Subbotina* spp. in blue, surface dwellers *Morozovella* spp. and *Acarinina* spp. in red and green, respectively.

Core holes	Distance in the NJ map (mm	Distance between coreholes (km)	Paleodepth estimates based on paleoslope 1:1000 (m)		Paleodepth estimates based on paleoslope 1:750 (m)		Paleodepth estimates based on paleoslope 1:500 (m)	
			Relative	Vincen-town	Relative	Vincen-town	Relative	Vincen-town
MD	23	5.75	5.75	25.00	8.63	25.00	11.50	25.00
WL	60	15.00	15.00	34.25	22.50	38.88	30.00	43.50
AN	98	24.50	24.50	43.75	36.75	53.13	49.00	62.50
MV	151	37.75	37.75	57.00	56.63	73.00	75.50	89.00
BR	201	50.25	50.25	69.50	75.38	91.75	100.50	114.00

Table 2.S1. Paleowater depths estimates for the Vincentown Formation at the New Jersey coastal plain sites (WL – Wilson Lake; AN – Ancora; MV – Millville; BR – Bass River) using possible end-member assumptions of the paleoslope gradient and errors in the anchor point at Medford (MD), NJ and site projections to a dip profile (±5 m in the relative placement).

Depth interval (ft)		Mean depth (ft)	Mean depth (m)	$\delta^{13}C$ PDB (‰) [250-300 μm]	$\delta^{13}C$ PDB, ‰ [150-212 μm]	$\delta^{13}C$ PDB offset (‰)
Bottom	Top					
321.00	321.10	321.05	97.86	-2.02	-2.37	0.35
330.15	330.25	330.20	100.64	-2.00	-2.41	0.41
339.50	339.60	339.55	103.49	-2.26	-2.67	0.41
350.20	350.30	350.25	106.76	-2.15	-2.62	0.47

Table 2.S2. Stable carbon isotopic values of *Subbotina roesnaesensis* from the 150-212 μm and 300-350 μm size fractions at Wilson Lake Hole B, NJ with indicated offset in $\delta^{13}C$ values between small (150-212 μm) and large specimens (300-350 μm) due to the vital effect.

III CHAPTER THREE

Blackout of planktonic foraminifera: seasonality effects on surface ocean climate reconstructions at the Paleocene-Eocene thermal maximum

3.1 Abstract

The largest global warming event of the Cenozoic, the Paleocene-Eocene thermal maximum (PETM, ca. 56 million years ago), is often used as an analog for anthropogenic climate studies yet the thermal evaluation during this event is still puzzling despite abundant data. Most environmental reconstructions of the PETM rely on foraminiferal tracers from marine sections. Here, I examine seasonality of planktonic foraminifera as a mediator in sea surface temperature reconstructions. Comparison of oxygen stable isotopes in foraminifera and two paleotemperature proxies (Mg/Ca, TEX_{86}) at Millville, the U.S. North Atlantic continental margin, implies a shift to winter blooms in mid-latitudinal surface dwelling foraminifera. High sea surface temperatures above foraminiferal limit of calcification (~33°C) during the PETM would restrict surface dwellers production to colder months, therefore their $\delta^{18}O$ records cannot register the full warming. I suggest a 6-7°C temperature increase on the North Atlantic paleoshelf based on the organic paleothermoter TEX^{H}_{86} and $\delta^{18}O$ of thermocline dwelling *Subbotina* spp. Oxygen isotopic records of foraminifera from low latitudinal marine locations show similar responses and support the seasonality shift in subtropical surface dwellers due to the extreme PETM warmth.

3.2 Introduction

The Paleocene-Eocene thermal maximum (PETM, ca. 56 Ma) was a transient global warming event characterized by a massive input of carbon into the Earth's system. Estimates of sea surface temperature (SST) rise vary from 4°C to 9°C depending on location and proxy used [e.g., Dunkley Jones et al., 2013]. Many temperature estimates of the PETM warming use stable oxygen isotopes of planktonic foraminifera [Kennett and Stott, 1991; Lu et al., 1998; Thomas et al., 1999; Thomas et al., 2002; Zachos et al., 2003; Zachos et al., 2006; John et al., 2008; Hollis et al., 2015; Babila et al., 2016]; however, the $\delta^{18}O$ of pristine foraminiferal tests might have been also affected by variations in seasonality and evaporation/precipitation reflected in salinity. Culture studies show that temperature is a limiting factor in foraminiferal survival, although salinity plays minor role [Bijma et al., 1990]. Therefore, it is critical to estimate SSTs and salinity impact to interpret $\delta^{18}O$ values of surface dwellers correctly.

Here, I use a multiproxy approach to evaluate amount of warming on the New Jersey paleoshelf at the PETM. Makarova et al. [2017] documented a smaller $\delta^{18}O$ anomaly in surface dwelling foraminifera associated with the PETM onset at Millville, NJ suggesting ecologic and hydrographic scenarios (Chapter Two). They also discussed a possible shift of surface dwellers production to colder seasons due to temperature restrictions on foraminiferal calcification. SSTs of ~35°C on the mid-Atlantic margin [Zachos et al., 2006; Sluijs et al., 2007] could have precluded year-long blooms of surface dwelling species; calcification in cooler season may have caused smaller $\delta^{18}O$ anomaly in surface dwellers associated with the PETM onset. Frieling et al. [2017] estimated SSTs exceeding 36°C in tropics during the PETM and also suggested heat

stress of planktonic organisms to explain changes in dinoflagellate and planktonic foraminifera, as did Si and Aubry [2018].

To estimate SST increase on the New Jersey paleoshelf during the PETM, I use organic paleothermometer TEX_{86} and Mg/Ca in planktonic foraminifera. I supplement existing oxygen isotopic records of foraminifera at Millville (Fig. 3.1) [Makarova et al., 2017; Si and Aubry, 2018] with temperature estimates from these two independent paleothermometers and discuss potential effects of seasonality on foraminiferal $\delta^{18}O$ values. I also apply Mg/Ca and TEX_{86}-based temperatures to decipher possible variations in salinity on the mid-Atlantic shelf embedded in planktonic foraminiferal $\delta^{18}O$ signals.

3.3 Geological Setting and Methods

The Millville site (ODP Leg 174AX) is located on the New Jersey coastal plain recovering a thick shelf PETM section [Makarova et al., 2017]. Paleoslope reconstruction of the New Jersey paleoshelf using a 1:750 gradient suggest ~70±20 m water depth during the latest Paleocene and a ~20 m deeper setting in the Early Eocene [Makarova et al., 2017]. Deposition at the Paleocene/Eocene transition shifts from glauconitic sandy silts to kaolinitic fine clays [Gibson et al., 1993; Cramer et al., 1999; Miller et al., 2005; Lombardi, 2013], facilitating excellent/pristine preservation of foraminifera in the PETM section at Millville, NJ (Fig. 3.S1) [Makarova et al., 2017]. More detailed geological setting on the New Jersey paleoshelf and lithologic description of the Millville core are given in sections 2.3 “ODP Leg 174AX Millville site” and 2.12.2 “Geological Setting” of Chapter Two.

3.3.1 Lipid biomarker analyses (TEX_{86})

Powdered freeze-dried sediments (~20 g dry mass) were extracted with a Dionex accelerated solvent extractor (ASE 200) using a 9:1 mixture (v:v) of dichloromethane (DCM) and methanol (MeOH) at a temperature of 150°C and a pressure of 1500 psi. The polar fraction containing glycerol dialkyl glycerol tetraethers (GDGTs) was separated from the total lipid extract through the alumina (Al_2O_3) column. The GDGT analyses were performed in 2013 and 2018, as indicated in Table 3.1. The 2013 analysis was performed by normal phase chromatography on an Agilent 1100 series high-performance liquid chromatography (HPLC) using the Prevail Cyano column (3 mm, 150 × 2.1 mm). A 99:1 (v:v) mixture of hexane:isopropanol was used to elute GDGTs at a flow rate 0.2 ml/min and column temperature 30°C according to the Hopmans et al. [2000] and Schouten et al. [2007a] methodology. The 2018 analysis used a modified HPLC high resolution method proposed by Hopmans et al. [2016]. GDGTs were eluted isocratically for 25 min with 18% of solvent A, followed by a linear gradient to 35% of A in 25 min, then a linear gradient to 100% of A in 30 min, where solvent A is a 9:1 mixture of hexane:isopropanol (v:v) and B is hexane. Flow rate was 0.2 ml/min, resulting in a maximum back pressure of 200 bar for this chromatographic system. Total run time is 80 min with a 20 min re-equilibration. The APCI source was kept at 200°C (gas temperature) and 400°C (vaporizer). The drying gas flow is set at 6 L/min^{-1}. The source was tuned in positive polarity. The two ACQUITY UPLC BEH HILIC columns used were purchased from Waters (2.1 x 150 mm, 1.7 μm). Blanks and standards were running along with the samples at daily basis to ensure analytical quality. Detection of GDGTs was accomplished via Single Ion Monitoring mode using Agilent OpenLAB Software.

3.3.2 Trace element analyses of foraminifera

Foraminiferal tests were gently crushed between two glass plates to open the chambers to facilitate cleaning following the protocol reported by Boyle and Keigwin [1985] later modified by Rosenthal et al. [1997]. Trace element analyses were measured on a Thermo Finnigan Element XR Sector Field Inductively Coupled Plasma Mass Spectrometer (SF-ICP-MS) operated in low resolution ($m/\Delta m$ =300) and medium resolution ($m/\Delta m$ =4300) settings outlined in the protocol of Rosenthal et al. [1999]. For robust interpretation of trace elements data, samples with unreasonably low or high calcium elemental ratios (B/Ca, Mg/Ca, Al/Ca, Ti/Ca, Mn/Ca, Sr/Ca, Fe/Ca) were considered as contaminated or possibly altered due to diagenesis and thus rejected from the reconstructions (Appendix 1; Fig. 3.S2). Elemental ratios were monitored and corrected for matrix effects for each analytical run by analyzing a suite of standards using an internal spiked gravimetric standard (SGS) with the same elemental ratios but varying [Ca] (1.5mmol/l to 8mmol/l) [Rosenthal et al., 1999]. [Ca] concentrations in sample solutions were typically maintained in the range of 1.5 to 4mmol/l to minimize matrix effects on Mg/Ca.

3.4 Results

3.4.1 TEX_{86}-based temperature estimates

I apply TEX^{H}_{86} and TEX^{L}_{86} indices from Kim et al. [2010] to convert the change in relative distribution of GDGTs to temperatures across the Paleocene/Eocene (P/E) boundary at Millville, NJ (Table 3.1). Two indices use different GDGT ratios, where GDGT ratio-2 (TEX^{H}_{86}) includes crenarchaeol regio-isomer and GDGT ratio-1 (TEX^{L}_{86})

does not (Fig. 3.S3). The total change in GDGT ratio-1 is 0.12 from 0.44 to 0.56 and the change in GDGT ratio-2 is 0.16 from 0.74 to 0.90 (Table 3.1; Fig. 3.2). The BIT index ranges from 0.05 to 0.15 (Table 3.2), indicating predominantly marine origin of organic fractions used for TEX_{86} with low soil organic matter input [Schouten et al., 2013 and references therein]. The TEX^{H}_{86} and TEX^{L}_{86} calibrations represent the best relationships between the relative distribution of thaumarchaeotal lipids (GDGTs) at temperatures higher than 15°C, though no modern calibration above 30°C is possible. Application of the TEX^{H}_{86} calibration reveals a 6°C warming (29.5-35.5°C) across the PETM onset (Fig. 3.3). The TEX^{H}_{86} temperature estimates reach a maxima at 35.5°C within the CIE "core" (see Chapter Two for the CIE "core" definition at Millville, NJ) and shows a two-step warming across the onset with a plateau around 33.5°C (Fig. 3.3). A 2 ft (0.6 m) thick temperature plateau interval appears above the CIE onset corresponding to a low (< 1% $CaCO_3$) carbonate zone [Makarova et al., 2017]. The TEX^{L}_{86} calibration shows a 7°C warming with cooler temperatures (23-30°C) and a plateau at 27.5°C (Fig. 3.3). Both calibrations indicate the recovery of temperatures to the pre-PETM values by 855 ft (260.6 m) in the upper part of the section (Fig. 3.3). The precursor warming suggested by TEX_{86} estimates at Bass River, NJ [Sluijs et al., 2007] is vague at Millville. The TEX^{H}_{86} calibration hints a 1-2°C warming preceding the main inflection in bulk sediment $\delta^{13}C$ values, whereas the TEX^{L}_{86} calibration shows no warming prior the CIE onset (Fig. 3.3). The lead/lag relationship between the CIE onset and TEX_{86} estimated warming is discussed in Chapter Four that provides data from expanded section of the PETM onset at Medford, NJ.

3.4.2 Mg/Ca-based temperature estimates

Mg/Ca data from surface dwelling *Morozovella* and *Acarinina* spp. are not sufficient to reconstruct the temperature anomaly associated with the PETM onset and only present in the upper part of the section (Fig. 3.2; Table 3.3). The total change in Mg/Ca ratio of thermocline dwelling *Subbotina* spp. across the PETM onset is 1.6 mmol/mol that is equivalent to a ~5.5°C warming applying the multispecies equation of Anand et al. [2003] (Figs. 3.2 and 3.5; Table 3.3). The Mg/Ca ratio of seawater during the PETM is not well known ranging from 1.5 to 3.5 mmol/mol with a best estimate of 2.5 mmol/mol [Cramer et al., 2011; Evans et al., 2018]. Assuming that Mg/Ca of seawater was 2.5 mmol/mol during the PETM and the multispecies equation from Anand et al. [2003], temperatures in the thermocline indicated by *Subbotina* spp. Mg/Ca ratio increased from 29.5°C to 35°C (Table 3.3).

3.5 Discussion

3.5.1 Sea surface temperature anomaly at Millville, NJ

3.5.1.1 Oxygen isotopes of foraminifera

To evaluate warming associated with the PETM onset at Millville, NJ, I compare temperature anomalies derived from the organic paleothermometer TEX_{86} and Mg/Ca of planktonic foraminifera with $\delta^{18}O$ records of planktonic foraminifera (Figs. 3.4 and 3.5). Foraminiferal isotopic data from Makarova et al. [2017] and Si and Aubry [2018] represent compilations of isotopic values measured in mostly mono-specific samples from narrow size fractions and agree with each other (Fig. 3.1). The *Morozovella* spp. assemblage shifts from a *M. aequa*/*M. subbotinae*-dominated assemblage (*MAS* lineage

in Si and Aubry [2018]) to a *M. acuta*/*M. velascoensis*-dominated assemblage (*MAV* lineage in Si and Aubry [2018]) across the PETM onset. Si and Aubry [2018] suggested different depth niches for *MAS* and *MAV* linages during the PETM. Therefore, I plot *M. aequa* and *M. acuta* in distinct symbols to clarify the *Morozovella* spp. record (Fig. 3.1). Interspecies isotopic values in *Acarinina* and *Subbotina* are similar (Fig. 3.S4) and, therefore, are plotted as monogeneric records, i.e. *Acarinina* and *Subbotina* spp. (Fig. 3.1).

Surface dwelling *Acarinina* and *Morozovella* spp. show a -1 ‰ anomaly in oxygen isotopic values ($\Delta\delta^{18}O$ = $\delta^{18}O$ before the CIE onset minus $\delta^{18}O$ after the CIE onset) associated with the PETM onset (Figs. 3.1 and 3.S4). Thermocline dwelling *Subbotina* spp. $\delta^{18}O$ show a -1.75 ‰ anomaly. Makarova et al. [2017] attributed the smaller $\Delta\delta^{18}O$ in surface dwelling taxa either to changes in water column structure due to a more gradual thermocline and/or to a shift in seasonality of blooms. In contrast, Si and Aubry [2018] interpreted this difference to a depth migration as an adaptation of *Acarinina* spp. and the *MAV* lineage to the environmental stress associated with the PETM onset.

Since all foraminifera from the Millville core, i.e. *Morozovella* spp., *Acarinina* spp., *Subbotina* spp., and benthic taxa, show similar carbon isotope excursions (CIEs) of 3.6-4 ‰ across the P/E boundary (Figs. 3.1 and 3.S4), I argue against the species depth migration scenario. Recycling of organic matter in deeper parts of the water column lowers $\delta^{13}C$ of the dissolved inorganic carbon (DIC) in the seawater. Thus, the highest $\delta^{13}C$ values in symbiont-bearing mixed layer dwelling *Morozovella* and *Acarinina* spp. imply near surface niches, lower $\delta^{13}C$ values in symbiont barren thermocline dwelling

Subbotina spp. indicate residence in the nutricline/thermocline, and lowest $\delta^{13}C$ values in benthic taxa indicate seafloor habitats. Such $\delta^{13}C$ relationships among PETM taxa are reported in other shelf [Zachos et al., 2006, 2007; John et al., 2008; Babila, 2014; Babila et al., 2016] and pelagic sites [e.g., Kennett and Stott, 1991; Bralower et al., 1995; Lu and Keller, 1996; Thomas et al., 2002; Hollis et al., 2015] and interpreted as vertical $\delta^{13}C$ isotopic gradients. Consequently, migration of the mixed layer dwelling taxa to deeper habitats should have also lowered their $\delta^{13}C$ mimicking DIC isotopic profile. This would have resulted in larger CIEs recorded by the refuge species of *Morozovella* and *Acarinina*, than by *Subbotina* spp. and benthic foraminifera that remained their ecological niches during the PETM. Unchanged carbon isotopic gradients between all taxa at Millville imply little or no depth migration of surface dwellers during the PETM.

Oxygen isotopic relationships among the foraminifera are likewise interpreted by most studies as vertical rankings reflecting calcification at different depths. Accordingly, Makarova et al. [2017] inferred a thermally more homogeneous water column structure with smoother thermocline to explain diminished gradients in $\delta^{18}O$ values between surface dwellers and thermocline/benthic species during the PETM. They also mentioned a change in seasonality of foraminiferal blooms as another factor possibly affecting generic differences in $\delta^{18}O$ values that I elaborate on here, using TEX_{86} and Mg/Ca data to constrain the problem.

Blooms of planktonic foraminifera are mainly controlled by species thermal preferences and nutrient supply/food availability [e.g., Bé, 1960; Tolderlund and Bé, 1971; Curry et al., 1983; Thunell et al., 1983; Deuser and Ross, 1989; Fairbanks and Wiebe, 1980; Ravelo and Fairbanks, 1992]. Sediment trap studies of modern planktonic

foraminiferal fluxes from the North Atlantic (34°N, which is similar to the New Jersey paleoshelf latitude during the PETM) show seasonal changes in foraminiferal production [Wolfteich, 1994]. Maximum fluxes of most taxa in the modern subtropical study area occur during winter-early spring blooms of phytoplankton. *G. bulloides* occupies the niche above the thermocline [Fairbanks et al., 1982] and grows during the peak of phytoplankton production that supplies food for foraminifera [Wolfteich, 1994]. Thus, the $\delta^{18}O$ values of *G. bulloides* from mid latitudes should mainly reflect lower temperatures of winter-early spring calcification and subsurface habitat. At higher latitudes, however, *G. bulloides* peak production is delayed towards summer and fall as a response to changing food availability defined by seasonal variations in local phytoplankton blooms [Tolderlund and Bé, 1971]. When primary productivity is low, surface dwelling, symbiont bearing *G. ruber* prevails in foraminiferal flux for up to eight months in the North Atlantic mid latitudes.

Wolfteich [1994] pointed out that seawater temperature also plays a critical role in foraminiferal succession. In fact, *G. ruber* is the only species surviving spring-summer SST of 25°C and dominated *G. bulloides* in relative abundances at SSTs above 18.5°C [Wolfteich, 1994]. Seasonality of the main production of *G. ruber* and *G. bulloides* is potentially analogous to surface and thermocline dwelling foraminifera during the PETM. As a result of temperature limit on foraminiferal calcification, very hot summer temperatures above the tolerance threshold could have shifted surface dwelling foraminiferal blooms to colder seasons. If so, the $\Delta\delta^{18}O$ in *Morozovella* and *Acarinina* spp. would not reflect the full change in sea surface temperature as measured $\delta^{18}O$. In contrast, thermocline dwelling *Subbotina* spp., keeping usual season of calcification,

would reflect the full $\delta^{18}O$ anomaly in the thermocline during the PETM. Application of a 0.25 ‰/°C slope [O'Neil et al., 1969], therefore, gives a 7°C warming in the thermocline on the New Jersey paleoshelf based on $\Delta\delta^{18}O$ of *Subbotina* spp. at Millville, NJ.

3.5.1.2 TEX_{86}-derived temperature estimates

The TEX_{86} indices are calculated based on relative distribution of isoprenoidal GDGTs (membrane lipids of marine Thaumarchaeota) in surface sediments and correspond with mean annual SST in the range of 5 to 30°C derived from satellite measurements [Schouten et al., 2002; Kim et al., 2010]. The composition of thaumarchaeotal membranes changes with seawater temperature and does not depend on salinity or nutrients [Schouten et al., 2002; Wuchter et al., 2004, Schouten et al., 2007b]. However, there is a discrepancy in correlation of GDGTs abundancies to SSTs because of uncertain depths of main GDTGs production and their transport to sediments. In fact, Thaumarchaeota is the most abundant prokaryotic group that is ubiquitous throughout the water column with a maximum occurrence at depths less than 200 m [Karner et al., 2001; Pearson and Ingalls, 2013; Schouten et al., 2013; Tierney, 2014 and references therein]. Indifference to sun light and nitrifying metabolism of Thaumarchaeota are evidential of their residence below the photic zone [Könneke et al., 2005; 2014]. Moreover, radiocarbon and stable carbon isotopic measurements in archaeal C_{40} isoprenoids (constituents of GDGTs) also support the subsurface origin [Pearson et al., 2001; Shah et al., 2008]. Nonetheless, values of TEX_{86} from coretop sediments reflect modern SST well [Schouten et al., 2002; Liu et al., 2009; Kim et al., 2010; Tierney and Tingley, 2015] despite deeper habitats of GDGT producers.

The TEX_{86} calibrated temperature anomaly of 6-7°C is identical to the temperature change estimated from $\delta^{18}O$ of thermocline dwelling *Subbotina* spp. and contrasts with the lower change from surface dwellers at Millville, NJ (Fig. 3.4). It is remarkable how much temperatures registered by $\delta^{18}O$ of *Subbotina* spp. and TEX_{86} resemble each other (Fig. 3.4). The records show stable high temperatures during the peak PETM warmth between 881 ft and 896 ft (268.5-273.1 m) and the initial cooling of 2-3°C at 871-881 ft (265.5-268.5 m). There is a secondary warming and then the final cooling to the pre-PETM temperature values begins at 863 ft (263 m). The final decrease in temperature corresponds to the CIE recovery (Figs. 3.3 and 2.4 in Chapter Two) defined by $\delta^{13}C$ values in bulk carbonate and foraminifera [Makarova et al., 2017]. At this level oxygen isotopic records show a step-like decrease in $\delta^{18}O$ values of *Morozovella* and *Acarinina* spp. (Fig. 3.4) and reestablishment of the $\delta^{18}O$ gradient between surface and thermocline dwellers (Fig. 2.S1 in Chapter Two). The secondary episode of warming, not described in other locations, might indicate additional input of carbon in form of greenhouse gases before the system reached the main phase of recovery. Such possible cascade of multiple carbon injections may have facilitated the PETM warmth and CIE "core" to persist for 40 to 135 kyr based on various chronological estimates [Katz et al., 1999; Röhl et al., 2007; Murphy et al., 2010].

If the TEX_{86} indeed reflects SST changes as the calibration implies, then water column warmed uniformly from surface to thermocline during the PETM and lower temperature anomaly of ~4°C calculated from $\Delta\delta^{18}O$ in surface dwellers did not record the full warming in the mixed layer (Fig. 3.4). The proposed temporal shift in surface dwelling taxa blooms is supported by TEX^{H}_{86} calibrated SST of 35.5°C during the peak

PETM warmth that is above the limit of foraminiferal survival (~33°C; Bijma et al. [1990]).

On the other hand, if the TEX_{86}-derived temperature signal actually comes from the subsurface [Ho and Laepple, 2016], then similar anomalies from *Subbotina* spp. $\delta^{18}O$ and TEX_{86} are not surprising. If this is true, then neither this study nor previous studies of lower latitude sites provide firm constraints on the maximum surface temperatures and SST anomaly associated with the PETM onset. Since most TEX_{86}-based PETM temperature estimates come from marine sections containing no or insufficient foraminifera to compute $\delta^{18}O$ anomaly, it is difficult to decipher whether TEX_{86} embodies sea surface or thermocline signal. More TEX_{86}-foraminiferal $\delta^{18}O$ correlations from other low-mid latitudinal sites are needed to further address interpretation of TEX_{86} paleorecords. Because modern GDGT abundances correlate well with SSTs, I interpret temperatures estimated from TEX_{86} as surface, which implies that there was no change in surface salinities and surface dwelling foraminifera (*Morozovella* and *Acarinina* spp.) did not record SSTs.

3.5.1.3 Mg/Ca-derived temperature estimates

Subbotina spp. Mg/Ca-derived temperature record shows an overall similar anomaly associated with the CIE onset (898.17 ft; 273.76 m) as those from TEX_{86} and *Subbotina* spp. $\delta^{18}O$ at Millville, NJ (Fig. 3.5). Temperatures estimated from *Subbotina* spp. Mg/Ca remain constant above the CIE onset and then gradually decrease from 881 ft (268.5 m) upward matching the cooling recorded by TEX_{86} and *Subbotina* spp. $\delta^{18}O$. At the top section (855-863 ft; 260.6-263 m) *Subbotina* spp. Mg/Ca record does not agree with the trends from TEX_{86} and *Subbotina* spp. $\delta^{18}O$ (Fig. 3.5), with Mg/Ca showing a

minor warming than cooling versus all cooling in other proxies. Additional Mg/Ca measurements are required to resolve this issue.

Trace metals analyses at other New Jersey coastal plain sites (Ancora [Babila, 2014] and Bass River [Babila et al., 2016]) indicate identical warming recorded by *Subbotina* spp. as at Millville (Fig. 3.S5). Mg/Ca records of *Morozovella* and *Acarinina* spp. also show alike values among three sites (Fig. 3.S5). However, during the peak warmth, *Acarinina* spp. Mg/Ca calibrated temperatures are much lower than those from *Morozovella* and *Subbotina* spp. (Fig. 3.S5). This observation is not consistent with oxygen isotopic records (Fig. 3.1). Such differences in absolute Mg/Ca-derived temperatures among planktonic foraminifera probably originate from different mechanisms of trace element incorporation during biomineralization [e.g., Evans et al., 2018] and do not necessarily indicate lower temperatures recorded by *Acarinina* spp. Thus, inter-specific differences in Mg/Ca-derived temperatures should not be used in reconstructions of temperature gradients between surface and thermocline dwelling taxa and rather be applied for estimates of temperature anomaly in each taxa. Overall, only *Subbotina* spp. provides robust Mg/Ca calibrated temperatures that agree with estimates from oxygen stable isotopes and TEX_{86} (Fig. 3.5).

3.5.2 Spatial distribution of temperature anomalies on the New Jersey paleoshelf during the PETM: intersites comparison of TEX_{86}-based estimates

TEX^{H}_{86} and TEX^{L}_{86} indices from four New Jersey coastal plain sites, updip Medford MAP 3B [Chapter Four] and Wilson Lake A [Zachos at el., 2006], downdip Millville and Bass River [Sluijs et al., 2007], encompass spatial reconstruction of temperature variations across the shelf during the PETM (Fig. 3.6). In general, both

indices indicate larger temperature anomalies at proximal Medford and Wilson Lake than at distal Millville and Bass River (Fig. 3.6). TEX^{L}_{86} shows cooler temperatures and higher amplitude of warming than TEX^{H}_{86} during the PETM (Fig. 3.6), however in the modern ocean both TEX^{H}_{86} and TEX^{L}_{86} indices agree at SSTs >15°C [Kim et al., 2010]. Kim et al. [2010] suggested using TEX^{H}_{86} to compute temperature for the PETM sections due to its smaller error (±2.5°C versus ±4°C for TEX^{H}_{86} and TEX^{L}_{86}, respectively) and higher estimated temperatures (28-36°C) that are more expected with high CO_2 levels during the PETM. In contrast, Taylor et al. [2013] favored the TEX^{L}_{86} calibration for the Paleogene datasets. Taylor et al. [2013] found that the offset between TEX^{H}_{86} and TEX^{L}_{86} depends on the GDGT-2/GDGT-3 ratio that greatly varies with depth. The coretop dataset for the TEX^{H}_{86} calibration is mostly derived from deep-water settings (>1,000 m) and can be biased by GDGTs from benthic archaean community; therefore, the TEX^{L}_{86} should be more applicable for the PETM at "shallow" depths (<1,000 m). However, New Jersey sites were limited to less than 100-200 m water depths during the PETM based on various paleowater depth reconstructions [Stassen et al., 2015; Makarova et al., 2017] and shelf deposits should not contain GDGTs of deep origin (>1,000 m).

HPLS analysis detects a set of six isoprenoid GDGTs in polar fractions of organic extracts (Fig. 3.S3). The most abundant crenarchaeol (60-75% among GDGTs in PETM sediments from New Jersey coastal plain sites) is not used for TEX_{86} due to its much higher concentrations [Schouten et al, 2002]. Interestingly, only crenarchaeol abundances vary coherently among NJ sites, whereas relative abundances of less abundant GDGTs differ in proximal versus distal sites. To see which GDGTs drive different temperature estimates from TEX^{H}_{86} and TEX^{L}_{86} among NJ sites, I calculated fractions of each GDGT

normalized to the sum of GDGTs from corresponding calibrations (Figs. 3.S3, 3.S6, and 3.S7). The fractional analyses of lipids from TEX^{H}_{86} show that GDGT-2 and GDGT-3 covary similarly among NJ sites and change their relative abundances not at the CIE onset level but slightly higher, corresponding to the top of the low carbonate zone (Fig. 3.S6). In contrast, change in relative abundance of crenarchaeol regio-isomer across the CIE onset is larger at Medford than at Millville and Bass River (Fig. 3.S6). This may account for different temperature anomalies calculated from TEX^{H}_{86} at these sites (Fig. 3.5). Variations in TEX^{L}_{86} temperatures among NJ sites are driven by relative abundance of GDGT-2 with a larger increase in GDGT-2 abundance at Medford than at Millville and Bass River (Fig. 3.S7). In fact, reevaluation of the modern core-top and Paleogene datasets showed that GDGT-2/GDGT-3 ratio and percent of crenarchaeol regio-isomer control the offset between TEX^{H}_{86} and TEX^{L}_{86} estimates [Taylor et al., 2013], supporting observations from the PETM records discussed here (Fig. 3.7).

Spatial variability in TEX_{86}-based temperature estimates from the New Jersey coastal plain sites is consistent with TEX_{86} variability on shelves today. Study of modern coretops from the South China Sea showed lower TEX_{86}-based temperatures in coretops from <100 m depths [Wei et al., 2011]. A dataset from the Mediterranean Sea also revealed larger offsets between TEX_{86} estimated temperatures and satellite measured SSTs in the nearshore environments with TEX_{86} indicating colder temperatures [Leider et al., 2010; Kim et al., 2015]. Leider et al. [2010] suggested that TEX_{86} estimates cold-biased winter temperatures in the nearshore sites that are more affected by seasonal and spatial changes in nutrients, whereas further offshore sites record true summer temperatures. Kim et al. [2015] significantly extended the Mediterranean dataset and

concluded that TEX^{H}_{86} temperature estimates overall correspond well to satellite annual mean SSTs and are not determined by seasonal environmental variations. The main bias in TEX^{H}_{86}-derived temperatures comes from by organic matter imprint in coastal areas, also supported by high BIT values, and from water depth on continental shelves. They also indicated increased fractional abundances of GDGT-2 and crenarchaeol regio-isomer and decreased abundances of GDGT-1 and GDGT-3 with water depth. These are responsible for a bias towards higher temperatures imbedded in TEX^{H}_{86} in deeper water.

Observations from the South China Sea and the Mediterranean are similar to GDGT fractional analyses in the PETM records from New Jersey coastal plain sites. Thus, spatial variance of TEX_{86}-derived temperatures on the New Jersey paleoshelf during the PETM is mostly determined by water depth. However, there are still more uncertainties that might control TEX_{86} values, such as input of GDGTs from non-marine sources [Pearson et al., 2016] or other groups of Archaea [Turich et al., 2007], season of growth [Huguet et al., 2007], oxygen content [Qin et al., 2015], ammonia oxidation rates [Hurley et al., 2016], and other environmental factors [e.g., Elling et al., 2015; Zhu et al., 2016; Kim et al., 2016]. As suggested by Hurley et al. [2016], there is a need for regional calibrations to interpret TEX_{86} values from paleorecords. The current TEX_{86} dataset does not include coretops from the North Atlantic [Kim et al., 2010]. Thus, a calibration, analogous to the PETM settings on the New Jersey paleoshelf, should be developed on the modern North Atlantic margin to better understand factors controlling spatial distributions of GDGT ratios on the shelf.

Influences of other factors on TEX_{86}-derived temperature estimates in the New Jersey PETM records are also evident from comparison with foraminiferal $\delta^{18}O$ and

Mg/Ca data. All sites show similar anomalies in generic $\delta^{18}O$ (Fig. 2.S3 in Charter two) and Mg/Ca (Fig. 3.S5) values across the PETM onset suggesting spatially equal warming across the New Jersey paleoshelf. Therefore, a larger TEX_{86} temperature anomalies at Medford and Wilson Lake possibly come from their proximity/shallower depths. Since nearshore environments exhibit cold-biased TEX_{86} temperatures [Leider et al., 2010; Wei et al., 2011; Kim et al., 2015], distal/deeper Millville and Bass River would represent more trustful data because of fully marine conditions at their localities both prior and during the PETM. Between the two indices, TEX^{H}_{86}-based estimates show less variance in amount of warming during the PETM among New Jersey sites than TEX^{L}_{86} (Fig. 3.6), and thus probably reflect less bias by depth/proximity to the shore. Based on all above, the TEX^{H}_{86} estimates from more distal Millville and Bass River seem to reflect more robust temperature anomaly, i.e. 6°C warming during the PETM (Fig. 3.6).

3.5.3 Temperature estimates in other PETM sections from low-mid latitudes

Despite extensive research on the PETM for almost three decades there not many temperature records from low-mid latitudes [e.g., Dunkley Jones et al, 2013; Sluijs et al., 2014; Frieling et al., 2017]. TEX_{86}-based estimates were done on sections from the Gulf coastal plain [32°N paleolatitude; Sluijs et al., 2014] and east Atlantic equatorial sites offshore Nigeria and Ghana [1-7°S paleolatitude; Frieling et al., 2017; 2018]. Based on above discussion of uncertainties associated with the TEX_{86} signal, it should be noted that comparison of TEX_{86}-derived records from distinct settings might be overprinted by regional environmental effects. The TEX^{H}_{86} record from the Gulf coastal plain shows a 7°C warming from 28.5°C to 35.5°C [Sluijs et al., 2014], similar to the anomaly registered at New Jersey coastal plain sites and the absolute temperature estimates from

TEX^{H}_{86}. Equatorial sites from offshore Nigeria [Frieling et al., 2017] and Ghana [Frieling et al., 2018] show much smaller warming of ~3°C from 34.5°C to 37.5°C (the TEX^{H}_{86} calibration) in the tropics during the PETM that Frieling et al. [2017] attributed to polar amplification, which is generally suggested by proxy data [e.g., Bijl et al., 2009] and also reproduced by climate models for greenhouse world [Huber and Caballero, 2011; Lunt et al., 2012; Kiehl and Shields, 2013]. Such warm tropical TEX^{H}_{86}-based temperatures are above the limit of satellite-based SST calibrations (30°C) [Kim et al., 2010]. Therefore, Frieling et al. [2018] noted that a smaller amplitude of warming might be underestimated, though modern GDGT producers from mesocosm studies thrive and display positive correlation to temperatures up to 40°C [Wuchter et al., 2004; Schouten et al., 2007b]. Nonetheless, they hypothesized that heat stress might have been responsible for decline in dinoflagellate assemblages and reduced calcification in the tropics.

Isotopic records of planktonic foraminifera from low-mid latitudes are also scarce. Most of them are from open ocean sites that have condensed PETM sections with 20-40 cm thick CIE "core" intervals (compared to 10 m at Millville). Stable oxygen isotopic records from Alamedilla, Spain (Tethys, 30°N paleolatitude; Lu et al. [1998]), ODP Site 1209 (Shatsky Rise, north western Pacific, 22°N paleolatitude; Zachos et al. [2003]), ODP Site 865 (Allison Guyot, western central equatorial Pacific, 2°N paleolatitude; Bralower et al. [1995]), and DSDP Site 527 (Walvis Ridge, South Atlantic, 35°S paleolatitude; Thomas et al. [1999]) show smaller $\delta^{18}O$ anomalies ranging from 0 to 1 ‰ in surface dwelling *Morozovella* and *Acarinina* spp. than in thermocline *Subbotina* spp. and benthic taxa. Surface dwellers from southern hemisphere high latitudes recorded larger $\delta^{18}O$ anomalies ranging from 1 to 2.5 ‰ that is similar or even larger than in

deeper dwelling foraminifera [Kenneth and Stott, 1991; Lu and Keller, 1993; Thomas et al., 2002; Hollis et al., 2015]. These observations are consistent with the proposed shift in calcification season of *Morozovella* and *Acarinina* spp. during the PETM on the mid-Atlantic margin, i.e. surface dwelling foraminifera from low-mid latitudes recorded smaller $\delta^{18}O$ anomaly due to inability to calcify at extreme summer temperatures, whereas surface dwelling foraminifera from colder high latitudes recorded the full $\delta^{18}O$ anomaly. Similarly, Aze et al. [2014] estimated tropical SSTs over 40°C corresponding to $\delta^{18}O$ values of -5 ‰ in *Morozovella* spp. on the Tanzania shelf (19°S paleolatitude) and suggested surface dwellers exclusion due to heat stress. However, the ~11 m thick section from Tanzania does not have a defined CIE by foraminifera, n-alkanes, or bulk sediment organic carbon. Although foraminiferal tests are well-preserved, specimens are scarce making it difficult to interpret any isotopic changes.

Foraminiferal tests are in general subjected to diagenetic alterations that could bias isotopic values and trace element ratios [e.g., Pearson et al., 2001; Sexton et al., 2006]. Dunkley Jones et al. [2013] attributed smaller $\Delta\delta^{18}O$ at DSDP Site 527 and ODP Sites 865 and 1209 to poor preservation of foraminiferal tests and suggested cold-biased $\delta^{18}O$-based temperatures. In contrast to $\delta^{18}O$ temperature estimates, Mg/Ca records of the same species from these deep sea sections estimated larger warming anomalies during the PETM [Zachos et al., 2003; Tripati and Elderfield, 2004]. These larger anomalies were originally explained by changes in precipitation/evaporation dampening $\Delta\delta^{18}O$ [Zachos et al., 2003; Tripati and Elderfield, 2004] and later argued to represent less impact of recrystallization on trace element ratios [Dunkley Jones et al., 2013]. Despite offsets in warming estimates between $\delta^{18}O$ and Mg/Ca, each proxy shows larger temperature

anomalies in thermocline dwelling species than in surface dwellers. Therefore, this is consistent with the proposed changes in calcification seasons of surface dwelling taxa associated with the peak PETM warmth in low-mid latitudes.

Unfortunately, the lack of planktonic foraminifera in marine sections across the PETM onset and poor test preservation in deep sea sections complicate estimates of warming from foraminiferal stable isotopes and trace metals analyses. Most existing reconstructions of sea surface anomalies during the PETM are from *Acarinina* spp. that show puzzling $\delta^{18}O$ records and large variability among all sites. Instead, *Morozovella* and *Subbotina* spp. show more consistent records and less variability between different locations. Thus, monospecies samples of *Morozovella* and *Subbotina* spp. from narrow size fractions would represent better choice for warming estimates of the surface ocean and thermocline, respectively.

3.5.4 Salinity evaluations on the New Jersey paleoshelf during the PETM

$\delta^{18}O$ anomalies interpreted above from surface and thermocline dwelling foraminifera at Millville, NJ account only for temperature changes. However, variations in seawater $\delta^{18}O$ might have affected oxygen isotopic values of foraminifera as well. Various proxy data and models suggested an increased tropical heat and moisture transport in response to the PETM warming [e.g., Caballero and Langen, 2005; Pagani et al., 2006; Carmichael et al., 2016]. The proposed enhanced hydrological cycle would have increased precipitation and river discharge, resulting in higher sediment accumulation rates on the continental margins during the PETM [e.g., Schmitz and Pujalte, 2003; 2007; Giusberti et al., 2007; John et al., 2008; Cui et al., 2011; Harding et al., 2011]. Studies of New Jersey PETM sections supported enhanced hydrological cycle

and fresh water input by evidence of expanded flux of the fine sediment, development of a river-dominated shelf, and abundant low salinity dinoflagellates [Sluijs et al., 2007; John et al., 2008; Kopp et al., 2009; Sluijs and Brinkhuis, 2009]. Therefore, the mixing of river runoff and seawater might have affected foraminiferal $\delta^{18}O$ towards more negative values that would have resulted in increased foraminiferal $\Delta\delta^{18}O$ across the PETM onset. Following this logic, a fresh water lens should have lowered surface dwelling *Morozovella* and *Acarinina* spp. $\delta^{18}O$ values more than those of thermocline dwelling *Subbotina* spp. In contrast, foraminiferal oxygen isotopic records showed larger $\Delta\delta^{18}O$ recorded by *Subbotina* spp. than that by surface dwellers.

Despite these concerns, my comparisons show that salinity variations in the shelf thermocline can be neglected. Temperature anomalies of 5.5-7°C estimated from TEX_{86} and Mg/Ca in *Subbotina* spp. are comparable to $\Delta\delta^{18}O$ in *Subbotina* spp., suggesting that 1.75 ‰ decrease in $\delta^{18}O$ of *Subbotina* spp. was driven by warming. Though "The Appalachian Amazon" may be valid analog for the New Jersey paleoshelf during the PETM [Kopp et al., 2009], it should be noted that modern Amazon drainage system does not affect seawater salinity further offshore at water depths more than 20 m either through fresh water lens or by bottom fluid mud [see section 2.5.1 "Environmental and biotic controls on stable isotope records of foraminifera" in Chapter Two; Makarova et al., 2017]. Thus, the Millville site with paleowater depth estimates of >70 m during the PETM [Makarova et al., 2017] should have not been affected by river discharge at its offshore location (Figs. 2.1 and 2.7 in Chapter Two). Besides, absolute $\delta^{18}O$ values and $\Delta\delta^{18}O$ in all foraminifera are similar during the PETM among New Jersey coastal plain

sites (Figs. 2.S3 in Charter Two), suggesting shelf settings far from the river mouth and fresh water discharge.

The lower SST anomaly derived from a smaller $\Delta\delta^{18}O$ in *Morozovella* and *Acarinina* spp. could also reflect an increase in seawater $\delta^{18}O$ due to enhanced evaporation in the mixed layer. Use of the TEX_{86}-derived temperature anomaly yields an increase in salinity in surface water. Thus, application of $\Delta\delta^{18}O$ from surface dwellers for SST estimates during the PETM could be misleading, whereas $\Delta\delta^{18}O$ from *Subbotina* spp. represent more robust temperature anomaly.

3.6 Conclusions

Application of multiple paleotemperature proxies at Millville, NJ provide three sets of temperature anomaly estimates during the PETM. Thermocline dwelling *Subbotina* spp. recorded a 1.75 ‰ decrease in $\delta^{18}O$ in contrast to 1 ‰ in surface dwelling *Morozovella* and *Acarinina* spp. Stable isotopic records from other low-mid latitudinal locations likewise showed a smaller $\Delta\delta^{18}O$ in surface dwellers; however, this is not observed in sections from high latitudes. If SSTs in low-mid latitudes were above the limit of foraminiferal calcification (>33°C), this would have interrupted normal season of surface dwellers blooms and shifted their main production to colder months resulting in dampened $\delta^{18}O$ anomaly. A more robust $\delta^{18}O$-derived temperature anomaly during the PETM from low-mid latitudinal sections can be estimated using thermocline dwelling *Subbotina* spp. because surface dwellers *Morozovella* and *Acarinina* spp. did not record the full warming during the PETM. In fact, TEX_{86}-based temperature estimates mimic the $\delta^{18}O$ record of *Subbotina* spp. suggesting either both recorded thermocline temperature or

that thermocline and surface water temperature changes were similar. A spatial comparison of TEX_{86} records among New Jersey coastal plain sites revealed a larger warming in proximal sites Medford and Wilson Lake versus distal sites Millville and Bass River, which is attributed to other than temperature controls on lipid distributions in the nearshore environments. The TEX^{L}_{86} calibration showed larger variance between sites than the TEX^{H}_{86} calibration. However, Mg/Ca and $\delta^{18}O$ records indicated spatially similar anomalies during the PETM on the New Jersey paleoshelf. Thus, TEX^{H}_{86} from distal sites provided more plausible temperature estimates reflecting a warming of 6°C. Altogether, TEX^{H}_{86} and *Subbotina* spp. Mg/Ca, $\delta^{18}O$ suggested a ~6-7°C warming in the thermocline with minimal changes in salinity. Oxygen isotopic records of surface dwelling taxa from the low-mid latitudinal sections should be used cautiously in SST reconstructions for the PETM because of possible shifts in timing of their calcification.

3.7 Acknowledgments

My acknowledgements go to Rutgers Graduate School New Brunswick and Geological Society of America for research grants. I am grateful to Dr. Timothy D. Herbert for the opportunity to work in the organic geochemistry laboratory at Brown University and Shuo (Aaron) Yang, Dr. Alexandrina Tzanova, Rafael Tarozo, Dr. Marcelo Da Rosa Alexandre, and Laura Messier for their help with the lipid biomarker analyses. I also thank Dr. Yair Rosenthal, Dr. Tali L. Babila, Dr. Xiaoli Zhou, and Kaixuan (Ryan) Bu for the help with trace element analyses.

3.8 References

Anand, P., H. Elderfield, and M.H. Conte (2003), Calibration of Mg/Ca thermometry in planktonic foraminifera from a sediment trap time series, Paleoceanography, 18/2, 1–15; doi:10.1029/2002PA000846.

Aze, T., P.N. Pearson, A.J. Dickson, M.P.S. Badger, P.R. Bown, R.D. Pancost, S.J. Gibbs, B.T. Huber, M.J. Leng, A.L. Coe, A.S. Cohen, and G.L. Foster (2014), Extreme warming of tropical waters during the Paleocene–Eocene Thermal Maximum, Geology, 42(9), 739–742, doi:10.1130/G35637.1.

Babila, T.L. (2014), Boron/calcium in planktonic foraminifera: proxy development and application to the Paleocene-Eocene boundary, Ph.D. Thesis, Rutgers University, 140 p.

Babila, T.L., Y. Rosenthal, J.D. Wright, and K.G. Miller (2016), A continental shelf perspective of ocean acidification and temperature evolution during the Paleocene-Eocene Thermal Maximum, Geology, 44(4), 275–278, doi:10.1130/G37522.1.

Bé, A.W.H. (1960), Ecology of recent planktonic foraminifera: Part 2—Bathymetric and seasonal distributions in the Sargasso Sea off Bermuda, Micropaleontology, 6(4), 373–392.

Bijma, J., W.W. Faber Jr., and C. Hemleben (1990), Temperature and salinity limits for growth and survival of some planktonic foraminifers in laboratory cultures, Journal of Foraminiferal Research, 20(2), 95–116.

Boyle, E.A. and L.D. Keigwin (1985), Comparison of Atlantic and Pacific paleochemical records for the last 215,000 years: changes in deep ocean circulation and chemical inventories, Earth and Planetary Science Letters, 76, 135–150.

Bralower, T.J., J.C. Zachos, E. Thomas, M. Parrow, C.K. Paull, D.C. Kelly, I. Premoli Silva, W.V. Sliter, and K.C. Lohmann (1995), Late Paleocene to Eocene paleoceanography of the equatorial Pacific Ocean: stable isotopes recorded at Ocean Drilling Program Site 865, Allison Guyot, Paleoceanography, 10, 841–865.

Caballero, R. and P.L. Langen (2005), The dynamic range of poleward energy transport in an atmospheric general circulation model, Geophysical Research Letters, 32, L02705, doi:10.1029/2004GL021581.

Carmichael, M.J., D.J. Lunt, M. Huber, M. Heinemann, J. Kiehl, A. LeGrande, C.A. Loptson, C.D. Roberts, N. Sagoo, C. Shields, P.J. Valdes, A. Winguth, C. Winguth, and R.D. Pancost (2016), A model–model and data–model comparison for the early Eocene hydrological cycle, Climate of the Past, 12, 455–481, doi:10.5194/cp-12-455-2016.

Cui, Y., L.R. Kump, A.J. Ridgwell, A.J. Charles, C.K. Junium, A.F. Diefendorf, K.H. Freeman, N.M. Urban, and I.C. Harding (2011), Slow release of fossil carbon during the Palaeocene–Eocene Thermal Maximum, Nature Geoscience, 4, 481–485, doi:10.1038/NGEO1179.

Cramer, B.S., M.-P. Aubry, K.G. Miller, R.K. Olsson, J.D. Wright, and D.V. Kent (1999), An exceptional chronologic, isotopic, and clay mineralogic record at the

latest Paleocene thermal maximum, Bass River, NJ, ODP 174AX, Bulletin de la Société géologique de France, 170(6), 883–897.

Curry, W.B., R.C. Thunell, and S. Honjo (1983), Seasonal changes in the isotopic composition of planktonic foraminifera collected in Panama Basin sediment traps, Earth and Planetary Science Letters, 64, 33–43.

Deuser, W.G. and E.H. Ross (1989), Seasonally abundant planktonic foraminifera of the Sargasso Sea: Succession, deep-water fluxes, isotopic compositions, and paleoceanographic implications, Journal of Foraminiferal Research, 19(4), 268–293.

Dunkley Jones, T., D.J. Lunt, D.N. Schmidt, A. Ridgwell, A. Sluijs, P.J. Valdes, and M. Maslin (2013), Climate model and proxy data constraints on ocean warming across the Paleocene-Eocene Thermal Maximum, Earth-Science Reviews, 125, 123–145, doi:10.1016/j.earscirev.2013.07.004.

Elling, F.J., M. Könneke, M. Mußmann, A. Greve, and K.-U. Hinrichs (2015), Influence of temperature, pH, and salinity on membrane lipid composition and TEX_{86} of marine planktonic thaumarchaeal isolates, Geochimica et Cosmochimica Acta, 171, 238–255.

Evans, D., N. Sagoo, W. Renema, L.J. Cotton, W. Müller, J.A. Todd, P. Kumar Saraswati, P. Stassen, M. Ziegler, P.N. Pearson, P.J. Valdes, and H.P. Affek (2018), Eocene greenhouse climate revealed by coupled clumped isotope-Mg/Ca thermometry, PNAS, 201714744, 1–6, doi:10.1073/pnas.1714744115.

Fairbanks, R.G. and P.H Wiebe (1980) Foraminifera and chlorophyll maximum: vertical distribution, seasonal succession, and paleoceanographic significance, Science, 209(4464), 1524–1526, doi:10.1126/science.209.4464.1524.

Fairbanks, R.G., M. Sverdlove, R. Free, P.H. Wiebe, and A.W.H. Bé (1982), Vertical distribution and isotopic fractionation of living planktonic foraminifera in the Panama Basin, Nature, 298, 841–844.

Frieling, J., H. Gebhardt, M. Huber, O.A. Adekeye, S.O. Akande, G.-J. Reichart, J.J. Middelburg, S. Schouten, and A. Sluijs (2017), Extreme warmth and heat-stressed plankton in the tropics during the Paleocene-Eocene Thermal Maximum. Science Advances, 3, e1600891, 1–9.

Frieling, J., G.-J. Reichart, J.J. Middelburg, U. Röhl, T. Westerhold, S.M. Bohaty, and A. Sluijs (2018), Tropical Atlantic climate and ecosystem regime shifts during the Paleocene–Eocene Thermal Maximum, Climate of the Past, 14, 39–55.

Gibson, T.G., L.M. Bybell, and J.P. Owens (1993), Latest Paleocene lithologic and biotic events in neritic deposits of southwestern New Jersey, Paleoceanography, 8(4), 495–514.

Giusberti, L., D. Rio, C. Agnini, J. Backman, E. Fornaciari, F. Tateo, and M. Oddone (2007), Mode and tempo of the Paleocene-Eocene thermal maximum in an expanded section from the Venetian pre-Alps, Geological Society of America Bulletin, 119, 391–412, doi:10.1130/B25994.1.

Harding, I.C., A.J. Charles, J.E.A. Marshall, H. Pälike, A.P. Roberts, P.A. Wilson, E. Jarvis, R. Thorne, E. Morris, R. Moreman, R. Pearce, and S. Akbari, (2011), Sea

level and salinity fluctuations during the Palaeocene/Eocene thermal maximum in Arctic Spitsbergen. Earth and Planetary Science Letters, 303, 97–107.

Ho, S.L. and T. Laepple (2016), Flat meridional temperature gradient in the early Eocene in the subsurface rather than surface ocean, Nature Geoscience, 9, 606–610, doi:10.1038/NGEO2763.

Hollis, C.J., B.R. Hines, K. Littler, V. Villasante-Marcos, D.K. Kulhanek, C.P. Strong, J.C. Zachos, S.M. Eggins, L. Northcote, and A. Phillips (2015), Onset of the Paleocene–Eocene Thermal Maximum in the southern Pacific Ocean (DSDP Site 277, Campbell Plateau), Climate of the Past Discussions, 11, 243–278, doi:10.5194/cpd-11-243-2015.

Hopmans, E.C., S. Schouten, R.D. Pancost, M.T.J. van der Meer, and J.S. Sinninghe Damsté (2000), Analysis of intact tetraether lipids in archaeal cell material and sediments using high performance liquid chromatography/atmospheric pressure ionization mass spectrometry, Rapid Communications in Mass Spectrometry, 14, 585–589.

Hopmans, E.C., S. Schouten, and J.S. Sinninghe Damsté (2016), The effect of improved chromatography on GDGT-based palaeoproxies, Organic Geochemistry, 93, 1–6.

Huguet, C., A. Schimmelmann, R. Thunell, L.J. Lourens, J.S. Sinninghe Damsté, and S. Schouten (2007), A study of the TEX_{86} paleothermometer in the water column and sediments of the Santa Barbara Basin, California, Paleoceanography, PA3203, 1–9, doi:10.1029/2006PA001310.

Hurley, S.J., F.J. Elling, M. Könneke, C. Buchwald, C.D. Wankel, A.E. Santoro, J.S. Lipp, K.-U. Hinrichs, and A. Pearson (2016), Influence of ammonia oxidation rate on thaumarchaeal lipid composition and the TEX_{86} temperature proxy, PNAS, 113(28), 7762–7767.

John, C.M., S.M. Bohaty, J.C. Zachos, A. Sluijs, S. Gibbs, H. Brinkhuis, and T.J. Bralower (2008), North American continental margin records of the Paleocene-Eocene thermal maximum: Implications for global carbon and hydrological cycling, Paleoceanography, 23, 1–20, doi:10.1029/2007PA001465.

Katz, M.E., D.K. Pak, G.R. Dickens, and K.G. Miller (1999), The source and fate of massive carbon input during the latest Paleocene Thermal Maximum, Science, 286, 1531–1533.

Kennett, J.P. and L.D. Stott (1991), Abrupt deep-sea warming, palaeoceanographic changes and benthic extinctions at the end of the Palaeocene, Nature, 353, 225–229.

Karner, M.B., E.F. DeLong, and D.M. Karl (2001), Archaeal dominance in the Mesopelagic zone of the Pacific Ocean, Nature, 409, 507–510.

Kiehl, J.T. and C.A. Shields (2013), Sensitivity of the Palaeocene-Eocene Thermal Maximum climate to cloud properties, Philosophical Transactions of the Royal Society A: Mathematical, Physical and Engineering Sciences, 371(2001), 20130093–20130093, doi:10.1098/rsta.2013.0093.

Kim, J.-H., J. van der Meer, S. Schouten, P. Helmke, V. Willmott, F. Sangiorgi, N. Koc, E.C. Hopmans, and J.S. Sinninghe Damsté (2010), New indices and calibrations derived from the distribution of crenarchaeal isoprenoid tetraether lipids:

implications for past sea surface temperature reconstructions, Geochimica et Cosmochimica Acta, 74, 4639–4654.

Kim, J.-H., S. Schouten, M. Rodrigo-Gámiz, S. Rampen, G. Marino, C. Huguet, P. Helmke, R. Buscail, E.C. Hopmans, J. Pross, F. Sangiorgi, J.B.M. Middelburg, and J.S. Sinninghe Damsté (2015), Influence of deep-water derived isoprenoid tetraether lipids on the TEX^{H}_{86} paleothermometer in the Mediterranean Sea, Geochimica et Cosmochimica Acta, 150, 125–141.

Kim, J.-H., L. Villanueva, C. Zell, and J.S. Sinninghe Damsté (2016), Biological source and provenance of deep-water derived isoprenoid tetraether lipids along the Portuguese continental margin, Geochimica et Cosmochimica Acta, 172, 177–204.

Könneke, M, A.E. Bernhard, J.R. de la Torre, C.B. Walker, J.B. Waterbury, and D.A. Stahl (2005), Isolation of an autotrophic ammonia-oxidizing marine archaeon, Nature, 437, 543–546.

Könneke, M., D.M. Schubert, P.C. Brown, M. Hügler, S. Standfest, T. Schwander, L. Schada von Borzyskowski, T.J. Erb, D.A. Stahl, and I.A. Berg (2014), Ammonia-oxidizing archaea use the most energy-efficient aerobic pathway for CO_2 fixation, PNAS, 1–6.

Kopp, R.E., D. Schumann, T.D. Raub, D.S. Powars, L.V. Godfrey, N.L. Swanson-Hysell, A.C. Maloof, and H. Vali (2009), An Appalachian Amazon? Magnetofossil evidence for the development of a tropical river-like system in the mid-Atlantic United States during the Paleocene-Eocene thermal maximum, Paleoceanography, 24, 1–17, doi:10.1029/2009PA001783.

Leider, A., K.-U. Hinrichs, G. Mollenhauer, and G.J.M. Versteegh (2010), Core-top calibration of the lipid-based $U^{K'}_{37}$ and TEX_{86} temperature proxies on the southern Italian shelf (SW Adriatic Sea, Gulf of Taranto), Earth and Planetary Science Letters 300, 112–124.

Liu, Z., M. Pagani, D. Zinniker, R. DeConto, M. Huber, H. Brinkhuis, S.R. Shah, R.M. Leckie, A. Pearson (2009), Global Cooling During the Eocene-Oligocene Climate Transition, Science, 323(5918), 1187–1190, doi:10.1126/science.1166368.

Lombardi, C.J. (2013), Lithostratigraphy and clay mineralogy of Paleocene-Eocene thermal maximum sediments at Wilson Lake, NJ, M.S. Thesis, Rutgers University, 94 p.

Lu, G. and G. Keller (1993), The Paleocene-Eocene transition in the Antarctic Indian Ocean: Inference from planktic foraminifera, Marine Micropaleontology, 21, 101–142.

Lu, G., T. Adatte, G. Kelly, and N. Ortiz (1998), Abrupt climatic, oceanographic and ecologic changes near the Paleocene-Eocene transition in the deep Tethys basin: The Alademilla section, southern Spain, Eclogae Geologicae Helvetiae, 91, 293–306.

Makarova, M., J.D. Wright, K.G. Miller, T.L. Babila, Y. Rosenthal, and J.I.Park (2017), Hydrographic and ecologic implications of foraminiferal stable isotopic response across the U.S. mid-Atlantic continental shelf during the Paleocene-Eocene Thermal Maximum, Paleoceanography, 32, 1–18, doi:10.1002/2016PA002985.

Miller, K.G., P.J. Sugarman, J.V. Browning, M.-P. Aubry, G.J. Brenner, G.III Cobbs, L. de Romero, M.D. Feigenson, A. Harris, M.E. Katz, A. Kulpecz, P.P.Jr. McLaughlin, S. Misintseva, D.H. Monteverde, R.K. Olsson, L. Patrick, S.J. Pekar, and J. Uptegrove (2005), Millville site, in K.G. Miller, P.J. Sugarman, J.V. Browning et al., Proceedings of the Ocean Drilling Program, Scientific results, Volume 174AX (supplement): College Station, Texas, Ocean Drilling Program, 1–95.

Murphy, B.H., K.A. Farley, and J.C. Zachos (2010), An extraterrestrial ^{3}He-based timescale for the Paleocene-Eocene Thermal Maximum (PETM) from Walvis Ridge, IODP Site 1266, Geochimica et Cosmochimica Acta, 74, 5098–5108.

O'Neil, J. R., R. N. Clayton, and T. K. Mayeda (1969), Oxygen isotope fractionation in divalent metal carbonates, Journal of Chemical Physics, 51/12, 5547–5558.

Pagani, M., N. Pedentchouk, M. Huber, A. Sluijs, S. Schouten, H. Brinkhuis, J.S. Sinninghe Damsté, G.R. Dickens, and the Expedition 302 Scientists (2006), Arctic hydrology during global warming at the Palaeocene/Eocene thermal maximum, Nature, 442, 671–675.

Pearson, A., A.P. McNichol, B.C. Benitez-Nelson, J.M. Hayes, and T.I. Eglinton (2001) Origins of lipid biomarkers in Santa Monica Basin surface sediment: A case study using compound-specific Δ^{14}C analysis, Geochimica et Cosmochimica Acta, 65(18), 3123–3137.

Pearson, P.N., P.W. Ditchfield, J. Singano, K.G. Harcourt-Brown, C.J. Nicholas, R.K. Olsson, N.J. Shackleton, and M.A. Hall (2001), Warm tropical sea surface temperatures in the Late Cretaceous and Eocene epochs, Nature, 413, 481–487.

Pearson., A. and A.E. Ingalls (2013), Assessing the use of archaeal lipids as marine environmental proxies, Annual Review of Earth and Planetary Sciences, 41, 359–384, doi:10.1146/annurev-earth-050212-123947.

Pearson, A. S.J. Hurley, S.R. Shah Walter, S. Kusch, S. Lichtin, and Y. Ge Zhang (2016), Stable carbon isotope ratios of intact GDGTs indicate heterogeneous sources to marine sediments, Geochimica et Cosmochimica Acta, 181, 18–35.

Qin, W., L.T. Carlson, E.V. Armbrust, A.H. Devol, J.W. Moffett, D.A. Stahl, and A.E. Ingalls (2015), Confounding effects of oxygen and temperature on the TEX_{86} signature of marine Thaumarchaeota, PNAS, 112 (35), 10979–10984.

Ravelo, A.C., and R.G. Fairbanks (1992), Oxygen isotopic composition of multiple species of planktonic foraminifera: Recorders of the modern photic zone temperature gradient, Paleoceanography, 7(6), 815–831, doi:10.1029/92PA02092.

Röhl, U., T. Westerhold, T.J. Bralower, and J.C. Zachos (2007), On the duration of the Paleocene-Eocene Thermal Maximum (PETM), Geochemistry Geophysics Geosystems, 8, Q12002, doi:10.1029/2007GC001784.

Rosenthal, Y., E.A. Boyle, and N. Slowey (1997), Temperature control on the incorporation of magnesium, strontium, fluorine, and cadmium into benthic foraminiferal shells from Little Bahama Bank: Prospects for thermocline paleoceanography, Geochimica at Cosmochimica Acta, 61(17), 3633–3643.

Rosenthal, Y., M.P. Field, and R.M. Sherrell (1999), Precise Determination of Element/Calcium Ratios in Calcareous Samples Using Sector Field Inductively

Coupled Plasma Mass Spectrometry, Analytical Chemistry, 71, 3248–3253.

Schmitz, B., and V. Pujalte (2003), Sea-level, humidity, and land-erosion records across the initial Eocene thermal maximum from a continental-marine transect in northern Spain, Geology, 31, 689–692, doi:10.1130/ G19527.1.

Schmitz, B., and V. Pujalte (2007), Abrupt increase in seasonal extreme precipitation at the Paleocene-Eocene boundary, Geology, 35, 215–218, doi:10.1130/G23261A.1.

Schouten, S., E.C. Hopmans, E. Schefuß, and J.S. Sinninghe Damsté (2002), Distributional variations in marine crenarchaeotal membrane lipids: A new tool for reconstructing ancient sea water temperatures?, Earth and Planetary Science Letters, 204(1–2), 265–274.

Schouten, S., C. Huguet, E.C. Hopmans, M.V.M. Kienhuis, and J.S. Sinninghe Damsté (2007a), Analytical methodology for TEX_{86} paleothermometry by High-Performance Liquid Chromatography/Atmospheric Pressure Chemical Ionization-Mass Spectrometry, Analytical Chemistry, 79, 2940–2944.

Schouten, S., A. Forster, F.E. Panoto, and J.S. Sinninghe Damsté (2007b), Towards calibration of the TEX_{86} palaeothermometer for tropical sea surface temperatures in ancient greenhouse worlds, Organic Geochemistry, 38, 1537–1546.

Schouten, S., E.C. Hopmans, and J.S. Sinninghe Damsté (2013), The organic geochemistry of glycerol dialkyl glycerol tetraether lipids: A review, Organic Geochemistry, 54, 19–61.

Sexton, P.F., P.A. Wilson, and P.N. Pearson (2006), Microstructural and geochemical perspectives on planktic foraminiferal preservation: “Glassy” versus “frosty”, Geochemistry Geophysics Geosystems, 7, Q12P19, doi:10.1029/2006GC001291.

Si, W. and M.-P. Aubry (2018), Vital effects and ecologic adaptation of photosymbiont-bearing planktonic foraminifera during the Paleocene-Eocene Thermal Maximum, implications for paleoclimate, Paleoceanography and Paleoclimatology, 33, 1–14, https://doi.org/ 10.1002/2017PA003219.

Sluijs, A., H. Brinkhuis, S. Schouten, S.M. Bohaty, C.M. John, J.C. Zachos, G.J. Reichart, J.S. Sinninghe Damsté, E.M. Crouch, and G.R. Dickens (2007), Environmental precursors to rapid light carbon injection at the Palaeocene/Eocene boundary, Nature, 450(7173), 1218–1221, doi:10.1038/nature06400.

Sluijs, A., L. van Roij, G.J. Harrington, S. Schouten, J A. Sessa, L.J. LeVay, G.-J. Reichart, and C.P. Slomp (2014), Warming, euxinia and sea level rise during the Paleocene–Eocene Thermal Maximum on the Gulf Coastal Plain: implications for ocean oxygenation and nutrient cycling, Climate of the Past, 10, 1421–1439, doi:10.5194/cp-10-1421-2014.

Sluijs, A. and H. Brinkhuis (2009), A dynamic climate and ecosystem state during the Paleocene-Eocene Thermal Maximum: inferences from dinoflagellate cyst assemblages on the New Jersey Shelf, Biogeosciences, 6, 1755–1781.

Shah, S.R., G. Mollenhauer, N. Ohkouchi, T.I. Eglinton, and A. Pearson (2008), Origins of archaeal tetraether lipids in sediments: Insights from radiocarbon analysis, Geochimica et Cosmochimica Acta, 72, 4577–4594.

Taylor, K.W.R., M. Huber, C.J. Hollis, M.T. Hernandez-Sanchez, and R.D. Pancost (2013), Re-evaluating modern and Palaeogene GDGT distributions: Implications

for SST reconstructions, Global and Planetary Change, 108, 158–174.

Tierney, J.E. (2014), Biomarker-based inferences of past climate: The TEX_{86} paleotemperature proxy, in K.K. Turekian and H.D. Holland (eds.), Treatise on Geochemistry, 12, 379–393.

Tierney, J.E. and M.P. Tingley (2015), A TEX_{86} surface sediment database and extended Bayesian calibration, Scientific Data, 2:150029, 1–10, doi:10.1038/sdata.2015.29.

Thunell, R.C., W.B. Curry, and S. Honjo (1983), Seasonal variations in the flux of planktonic foraminifera: Time series sediment trap results from the Panama Basin, Earth and Planetary Science Letters, 64, 44–55.

Thomas, D.J., T.J. Bralower, and J.C. Zachos (1999), New evidence for subtropical warming during the late Paleocene thermal maximum: Stable isotopes from Deep Sea Drilling Project Site 527, Walvis Ridge, Paleoceanography, 14(5), 561–570.

Thomas, D.J., J.C. Zachos, T.M. Bralower, E. Thomas, and S. Bohaty (2002), Warming the fuel for the fire: Evidence for the thermal dissociation of methane hydrate during the Paleocene-Eocene thermal maximum, Geology, 30(12), 1067–1070.

Tolderlund, D.S and A.W.H. Bé (1971), Seasonal distribution of planktonic foraminifera in the western North Atlantic, Micropaleontology, 17(3), 297–329.

Tripati, A.K. and H. Elderfield (2004), Abrupt hydrographic changes in the equatorial Pacific and subtropical Atlantic from foraminiferal Mg/Ca indicate greenhouse origin for the thermal maximum at the Paleocene-Eocene Boundary, Geochemistry Geophysics Geosystems, 5(2), 1–11, doi:10.1029/2003GC000631.

Turich, C., K.H. Freeman, M.A. Bruns, M.H. Conte, A.D. Jones, and S.G. Wakeham (2007), Lipids of marine archaea: Patterns and provenance in the water-column and sediments, Geochimica et Cosmochimica Acta, 71, 3272–3291.

Wei, Y., J. Wang, J. Liu, L. Dong, L. Li, H. Wang, P. Wang, M. Zhao, and C.L. Zhang (2011), Spatial variations in Archaeal lipids of surface water and core-top sediments in the South China Sea: implications for paleoclimate studies. Applied and Environmental Microbiology 77, 7479–7489, doi:10.1128/AEM.00580-11.

Wolfteich, C.M. (1994), Satellite-derived sea surface temperature, mesoscale variability, and foraminiferal production in the North Atlantic, M.S. Thesis, the Massachusetts Institute of Technology/Woods Hole Oceanographic Institution, 91 p.

Wuchter, C., S. Schouten, M.J.L. Coolen, and J.S. Sinninghe Damsté (2004), Temperature-dependent variation in the distribution of tetraether membrane lipids of marine Crenarchaeota: Implications for TEX_{86} paleothermometry, Paleoceanography, 19, 1–10, PA4028, doi:10.1029/2004PA001041.

Zachos, J.C., M.W. Wara, S.M. Bohaty, M.L. Delaney, M. Rose-Petrizzo, A. Brill, T.J. Bralower, and I. Premoli-Silva (2003), A transient rise in tropical sea surface temperature during the Paleocene-Eocene thermal maximum, Science, 302, 1551–1554.

Zachos, J.C., S. Schouten, S. Bohaty, T. Quattlebaum, A. Sluijs, H. Brinkhuis, S.J. Gibbs, and T.J. Bralower (2006), Extreme warming of mid-latitude coastal ocean during the Paleocene-Eocene Thermal Maximum: Inferences from TEX_{86} and isotope data, Geology, 34(9), 737–740.

Zhu, C., S.G. Wakeham, F.J. Elling, A. Basse, G. Mollenhauer, G.J.M. Versteegh, M. Könneke, and K.-U. Hinrichs (2016), Stratification of archaeal membrane lipids in the ocean and implications for adaptation and chemotaxonomy of planktonic archaea, Environmental Microbiology, 18(12), 4324–4336, doi:10.1111/1462-2920.13289.

3.9 Figures

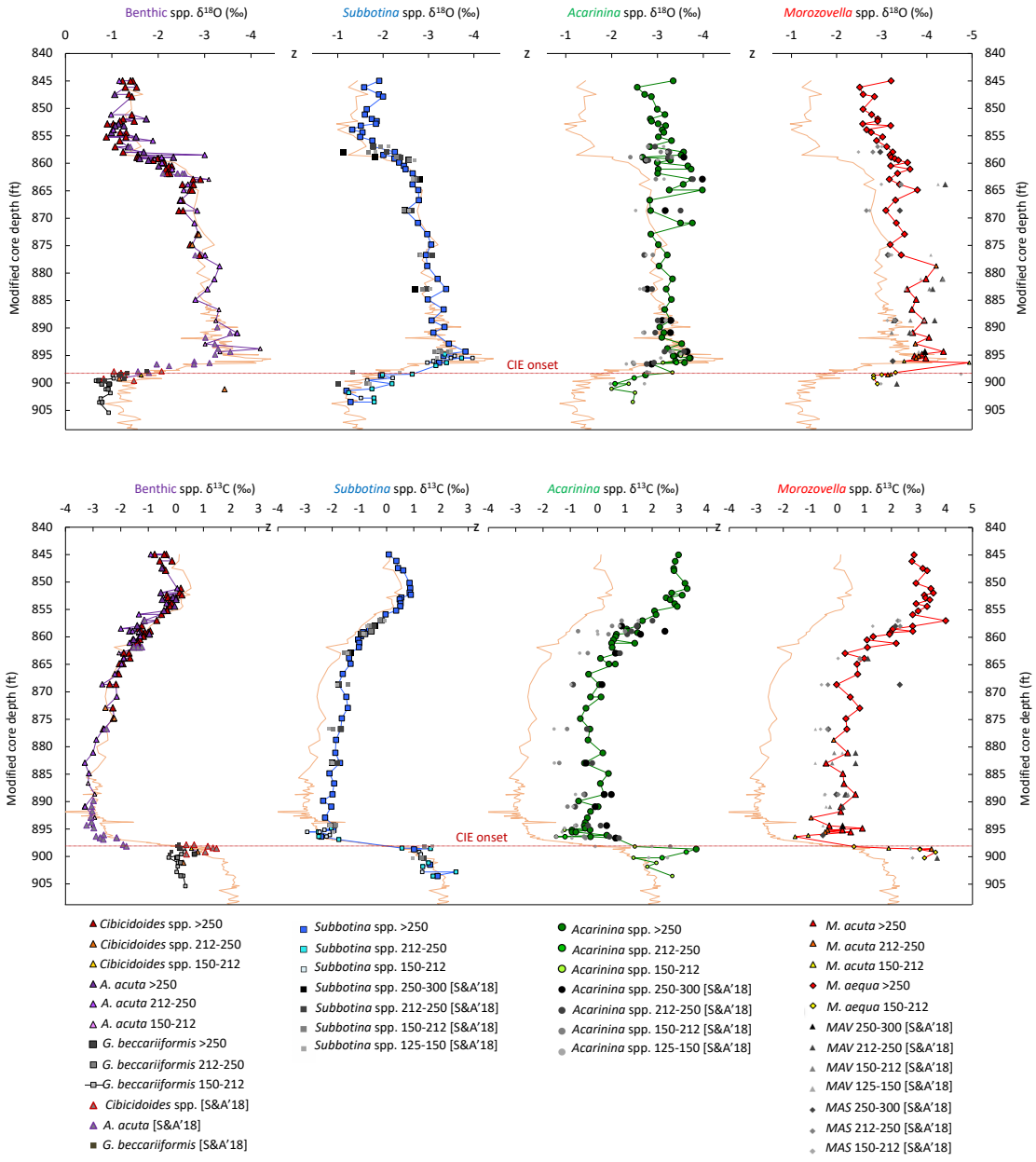

Fig. 3.1. Carbon (lower panel) and oxygen (upper panel) isotopic records of multispecimen samples of foraminifera at Millville, NJ: benthic *Cibicidoides* spp. (brown), *A. acuta* (purple), *G. beccariiformis* (gray); thermocline dwelling *Subbotina* spp. (blue); surface dwelling *Acarinina* spp. (green), *M. acuta* (red triangulars) and *M. aequa* (red diamonds). Samples contain spesimens from one size fraction (>250, 200-250, or 150-200 μm) with larger spesimens highlighted in darker shades and smaller spesimens in lighter. Isotopic values are given in Table 2.1 in Chapter Two. Data from Si and Aubry [2018] are plotted in black symbols.

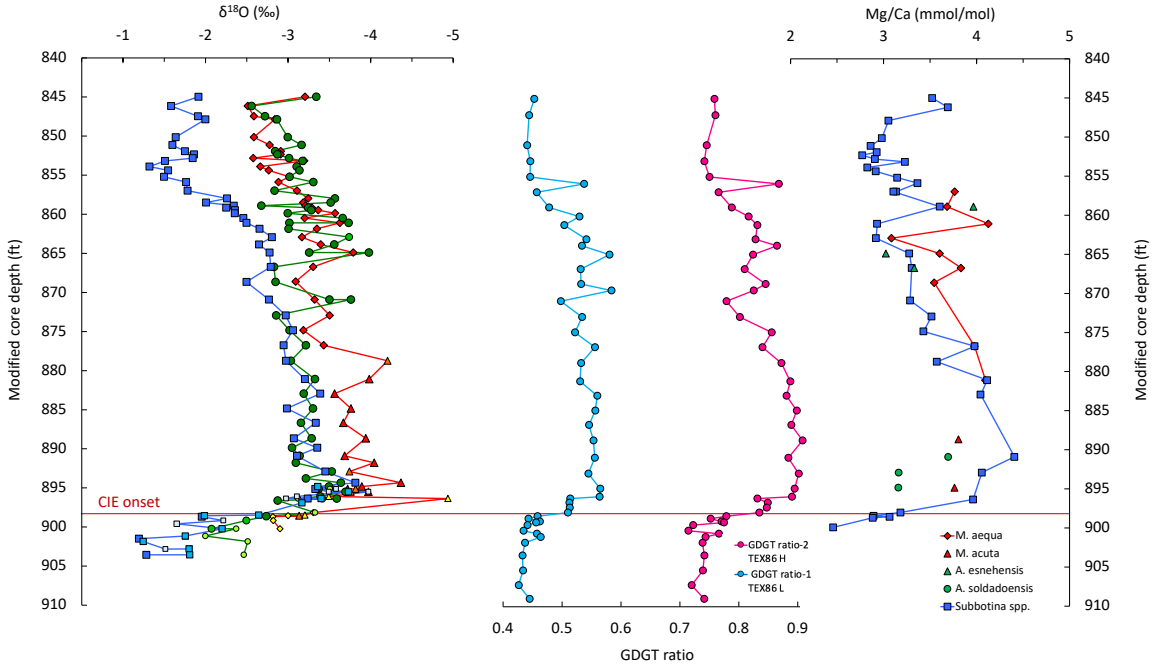

Fig. 3.2. Multiproxy records used for temperature reconstructions at Millville, NJ: $\delta^{18}O$ and Mg/Ca of surface dwelling (*Morozovella* spp. in red; *Acarinina* spp. in green) and thermocline dwelling (*Subbotina* spp. in blue) foraminifera and TEX_{86} expressed as GDGT ratio-1 (TEX^{L}_{86}) and GDGT ratio-2 (TEX^{H}_{86}) [Kim et al., 2010]. See fig. 3.1 for labels of planktonic foraminiferal $\delta^{18}O$ symbols.

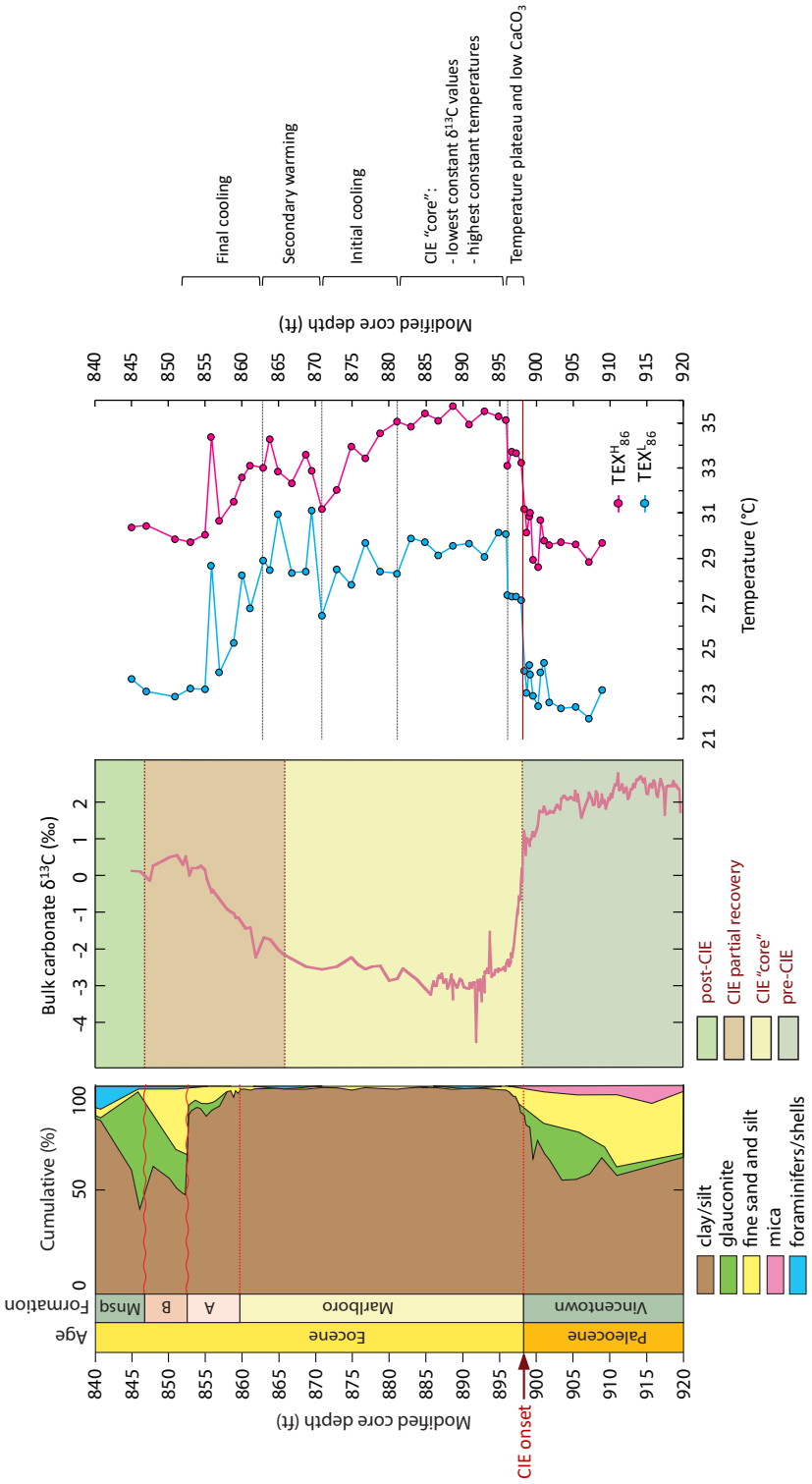

Fig. 3.3. TEX_{86}-derived temperature estimates at Millville, NJ. Calibration errors for TEX^{H}_{86} and TEX^{L}_{86} are ±2.5°C and ±4°C, respectively [Kim et al., 2010]. Lithology and bulk carbonate $\delta^{13}C$ record are from Makarova et al. [2017] and Wright and Schaller [2013].

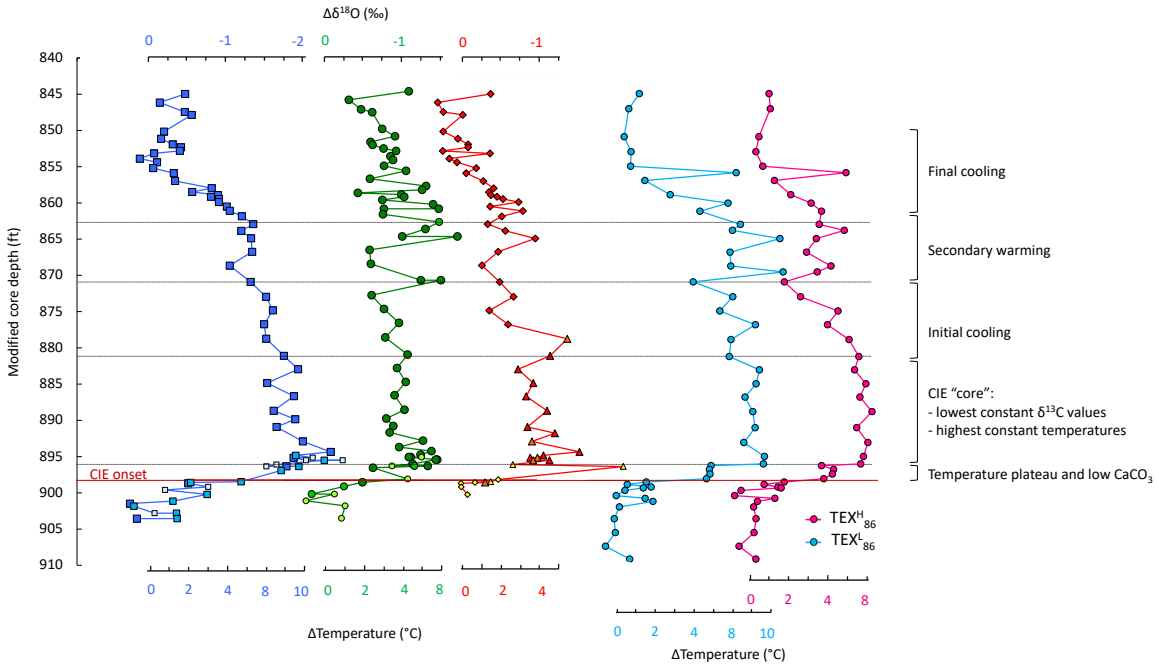

Fig. 3.4. Temperature anomaly (Δ) at Millville, NJ estimated from $\Delta\delta^{18}O$ values of surface dwelling (*Morozovella* spp. in red; *Acarinina* spp. in green) and thermocline dwelling dwelling (*Subbotina* spp. in blue) foraminifera considering a 0.25‰/°C gradient [O'Neil et al., 1969] and TEX_{86} indices from Kim et al. [2010]. Calibration errors for TEX^{H}_{86} and TEX^{L}_{86} are ±2.5°C and ±4°C, respectively [Kim et al., 2010]. See fig. 3.1 for labels of planktonic foraminiferal $\delta^{18}O$ symbols.

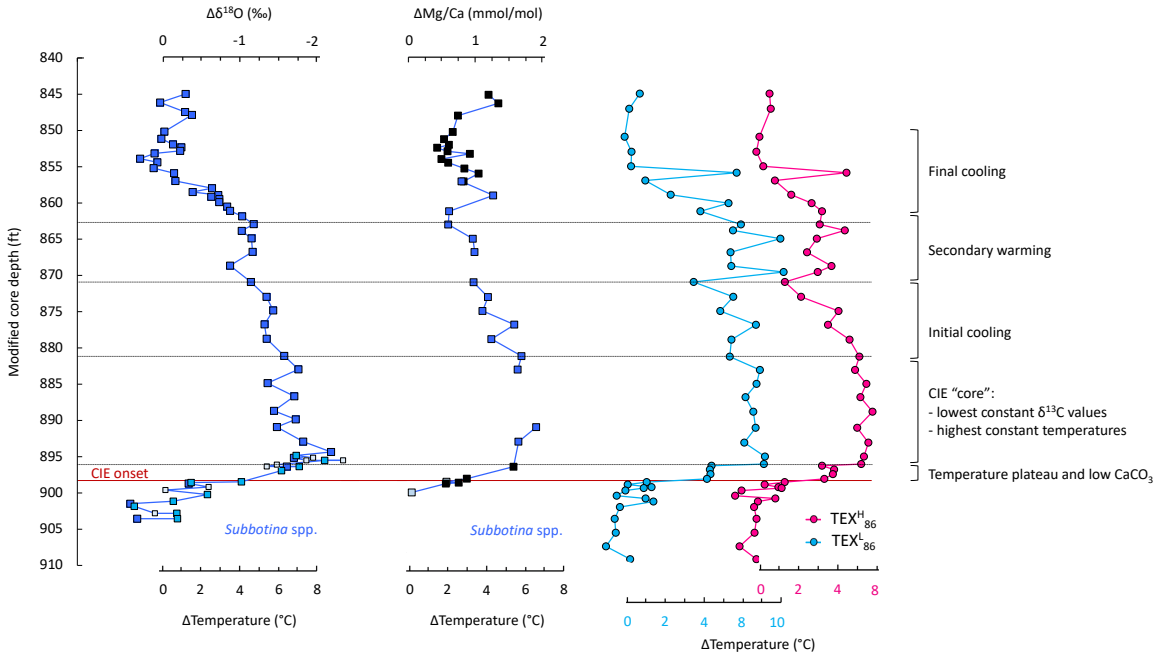

Fig. 3.5. Temperature anomaly (Δ) at Millville, NJ estimated from $\Delta\delta^{18}O$ (0.25‰/°C gradient; O'Neil et al. [1969]) and Mg/Ca values of thermocline dwelling *Subbotina* spp. and TEX_{86} indices from Kim et al. [2010]. Mg/Ca values calibrated to temperatures using Anand et al. [2003] multispecies equation (calibration error is ±1°C). Different colors for Mg/Ca symbols indicate separate analyses performed in May 2013 (light blue), October 2013 (blue), and June 2018 (black). Calibration errors for TEX^{H}_{86} and TEX^{L}_{86} are ±2.5°C and ±4°C, respectively [Kim et al., 2010]. See fig. 3.1 for labels of $\delta^{18}O$ symbols.

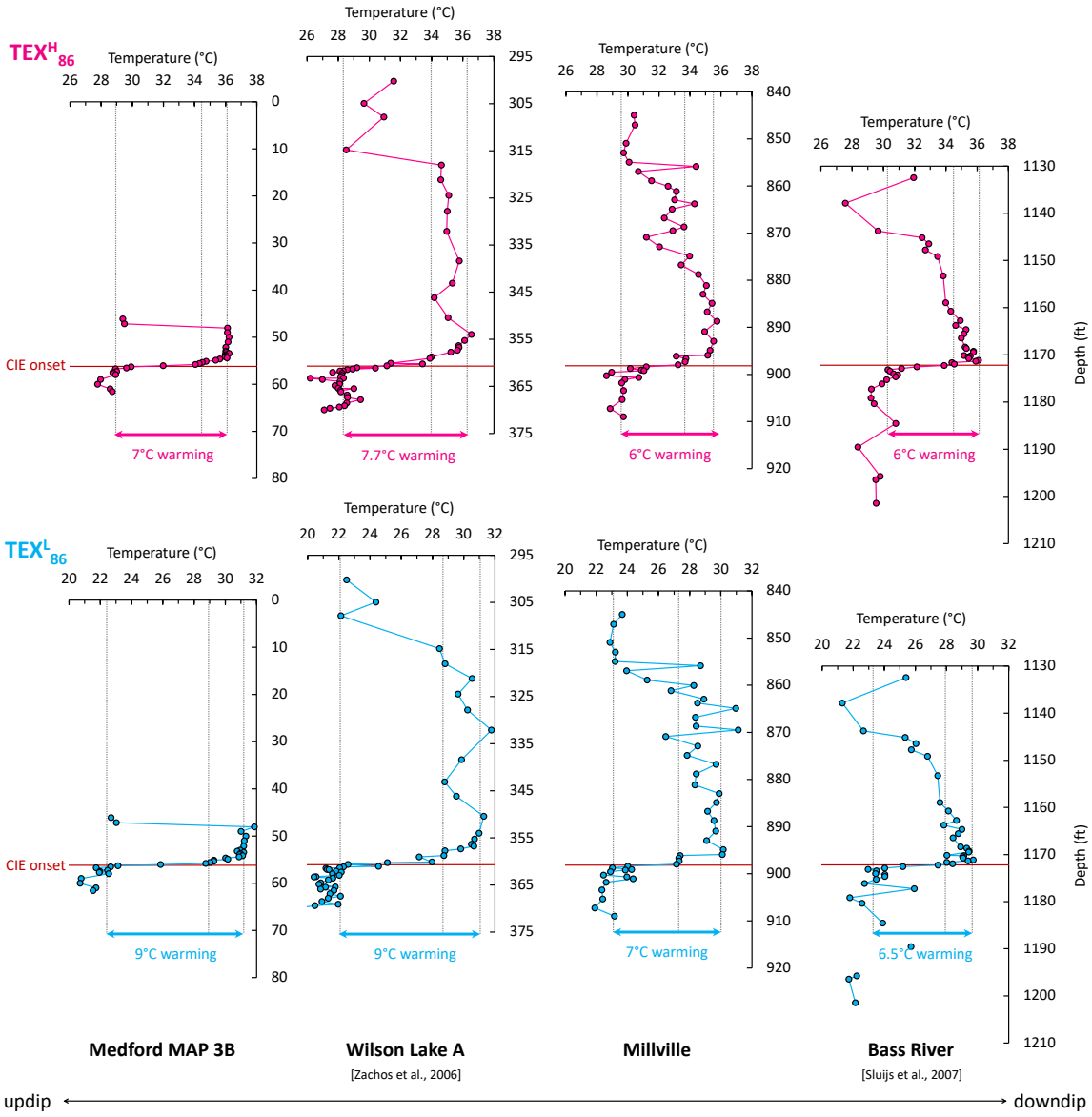

Fig. 3.6. TEX^H_{86} (upper panel) and TEX^L_{86} (lower panel) calibrated temperature records from New Jersey coastal plain sites Medford MAP 3B, Wilson Lake Hole A, Millville, and Bass River aligned by the PETM/CIE onset. See fig. 2.1 in Chapter Two for the location map. TEX^H_{86}-derived records at updip Medford and Wilson Lake show ~7°C temperature increase associated with the PETM onset and downdip Millville and Bass River indicate less warming of 6°C. TEX^H_{86}-based estimates from all sites reveal temperature maximum at 36°C and a two-step warming with a temperature plateau at 33.5-34°C. TEX^L_{86} estimated temperatures are lower and indicated a larger temperature anomaly than TEX^H_{86} in each site. Calibration errors for TEX^H_{86} and TEX^L_{86} are ±2.5°C and ±4°C, respectively [Kim et al., 2010].

Supporting figures

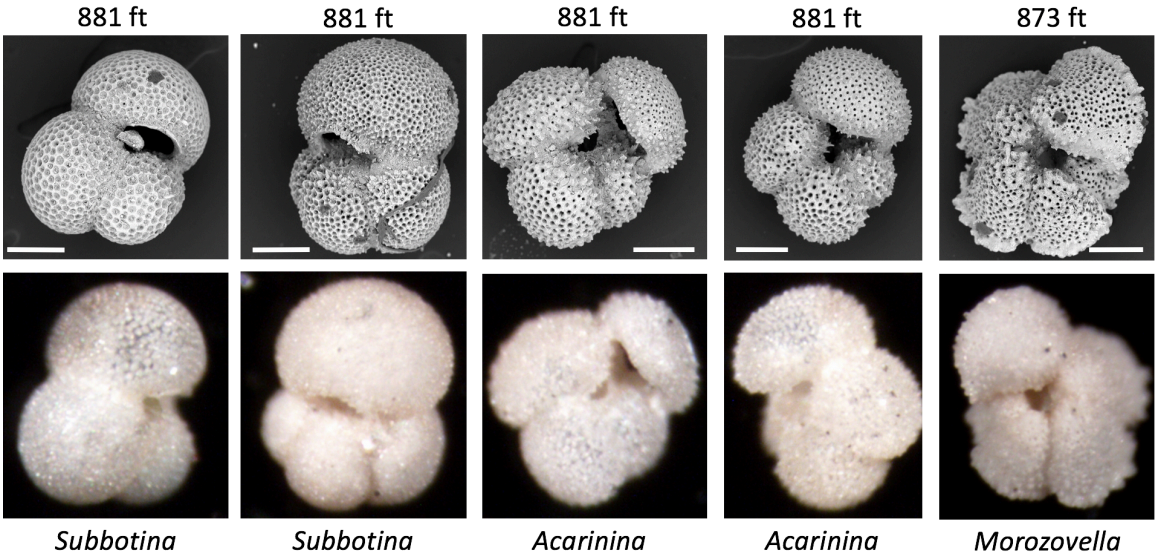

Fig. 3.S1. Scanning electron microscopy (SEM) and optical photographs of planktonic foraminifera from clayey silts of the Marlboro Formation at Millville, NJ showing excellent preservation of tests. Scale bar is 100 μm.

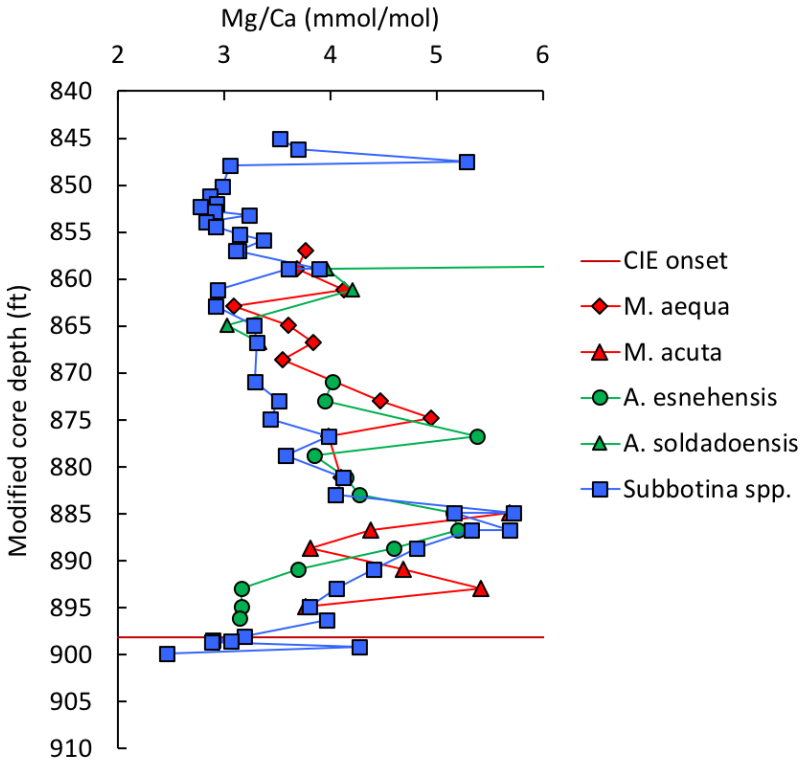

Fig. 3.S2. Mg/Ca of surface dwelling (*Morozovella* spp. in red; *Acarinina* spp. in green) and thermocline (*Subbotina* spp. in blue) dwelling foraminifera at Millville, NJ.

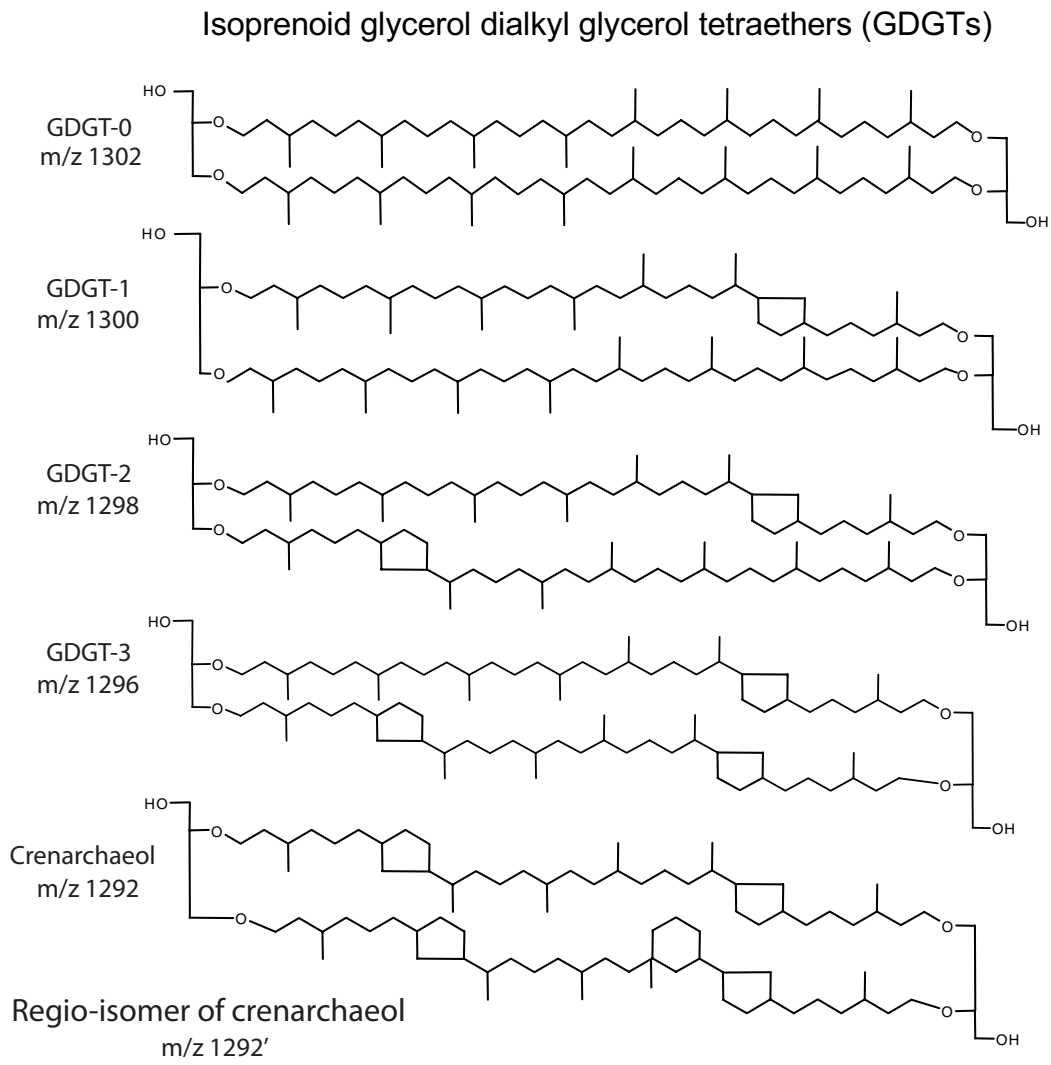

$$TEX^{H}_{86}\ (GDGT\ index\text{-}2) = \log \frac{GDGT\text{-}2 + GDGT\text{-}3 + cren'}{GDGT\text{-}1 + GDGT\text{-}2 + GDGT\text{-}3 + cren'}$$

$$SST = 64.8 \times TEX^{H}_{86} + 38.6\ (\pm 2.5°C;\ r^2 = 0.87;\ n = 255)$$

$$TEX^{L}_{86}\ (GDGT\ index\text{-}1) = \log \frac{GDGT\text{-}2}{GDGT\text{-}1 + GDGT\text{-}2 + GDGT\text{-}3}$$

$$SST = 67.5 \times TEX^{L}_{86} + 46.9\ (\pm 4°C;\ r^2 = 0.86;\ n = 396)$$

Fig. 3.S3. Structures of isoprenoid glycerol dialkyl glycerol tetraethers (GDGTs) used for TEX^{H}_{86} and TEX^{L}_{86} indices and their calibrations to modern sea surface temperatures (SSTs) [Kim et al., 2010].

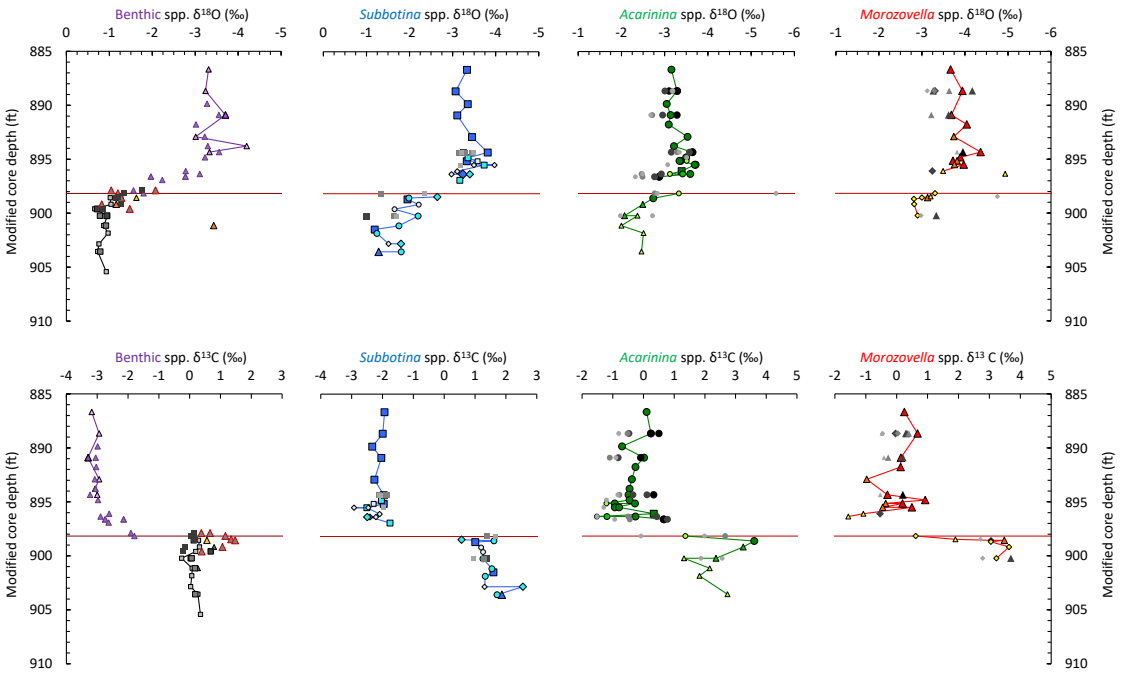

Fig. 3.S4. Carbon (lower panel) and oxygen (upper panel) isotopic records of multispecimen samples of foraminifera at Millville, NJ: benthic *Cibicidoides* spp. (brown), *A. acuta* (purple), *G. beccariiformis* (gray); thermocline dwelling *Subbotina* spp. (blue); surface dwelling *Acarinina* spp. (green), *M. acuta* (red triangulars) and *M. aequa* (red diamonds). Samples contain spesimens from one size fraction (>250, 200-250, or 150-200 μm) with larger spesimens highlighted in darker shades and smaller spesimens in lighter. Isotopic values are given in Table 2.1 in Chapter Two. Data from Si and Aubry [2018] are plotted in black symbols.

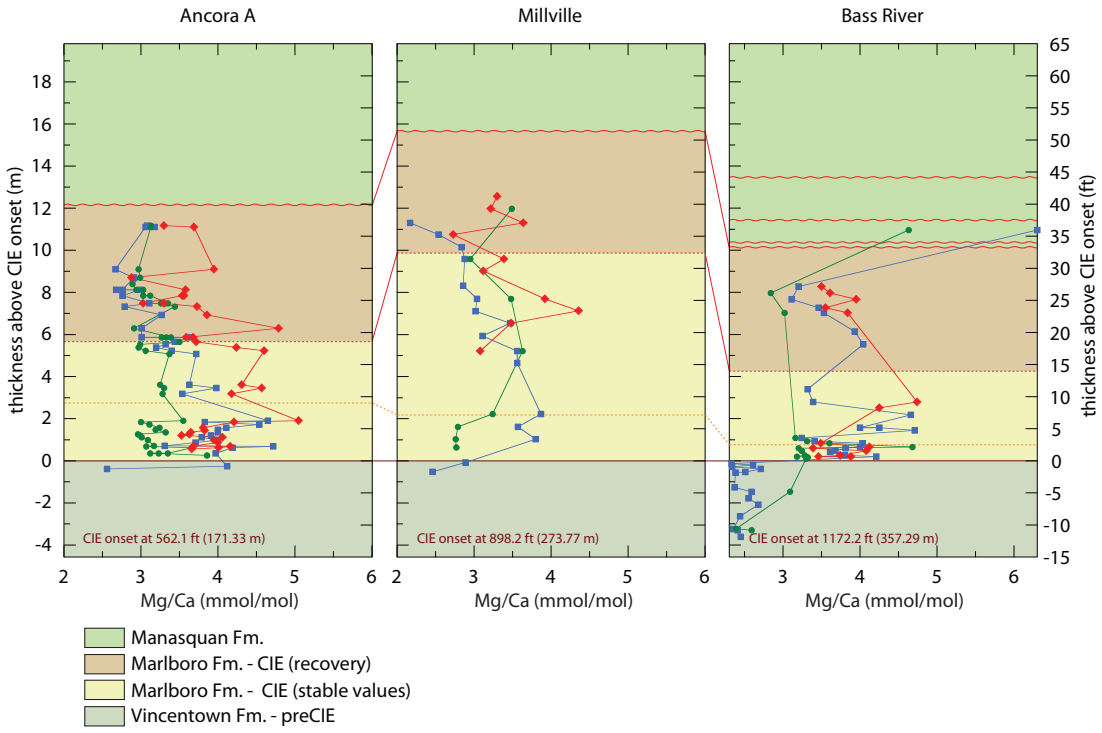

Fig. 3.S5. Mg/Ca of surface dwelling (*Morozovella* spp. in red; *Acarinina* spp. in green) and thermocline (*Subbotina* spp. in blue) dwelling foraminifera at Ancora [Babila, 2014], Millville, and Bass River [Babila et al., 2016], New Jersey coastal plain sites.

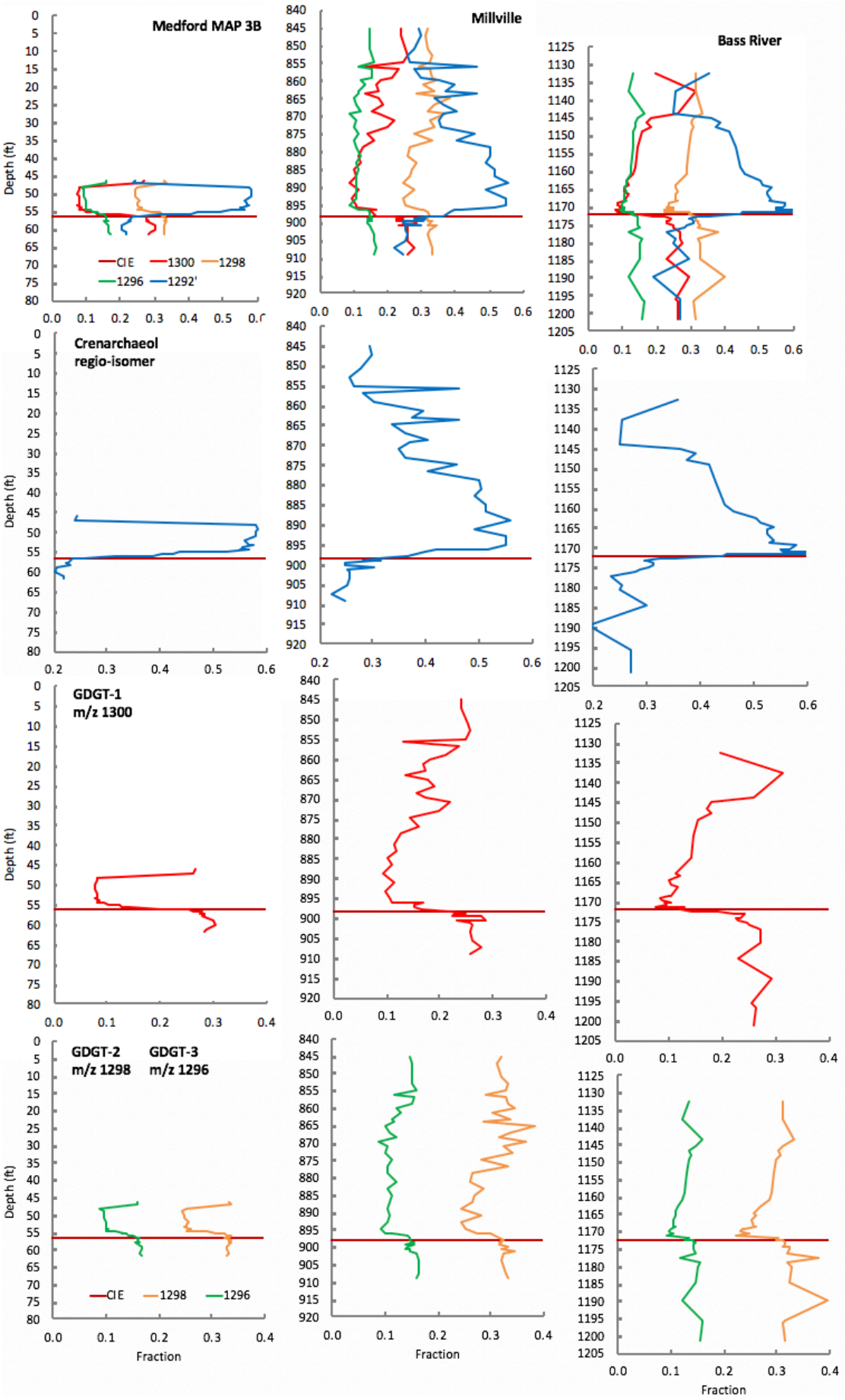
Medford MAP 3B
Millville
Bass River
Crenarchaeol
regio-isomer
GDGT-1
m/z 1300
GDGT-2
m/z 1298
GDGT-3
m/z 1296
CIE
1300
1298
1296
1292'
Depth (ft)
Fraction

Fig. 3.S6. Relative distribution of GDGTs used in TEX^{H}_{86} calibration: GDGT-1 (m/z 1300), GDGT-2 (m/z 1298), GDGT-3 (m/z 1296), and crenarchaeol regio-isomer (1292) in Medford MAP 3B [Chapter Four], Millville, and Bass River [Sluijs et al., 2007]. Top panel shows relative distribution of each GDGT in terms of their fractions normalized to the sum of GDGT-1, GDGT-2, GDGT-3, and crenarchaeol regio-isomer. Fractions of GDGT-1, GDGT-2, GDGT-3, and crenarchaeol regio-isomer are plotted separately in lower panels. Note that TEX^{H}_{86} uses the following ratio: (GDGT-2 + GDGT-3 + crenarchaeol regio-isomer) / (GDGT1 + GDGT-2 + GDGT-3 + crenarchaeol regio-isomer). Fractional GDGT abundances show that crenarchaeol regio-isomer is most variable among sites and, therefore, is responsible for larger temeprature anomaly in proximal Medford MAP 3B versus distal Millville and Bass River.

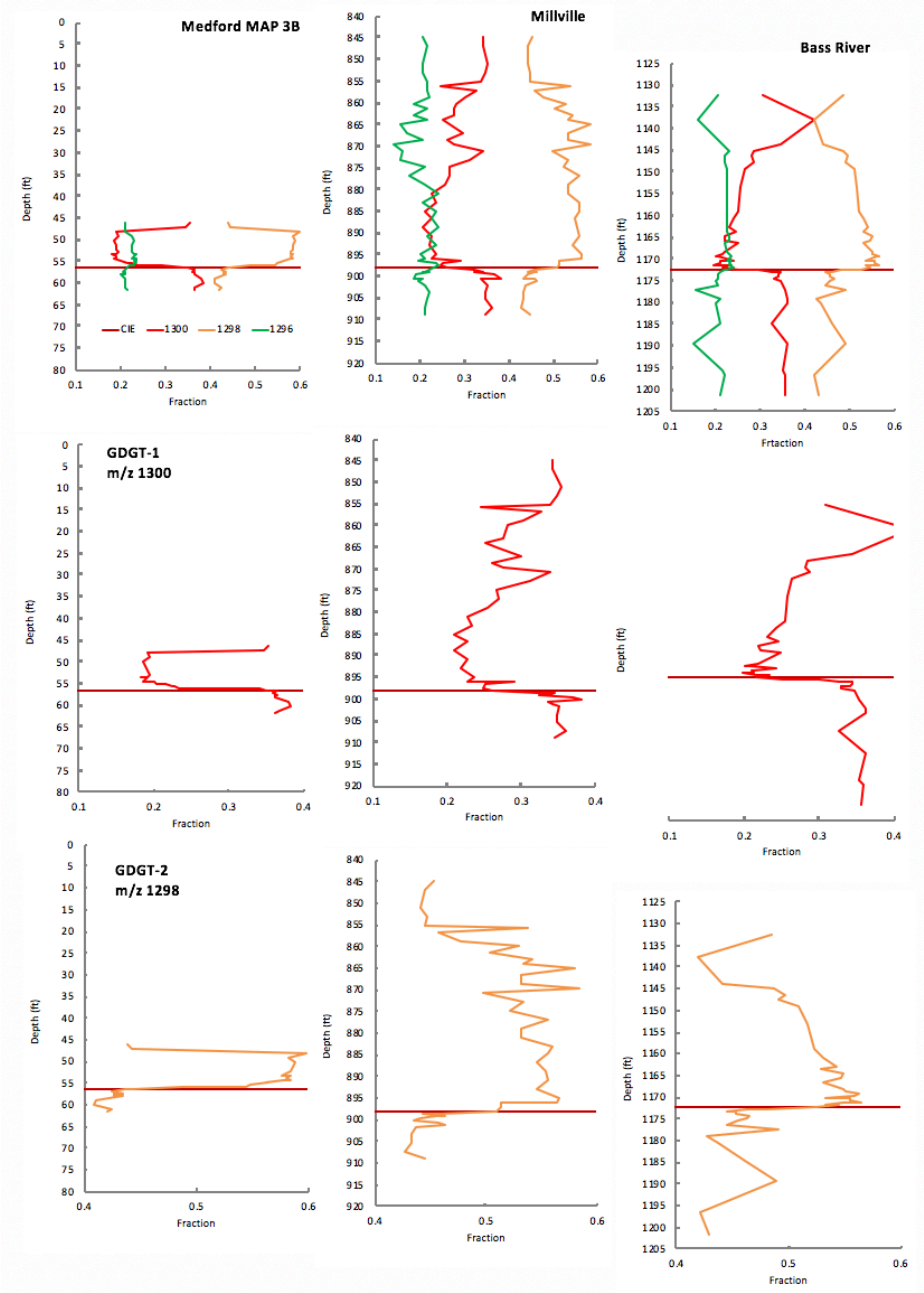

Fig. 3.S7. Relative distribution of GDGTs used in TEX^{L}_{86} calibration: GDGT-1 (m/z 1300), GDGT-2 (m/z 1298), and GDGT-3 (m/z 1296) in Medford MAP 3B [Chapter Four], Millville, and Bass River [Sluijs et al., 2007]. Top panel shows relative distribution of each GDGT in terms of their fractions normalized to the sum of GDGT-1, GDGT-2 and GDGT-3. Fractions of GDGT-1 and GDGT-2 are plotted separately in lower panels. Note that TEX^{L}_{86} uses the following ratio: GDGT-2 / (GDGT1 + GDGT-2 + GDGT-3) shown on the bottom panel. Fractions of each lipid show that only GDGT-2 relative abundance is variable among sites and, therefore, is responsible for larger temeprature anomaly in proximal Medford MAP 3B versus distal Millville and Bass River.

3.10 Tables

Table 3.1. GDGT abundances and TEX_{86} estimated temperatures [Kim et al., 2010] from Millville, NJ. Analyses performed in 2018 are marked in green. Table includes modified for core expansion depths (mcd). Samples from the core expansion are marked in quotes.

Interval depth (ft)		Mean depth (ft)	Mcd (ft)	Mcd (m)	Sample weight (g)	GDGT peak areas				
top	bottom					m/z 1302	m/z 1300	m/z 1298	m/z 1296	m/z 1292'
844.95	845.00	844.98	844.98	257.55	20.0	2137493	874763	1159211	526865	1063435
847.02	847.10	847.06	847.06	258.18	20.0	2942828	1268134	1649597	795782	1576526
850.90	850.95	850.93	850.92	259.36	20.0	2115070	863267	1079972	507629	939654
852.95	853.03	852.99	852.96	259.98	17.2	3394815	1143396	1466292	677673	1134855
854.98	855.05	855.02	854.97	260.59	17.7	2627547	1026599	1349901	652384	1082278
855.87	855.95	855.91	855.85	260.86	20.0	588440	153993	337250	136394	537787
856.90	857.10	857.00	856.93	261.19	20.2	1100427	466325	653633	309982	560445
858.88	859.07	858.98	858.89	261.79	20.0	908916	395340	623617	285317	560805
860.00	860.10	860.05	860.05	262.14	19.1	661452	293237	550638	195793	559221
861.10	861.30	861.20	861.14	262.48	19.9	246053	112068	202713	87573	263003
863.00	863.20	863.10	862.95	263.03	20.2	125445	43340	85436	29040	94521
863.95	864.00	863.98	863.79	263.28	17.7	1001105	256667	544690	219107	883780
865.10	865.24	865.17	864.92	263.63	20.2	179351	57236	124989	33084	110017
867.00	867.25	867.13	866.79	264.20	20.2	329218	104850	186989	60022	199741
869.00	869.25	869.13	868.69	264.78	20.2	148534	49835	101984	39810	130638
869.95	870.00	869.98	869.50	265.02	18.0	873670	343418	724638	173173	723717
870.82	871.00	870.91	870.87	265.44	19.7	120935	54609	80068	26125	86512
872.94	873.13	873.04	872.90	266.06	20.1	178659	59570	102424	29775	108586
875.00	875.20	875.10	874.88	266.66	20.1	190356	56955	111386	45081	181751
876.95	877.20	877.08	876.77	267.24	20.2	298648	93501	193946	61381	235958
879.07	879.32	879.20	878.80	267.86	19.1	288485	118693	247236	98446	466256
881.10	881.30	881.20	881.14	268.57	20.1	217234	73629	171705	78182	330938
883.05	883.23	883.14	882.98	269.13	20.3	219157	72714	174121	64189	299406
885.06	885.25	885.16	884.89	269.71	20.5	207393	91501	243123	102260	463824
886.99	887.20	887.10	886.73	270.27	20.1	92229	34626	82908	34380	160291
889.08	889.30	889.19	888.71	270.88	20.3	71731	32065	85493	36921	194813
890.90	891.06	890.98	890.92	271.55	20.2	171268	53167	129311	50242	225913
893.04	893.26	893.15	892.96	272.17	20.2	178789	64659	160617	69650	362381
895.09	895.30	895.20	894.88	272.76	20.2	312908	109203	262773	93201	572069
896.25	896.35	896.30	895.92	273.08	20.0	576391	76661	190026	70399	361499
896.44	896.64	896.54	896.14	273.14	20.0	26496	9044	15973	6063	22559
896.98	897.22	897.10	896.67	273.30	20.3	413787	193057	394436	182203	509701
897.66	897.90	897.78	897.31	273.50	19.1	343773	123030	255642	119682	308081
898.34	898.60	898.47	897.95	273.70	20.3	209932	83251	162991	73447	184332
898.80	899.09	898.95	898.40	273.83	20.3	358423	125719	179270	86212	177464
899.20	899.40	899.30	898.73	273.93	20.3	465893	174945	225370	108353	197533
899.65	899.70	899.68	899.08	274.04	20.4	22581	8882	12285	5414	12131
899.73	899.88	899.81	899.21	274.08	20.3	459031	169610	239257	115996	228621
"900.07"	"900.29"	900.18	899.56	274.19	20.3	348861	116142	138812	59633	103890
900.18	900.40	900.29	900.28	274.40	20.3	616245	189676	217021	92795	164730
900.65	900.70	900.68	900.64	274.52	15.5	861606	317805	434038	197159	410909
900.95	901.30	901.13	901.07	274.65	20.5	312118	124147	168085	70257	121503
901.81	902.00	901.91	901.81	274.87	20.4	273234	119220	148307	71845	116607
903.42	903.80	903.61	903.44	275.37	20.2	261716	115572	143996	72980	114725
905.50	905.74	905.62	905.35	275.95	20.2	316410	136075	169529	85202	130541
907.45	907.75	907.60	907.24	276.53	20.1	32231	14899	17619	8808	11892
909.36	909.52	909.44	908.99	277.06	20.1	260443	120329	155415	73490	115964

Table 3.1. Cont.

Interval depth (ft)		Mean depth (ft)	Mcd (ft)	Mcd (m)	GDGT ratio-1	TEX^{L}_{86}	T^{L} (°C)	GDGT ratio-2	TEX^{H}_{86}	T^{H} (°C)
top	bottom									
844.95	845.00	844.98	844.98	257.55	0.45	-0.34	23.7	0.76	-0.12	30.4
847.02	847.10	847.06	847.06	258.18	0.44	-0.35	23.1	0.76	-0.12	30.5
850.90	850.95	850.93	850.92	259.36	0.44	-0.36	22.9	0.75	-0.13	29.9
852.95	853.03	852.99	852.96	259.98	0.45	-0.35	23.2	0.74	-0.13	29.7
854.98	855.05	855.02	854.97	260.59	0.45	-0.35	23.2	0.75	-0.12	30.1
855.87	855.95	855.91	855.85	260.86	0.54	-0.27	28.7	0.87	-0.06	34.4
856.90	857.10	857.00	856.93	261.19	0.46	-0.34	24.0	0.77	-0.12	30.7
858.88	859.07	858.98	858.89	261.79	0.48	-0.32	25.3	0.79	-0.10	31.5
860.00	860.10	860.05	860.05	262.14	0.53	-0.28	28.3	0.82	-0.09	32.6
861.10	861.30	861.20	861.14	262.48	0.50	-0.30	26.8	0.83	-0.08	33.1
863.00	863.20	863.10	862.95	263.03	0.54	-0.27	28.9	0.83	-0.08	33.0
863.95	864.00	863.98	863.79	263.28	0.53	-0.27	28.5	0.87	-0.06	34.3
865.10	865.24	865.17	864.92	263.63	0.58	-0.24	31.0	0.82	-0.08	32.9
867.00	867.25	867.13	866.79	264.20	0.53	-0.27	28.4	0.81	-0.09	32.3
869.00	869.25	869.13	868.69	264.78	0.53	-0.27	28.4	0.85	-0.07	33.6
869.95	870.00	869.98	869.50	265.02	0.58	-0.23	31.1	0.83	-0.08	32.9
870.82	871.00	870.91	870.87	265.44	0.50	-0.30	26.5	0.78	-0.11	31.2
872.94	873.13	873.04	872.90	266.06	0.53	-0.27	28.5	0.80	-0.10	32.0
875.00	875.20	875.10	874.88	266.66	0.52	-0.28	27.8	0.86	-0.07	34.0
876.95	877.20	877.08	876.77	267.24	0.56	-0.25	29.7	0.84	-0.08	33.4
879.07	879.32	879.20	878.80	267.86	0.53	-0.27	28.4	0.87	-0.06	34.5
881.10	881.30	881.20	881.14	268.57	0.53	-0.28	28.3	0.89	-0.05	35.1
883.05	883.23	883.14	882.98	269.13	0.56	-0.25	29.9	0.88	-0.06	34.8
885.06	885.25	885.16	884.89	269.71	0.56	-0.25	29.7	0.90	-0.05	35.4
886.99	887.20	887.10	886.73	270.27	0.55	-0.26	29.1	0.89	-0.05	35.1
889.08	889.30	889.19	888.71	270.88	0.55	-0.26	29.6	0.91	-0.04	35.7
890.90	891.06	890.98	890.92	271.55	0.56	-0.26	29.7	0.88	-0.05	34.9
893.04	893.26	893.15	892.96	272.17	0.54	-0.26	29.1	0.90	-0.04	35.5
895.09	895.30	895.20	894.88	272.76	0.56	-0.25	30.2	0.89	-0.05	35.3
896.25	896.35	896.30	895.92	273.08	0.56	-0.25	30.1	0.89	-0.05	35.1
896.44	896.64	896.54	896.14	273.14	0.51	-0.29	27.4	0.83	-0.08	33.1
896.98	897.22	897.10	896.67	273.30	0.51	-0.29	27.3	0.85	-0.07	33.7
897.66	897.90	897.78	897.31	273.50	0.51	-0.29	27.3	0.85	-0.07	33.7
898.34	898.60	898.47	897.95	273.70	0.51	-0.29	27.2	0.83	-0.08	33.2
898.80	899.09	898.95	898.40	273.83	0.46	-0.34	24.0	0.78	-0.11	31.2
899.20	899.40	899.30	898.73	273.93	0.44	-0.35	23.0	0.75	-0.12	30.1
899.65	899.70	899.68	899.08	274.04	0.46	-0.34	24.3	0.77	-0.11	30.9
899.73	899.88	899.81	899.21	274.08	0.46	-0.34	23.9	0.77	-0.11	31.0
"900.07"	"900.29"	900.18	899.56	274.19	0.44	-0.36	22.9	0.72	-0.14	28.9
900.18	900.40	900.29	900.28	274.40	0.43	-0.36	22.5	0.71	-0.15	28.6
900.65	900.70	900.68	900.64	274.52	0.46	-0.34	24.0	0.77	-0.12	30.7
900.95	901.30	901.13	901.07	274.65	0.46	-0.33	24.4	0.74	-0.13	29.8
901.81	902.00	901.91	901.81	274.87	0.44	-0.36	22.6	0.74	-0.13	29.6
903.42	903.80	903.61	903.44	275.37	0.43	-0.36	22.4	0.74	-0.13	29.7
905.50	905.74	905.62	905.35	275.95	0.43	-0.36	22.4	0.74	-0.13	29.6
907.45	907.75	907.60	907.24	276.53	0.43	-0.37	21.9	0.72	-0.14	28.8
909.36	909.52	909.44	908.99	277.06	0.45	-0.35	23.2	0.74	-0.13	29.7

Table 3.2. GDGT abundances and BIT values from Millville, NJ. Analyses performed in 2018 are marked in green. Table includes modified for core expansion depths (mcd). Samples from the core expansion are marked in quotes.

Interval depth (ft)		Mean	Mcd	Mcd	GDGT peak areas				BIT
top	bottom	depth (ft)	(ft)	(m)	m/z 1292	m/z 1050	m/z 1036	m/z 1022	
844.95	845.00	844.98	844.98	257.55	10313853	35808	63959	611959	0.06
847.02	847.10	847.06	847.06	258.18	15611075	37075	69722	579887	0.04
850.90	850.95	850.93	850.92	259.36	10232863	29405	51898	452723	0.05
852.95	853.03	852.99	852.96	259.98	12784604	41829	91385	719069	0.06
854.98	855.05	855.02	854.97	260.59	12093590	38044	87409	749776	0.07
855.87	855.95	855.91	855.85	260.86	3187794	8681	20692	285520	0.09
856.90	857.10	857.00	856.93	261.19	5921114	44881	357360	370843	0.12
858.88	859.07	858.98	858.89	261.79	5269858	30018	297012	333751	0.11
860.00	860.10	860.05	860.05	262.14	3668361	11483	26555	380694	0.10
861.10	861.30	861.20	861.14	262.48	1763461	10380	121037	161364	0.14
863.00	863.20	863.10	862.95	263.03	654761	4246	38336	53250	0.13
863.95	864.00	863.98	863.79	263.28	5293520	13145	31578	416217	0.08
865.10	865.24	865.17	864.92	263.63	684958	3748	35130	53998	0.12
867.00	867.25	867.13	866.79	264.20	1277956	5609	65933	101418	0.12
869.00	869.25	869.13	868.69	264.78	876081	4406	39246	56311	0.10
869.95	870.00	869.98	869.50	265.02	4310965	8016	20271	288390	0.07
870.82	871.00	870.91	870.87	265.44	597682	5626	30757	43902	0.12
872.94	873.13	873.04	872.90	266.06	677609	5319	31599	45381	0.11
875.00	875.20	875.10	874.88	266.66	1204090	6160	50573	73546	0.10
876.95	877.20	877.08	876.77	267.24	1541796	7420	50954	78415	0.08
879.07	879.32	879.20	878.80	267.86	2664074	16052	83227	115891	0.07
881.10	881.30	881.20	881.14	268.57	2085924	8376	61709	92297	0.07
883.05	883.23	883.14	882.98	269.13	1840454	5458	52641	76538	0.07
885.06	885.25	885.16	884.89	269.71	3010298	11070	81443	123023	0.07
886.99	887.20	887.10	886.73	270.27	979729	2326	26459	38963	0.06
889.08	889.30	889.19	888.71	270.88	1102632	3237	27525	42803	0.06
890.90	891.06	890.98	890.92	271.55	1385388	3733	46399	72795	0.08
893.04	893.26	893.15	892.96	272.17	2070419	4036	55128	82347	0.06
895.09	895.30	895.20	894.88	272.76	3257431	5715	87423	135049	0.07
896.25	896.35	896.30	895.92	273.08	2210298	3581	63314	97016	0.07
896.44	896.64	896.54	896.14	273.14	155422	352	4546	6501	0.07
896.98	897.22	897.10	896.67	273.30	4331714	11529	125681	163756	0.06
897.66	897.90	897.78	897.31	273.50	2623008	7799	83856	114614	0.07
898.34	898.60	898.47	897.95	273.70	1499069	5164	56866	79209	0.09
898.80	899.09	898.95	898.40	273.83	1655160	8076	78592	92917	0.10
899.20	899.40	899.30	898.73	273.93	2064158	9890	80291	85092	0.08
899.65	899.70	899.68	899.08	274.04	100430	357	2662	3023	0.06
899.73	899.88	899.81	899.21	274.08	2242602	9266	81470	90948	0.07
"900.07"	"900.29"	900.18	899.56	274.19	1049804	6696	58852	66061	0.11
900.18	900.40	900.29	900.28	274.40	1704168	11624	97274	108445	0.11
900.65	900.70	900.68	900.64	274.52	3850703	14404	25388	301714	0.08
900.95	901.30	901.13	901.07	274.65	1215816	8985	96772	107376	0.15
901.81	902.00	901.91	901.81	274.87	1229323	8632	77969	87286	0.12
903.42	903.80	903.61	903.44	275.37	1284453	9463	75745	81241	0.11
905.50	905.74	905.62	905.35	275.95	1514842	9502	93334	101840	0.12
907.45	907.75	907.60	907.24	276.53	132365	852	5811	5924	0.09
909.36	909.52	909.44	908.99	277.06	1256378	6810	72015	79296	0.11

Table 3.3. Mg/Ca ratios in *Morozovella*, *Acarinina*, and *Subbotina* spp. at Millville, NJ. Mg/Ca values calibrated to temperatures using Anand et al. [2003] multispecies equation (calibration error is ±1°C) and seawater Mg/Ca of 2.5 mmol/mol. Values in red were rejected due to potential contamination and diagenesis. Table includes modified for core expansion depths (mcd). Samples from the core expansion are marked in quotes.

Top (ft)	Bottom (ft)	Mean depth (ft)	Mcd (ft)	Mcd (m)	Species	Size (µm)	#	Mg25/Ca43 (mmol/mol)	T (°C)
857.00	857.10	857.05	856.98	261.21	*M. aequa*	300-400	21	3.77	
858.92	859.07	859.00	858.91	261.79	*M. aequa*	300-400	30	3.68	
861.10	861.20	861.15	861.10	262.46	*M. aequa*	300-400	16	4.13	
863.00	863.15	863.08	862.93	263.02	*M. aequa*	300-400	10	3.09	
865.10	865.18	865.14	864.90	263.62	*M. aequa*	300-400	14	3.60	
867.00	867.15	867.08	866.74	264.18	*M. aequa*	300-400	14	3.83	
869.00	869.10	869.05	868.62	264.76	*M. aequa*	300-400	21	3.54	
873.02	873.13	873.08	872.94	266.07	*M. aequa*	300-400	20	4.47	
875.00	875.10	875.05	874.83	266.65	*M. aequa*	300-400	12	4.94	
876.95	877.16	877.06	876.75	267.23	*M. aequa*	300-400	25	3.98	
881.10	881.20	881.15	881.09	268.56	*M. aequa*	300-400	11	4.10	
885.06	885.17	885.12	884.85	269.70	*M. acuta*	300-400	12	5.69	
886.99	887.10	887.05	886.68	270.26	*M. acuta*	300-400	14	4.38	
889.08	889.20	889.14	888.66	270.86	*M. acuta*	300-400	28	3.81	
890.90	891.02	890.96	890.90	271.55	*M. acuta*	300-400	25	4.69	
893.04	893.16	893.10	892.91	272.16	*M. acuta*	300-400	13	5.41	
895.09	895.19	895.14	894.83	272.74	*M. acuta*	300-400	30	3.76	
857.00	857.10	857.05	856.98	261.21	*A. esnaensis*	300-400	20	21.80	
858.92	859.07	859.00	858.91	261.79	*A. esnaensis*	300-350	20	3.97	
861.10	861.20	861.15	861.10	262.46	*A. esnaensis*	300-350	18	4.21	
865.10	865.18	865.14	864.90	263.62	*A. esnaensis*	300-350	15	3.03	
867.00	867.15	867.08	866.74	264.18	*A. esnaensis*	300-400	15	3.33	
870.88	871.00	870.94	870.90	265.45	*A. esnaensis, angulosa, soldadoensis*	300-350	14	4.02	
873.02	873.13	873.08	872.94	266.07	*A. soldadoensis*	**350**-400	14	3.95	
876.95	877.16	877.06	876.75	267.23	*A. soldadoensis*	300-350	15	5.38	
879.07	879.20	879.14	878.74	267.84	*A. soldadoensis*	300-350	20	3.85	
881.10	881.20	881.15	881.09	268.56	*A. soldadoensis*	300-350	20	4.14	
883.05	883.16	883.11	882.94	269.12	*A. soldadoensis*	300-350	20	4.27	
885.06	885.17	885.12	884.85	269.70	*A. soldadoensis*	300-350	20	5.15	
886.99	887.10	887.05	886.68	270.26	*A. soldadoensis*	300	20	5.20	
889.08	889.20	889.14	888.66	270.86	*A. soldadoensis*	300-350	20	4.59	
890.90	891.02	890.96	890.90	271.55	*A. soldadoensis*	300-350	20	3.70	
893.04	893.16	893.10	892.91	272.16	*A. soldadoensis*	300-350	15	3.16	
895.09	895.19	895.14	894.83	272.74	*A. soldadoensis*	300-350	20	3.16	
896.44	896.54	896.49	896.09	273.13	*A. soldadoensis*	300-400	12	3.14	
844.92	845.02	844.97	845.02	257.56	*S. roesnaesensis*	250-300	30	3.52	33.5
846.10	846.20	846.15	846.20	257.92	*S. roesnaesensis*	250-300	33	3.69	34.0
847.40	847.50	847.45	847.50	258.32	*S. roesnaesensis*	250-300	30	5.28	
847.82	847.90	847.86	847.90	258.44	*S. roesnaesensis*	250-300	34	3.05	31.9
850.10	850.20	850.15	850.15	259.13	*S. roesnaesensis*	250-300	34	2.98	31.6
851.10	851.20	851.15	851.14	259.43	*S. roesnaesensis*	250-300	30	2.86	31.2
851.90	852.00	851.95	851.93	259.67	*S. roesnaesensis*	250-300	30	2.93	31.4
852.30	852.40	852.35	852.33	259.79	*S. roesnaesensis*	250-300	30	2.77	30.8
852.80	852.90	852.85	852.82	259.94	*S. roesnaesensis*	250-300	30	2.91	31.4
853.14	853.26	853.20	853.17	260.05	*S. roesnaesensis*	250-300	30	3.23	32.5
853.90	853.96	853.93	853.89	260.27	*S. roesnaesensis*	250-300	30	2.83	31.0
854.38	854.48	854.43	854.39	260.42	*S. roesnaesensis*	250-300	30	2.92	31.4

855.20	855.30	855.25	855.20	260.66	*S. roesnaesensis*	250-300	30	3.15	32.2
855.90	856.00	855.95	855.89	260.88	*S. roesnaesensis*	250-300	30	3.37	33.0
857.00	857.10	857.05	856.98	261.21	*S. roesnaesensis*	325-**425**	32 (250)	3.14	32.2
857.00	857.10	857.05	856.98	261.21	*S. roesnaesensis*	300-350	30	3.11	32.1
858.92	859.07	859.00	858.91	261.79	*S. roesnaesensis*	350-**400**	31 (250)	3.90	
858.92	859.07	859.00	858.91	261.79	*S. roesnaesensis*	300-**350**	30	3.61	33.7
861.10	861.20	861.15	861.10	262.46	*S. roesnaesensis*	300-400 (**350**)	29	2.93	31.4
863.00	863.15	863.08	862.93	263.02	*S. roesnaesensis*	300-**350**	29	2.92	31.4
865.10	865.18	865.14	864.90	263.62	*S. roesnaesensis*	300-350	30	3.28	32.7
867.00	867.15	867.08	866.74	264.18	*S. roesnaesensis*	300-350	28	3.30	32.8
870.88	871.00	870.94	870.90	265.45	*S. roesnaesensis*	300-**350**	30	3.29	32.7
873.02	873.13	873.08	872.94	266.07	*S. roesnaesensis*	300-**350**	31	3.52	33.5
875.00	875.15	875.08	874.86	266.66	*S. roesnaesensis*	300-**350**	20	3.43	33.2
876.95	877.16	877.06	876.75	267.23	*S. roesnaesensis*	300-350	30	3.98	34.8
879.07	879.20	879.14	878.74	267.84	*S. roesnaesensis*	300-350	30	3.57	33.6
881.10	881.20	881.15	881.09	268.56	*S. roesnaesensis*	300-350	30	4.12	35.2
883.05	883.16	883.11	882.94	269.12	*S. roesnaesensis*	300-**350**	25	4.04	35.0
885.06	885.17	885.12	884.85	269.70	*S. roesnaesensis, few patagonica & velascoensis*	275-400 (**375**)	30 (20x250, 10x212, 1x150)	5.73	
885.06	885.17	885.12	884.85	269.70	*S. roesnaesensis*	300-350	30	5.16	
886.99	887.10	887.05	886.68	270.26	*S. roesnaesensis, few patagonica & velascoensis*	300-**375**	50 (212-250, 250-300)	5.68	
886.99	887.10	887.05	886.68	270.26	*S. roesnaesensis*	300-350	30	5.33	
889.08	889.20	889.14	888.66	270.86	*S. roesnaesensis*	300-350	30	4.81	
890.90	891.02	890.96	890.90	271.55	*S. roesnaesensis*	300-350	30	4.41	36.0
893.04	893.16	893.10	892.91	272.16	*S. roesnaesensis*	300-350	18	4.06	35.1
895.09	895.19	895.14	894.83	272.74	*S. roesnaesensis*	250-350	35	3.80	
896.44	897.11	896.78	896.35	273.21	*S. patagonica, velascoensis & Parasubbotina (?)*	225-**375**	27 (2x250, 18x212)	3.96	34.8
898.34	898.74	898.54	898.02	273.72	*S. velascoensis, patagonica*	225-300	18 (9x212, 9x150)	3.18	32.4
898.94	899.04	898.99	898.44	273.84	*S. roesnaesensis, velascoensis*	250-350	15	2.89	31.3
899.05	899.20	899.13	898.57	273.88	*S. velascoensis, patagonica*	225-300	31 (10x212, 21x150)	3.07	31.9
899.20	899.31	899.26	898.69	273.92	*S. velascoensis, patagonica*	225-300	25 (6x212, 22x150, 28 total?)	2.89	31.3
899.73	899.82	899.78	899.18	274.07	*S. velascoensis, patagonica*	225-300	21 (1x250, 3x212, 17x150)	4.27	
"900.16"	900.3		899.92	274.29	*S. roesnaesensis, velascoensis*	250-350	12	2.46	29.5

IV CHAPTER FOUR

Proximity does it: Reconstructions of the PETM onset at Medford, New Jersey (USA)

4.1 Abstract

Expanded sections are required to evaluate lead/lag relationships of the Paleocene-Eocene thermal maximum (PETM) and the carbon isotopic excursion (CIE) to possibly constrain causal mechanism(s). The Salisbury Embayment contains expanded PETM sections, with auger cores at Medford, NJ providing the most proximal records among New Jersey Coastal Plain (NJCP) sites. The Medford cores recorded the most expanded CIE onset on the NJCP and arguably elsewhere, with gradational lithologic change from uppermost Paleocene glauconitic silts to lowermost Eocene kaolinitic clays. TEX_{86}-based temperature estimates indicated no warming prior the CIE onset, rejecting the precursor warming hypothesis that was based on studies of downdip NJCP sites. A drop in carbonate content associated with the CIE initiation, attributed to dissolution in deep ocean locations, represents a dilution event on the New Jersey paleoshelf associated with rapid, massive input of clay. This is supported by well-preserved foraminiferal tests found in the low (<1% $CaCO_3$) carbonate zone at Medford, NJ. Very fast deposition of clays facilitated preservation of foraminifera, whereas dissolution would have dissolved calcite tests. I/Ca ratios and benthic fauna do not suggest anoxia on the shelf floor, but generally low O_2.

4.2 Introduction

The Paleocene/Eocene (P/E) transition (~56 Ma) is marked by a global temperature increase of 4-9°C and the carbon isotope excursion (CIE) of 2-7 ‰ found ubiquitously in marine and terrestrial realms [e.g., McInerney and Wing, 2011; Dunkley Jones et al., 2013]. However, the mechanisms of warming and overall changes in the ocean-atmosphere system during the Paleocene-Eocene thermal maximum (PETM) are uncertain. Following the rough estimate from early survey work that the CIE occurred in less than 5-10 kyr [Kennett and Stott, 1991], the rapidity of the PETM onset has been debated, with estimates ranging from years [Wright and Schaller, 2013] to ~ 4 kyr [Zeebe et al., 2016; Kirtland Turner and Ridgwell, 2016]. The rate of change is needed to constrain the causal mechanism(s). An instantaneous release of carbon would imply catastrophic mechanism, such as cometary impact [Kent et al., 2003; Cramer and Kent, 2005; Schaller et al., 2016; Kent et al., 2017], whereas a prolonged CIE onset would suggest alternative mechanisms, e.g. methane hydrates dissociation [Dickens et al., 1995, 1997; Katz et al., 2001; Thomas et al., 2002], sill intrusion, or extrusive volcanism [Svensen et al., 2004; Storey et al., 2007; Dickson et al., 2015; Gutjahr et al., 2017]. See review of all proposed mechanisms in section 1.1 “Introduction” of Chapter One.

Sections from continental margins with high sedimentation rates and thus high resolution provide a possible way to resolve the timing of the onset and causal mechanism(s). Marine PETM records over 10 m thick are found on the New Jersey Coastal Plain (NJCP) (35-40°N paleolatitude) [Makarova et al., 2017]. Sections at Medford, NJ are most proximal among NJCP sites (Fig. 4.1) and were originally drilled by ODP at the Medford Maintenance Yard in 2007 [Sugarman et al., 2010], but the

PETM recovery was incomplete. The United States Geological Survey (USGS) and Rutgers University auger drilled six sites (Fig. 4.S1) and nine holes at Medford, NJ in Summer 2016 [Podrecca, 2018]. The P/E boundary at Medford Auger Project (MAP) cores is represented by gradual lithologic change (Fig. 4.2) from the uppermost Paleocene glauconitic silts of the Vincentown Formation to the lowermost Eocene kaolinitic clays of the Marlboro contrasting with the sharp, possibly unconformable or diastemic boundary at distal Bass River site [Miller et al., 1998; Stassen et al., 2012; 2015].

The PETM onset at Medford, NJ is not only associated with a gradual reduction in coarse fraction due to clay input, but also with a gradual decrease in bulk sediment $\delta^{13}C$ values within a 1.65 ft (0.5 m) thick interval (Fig. 4.3; Podrecca [2018]). In contrast, carbon isotopic records from most PETM sections show sharp (<<0.5 m) decreases that are used to delineate the CIE/PETM onset [e.g., Aubry et al., 2007]. Thus, the MAP cores enable evaluation of the initiation of the PETM at higher resolution and to resolve the timing and lead/lag relationships of the warming and CIE. In this chapter, I focus on three questions regarding the PETM onset using multiproxy data from Medford cores: 1) duration of the onset; 2) precursor warming; and 3) change in productivity on shelves and deoxygenation of water column.

The timing of the PETM onset can be potentially reconciled from the relationship among chemical signals imbedded in bulk carbonate and foraminiferal tracers. High-resolution bulk sediment isotopic records from Millville and Wilson Lake NJCP sites showed different responses in $\delta^{13}C$ and % $CaCO_3$ to the PETM onset, i.e. gradual decrease (24 cm) in $\delta^{13}C$ values versus sharp (4 mm) drop in % $CaCO_3$ [Wright and Schaller, 2013]. This was explained by instantaneous injection of CO_2, in regards to

faster rates of CO_2 invasion (displayed by % $CaCO_3$) than the timing of carbon isotopic equilibration ($\delta^{13}C$) [Wright and Schaller, 2013]. Following this, Schaller et al. [2016] reported microtektite spherules at the PETM onset level from the North Atlantic shelf (Millville, Wilson Lake, and Medford; Fig. 4.S4) and slope (Ocean Drilling Program (ODP) Site 1051B, Blake Nose) sections suggesting their origin from extraterrestrial impact ejecta and supporting instantaneous trigger for the PETM onset.

Isotopic analyses of single foraminiferal specimens provide possible constraints on the lead-lags of $\delta^{13}C$ and temperature. High-resolution stable isotopic records of single foraminiferal tests from open ocean ODP Site 690 [Thomas et al., 2002] showed a bimodal distribution of isotopic values with the $\delta^{18}O$ anomaly preceding the CIE onset. This apparent lead of temperatures led Thomas et al. [2002] to suggest an instantaneous release of methane from dissociation of clathrates that had been triggered by initial warming. However, the CIE "core" at Site 690 is 1 m thick [Bains et al., 1999; Thomas et al., 2002], and the decrease in $\delta^{18}O$ values of surface dwelling *Acarinina* spp. preceded the CIE, recorded by same species, by only 7 cm [Thomas et al., 2002]. This is within the 10 cm bioturbation thickness typically seen in pelagic sediments; therefore, the single specimen data of foraminiferal isotopes from more expanded sections of the PETM onset are required for more accurate timing estimates.

In contrast to the deep sea where Site 690 provides the thickest section of the CIE "core" (1 m), NJCP sections have much thicker intervals (>10 m) representing the "core" (Fig. 2.2 in Chapter Two). Isotopic studies of foraminifera at Millville used multi-specimen samples of foraminifera, which indicated intermediate $\delta^{13}C$ and $\delta^{18}O$ values spanning the PETM onset [Makarova et al., 2017; Si and Aubry, 2018]. Bass River single

and multi-specimen foraminiferal studies showed bimodal distribution of $\delta^{13}C$ and $\delta^{18}O$ values [Zachos et al., 2007; John et al., 2008]; however the onset there is apparently truncated [John et al., 2008; Stassen et al., 2012]. The MAP Hole 3A core recovered well-preserved foraminifera in the expanded section of the PETM onset. Thus, stable isotopic measurements of single tests of planktonic and benthic foraminifera across the expanded onset section in the Medford core may reveal the timing of the onset.

The relationship between temperature and carbon isotopic records is critical to evaluate mechanisms. Temperature estimates from the organic paleothermometer TEX_{86} provide high-resolution temperature records. Based on TEX_{86}-derived temperature estimates at Wilson Lake and Bass River, NJ, Sluijs et al. [2007] suggested a precursor warming (i.e., with temperature leading the $\delta^{13}C$ decrease) as the trigger to clathrate destabilization that caused methane release and further temperature increase. The updated TEX_{86} calibrations [Kim et al., 2010] together with the new TEX_{86} record from the Millville site (see Chapter Three), however, question the precursor warming previously reported from the New Jersey cores. To evaluate the relation between the CIE onset and warming initiation, I compare a high-resolution (0.1 ft; 3 cm sampling interval) $\delta^{13}C$ record of bulk sediment supported by planktonic and benthic foraminiferal $\delta^{13}C$ values with TEX_{86}-derived temperature estimates (~0.25 ft; 8 cm sampling interval) across the expanded section of the PETM onset at Medford MAP 3B core. The CIE onset at Medford and elsewhere is associated by a drop in carbonate content and rare foraminiferal tests; therefore, the lipid biomarker analysis provides the best tool for high resolution temperature reconstructions of the event initiation, especially in the low carbonate zone.

The PETM warming is accompanied globally by increased flux of sediments on continental shelves through enhanced weathering and river runoff [e.g. Kopp et al., 2009]. Supposedly higher phytoplankton productivity and nutrients supply from the terrestrial realm should have resulted in the anoxia/dysoxia in the water column, especially near the seafloor. Previous studies of the NJCP cores suggested an increase of nutrients supply, productivity, and stratification on shelf resulting in bottom water hypoxia, though the extent of low O_2 has not been fully evaluated [Zachos et al., 2006; John et al., 2008; Stassen et al. 2012; 2015]. Here, I use I/Ca ratio, a novel paleoredox proxy [Lu et al., 2010], in planktonic and benthic foraminifera from MAP 3A core at Medford, NJ to examine the water column deoxygenation on the New Jersey paleoshelf.

Overall, this chapter provides a detailed investigation of lithology and foraminiferal assemblages, results of stable isotopes and trace metals analyses in planktonic and benthic foraminifera, and temperature estimates form the organic paleothermometer TEX_{86} at nearshore site Medford, NJ.

4.3 Geological Setting and Methods

Six sites from Medford, NJ located on the New Jersey coastal plain represent the most updip locations along the New Jersey paleoshelf (Figs. 4.1 and 4.S1). The Medford sections were used as an anchor point in paleowater depth reconstructions of the New Jersey paleoshelf during the PETM. The Paleocene Vincentown Formation contains wispy cross laminations suggesting inner neritic, lower shoreface (~25 ± 5 m water depth) environments near storm wave base [Sugarman et al., 2005]. Benthic foraminiferal assemblages in the Vincentown Formation from the MAP 3A core indicated slightly

deeper settings (30-50 m water depths) of the middle shelf. However, Stassen et al. [2012; 2015] estimated that the Vincentown Formation was deposited in outer neritic (>100 m) paleodepths, and attributed the low percentage of planktonic foraminifera to dissolution. I reject this interpretation based on the following: 1) the assemblage of benthic foraminifera shows a lower diversity of inner to middle neritic assemblage consisting of *Cibicidoides alleni*, *Cibicidoides succedens*, *Guttulina*, *Saracenaria, Tritaxia, Globulimina,* and *Bolivina*; 2) the regional depth transect shows an expected change from glauconitic-quartz sands (with reworked glauconite) typical of lower shoreface environments in outcrops along strike and Medford outcrops and cores to sandy silts typical of offshore, middle neritic (30-50 m) environments in intermediate sites (Wilson Lake, Millville) to silty clays with common planktonic foraminifera at Bass River (Fig. 4.S2). The paleoslope model in fact requires paleodepths of the Vincentown to be less than 50 m at Medford.

More detailed geological setting on the New Jersey paleoshelf is given in section 2.12.2 “Geological Setting” of Chapter Two.

4.3.1 Lithological description of the MAP 3A, 3B, and 5A cores

MAP recovered nine cores from six sites at Medford, NJ (Fig. 4.S1). The P/E boundary at Medford is characterized by a gradational change from the Upper Paleocene glauconitic silts of the Vincentown Formation (65-80% coarse fraction >63 μm) to the Lower Eocene kaolinitic clays of the Marlboro Formation (mean grain size 1-2 μm; Podrecca [2018]) (Figs. 4.2 and 4.4; Table 4.1). A transitional lithology records a gradual decrease in coarse fraction from 70% to 2% at MAP sections; this transitional unit is 1.5-2.5 ft (0.46-0.76 m) thick in MAP Holes 5A, 3A, and 3B cores, allowing a detailed study

of the PETM onset (Fig. 4.2). The thickness of the "pure" clay unit of the Marlboro Formation that I define by the coarse fraction cutoff of <2% by weight varies among MAP sites due to erosion by a regional unconformity on top of the Marlboro Formation (Fig. 4.S2). The thickness of recovered clay is greater in the MAP 5A core (7.2.ft; 2.2 m). However, planktonic foraminifera are absent in the clay unit at MAP 5A due to shallow burial depth of this core (the top of the Marlboro Formation is at 17.7 ft; 5.4 m) and fractured structure of clay that allowed groundwater percolation (Fig. 4.2). Thus, I studied deeper MAP 3A and MAP 3B cores (Figs. 4.2 and 4.S2) that were drilled 8 ft (2.4 m) apart, that have thinner clay units yet abundant, well-preserved foraminifera. The recovered thickness of the Marlboro Formation is 4 ft (1.1 m) at MAP 3A and 6.2 ft (1.9 m) at MAP 3B. This difference can be explained by both a coring gap of 2 ft (0.6 m) and differences in truncation by the overlaying unconformity. Among the NJCP sites, the Medford sites recovered the thickest section of the onset but a truncated CIE "core". Here, I focus on the transitional interval that has recorded the PETM onset, arguably the most expanded across the New Jersey paleoshelf as suggested by the delta clinoform model of fluid mud deposition (Fig. 4.S3; Podrecca [2018]). Figure 4.4 shows a more detailed lithological summary of the MAP 3A core that has been used for foraminiferal studies.

4.3.2 Methods

Core samples were disaggregated in a sodium metaphosphate solution (5.5 g of sodium metaphosphate per liter) to deflocculate clays and then washed through a 63 μm sieve to separate the fine fraction (<63 μm). The >63 μm fraction was dried overnight in a 50°C oven and weighed dry to compute the percentage of coarse sediment.

For stable isotope analyses of single- and multi-specimen planktonic foraminifera, specimens of *Morozovella* (*M. aequa, M. acuta*), *Acarinina* (*A. soldadoensis, A. coalingensis, A. angulosa*), and *Subbotina* (mostly *S. roesnaesensis*) were picked from the >300 μm, 250-300 μm, 212-250 μm, and 150-212 μm size fractions using the taxonomy of Olsson et al. [1999] and Pearson et al. [2006]. For stable isotope analyses of single- and multi-specimen benthic foraminifera, specimens of *Anomalinoides* (mostly *A. acuta*) and *Cibicidoides* (*C. alleni, C. howelli, C. succedens*) were picked mainly from the >300 μm, 250-300 μm, 212-250 μm, and 150-212 μm size fractions using the taxonomy of Cushman [1951] and Berggren and Aubert [1975]. To avoid species bias, most of the samples analyzed consisted of single species of one size fraction (Table 4.2).

Stable isotope analyses of foraminifera were conducted on a Micromass Optima Mass Spectrometer with an attached multi-prep device. See method description in section 2.4.1 “Analyses” of Chapter Two.

Glycerol dialkyl glycerol tetraethers (GDGTs) used for the TEX_{86} paleothermometer were extracted from powdered freeze-dried sediments (~20 g dry mass) and analyzed on an Agilent 1100 series high-performance liquid chromatographer (HPLC) using high resolution method proposed by Hopmans et al. [2016]. See method description in section 3.3.1 “Lipid biomarker analyses (TEX_{86})” of Chapter Three.

For trace elemental analyses foraminiferal tests were crushed and cleaned following the protocol reported by Boyle and Keigwin [1985] and Rosenthal et al. [1997]. Elemental ratios were measured on a Thermo Finnigan Element XR Sector Field Inductively Coupled Plasma Mass Spectrometer (SF-ICP-MS) operated in low resolution ($m/\Delta m$ =300) and medium resolution ($m/\Delta m$ =4300) settings outlined in the protocol of

Rosenthal et al. [1999]. See method description in section 3.3.2 “Trace element analyses of foraminifera” of Chapter Three.

Depths of lithologic boundaries and samples at Medford cores MAP 3A, 3B, and 5A reported here are modified for core expansion (modified core depth; mcd), by adjusting the core recovery length to a 5 ft (1.5 m) interval per run. The true core depths of analyzed samples are given in data tables.

4.3.3 Paleoredox reconstructions from I/Ca in foraminifera

I/Ca ratio is a novel proxy for reconstruction of paleoredox conditions. The modern ocean contains two species of iodine in the seawater, iodate [IO^{3-}] and iodide [I^-]. Only iodate is incorporated in $CaCO_3$ and under dysoxic conditions iodate is reduced to iodide [Lu et al., 2010; Zhou et al., 2014 and references therein]. Therefore, I/Ca ratio in foraminiferal calcite is controlled by redox conditions: lower concentrations of dissolved O_2 in the seawater cause decrease of I/Ca ratios in foraminifera. Iodine speciation is affected by productivity. The biologic uptake (primary production) and release (decomposition of organic matter) may result in lower iodate concentrations in surface waters and higher iodide contents deeper in the ocean. Nonetheless, both increased productivity and lower oxygen levels cause decrease of I/Ca in planktonic foraminifera [Lu et al., 2010; Zhou et al., 2014 and references therein].

The I/Ca proxy has been applied for pelagic PETM sections. Zhou et al. [2014] measured I/Ca in planktonic foraminifera from open ocean cores in Atlantic, Sothern, Indian, and Pacific Oceans and observed overall decrease in I/Ca at the onset of the PETM. They interpreted this decrease as widespread deoxygenation in the upper ocean

waters caused by enhanced stratification and productivity. This chapter presents the first study to measure I/Ca ratio in foraminifera from shelf sections.

4.4 Results

4.4.1 Bulk sediment isotopic records from Medford Sites MAP 3A and 3B

The CIE onset is marked by sharp decreases in $\delta^{13}C$ values recognized globally from isotopic records of carbonate and organic carbon. However, the CIE onset in bulk $\delta^{13}C$ at Medford, NJ is gradational (Fig. 4.3), unlike the $\delta^{13}C$ excursion seen from bulk sediment record at distal Bass River that is sharp [Kent et al., 2003; John et al., 2008] (Fig. 4.S4). The decrease of 3.5 ‰ in bulk carbonate $\delta^{13}C$ values at MAP 3A and MAP 3B cores occurs over a 1.65 ft (0.5 m) interval (Fig. 4.3) and is comparable to that at proximal Wilson Lake site [Wright and Schaller, 2013] (Fig. 4.S4). Bulk carbonate analyses at MAP 3A and MAP 3B [Podrecca, 2018] showed not only a lower CIE magnitude (3.5 ‰ versus 4.5-6.5 ‰ at other sites; Wright and Schaller [2013]), but also lower absolute $\delta^{13}C$ values (-5 ‰), than in other NJCP sites (Fig. 4.S4). This can be explained by shallower depths and more proximal location of Medford sites on the New Jersey paleoshelf during the PETM with a greater influence of riverine dissolved inorganic carbon and a shift in relative abundances of carbonate species associated with the PETM onset (i.e. changing abundances of planktonic foraminifera, benthic foraminifera, and calcareous nannoplankton taxa). The CIE magnitude of 3.5 ‰ taken from bulk sediment is also confirmed by $\delta^{13}C$ values from surface dwelling *Acarinina* spp. and benthic species of *Cibicidoides* and *Anomalinoides* (Fig. 4.5).

The bulk sediment $\delta^{13}C$ records from MAP 3A and MAP 3B cores show slightly different geometry of the $\delta^{13}C$ decrease complicating firm placement of the CIE onset (Fig. 4.3). Isotopic and percent $CaCO_3$ records generally agree between the two cores when applying adjusted for core expansion depths, i.e. modified core depth (Fig. 4.S5). MAP 3A recorded a gradual decrease in bulk sediment $\delta^{13}C$ values from 57 ft (17.4 m) to 55.4 ft (16.9 m) (Fig. 4.3) that is confirmed by $\delta^{13}C$ decreases in benthic foraminifera and surface dwelling *Acarinina* spp. (Fig. 4.5). Foraminifera showed the excursion between 56.5 ft (17.2 m) and 56 ft (17.1 m) defining the *sensu stricto* placement of CIE onset below 56 ft at MAP 3A (Fig. 4.3). MAP 3B showed sharp decrease at 55.9 ft (17 m) with sporadic PETM $\delta^{13}C$ values occurring below in the 56.3-56.7 ft interval (17.2-17.3 m) (Fig. 4.3). In contrast to discrepancy in the CIE onset placement, the onset of low carbonate (<1% $CaCO_3$) zone appeared at the same depth (56.3 ft; 17.2 m) in both cores corresponding with the decrease in coarse fraction due to clay input (Fig. 4.3). Altogether these suggest a firm CIE onset placement at 55.9-56.3 ft (17-17.2 m) with initial decrease in $\delta^{13}C$ values striking below at 57 ft (17.4 m) at MAP 3A and MAP 3B.

4.4.2 Foraminiferal assemblages at MAP 3A, Medford, NJ

The foraminiferal assemblages of the Vincentown Formation are dominated by benthic species (Figs. 4.4 and 4.6). The benthic foraminifera assemblage represents typical Paleocene Midway fauna [Berggren and Aubert, 1975], suggesting middle shelf settings with paleowater depths of ~30-50 m. *Cibicidoides* spp. are most abundant benthic taxa in the Vincentown Formation. Planktonic foraminifera are dominated by *Acarinina* spp. with fewer *Subbotina* spp. and rare *M. aequa* in the Vincentown Formation. The planktonic to benthic ratio (P/B) is less than 1 in the Vincentown

Formation (Fig. 4.6). With the onset of the low (<1% $CaCO_3$) zone, the P/B in the 212-250 μm and 250-300 μm size fractions increases to 2-3 and is above 25 in the Marlboro Formation (Figs. 4.6 and 4.7). The increased abundances of % planktonics in larger size fractions (higher P/B ratio; Fig. 4.7) in the low carbonate zone argue against a cause by dissolution since planktonics are less resistant to dissolution. Rather, this argues for a strong dilution control.

A low carbonate zone at Medford, NJ (54.8-56.3 ft; 16.7-17.2 m) spanning the interval of transitional lithology (10-75% coarse fraction) is characterized by a decrease of foraminiferal number per gram dry sediment (Fig. 4.6). However, foraminiferal tests are well preserved (Fig. 4.S6) within this 1.5 ft (0.5 m) thick zone and the assemblage mostly consists of *Acarinina* spp. and *Anomalinoides* spp, and a few smaller specimens of *Morozovella* and *Subbotina*. Highest occurrence of *G. beccariiformis* is at 55.55 ft (16.9 m) and *Cibicidoides* spp. disappear from 55.3 ft (16.9 m) upward. Rare malformed tests of planktonic foraminifera with abnormal chamber shapes and additional champers (Fig. 4.S7) are present in 54.0-55.75 (16.5-17 m).

The Marlboro Formation is dominated by large planktonic foraminifera with abundant *M. acuta*, *Acarinina* spp., and *Subbotina* spp. *M. acuta* is the dominant *Morozovella* species in the Marlboro Clay in contrast to *M. aequa*-dominated Vincentown Formation. Benthic foraminifera are only present in the <212 μm size fraction and the most abundant benthic species are *A. acuta* and *A. midwayensis* (Fig. 4.S8). Planktonic foraminifera reached maximum abundance at 52.85-54.55 ft (16.1-16.6 m) and gradually decreased in abundance from 52.85 ft (16.1 m) upward (Fig. 4.6). Foraminiferal wall textures are well preserved; however, both benthic and planktonic

species have pyrite framboids, infilling and coatings, giving them “dirty” appearance (Fig. 4.S8).

The foraminiferal assemblage in the Manasquan Formation shows a return to settings similar to those during the latest Paleocene. Benthic taxa are dominated by *Cibicidoides* spp. and planktonic foraminifera are present by most abundant *Subbotina* spp., *M. aequa* and fewer *Acarinina* spp. (Fig. 4.4). P/B is less than 1 in the >300 μm fraction and is 2-3 in smaller size fractions (Fig. 4.6).

4.4.3 Foraminiferal stable isotopes from multiple-specimen analysis at MAP 3A, Medford, NJ

Multiple specimen $\delta^{13}C$ records showed 3.5 ‰ decreases in all genera (*Morozovella* spp., *Acarinina* spp., *Subbotina* spp., benthic taxa) mimicking the CIE in bulk sediment (Fig. 4.8; Table 4.2). Among foraminiferal isotopic records *Acarinina* are the only species spanning the low carbonate zone and recording intermediate $\delta^{13}C$ values of the gradual CIE onset at MAP 3A (Fig. 4.8). Species of *Subbotina* and *Morozovella* are too rare within the low carbonate zone to reconstruct changes in isotopic values across the PETM onset. Oxygen isotopic records revealed -1.5 ‰ $\delta^{18}O$ anomalies in benthic taxa and *Subbotina* spp. ($\Delta\delta^{18}O$ = $\delta^{18}O$ before the CIE onset minus $\delta^{18}O$ after the CIE onset), whereas $\Delta\delta^{18}O$ in surface dwelling *Morozovella* spp. and *Acarinina* spp. were ~1.0-1.2 ‰ (Fig. 4.8). Specifically, *Acarinina* spp. show a 0.5 ‰ increase in $\delta^{18}O$ values associated with the CIE onset and then a steplike decrease of 1.2 ‰ above the low carbonate zone (Fig. 4.8). Moreover, the oxygen isotopic record of *Acarinina* spp. shows a delayed anomaly ($\Delta\delta^{18}O$) in regards to the CIE onset. The decrease in $\delta^{13}C$ values of *Acarinina* spp. preceded the $\delta^{18}O$ decrease by at least 1 ft (30 cm) (Fig. 4.8). Benthic

foraminiferal species recorded a gradual decrease in $\delta^{18}O$ values in contrast to abrupt change in $\delta^{13}C$ values (Fig. 4.8). Interestingly, surface dwelling *Acarinina* spp. recorded values similar to benthic *A. acuta* and thermocline *Subbotina* spp. $\delta^{18}O$ values within the Marlboro Formation (Figs. 4.5 and 4.8). Also, the $\delta^{18}O$ isotopic gradient between surface to thermocline to benthic foraminifera is less than 1 ‰ in the Marlboro Formation in contrast to the 1.75 % $\delta^{18}O$ gradient in the Vincentown Formation (Fig. 4.8). Overall, foraminiferal isotopic records from the MAP 3A core are consistent with observations from other NJCP sites [Makarova et al., 2017].

4.4.4 Preliminary results of foraminiferal stable isotopes from single-specimen measurements at MAP 3A, Medford, NJ

The averaged $\delta^{13}C$ and $\delta^{18}O$ values measured in single tests of foraminifera agree with the isotopic records from multi-specimen measurements (Tables 4.2 and 4.3). Stable isotopes analyses of single foraminiferal tests showed bimodal distribution of $\delta^{13}C$ and $\delta^{18}O$ values between specimens from the Vincentown Formations and those from the Marlboro Formation (Fig. 4.9). Single specimens from the important transitional interval that spans the PETM onset at the MAP 3A core (54.5-56.5 ft; 16.6-17.2 m) are pending. A bimodal distribution in $\delta^{13}C$ values in the transition zone would imply very rapid onset of the CIE and the observed gradual carbon excursion in bulk sediment at MAP 3A would represent artifact of bioturbation and mixing of the pre- and post-CIE $\delta^{13}C$ values. Intermediate values mimicking changes in bulk sediment would suggest slower rates of the PETM onset. Similarly, distributions of $\delta^{18}O$ values would reveal fast versus gradual, slow warming. Therefore, additional data from the 54.5-56.5 ft (16.6-17.2 m) interval is

critical to reconcile the timing of the PETM onset from the high-resolution record of single specimen foraminiferal stable isotopes at Medford, NJ.

4.4.5 Trace elements (Mg/Ca, I/Ca) in foraminifera at MAP 3A, Medford, NJ

Trace elements analyses of planktonic and benthic foraminifera showed increases in Mg/Ca ratios in all species associated with the PETM onset at the MAP 3A core (Fig. 4.10; Table 4.4). *Subbotina* spp. indicated a 1.05 mmol/mol increase in Mg/Ca from 3.2 mmol/mol to 4.25 mmol/mol (Fig. 4.10). *Acarinina* spp. recorded a 0.75 mmol/mol increase in Mg/Ca from 2.94 mmol/mol to 3.7 mmol/mol (Fig. 4.10). The *M. acuta* Mg/Ca record shows average values of 3.8 mmol/mol in the Marlboro Formation (Fig. 4.10). The absolute values of Mg/Ca in surface dwelling *Morozovella* and *Acarinina* spp. are generally lower than in thermocline dwelling *Subbotina* spp. in the recovered at the MAP 3A core Marlboro Formation. The observed absolute values and changes of Mg/Ca ratios in planktonic foraminifera at MAP 3A are consistent with records from Ancora, Millville, and Bass River NJCP sites (Fig. 4.S9). The benthic foraminifera trace elemental ratios have been never reported for the PETM section from NJCP sites. The benthic *A. acuta* Mg/Ca record indicated a 1.05 mmol/mol increase from 3.34 mmol/mol to 4.34 mmol/mol at the MAP 3A core (Fig. 4.10). Mg/Ca anomalies recorded by benthics, thermocline dwelling *Subbotina* spp., and *A. acuta* correspond to warming of 3.1-3.2°C based on multi-species calibration of Anand et al. [2003].

Measurements of I/Ca showed distinct differences in values from planktonic versus benthic foraminifera at the MAP 3A core (Fig. 4.11). Surface dwelling *Morozovella* spp. and thermocline dwelling *Subotina* spp. recorded I/Ca values of less than 2 μmol/mol (Fig. 4.11). Within the Marlboro Clay, *Subbotina* spp. show slightly

elevated I/Ca values at 53.8-54.25 ft (16.4-16.53 m), *Morozovella* spp. have negligibly small I/Ca values, and I/Ca values in *Acarinina* spp. were below the detectable limit (Fig. 4.11). In contrast, benthic foraminifera recorded higher I/Ca values in the ~9-27 μmol/mol range (Fig. 4.11). *A. acuta* show I/Ca of 9-11 μmol/mol within the Marlboro Formation *Cibicidoides* spp. show I/Ca values of 11-18 μmol/mol in the Vincentown Formation (Fig. 4.11). Generally, I/Ca values in benthic foraminifera in the Marlboro Clay are lower than in above and below units (Fig. 4.11).

Ratios of other trace elements to calcium showed elevated values above the low carbonate zone at the base of the Marlboro Clay in the MAP 3A core (Fig. 4.12). There are noticeable spikes in Ba/Ca, Mn/Ca, U/Ca, and Fe/Ca at 54.55-54.65 ft (16.63-16.66 m). Values of Mn/Ca, Ba/Ca, U/Ca, and Fe/Ca remain elevated at 53.8-54.25 (16.4-16.53 m). All taxa showed higher Nd^{143}/Ca values within the Marlboro Formation than in over- and underlying sediments.

4.4.6 TEX_{86} derived temperature estimates at MAP 3B, Medford, NJ

Temperature records derived from TEX^{H}_{86} and TEX^{L}_{86} indices [Kim et al., 2010] showed an abrupt warming starting at 56.3 ft (17.2 m) at the MAP 3B core (Fig. 4.13; Table 4.5). Using TEX^{H}_{86}, I estimated a total warming of 6.2°C from 29.9°C to 36.1°C, whereas TEX^{L}_{86} showed larger warming of 8°C and cooler temperatures increasing from 23.1°C to 31.1°C (Fig. 4.13). Lower absolute temperature values and larger warming anomaly estimated by the TEX^{L}_{86} calibration are consistent with TEX_{86}-based estimates in other NJCP sites (Fig. 3.6 in Chapter Three). Warming at MAP 3B appeared in two steps with a temperature plateau at 55.1-55.8 ft (16.8-17 m): 1) a larger initial sharp temperature increase of 4.8-6.2°C from 56.3 ft (17.2 m) to 55.8 ft (17 m); and 2) a

smaller second temperature increase of 1.4-1.8°C from 55.1 (16.8 m) to 54.4 ft (16.6) (Fig. 4.13). The total warming with two steps and a temperature plateau appeared within a low (<1% $CaCO_3$) carbonate zone (Fig. 4.13), which corresponded to the decrease in coarse fraction and input of the Marlboro Clay at MAP 3B (Fig. 4.3). Although the placement of the CIE onset is arguable at MAP 3B (see section 4.4.1 "Bulk sediment isotopic records from Medford Sites MAP 3A and 3B"), the TEX_{86}-derived warming initiated either at the same level or above the CIE onset based on *sensu stricto* onset definition at 55.9-56.3 ft (17-17.2 m) or initial decrease in $\delta^{13}C$ values at 57 ft (17.4 m), respectively (Fig. 4.13). Particularly important, the MAP 3B TEX_{86} records indicated no warming below the CIE onset (Fig. 4.13). The BIT values are below 0.1 suggesting low soil organic matter input (Table 4.6).

4.5 Discussion

4.5.1 Depositional model for the New Jersey paleoshelf during the PETM

The distribution of PETM strata on the NJCP suggests increased sedimentation rates on the New Jersey paleoshelf associated with the PETM onset. Given >10 m in <<200 kyr mean sedimentation rate must be >>5 cm/kyr. Units of transitional from glauconitic silts of the Vincentown Formation to kaolinitic clays of the Marlboro Formation lithologies are the thickest in the MAP cores from Medford, NJ and are progressively thinner in more distal sections (Fig. 4.S2). Similarly, the low carbonate (<1% $CaCO_3$) zones are thicker in proximal and middle shelf sites than at distal Bass River. Moreover, good preservation of planktonic foraminifera within the low carbonate zone at the MAP 3A core suggests very rapid sedimentation rates and dilution associated

with the clay input rather than the dissolution. The interpretation of increased sedimentation rates was based on observations from sediment lithologies, carbonate content, and bulk $\delta^{13}C$ records that were explained by deltaic progradational deposition [Podrecca, 2018]. The clinoform depositional model implies a fluid mud reservoir source bypassing shallow zones and rapidly building foresets seaward of the rollover point (Fig. 4.S3). Therefore, the build up of successive clinoforms prograding offshore would result in thicker sections of the PETM onset in more proximal sites and thicker sections of later phases of the PETM in more distal sites, as seen in records of % coarse fraction, % $CaCO_3$, and bulk $\delta^{13}C$ values from NJCP sites (Fig. 4.S2, 4.S3, and 4.S4) [Podrecca, 2018].

4.5.2 Precursor warming? Results of multi proxy temperature estimates at Medford, NJ

The TEX_{86}-derived temperature records at the expanded section of the PETM onset at MAP Hole 3B core refutes the precursor warming hypothesis. Previously published TEX_{86} temperature calibrations showed a possible precursor warming at Wilson Lake Hole A [Zachos et al., 2006; Sluijs et al., 2007] and Bass River [Sluijs et al., 2007]. However, the precursor warming may be spurious when applying the TEX^{H}_{86} and TEX^{L}_{86} calibrations from Kim et al. [2010]. In fact, only the distal Bass River record showed a precursor warming (less than 2°C using the TEX^{L}_{86} calibration and ~ 4°C using the TEX^{H}_{86} calibration) in relation to the CIE onset, whereas the Wilson Lake Hole A and Millville (Fig. 3.6 in Chapter Three) TEX_{86}-based temperature records showed a little to no precursor warming. The record at MAP Hole 3B explicitly indicates no warming based on TEX_{86} temperature estimates prior to the CIE onset, even despite the slightly

uncertain level of CIE onset in the core (see section 4.4.1 “Bulk sediment isotopic records from Medford Sites MAP 3A and 3B”). The abrupt warming indicated by TEX_{86}-based temperature records at MAP 3B corresponds to the base of low carbonate zone and decrease in coarse fraction (Fig. 4.13) suggesting that the temperature increase was syncronous with the beginning of rapid clay deposion on the New Jersey paleoshelf at the initiation of the PETM, but lagged the carbon input.

Temperature estimates from stable oxygen isotopes and Mg/Ca ratios of foraminifera showed smaller warming anomalies (3.1-3.2°C) than TEX_{86}-based temperature records (6.2-8°C). Values of TEX_{86} might be influenced by factors other than factors in the nearshore environments (see section 3.5.2 “Spatial distribution of temperature anomalies on the New Jersey paleoshelf during the PETM: intersite comparisons of TEX_{86}-based estimates” and Fig. 3.6 in Chapter Three). Therefore, most proximal, shallow settings of the Medford site during the PETM might have resulted in a slightly overestimated TEX_{86}-derived warming anomaly than that recorded by foraminifera.

In general, specific Mg/Ca records at MAP 3 Hole A resemble the $\delta^{18}O$. However, Mg/Ca-based temperature anomalies are not consistent with $\Delta\delta^{18}O$. Surface and thermocline species $\Delta\delta^{18}O$ are larger than Mg/Ca-derived temperature increases (Fig. 4.10). This is seen in $\delta^{18}O$ and Mg/Ca records of planktonic foraminifera from other NJCP sites. In contrast to planktonic foraminifera, the oxygen isotopic record of benthic *A. acuta* shows minimal changes in $\delta^{18}O$ values within the Marlboro Formation at MAP Hole 3A, whereas Mg/Ca-based temperature estimates suggest a warming of ~3°C (Fig. 4.10). The discrepancy between $\delta^{18}O$- and Mg/Ca-derived temperature anomalies might

be associated with various degree of trace element inclusion during growth of different foraminiferal species and with the application of single Mg/Ca calibration equation for all species (i.e., the multispecies equation from Anand et al. [2003]).

The TEX_{86} estimated warming and bulk sediment $\delta^{18}O$ records from Medford cores revealed sharp two-step changes associated with the PETM onset, whereas bulk sediment $\delta^{13}C$ records showed gradual changes (over 50 cm) not recording such a sharp step (Figs. 4.3 and 4.13). The intermediate values of the "step interval" occur within the low carbonate zone. The same step-like changes in TEX_{86} and $\delta^{18}O$ values associated with the onset of low carbonate zone and decrease in coarse fraction were observed in records from other NJCP sites. Since carbon isotopic records displayed gradual decreases in $\delta^{13}C$ values, the step-like intermediate values in TEX_{86} and $\delta^{18}O$ were not an artifact of sediment mixing due to bioturbation.

Among the foraminiferal stable isotopes data from MAP Hole 3A, only *Acarinina* spp. provided continuous $\delta^{13}C$ and $\delta^{18}O$ records through the low carbonate zone (Fig. 4.8). *Acarinina* spp. showed a gradual decrease in $\delta^{13}C$ values within the low carbonate zone that is similar to bulk sediment. In contrast, oxygen isotopic values are stable and high in the low carbonate zone and the main negative $\delta^{18}O$ anomaly recorded by *Acarinina* spp. occurs at the top of the low carbonate zone (Fig. 4.8). Such step-like changes observed in TEX_{86} and bulk sediment and *Acarinina* spp. $\delta^{18}O$ records from Medford cores and confirmed by records from other NJCP sites can be associated either with: 1) much higher initial sedimentation rates during the PETM onset thus creating intermediate values in dilution (low carbonate) interval; and/or 2) by indeed two-step structure of the PETM warming. Stable isotopic measurements from single tests of

foraminifera from the low carbonate zone are required to further address this issue and constrain the nature of the PETM onset.

4.5.3 Paleoredox evaluation from trace metals in planktonic and benthic foraminifera from Medford, NJ

Variations in foraminiferal I/Ca ratios suggest lowered oxygen concentrations on the New Jersey paleoshelf, but not completely deoxygenated water column during the PETM. In general, lower I/Ca values recorded by planktonic foraminifera and higher I/Ca values recorded by benthic foraminifera at the MAP 3A core (Fig. 4.11) can be explained by higher productivity in the upper water column (lower [IO^{3-}]) and remineralization of organic matter near at the bottom water (higher [IO^{3-}]). The decrease in I/Ca of *Cibicidoides* spp. from 16-18 μmol/mol to 11 μmol/mol associated with the PETM onset (Fig. 4.11) is interpreted as a decrease in bottom water oxygen concentrations. The lower I/Ca ratios of 9-11 μmol/mol recorded by *A. acuta* within the Marlboro Formation could represent even less oxygenated bottom waters after the PEMT onset. However, bottom water did no go fully anoxic, otherwise benthic foraminifera would not detect iodine at any trace concentrations.

Other trace elemental ratios from foraminifera at the MAP 3A core also suggest lower oxygen concentrations on the New Jersey paleoshelf during the PETM. Elevated Fe/Ca and Mn/Ca indicate dysoxic sediments and low oxygen stress even in the nearshore environments. Development of fluid mud belt, abundant pyrite framboids in the Marlboro Clay, and a change in benthic foraminiferal assemblage to impoverished, oligotrophic taxa altogether support the suggested development of dysoxia in sediments coincident with PETM onset. Moreover, other paleoredox indicators from bulk sediment

at the Bass River section, NJ (vanadium enrichment and reactive iron concentration) are along the lines of evidence for transition toward dysoxia on the New Jersey paleoshelf during the PETM [Chen, 2014].

Changes in productivity are hard to decipherer based on trace elemental concentrations from foraminiferal calcite in the Medford PETM section. Elevated Nd/Ca ratio at the MAP 3A core (Fig. 4.12), however, suggest an increased influence of river discharge [e.g. Goldstein and Jacobsen, 1987]. Different redox signals from the North Atlantic and Tethyan shelf sections implied eutrophication associated with the riverine water influx on shelves [e.g., Crouch et al., 2003; Egger et al.., 2003; Gavrilov et al., 2003; Zachos et al., 2006; John et al., 2008; Aleksandrova and Shcherbinina, 2011; Schulte et al., 2011; Stassen et al. 2012; 2015; Khozyem et al., 2013; 2015; Shcherbinina et al., 2016]. The increased surface productivity in its turn would have caused higher concentrations of organic matter trapped in sediment, whereas sediment dysoxia and increased rates of mud deposition would have facilitated preservation of organic matter on the New Jersey paleoshelf. However, none of the NJCP sections showed much variation in percent of total organic matter in the sediment during the PETM (Fig. 4.S10). Thus, the eutrophication of the New Jersey paleoshelf associated with the PETM onset is debatable based on the availbale data.

4.6 Conclusions

Cores drilled at Medford, NJ provide a great potential to study the PETM onset on the mid-Atlantic shelf at a much higher resolution than in other New Jersey Coastal Plain (NJCP) sites and elsewhere in the marine realm due to its expanded section of the base of

the Marlboro Formation. The CIE at MAP sections is associated with input of kaolinitic clays, a gradual decrease in coarse fraction, and the onset of a low (<1% $CaCO_3$) carbonate zone. Foraminifera are rare but well preserved in the onset interval. All together this implies higher sedimentation rates and dilution of carbonate rather than dissolution. Thicker sections of the PETM onset at proximal Medford sites and progressively thinner onset sections in further offshore locations are explained by the depositional model of fluid mud in series of prograding seaward clinoforms. Thicker onset sections at Medford suggest higher sedimentation rates in the nearshore locations than in distal areas corresponding to the initiation of the PETM.

All foraminiferal taxa recorded a ~3.5 ‰ $\delta^{13}C$ decrease associated with the PETM onset similar to the bulk sediment CIE, validating the fidelity of the bulk records, whereas thermocline dwellers and benthic foraminiferal species showed larger $\delta^{18}O$ decreases compared to surface dwellers. This is consistent with observations from other NJCP sites interpreted as a change in the water column structure and/or a change in calcification season of the surface dwellers due to environmental stress [Makarova et al., 2017]. TEX_{86}-based temperature estimates showed a larger warming (anomaly of 6.2-8°C) than in foraminiferal tracers that occurred in two step-like increases within the low carbonate zone. No warming is observed the TEX_{86} record prior to the CIE onset at Medford refuting the precursor warming hypothesis.

Trace element analyses showed development of dysoxic conditions on the New Jersey paleoshelf during the PETM. Decreased benthic foraminiferal I/Ca values in the Marlboro Formation imply lower oxygen concentration, but not fully anoxic bottom waters. Higher Nd/Ca ratio within the Marlboro clay supports the increased river

discharge on shelf associated with the mud deposition. Enhanced riverine input and attendant eutrophication on the shelf has been suggested from studies of magnetotactic bacteria [Kopp et al., 2009], but are difficult to validate based on trace elemental ratios from foraminifera.

4.7 Acknowledgements

This work was supported by a Graduate Fellowship from the Department of Earth and Planetary Sciences at Rutgers University and two Geological Society of America research grants. I am grateful to Dr. Timothy D. Herbert for the opportunity to work in the organic geochemistry laboratory at Brown University and Dr. Marcelo Da Rosa Alexandre and Laura Messier for their help with the lipid biomarker analyses. I thank Dr. James D. Wright, Dr. Rick Mortlock, and Mark Yu for measuring stable isotopes. I also thank Dr. Yair Rosenthal, Dr. Xiaoli Zhou, and Kaixuan (Ryan) Bu for the help with trace element analyses. I am grateful to Luca Podrecca and Dr. James V. Browning for assistance in the core repository and discussions.

4.8 References

Aleksandrova, G.N. and E.A. Shcherbinina (2011), Stratigraphy and Paleoenvironmental Interpretation of the Paleocene–Eocene Transition in the Eastern Crimea, Stratigraphy and Geological Correlation, 19(4), 424–449.

Anand, P., H. Elderfield, and M.H. Conte (2003), Calibration of Mg/Ca thermometry in planktonic foraminifera from a sediment trap time series, Paleoceanography, 18/2, 1–15; doi:10.1029/2002PA000846.

Aubry, M.-P., K. Ouda, C. Dupuis, W.A. Berggren, J.A. Van Couvering, and the Members of the Working Group on the Paleocene/Eocene Boundary (2007), The Global Standard Stratotype-section and Point (GSSP) for the base of the Eocene Series in the Dababiya section (Egypt), Episodes, 30(4), 271–286.

Bains, S., R.M. Corfield, and R.D. Norris (1999), Mechanisms of climate warming at the end of the Paleocene, Science, 285, 724–727.

Berggren W.A. and J. Aubert (1975), Paleocene Benthonic Foraminiferal Biostratigraphy, Paleobiogeography and Paleoecology of Atlantic-Tethyan Regions: Midway-Type Fauna, Palaeogeography, Paleoclimatology, Palaeoecology, 18, 73–192.

Boyle, E.A. and L.D. Keigwin (1985), Comparison of Atlantic and Pacific paleochemical records for the last 215,000 years: changes in deep ocean circulation and chemical inventories, Earth and Planetary Science Letters, 76, 135–150.

Chen, A.P. (2014), Rock magnetic properties of uncultivated magnetotactic bacteria and paleo-redox changes across the Paleocene-Eocene boundary, New Jersey Coastal Plain, Ph.D. Thesis, Macquarie University, 139 p.

Cramer, B.S. and D.V. Kent (2005), Bolide summer: The Paleocene/Eocene thermal maximum as a response to an extraterrestrial trigger, Palaeogeography, Palaeoclimatology, Palaeoecology, 224, 144–166.

Cushman, J.A. (1951), Paleocene Foraminifera of the Gulf Coastal Region of the United States and Adjacent Areas, Geological Survey Professional Paper 232, United States Government Printing Office, 1–75.

Dickens, G.R., M.M. Castillo, and J.C.G. Walker (1997), A blast of gas in the latest Paleocene: Simulating first-order effects of massive dissociation of oceanic methane hydrate, Geology, 25(3), 259–262.

Dunkley Jones, T., D.J. Lunt, D.N. Schmidt, A. Ridgwell, A. Sluijs, P.J. Valdes, and M. Maslin (2013), Climate model and proxy data constraints on ocean warming across the Paleocene-Eocene Thermal Maximum, Earth-Science Reviews, 125, 123–145, doi:10.1016/j.earscirev.2013.07.004.

Dickson, A.J., A.S. Cohen, A.L. Coe, M. Davies, E.A. Shcherbinina, Y.O. Gavrilov (2015), Evidence for weathering and volcanism during the PETM from Arctic Ocean and Peri-Tethys osmium isotope records, Palaeogeography, Palaeoclimatology, Palaeoecology, 438, 300–307.

Dunkley Jones, T., D.J. Lunt, D.N. Schmidt, A. Ridgwell, A. Sluijs, P.J. Valdes, and M. Maslin (2013), Climate model and proxy data constraints on ocean warming across the Paleocene-Eocene Thermal Maximum, Earth-Science Reviews, 125, 123–145, doi:10.1016/j.earscirev.2013.07.004.

Gavrilov, Y.O., E.A. Shcherbinina, and H. Oberhänsli (2003), Paleocene-Eocene boundry events in the northeastern Peri-Tethys, Special Paper of the Geological Society of America, 369, 147–168, doi:10.1130/0-8137-2369-8.147.

Giusberti, L., D. Rio, C. Agnini, J. Backman, E. Fornaciari, F. Tateo, and M. Oddone (2007), Mode and tempo of the Paleocene-Eocene thermal maximum in an expanded section from the Venetian pre-Alps, Geological Society of America Bulletin, 119 (3/4), 391–412; doi:10.1130/B25994.1.

Goldstein, S.J and S.B. Jacobsen (1987), The Nd and Sr isotopic systematics of river-water dissolved material: Implications for the sources of Nd and Sr in seawater, Chemical Geology: Isotope Geoscience section, 66 (3-4), 245–272.

Gutjahr, M., Andy Ridgwell, P.F. Sexton, E. Anagnostou, P.N. Pearson, H. Pälike, R.D. Norris, E. Thomas, and G.L. Foster (2017), Very large release of mostly volcanic

carbon during the Palaeocene–Eocene Thermal Maximum, Nature, 548, 573–577, doi:10.1038/nature23646.

Hopmans, E.C., S. Schouten, and J.S. Sinninghe Damsté (2016), The effect of improved chromatography on GDGT-based palaeoproxies, Organic Geochemistry, 93, 1–6.

John, C.M., S.M. Bohaty, J.C. Zachos, A. Sluijs, S. Gibbs, H. Brinkhuis, and T.J. Bralower (2008), North American continental margin records of the Paleocene-Eocene thermal maximum: Implications for global carbon and hydrological cycling, Paleoceanography, 23, 1–20, doi:10.1029/2007PA001465.

Katz, M.E., B.S. Cramer, G.S. Mountain, S. Katz, and K.G. Miller (2001), Uncorking the bottle: What triggered the Paleocene/Eocene thermal maximum methane release? Paleoceanography, 16(6), 549–562.

Kent, D.V., B.S. Cramer, L. Lanci, D. Wang, J.D. Wright, and R. Van der Voo (2003), A case for a comet impact trigger for the Paleocene/Eocene thermal maximum and carbon isotope excursion, Earth and Planetary Science Letters, 211, 13–26.

Kent, D.V., L. Lanci, H. Wang, and J.D. Wright (2017), Enhanced magnetization of the Marlboro Clay as a product of soil pyrogenesis at the Paleocene–Eocene boundary? Earth and Planetary Science Letters, 473, 303–312.

Khozyem, H., T. Adatte, J..E. Spangenberg, A.A. Tantawy, and G. Keller (2013), Palaeoenvironmental and climatic changes during the Palaeocene–Eocene Thermal Maximum (PETM) at the Wadi Nukhul Section, Sinai, Egypt, Journal of the Geological Society, London, 170, 341–352. doi:10.1144/jgs2012-046.

Khozyem, H., T. Adatte, J.E. Spangenberg, G. Keller, A.A. Tantawy, and A. Ulianov (2015), New geochemical constraints on the Paleocene–Eocene thermal maximum: Dababiya GSSP, Egypt, Palaeogeography, Palaeoclimatology, Palaeoecology, 429, 117–135.

Kim, J.-H., J. van der Meer, S. Schouten, P. Helmke, V. Willmott, F. Sangiorgi, N. Koc, E.C. Hopmans, and J.S. Sinninghe Damsté (2010), New indices and calibrations derived from the distribution of crenarchaeal isoprenoid tetraether lipids: implications for past sea surface temperature reconstructions, Geochimica et Cosmochimica Acta, 74, 4639–4654.

Kirtland Turner, S. and A. Ridgwell (2016), Development of a novel empirical framework for interpreting geological carbon isotope excursions, with implications for the rate of carbon injection across the PETM, Earth and Planetary Science Letters, 435, 1–13, doi:10.1016/j.epsl.2015.11.027.

Kopp, R.E., D. Schumann, T.D. Raub, D.S. Powars, L.V. Godfrey, N.L. Swanson-Hysell, A.C. Maloof, and H. Vali (2009), An Appalachian Amazon? Magnetofossil evidence for the development of a tropical river-like system in the mid-Atlantic United States during the Paleocene-Eocene thermal maximum, Paleoceanography, 24, 1–17, doi:10.1029/2009PA001783.

Lu. Z., H.C. Jenkyns, and R.E.M. Rickaby (2010), Iodine to calcium ratios in marine carbonate as a paleo-redox proxy, Geology, 38(12), 1107–1110, doi:10.1130/G31145.1.

Makarova, M., J.D. Wright, K.G. Miller, T.L. Babila, Y. Rosenthal, and J.I.Park (2017), Hydrographic and ecologic implications of foraminiferal stable isotopic response across the U.S. mid-Atlantic continental shelf during the Paleocene-Eocene Thermal Maximum, Paleoceanography, 32, 1–18, doi:10.1002/2016PA002985.

McInerney, F.A. and S.L. Wing (2011), The Paleocene-Eocene thermal maximum: a perturbation of carbon cycle, climate, and biosphere with implications for the future, Annual Review of Earth and Planetary Sciences, 39, 489–516.

Miller, K.G., P.J. Sugarman, J.V. Browning, R.K. Olsson, S.F. Pekar, T.J. Reilly, B.S. Cramer, M.-P. Aubry, R.P. Lawrence, J. Curran, M. Stewart, J.M. Metzger, J. Uptegrove, D. Bukry, L.H. Burckle, J.D. Wright, M.D. Feigenson, G.J. Brenner, and R.F. Dalton (1998), Bass River Site, in K.G. Miller, P.J. Sugarman, J.V. Browning et al., eds., Proceedings of the Ocean Drilling Program, Initial reports, Volume 174AX: College Station, TX, Ocean Drilling Program, 5–43.

Olsson, R.K., C. Hemleben, W.A. Berggren, and B.T. Huber eds. (1999), Atlas of Paleocene planktonic foraminifera, Smithsonian contributions to paleobiology, 85, Smithsonian Institution Press, Washington D.C., 252 p.

Pearson, P.N., R.K. Olsson, B.T. Huber, C. Hemleben, and W.A. Berggren eds. (2006), Atlas of Eocene planktonic foraminifera, Cushman Foundation for foraminiferal research special publications, 41, 513 p.

Podrecca, L.G. (2018), Clear as mud: Assessing the paleoshelf environment and depositional setting at Medford, New Jersey during the Paleocene-Eocene Thermal Maximum, M.S. Thesis, Rutgers University, 81 p.

Rosenthal, Y., E.A. Boyle, and N. Slowey (1997), Temperature control on the incorporation of magnesium, strontium, fluorine, and cadmium into benthic foraminiferal shells from Little Bahama Bank: Prospects for thermocline paleoceanography, Geochimica at Cosmochimica Acta, 61(17), 3633–3643.

Schaller, M.F., M.K. Fung, J.D. Wright, M.E. Katz, and D.V. Kent (2016), Impact ejecta at the Paleocene-Eocene boundary, Science, 354(6309), 225–229, doi:10.1126/science.aaf5466.

Schulte, P., C. Scheibner, and R.P. Speijer (2011), Fluvial discharge and sea-level changes controlling black shale deposition during the Paleocene–Eocene Thermal Maximum in the Dababiya Quarry section, Egypt, Chemical Geology, 285, 167–183.

Shcherbinina, E., Y. Gavrilov, A. Iakovleva, B. Pokrovsky, O. Golovanova, and G. Aleksandrova (2016), Environmental dynamics during the Paleocene–Eocene thermal maximum (PETM) in the northeastern Peri-Tethys revealed by high-resolution micropalaeontological and geochemical studies of a Caucasian key section, Palaeogeography, Palaeoclimatology, Palaeoecology, 456, 60–81.

Si, W. and M.-P. Aubry (2018), Vital effects and ecologic adaptation of photosymbiont-bearing planktonic foraminifera during the Paleocene-Eocene Thermal Maximum, implications for paleoclimate, Paleoceanography and Paleoclimatology, 33, 1–14, https://doi.org/ 10.1002/2017PA003219.

Sluijs, A., H. Brinkhuis, S. Schouten, S.M. Bohaty, C.M. John, J.C. Zachos, G.J. Reichart, J.S. Sinninghe Damsté, E.M. Crouch, and G.R. Dickens (2007), Environmental precursors to rapid light carbon injection at the Palaeocene/Eocene boundary, Nature, 450(7173), 1218–1221, doi: 10.1038/nature06400.

Stassen, P., E. Thomas, and R.P. Speijer (2012), Integrated stratigraphy of the Paleocene-Eocene thermal maximum in the New Jersey Coastal Plain: Toward understanding the effects of global warming in a shelf environment, Paleoceanography, 27, 1–17, doi:10.1029/2012PA002323.

Stassen, P., E. Thomas, and R.P. Speijer (2015), Paleocene–Eocene Thermal Maximum environmental change in the New Jersey Coastal Plain: benthic foraminiferal biotic events, Marine Micropaleontology, 115, 1–23, doi:10.1016/j.marmicro.2014.12.001.

Storey, M., R.A. Duncan, and C.C. Swisher III (2007), Paleocene-Eocene thermal maximum and the opening of the Northeast Atlantic, Science, 316, 587–589.

Sugarman, P.J., K.G. Miller, J.V. Browning, M.-P. Aubry, G.J. Brenner, G. Cobbs III, L. de Romero, M.D. Feigenson, A. Harris, M.E. Katz, A. Kulpecz, P.P. McLaughlin Jr., S. Misintseva, D.H. Monteverde, R.K. Olsson, L. Patrick, S.J. Pekar, and J. Uptegrove (2005), Millville site, in K.G. Miller, P.J. Sugarman, J.V. Browning et al., eds., Proceedings of the Ocean Drilling Program, Scientific results, Vol. 174AX (supplement): College Station, Texas, Ocean Drilling Program, 1–95.

Sugarman, P.J., K.G. Miller, J.V. Browning, M.-P. Aubry, G.J. Brenner, D. Bukry, B. Butari, M.D. Feigenson, A.A. Kulpecz, P.P. McLaughlin Jr., S. Mizintseva, D.H. Monteverde, R.K. Olsson, A. Pusz, H. Rancan, J. Tomlinson, J. Uptegrove, and C.C. Velez (2010), Medford Site, in K.G. Miller, P.J. Sugarman, J.V. Browning et al., eds., Proceedings of the Ocean Drilling Program, Initial reports, Vol. 174AX (supplement): College Station, TX, 1–93.

Svensen, H., S. Planke, A. Malthe-Sørenssen, B. Jamtveit, R. Myklebust, T. Rasmussen Eidem, and S.S. Rey (2004), Release of methane from a volcanic basin as a mechanism for initial Eocene global warming, Nature, 429, 542–545.

Thomas, D.J., J.C. Zachos, T.M. Bralower, E. Thomas, and S. Bohaty (2002), Warming the fuel for the fire: Evidence for the thermal dissociation of methane hydrate during the Paleocene-Eocene thermal maximum, Geology, 30(12), 1067–1070.

Wright, J.D. and M.F. Schaller (2013), Evidence for a rapid release of carbon at the Paleocene-Eocene thermal maximum, Proceedings of the National Academy of Sciences of the United States of America, 110(40), 15908–15913.

Zachos, J.C., S. Schouten, S. Bohaty, T. Quattlebaum, A. Sluijs, H. Brinkhuis, S.J. Gibbs, and T.J. Bralower (2006), Extreme warming of mid-latitude coastal ocean during the Paleocene-Eocene Thermal Maximum: Inferences from TEX_{86} and isotope data, Geology, 34(9), 737–740.

Zeebe, R.E., A. Ridgwell, and J.C. Zachos (2016), Anthropogenic carbon release rate unprecedented during the past 66 million years, Nature Geoscience, 9, 325–329, doi:10.1038/ngeo2681.

Zhou, X., E. Thomas, R.E. Rickaby, A.M. Winguth, and Z. Lu (2014), I/Ca evidence for upper ocean deoxygenation during the PETM, Paleoceanography, *29*(10), 964–975, doi:10.1002/2014PA002702.

4.9 Figures

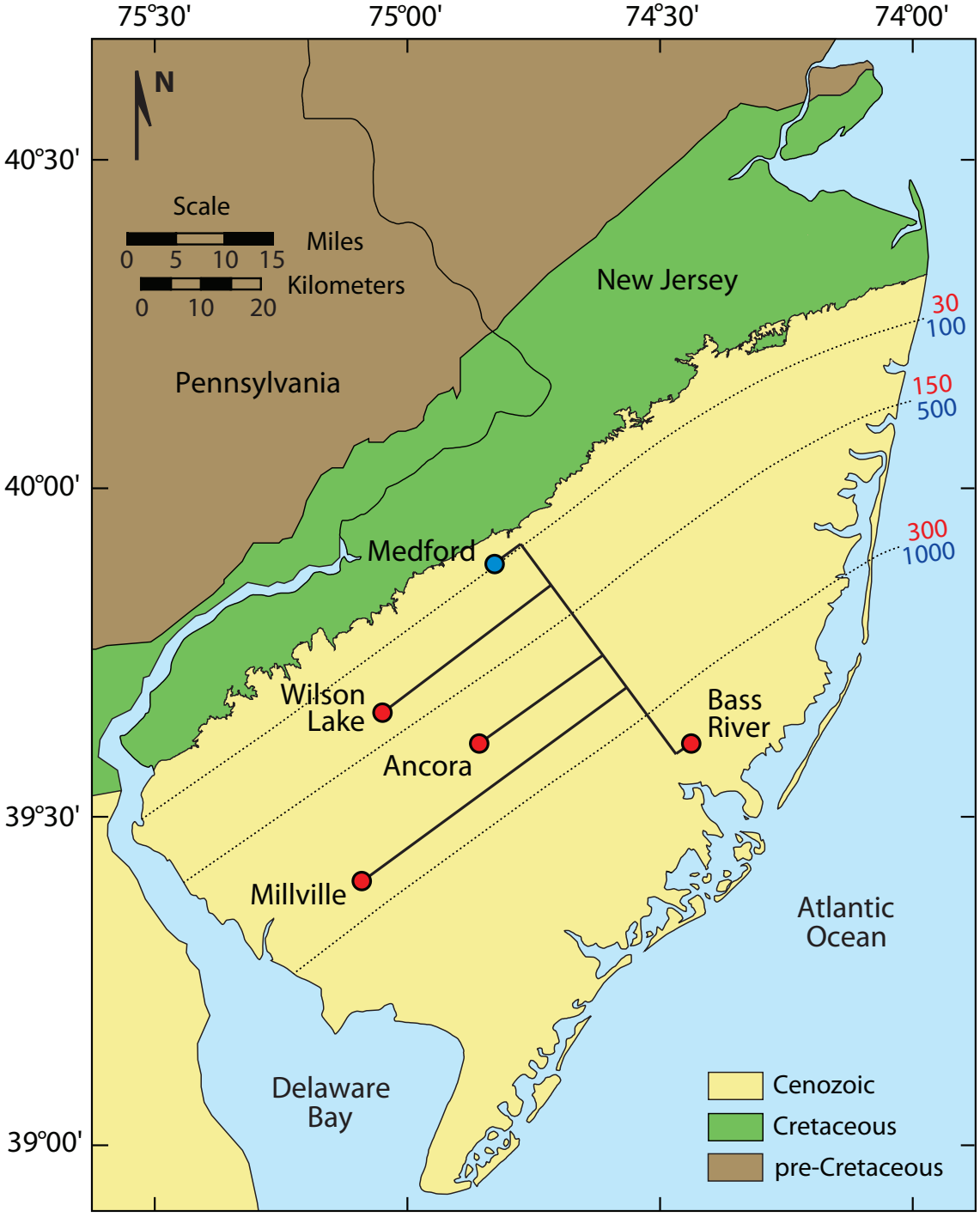

Fig. 4.1. Location map of the PETM sections on the New Jersey coastal plain: Medford, Wilson Lake, Ancora, Millville, and Bass River. Black solid lines represent projection of sites onto a dip profile drawn through Medford outcrop and Bass River [Makarova et al., 2017].

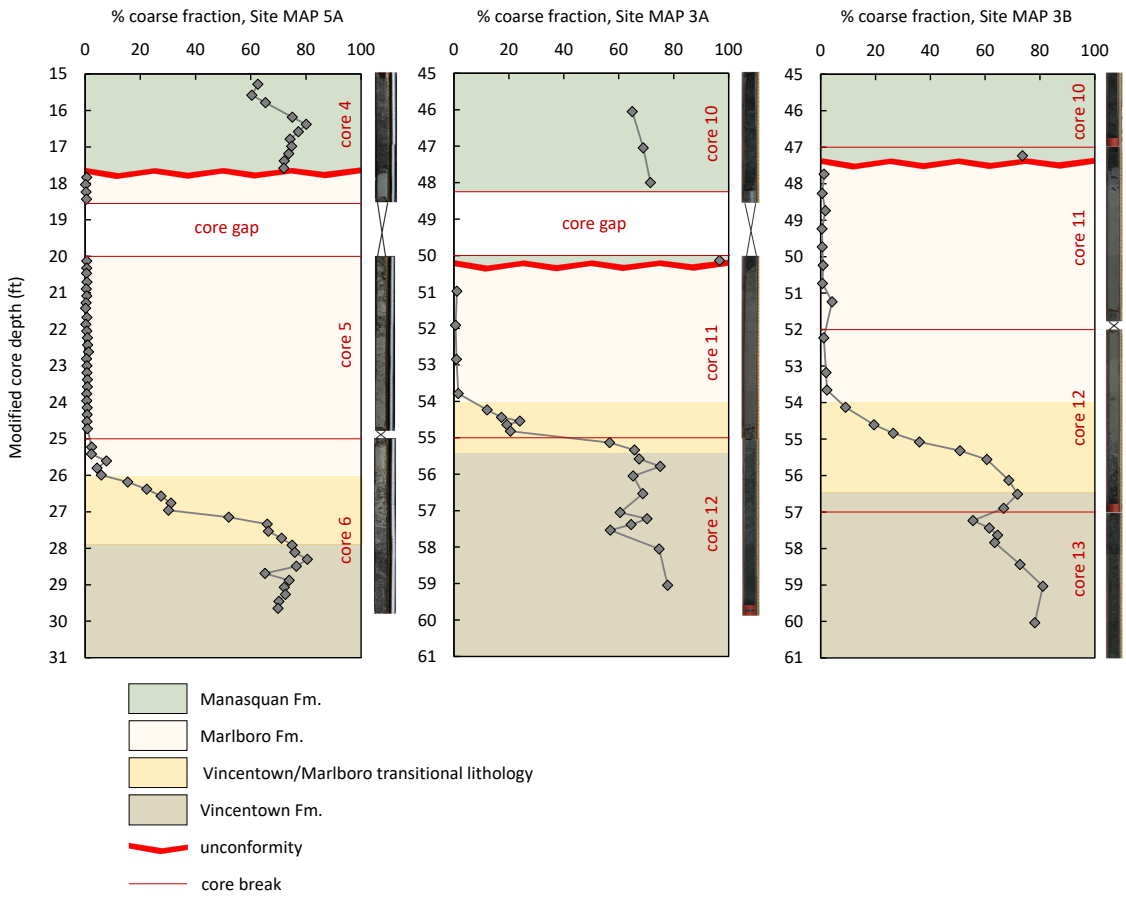

Fig. 4.2. Percent coarse fraction (>63 μm) records from MAP Sites 5A, 3A, and 3B, Medford, NJ.

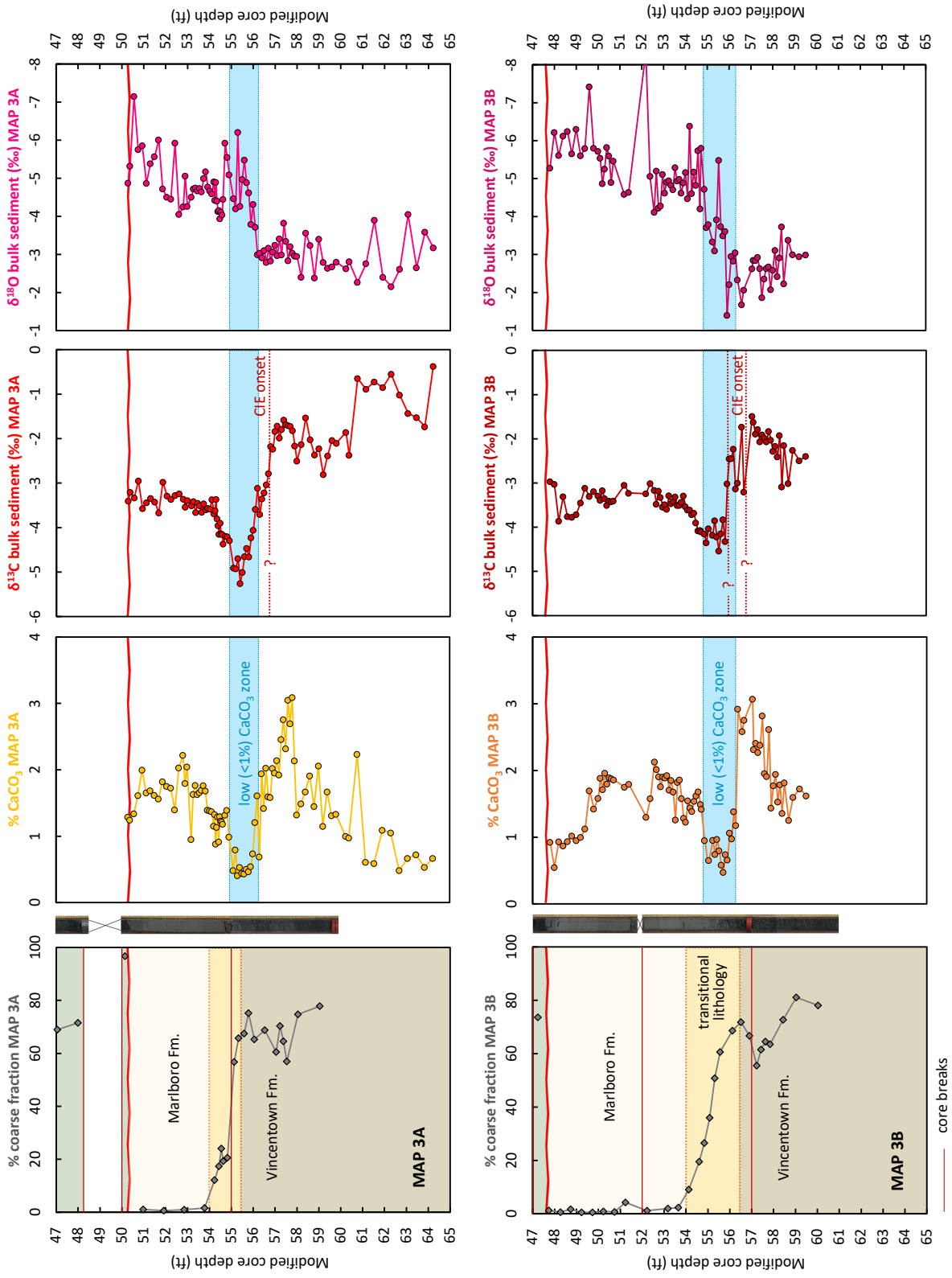

Fig. 4.3. Bulk sediment records (% $CaCO_3$, $\delta^{13}C$, $\delta^{18}O$; Podrecca [2018]) from MAP 3A and 3B cores, Medford, NJ.

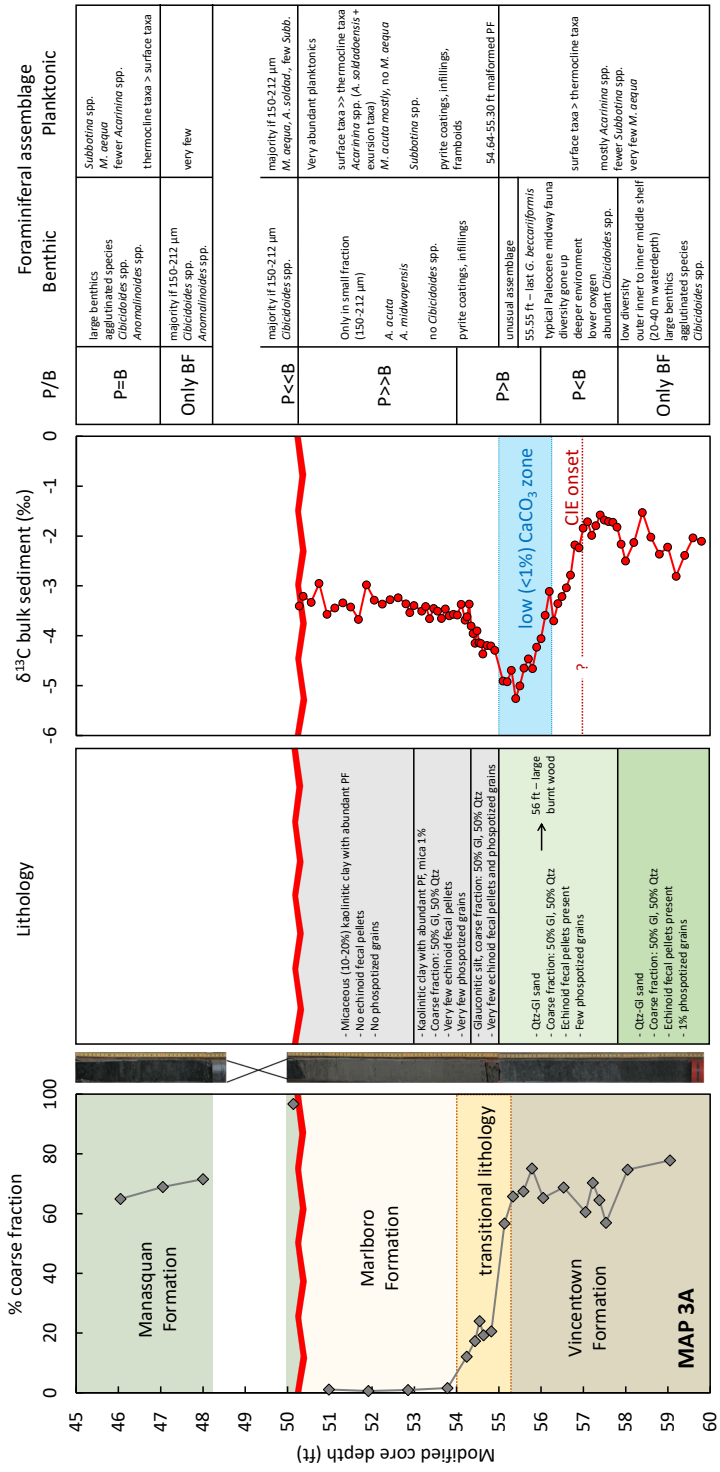

Fig. 4.4. Summary of the MAP 3A core from Medford, NJ: % coarse (>63 µm) fraction; lithological description; bulk sediment $\delta^{13}C$ with highlighted in blue low (<1%) $CaCO_3$ zone [Podrecca, 2018]; planktonic to benthic foraminifera relative abundance (P stands for planktonic foraminifera and B for benthic foraminifera); general description of planktonic and benthic foraminifera assemblages.

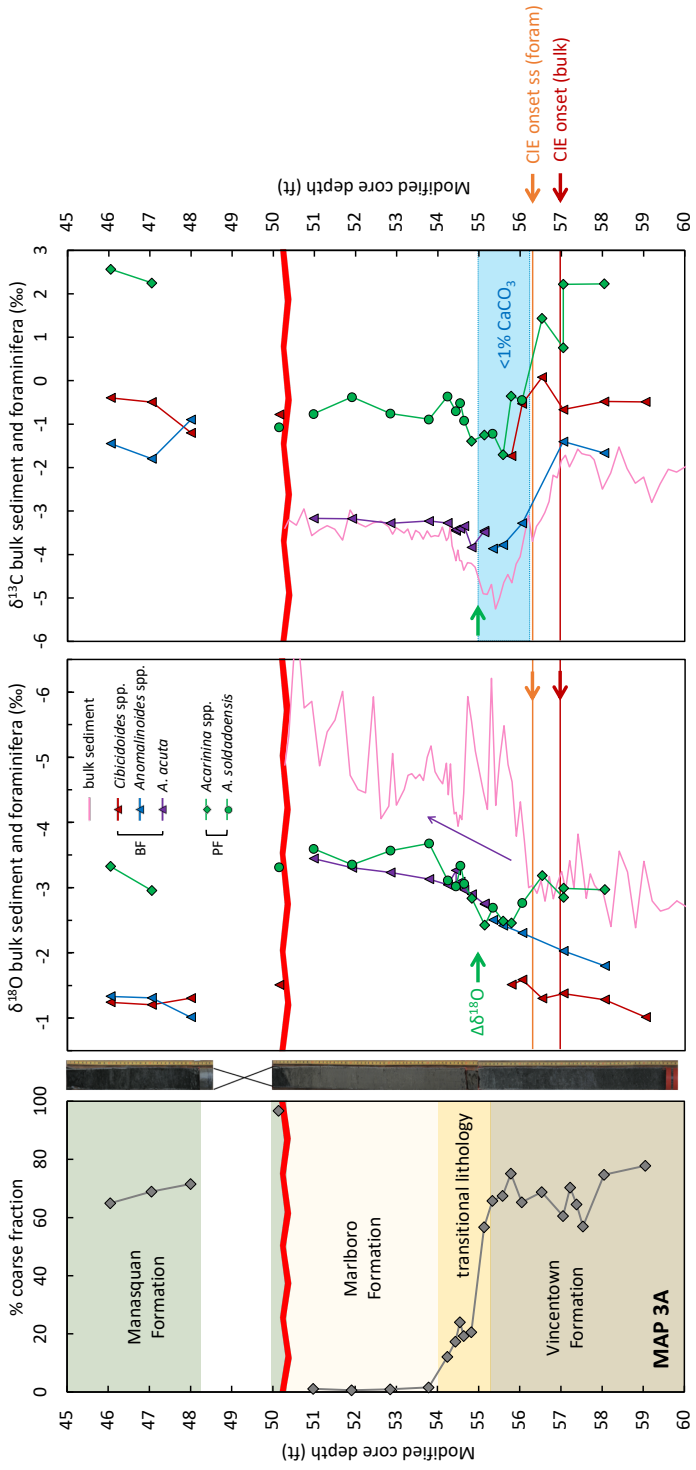

Fig. 4.5. Bulk sediment [Podrecca, 2018], planktonic (*Acarinina* spp. in green), and benthtic foraminiferal (*Cibicidoides* spp. in brown; *Anomalinoides* spp. in blue; *A. acuta* in purple) $\delta^{13}C$ records confirming the CIE onset at the MAP 3A core from Medford, NJ. SS stands for *sensu stricto*. Oxygen isotopic records show delayed anomaly in *Acarinina* spp. and *Anomalinoides* spp. in regards to the CIE.

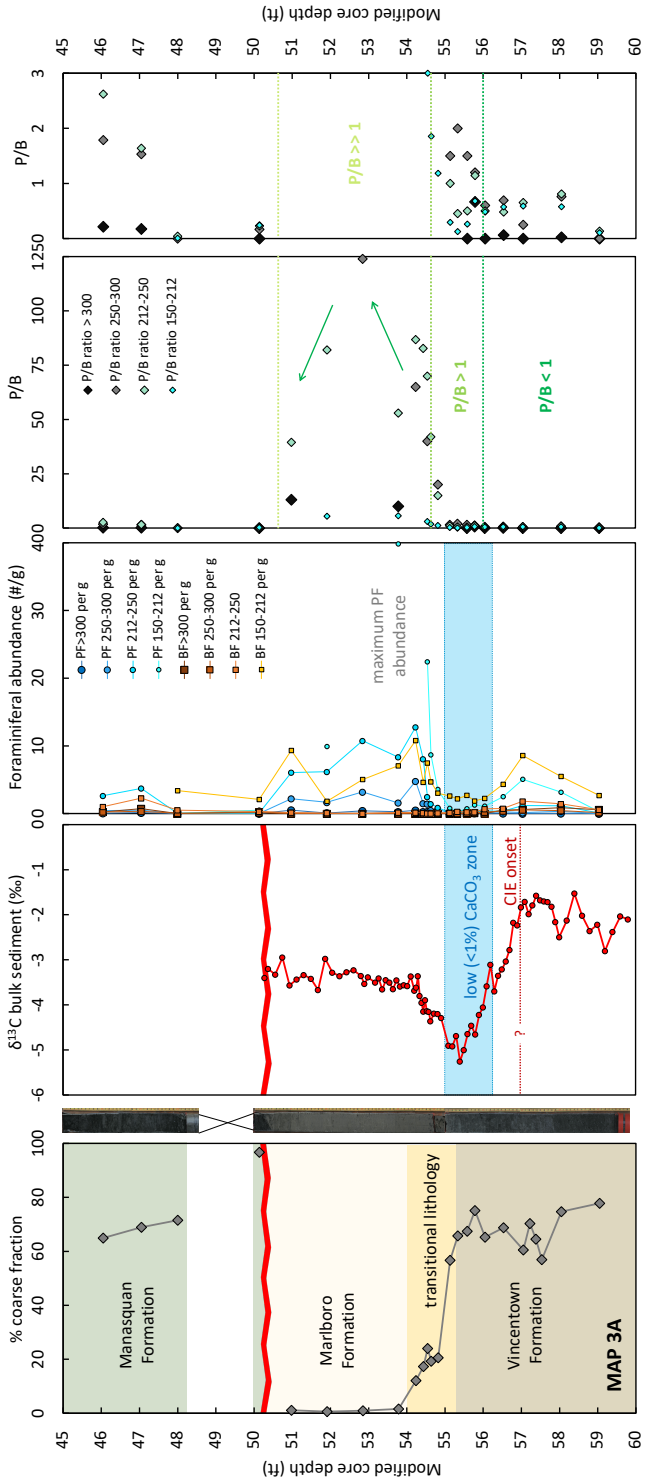

Fig. 4.6. Foraminiferal abundances in the MAP 3A core from Medford, NJ: number of planktonic to benthic foraminifera from >300 µm, 250-300 µm, 212-250 µm, and 150-212 µm size fractions per gram dry sediment; P/B ratio in >300 µm, 250-300 µm, 212-250 µm, and 150-212 µm size fractions. Bulk sediment $\delta^{13}C$ with highlighted in blue low (<1%) $CaCO_3$ zone are from Podrecca [2018].

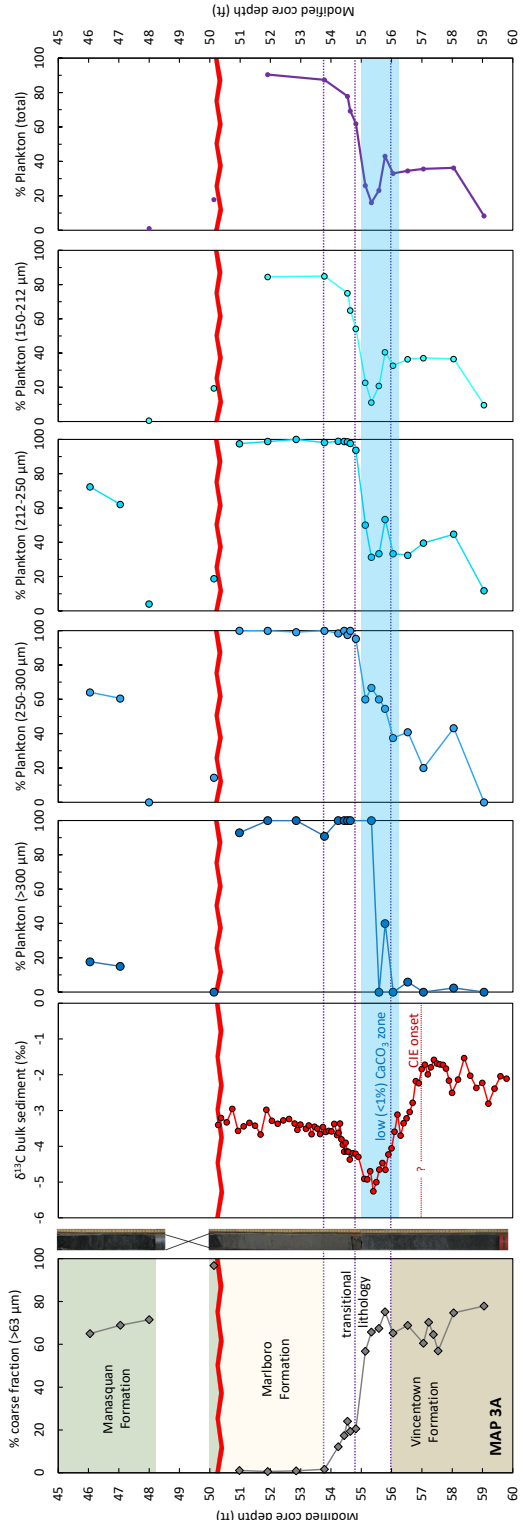

Fig. 4.7. Percent plankton in each fraction(>300 µm, 250-300 µm, 212-250 µm, and 150-212 µm) and total percent plankton in the MAP 3A core from Medford, NJ. Bulk sediment $\delta^{13}C$ with highlighted in blue low (<1%) $CaCO_3$ zone are from Podrecca [2018].

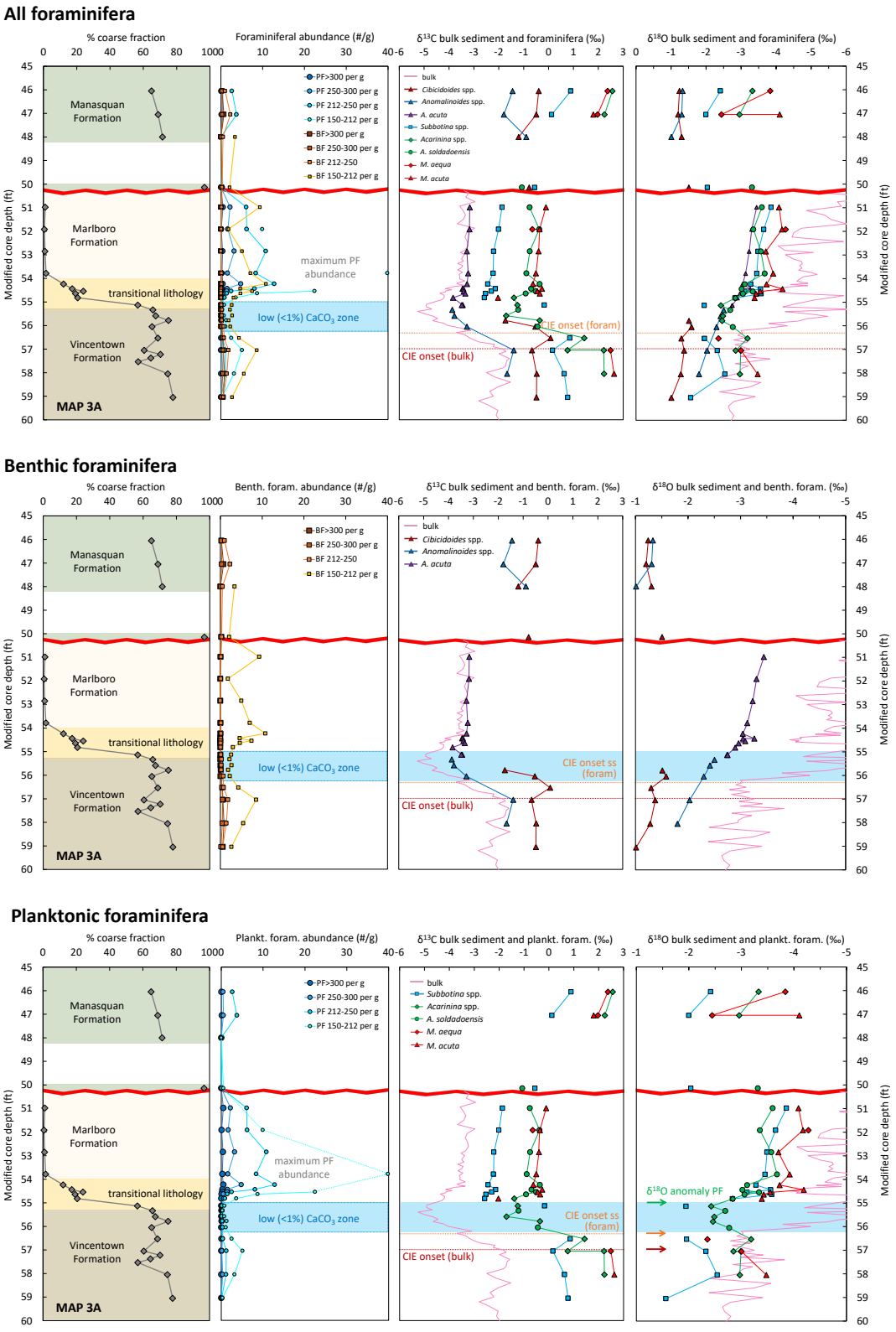

Fig. 4.8. Carbon and oxygen isotopic records from multi-specimen samples of foraminifera in the MAP 3A core from Medford, NJ. Bulk sediment $\delta^{13}C$ with highlighted in blue low (<1%) $CaCO_3$ zone are from Podrecca [2018].

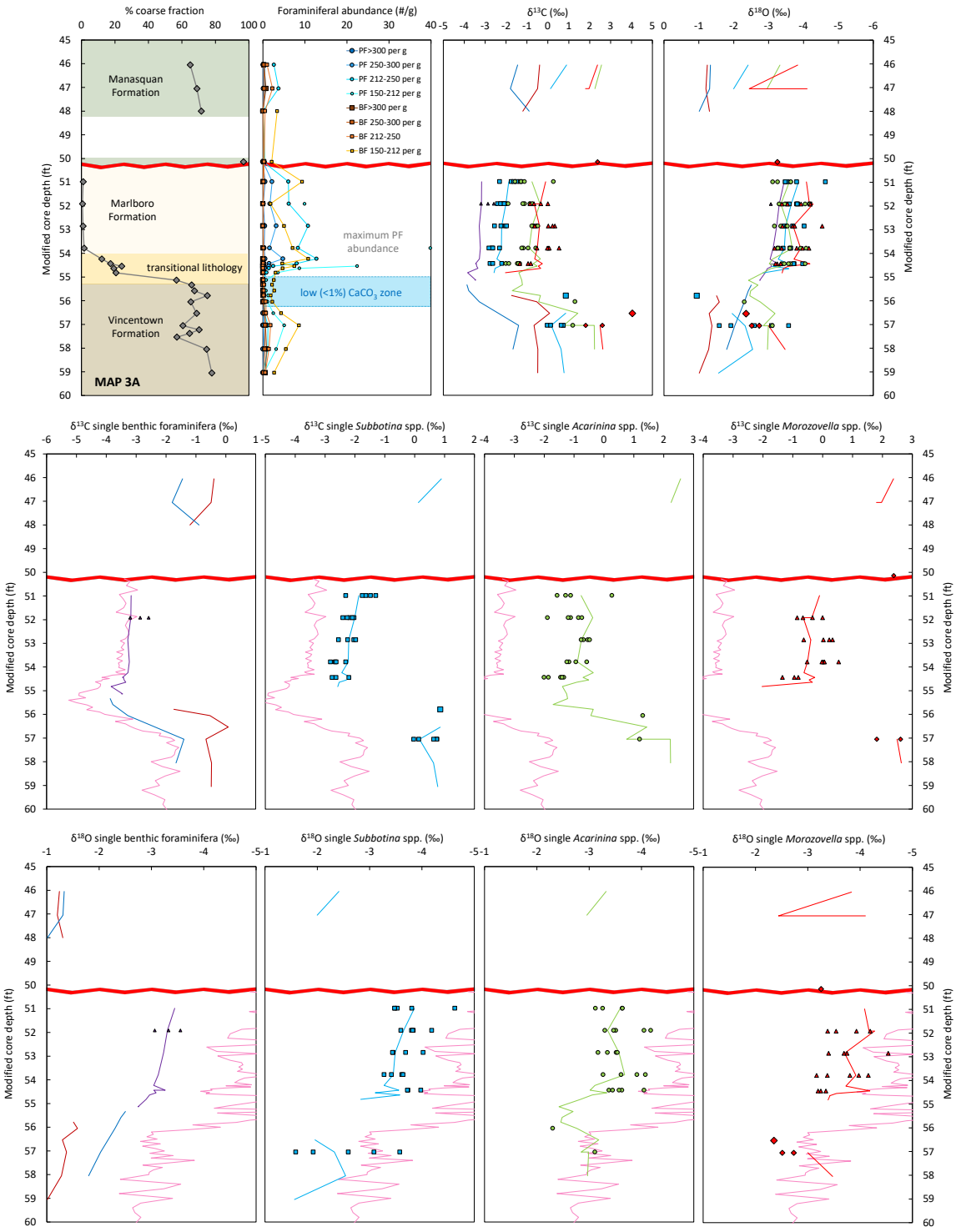

Fig. 4.9. Carbon and oxygen isotopic records from single-specimen samples of foraminifera in the MAP 3A core from Medford, NJ. Bulk sediment $\delta^{13}C$ and $\delta^{18}O$ (pink lines) and % $CaCO_3$ (<1% $CaCO_3$ zone highlighted in blue) are from Podrecca [2018]. See legend for foraminiferal symbols in Fig. 4.5. Lines indicate multi-specimen foraminiferal isotopic records.

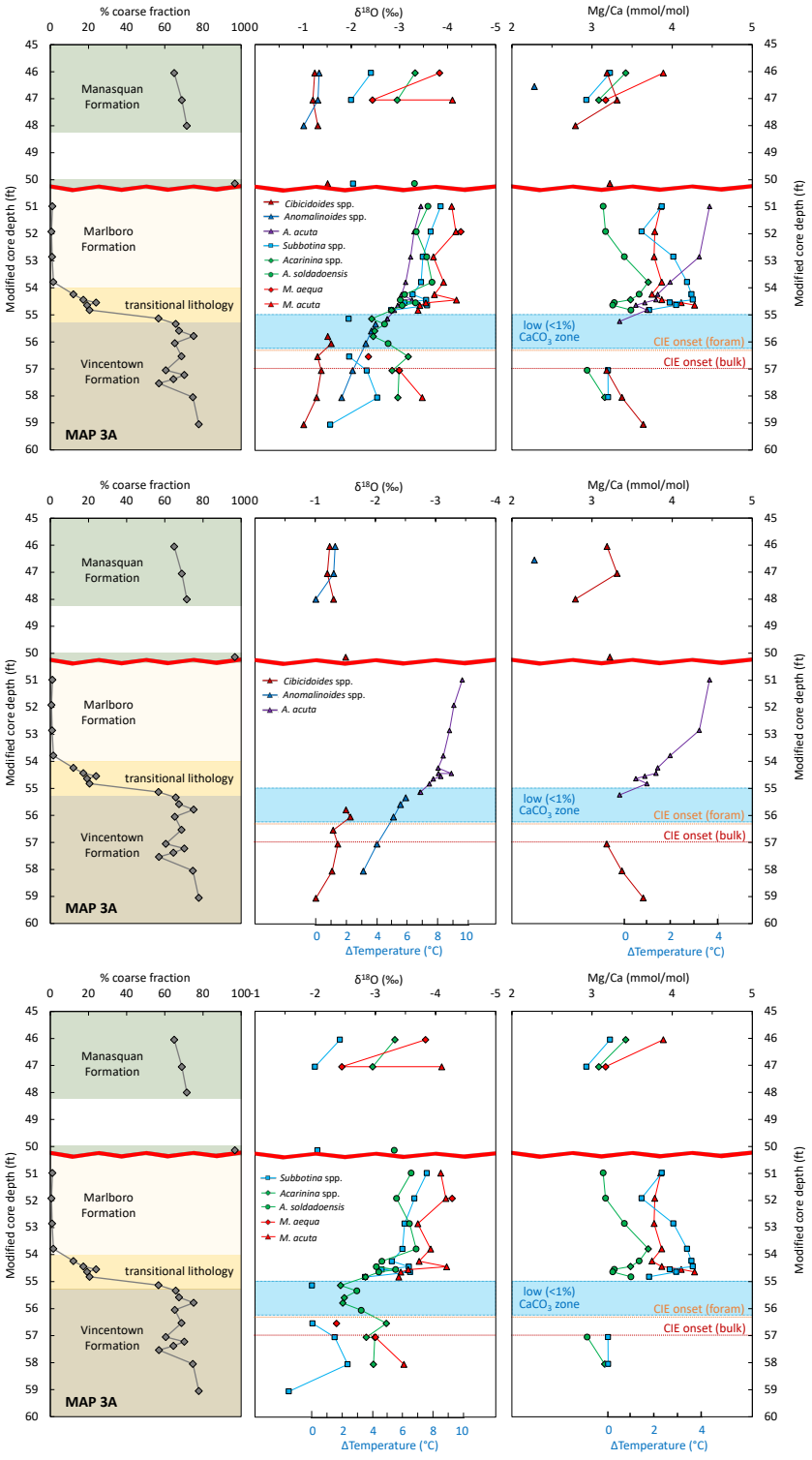

Fig. 4.10. Mg/Ca records of foraminifera in the MAP 3A core from Medford, NJ: top panels – all foraminifera; middle panels – benthic foraminifera; bottom panels – planktonic foraminifera. Temperature scale is given for a relative change in tempertature for each species.

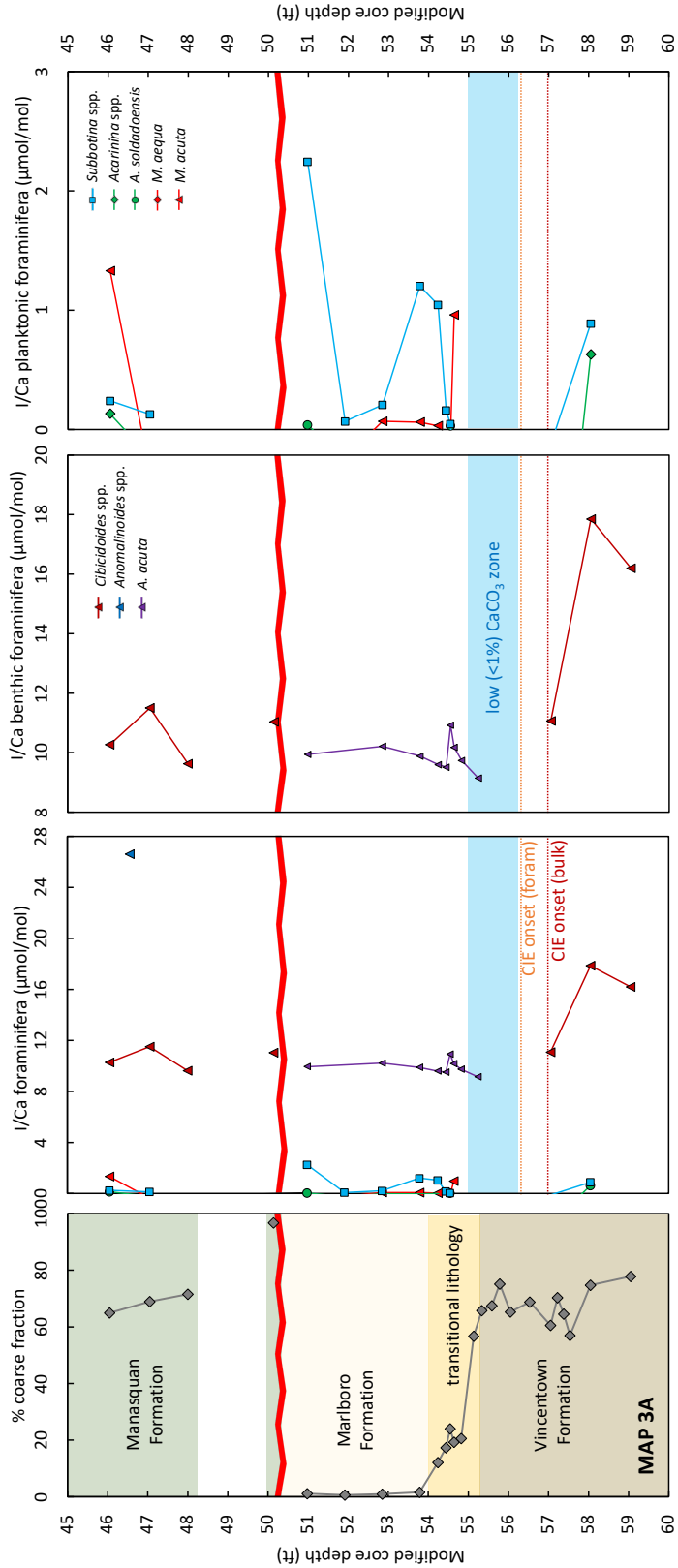

Fig. 4.11. I/Ca records of foraminifera in the MAP 3A core from Medford, NJ.

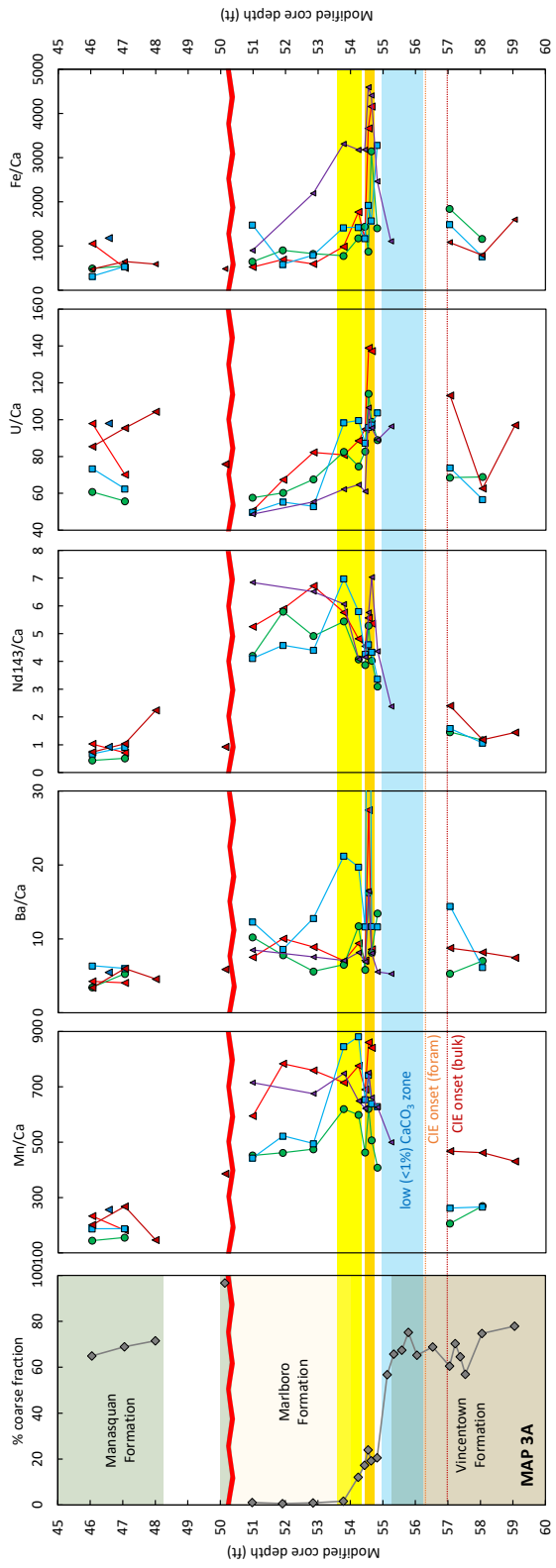

Fig. 4.12. Trace elemental ratios of foraminifera in the MAP 3A core from Medford, NJ: Mn/Ca, Ba/Ca, Nd/Ca, U/Ca, Fe/Ca.

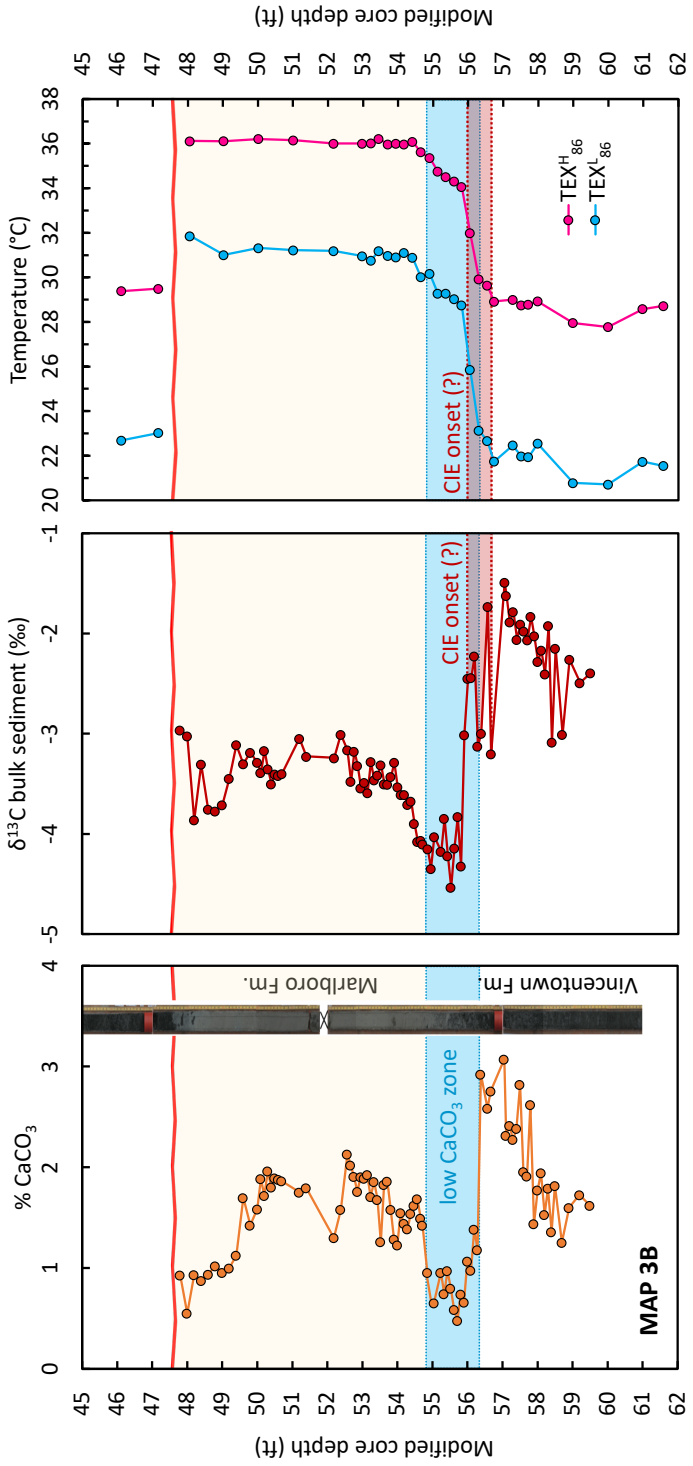

Fig. 4.13. Bulk sediment records (% $CaCO_3$, $\delta^{13}C$; Podrecca [2018]) and TEX_{86}-derived temperature estimates from MAP 3B core, Medford, NJ. Calibration errors for TEX^H_{86} and TEX^L_{86} are ±2.5°C and ±4°C, respectively [Kim et al., 2010]. The CIE onset at the MAP 3B core is shaded in red with top level representing *sensu stricto* placement of the CIE onset.

Supporting figures

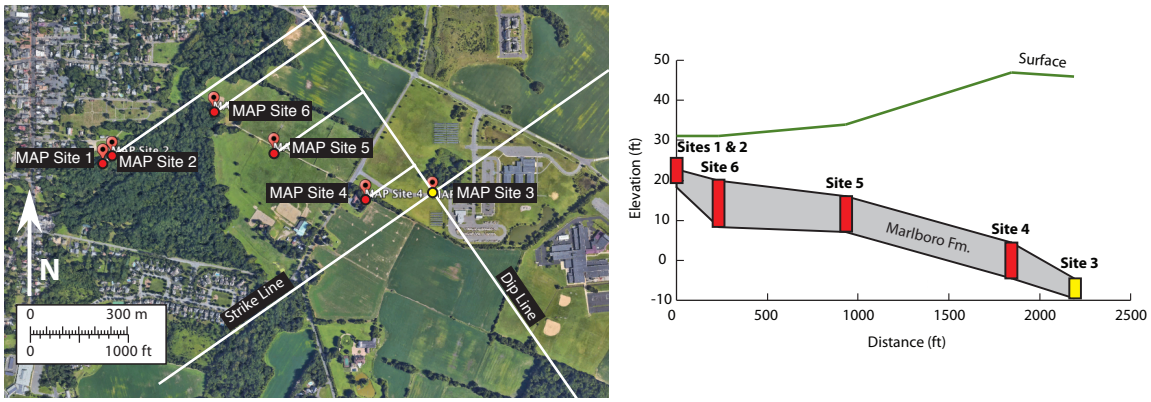

Fig. 4.S1. Medford Auger Project (MAP) holes location and cross section through the dip line with surface elevation, top and bottom of the Marlboro Formation, containing kaolinitic clay deposits of the PETM at Medford, NJ [Podrecca, 2018].

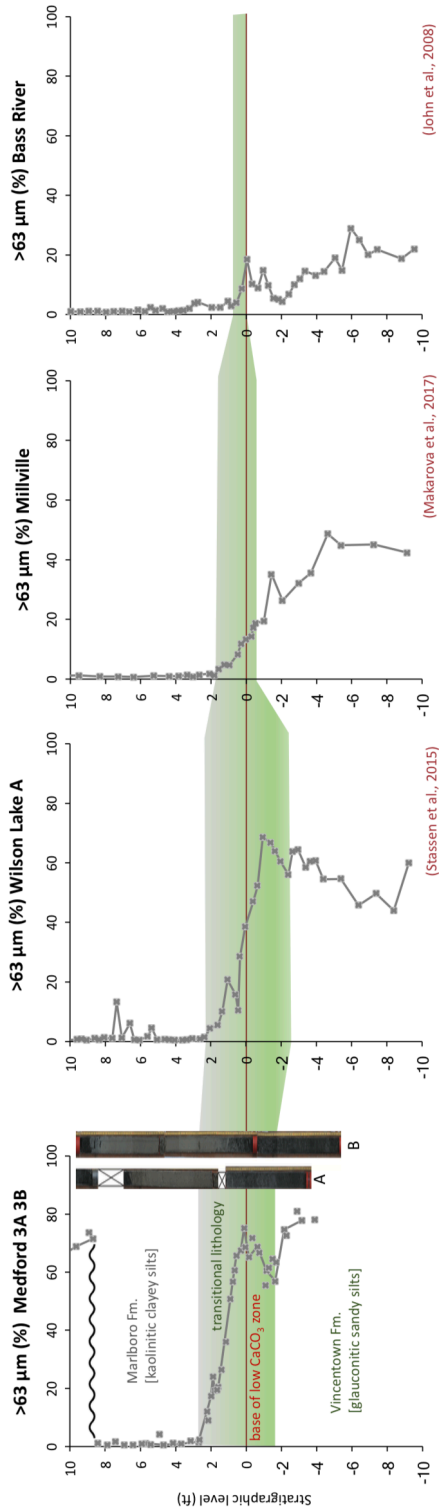

Fig. 4.S2. Percent coarse fraction (>63 µm) records from Medford (MAP Sites 3A and 3B), Wilson Lake A [Stassen et al., 2015], Millville [Makarova et al., 2017], and Bass River [John et al., 2008]. Units of transitional from Upper Paleocene Vincentown Formation to the Lower Eocene Marlboro Formation lithologies are shown in green.

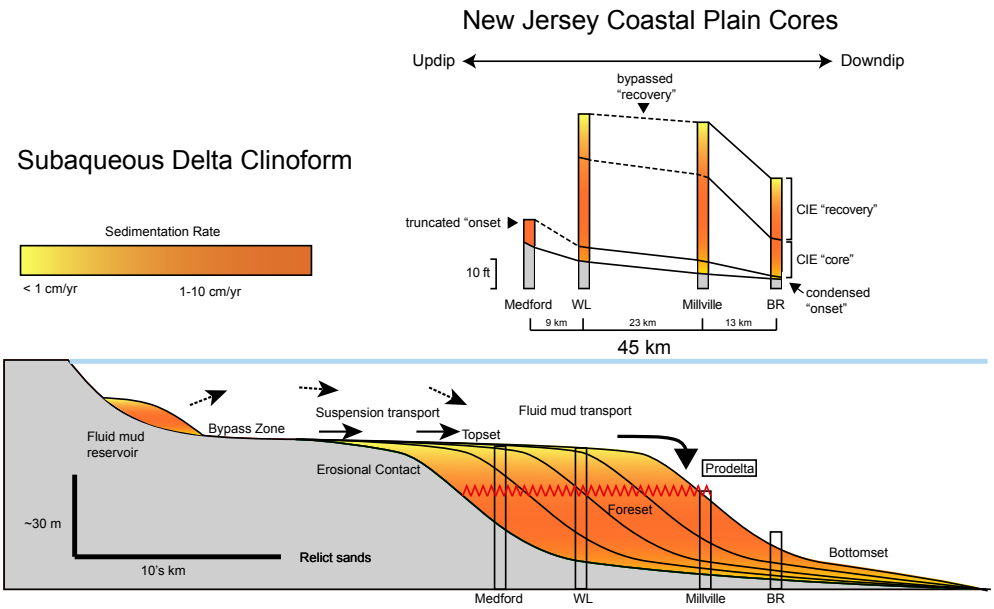

Fig. 4.S3. Clinoform depositional model showing a fluid mud reservoir source bypassing shallow zones and rapidly building foresets at the rollover point. Overlaying NJCP sections from Medford, Wilson Lake, Millville, and Bass River support variation in CIE preservation between sites [Podrecca, 2018].

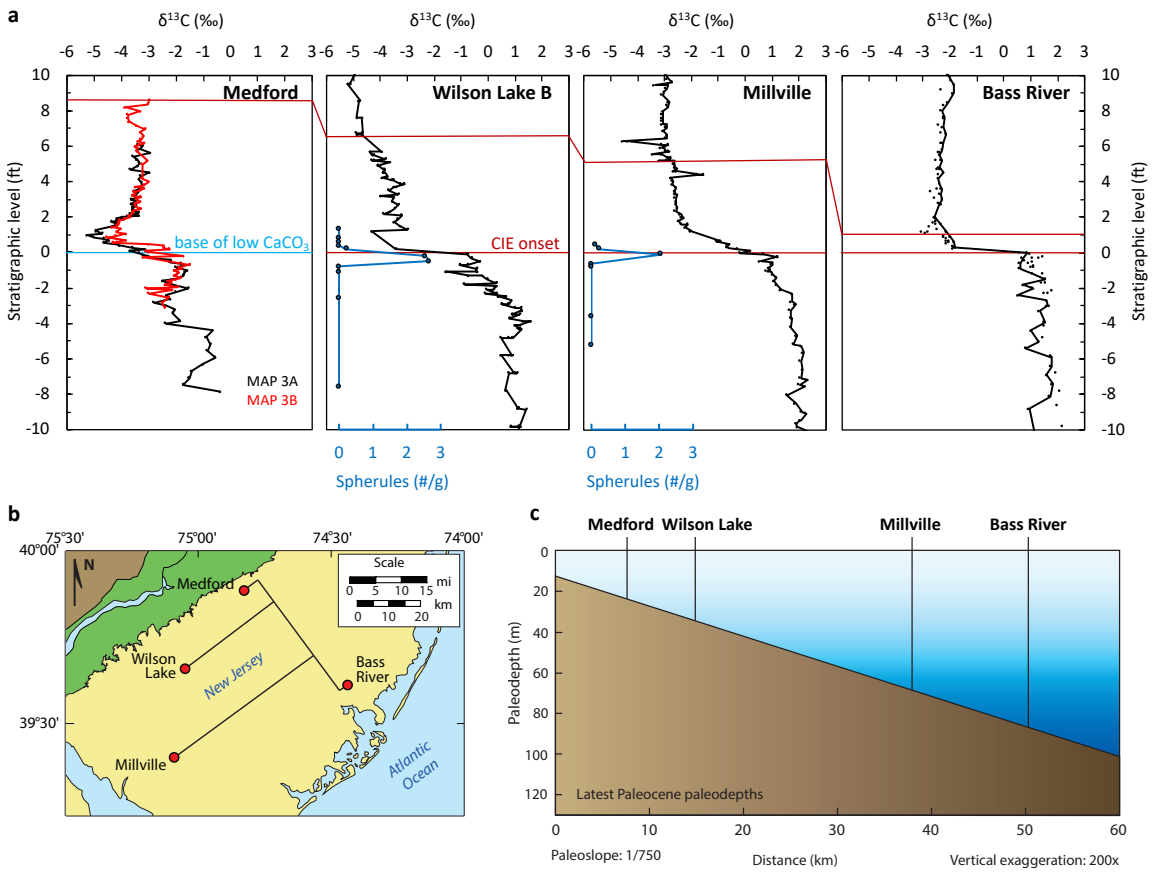

Fig. 4.S4. Correlation of bulk sediment $\delta^{13}C$ records from Medford MAP 3A and 3B [Podrecca, 2018], Wilson Lake B [Wright and Schaller, 2013], Millville [Wright and Schaller, 2013; Makarova et al., 2017], and Bass River [Kent et al., 2003; John et al., 2008] New Jersey coastal plain cores leveled to the base of low (<1%) $CaCO_3$ zone (a) with the map of site locations (b) and New Jersey paleoshelf reconstruction during the latest Paleocene (c). Spherules counts per gram from Wilson Lake B and Millville are from Schaller et al. [2016].

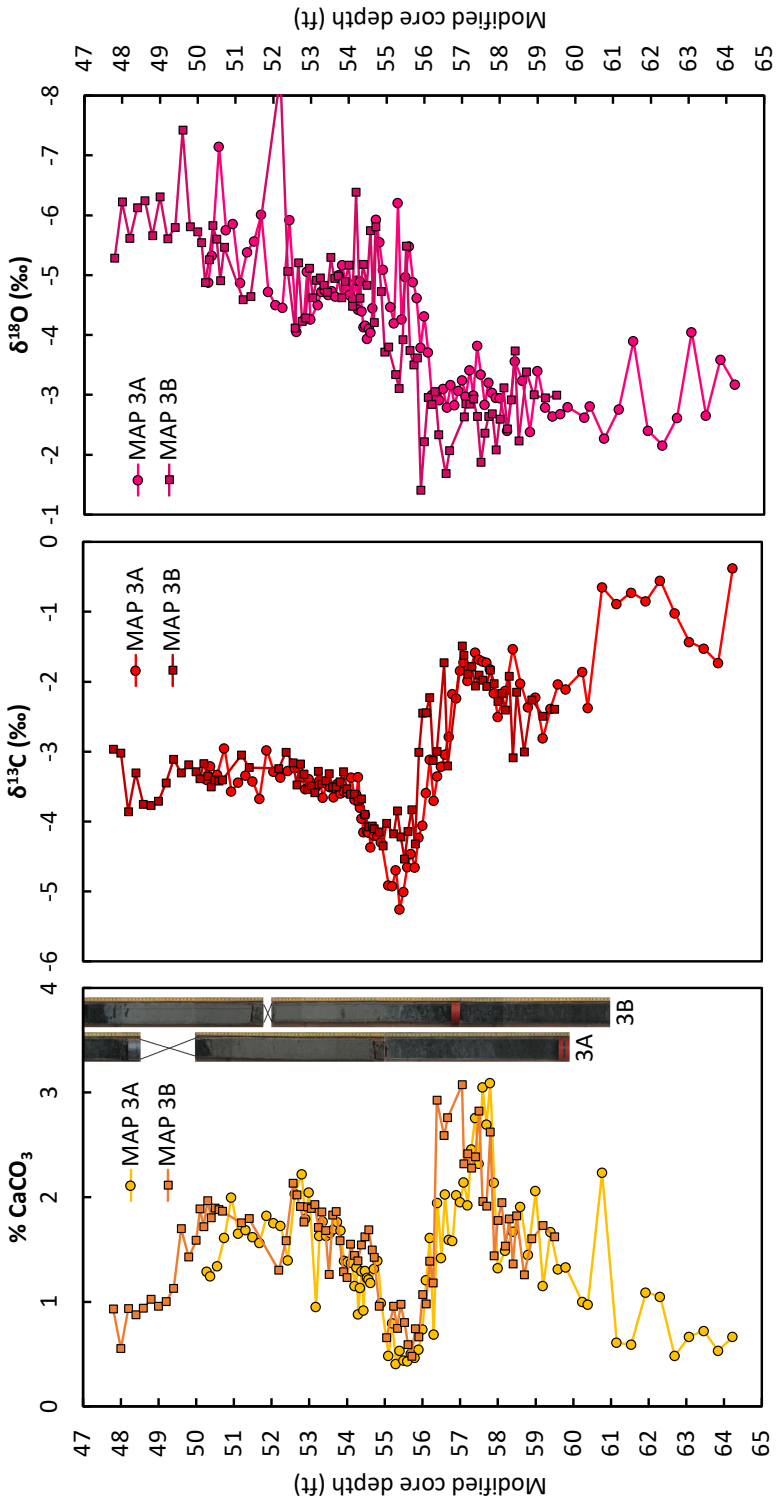

Fig. 4.S5. Corelation of bulk sediment records (% $CaCO_3$, $\delta^{13}C$, $\delta^{18}O$; Podrecca [2018]) from MAP 3A and 3B cores, Medford, NJ based on drilling depths modified for core expansion.

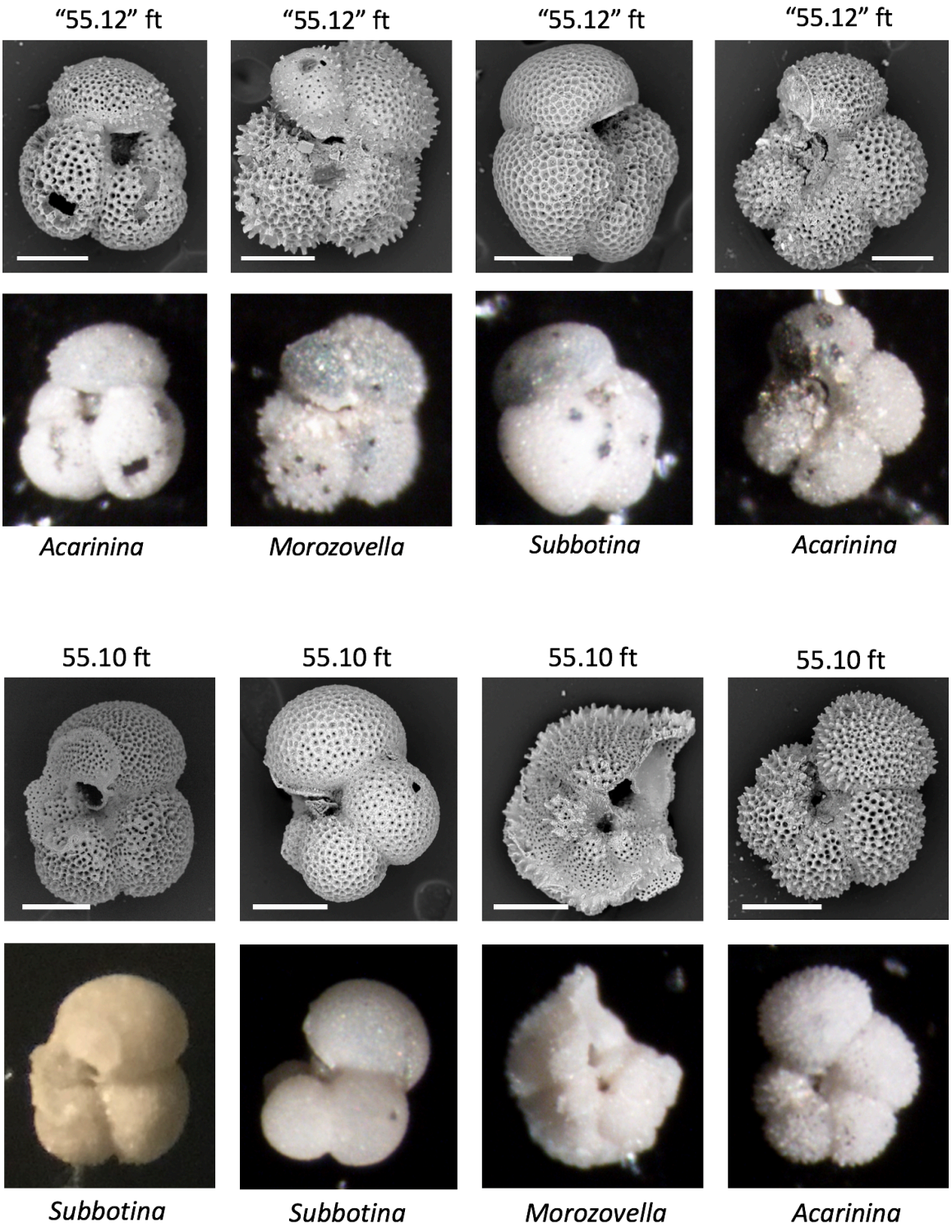

Fig. 4.S6. Scanning electron microscopy (SEM) and optical photographs of planktonic foraminifera from low carbonate (<1% $CaCO_3$) zone in MAP 3A core at Medford, NJ. Scale bar is 100 μm. Quotation marks indicate depths from core catcher.

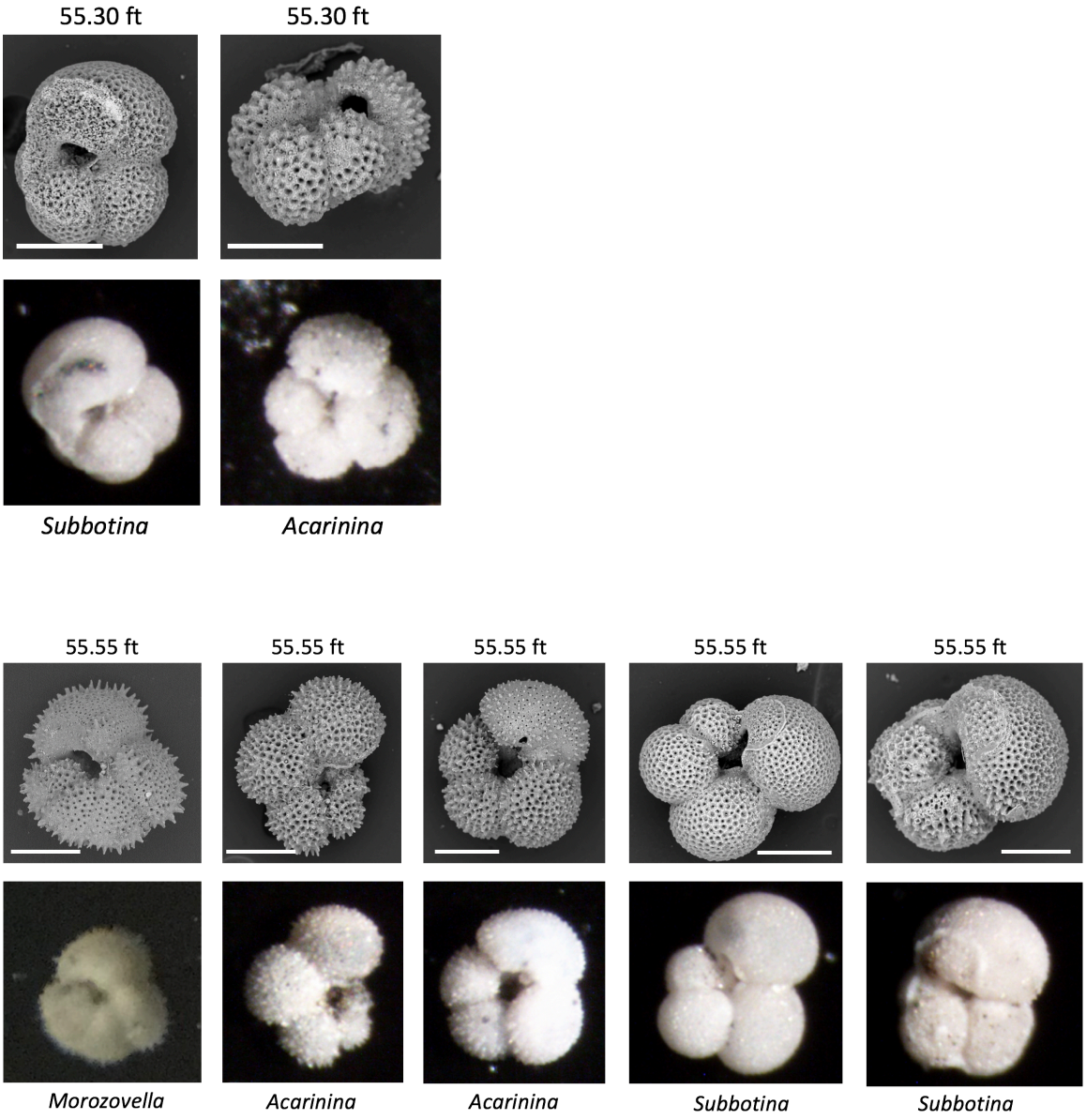
55.30 ft
55.30 ft
Subbotina
Acarinina
55.55 ft
55.55 ft
55.55 ft
55.55 ft
55.55 ft
Morozovella
Acarinina
Acarinina
Subbotina
Subbotina

Fig. 4.S6. Cont.

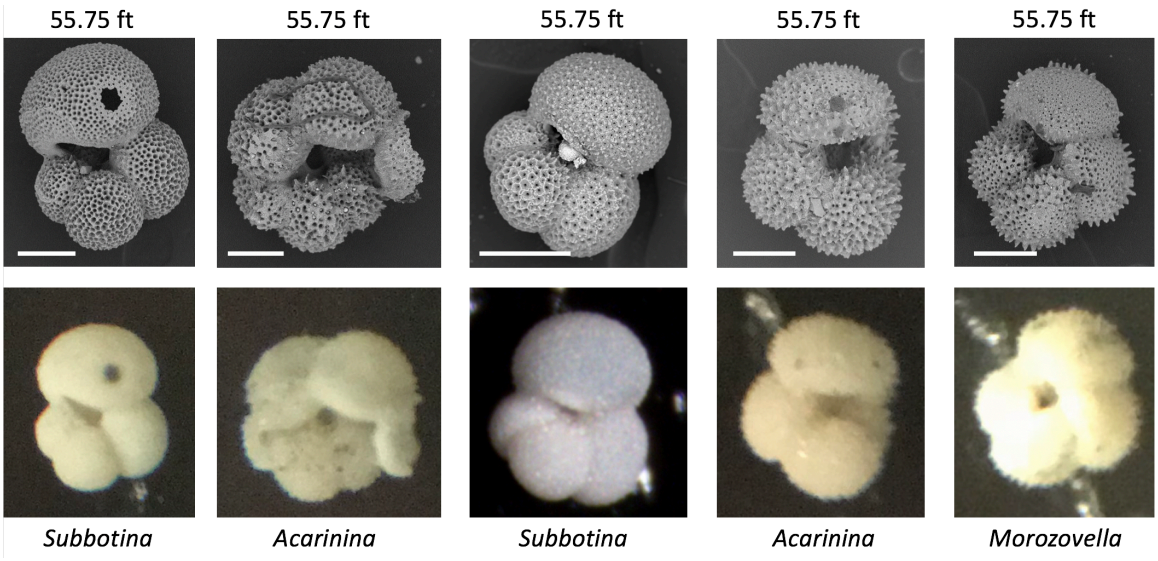
55.75 ft
55.75 ft
55.75 ft
55.75 ft
55.75 ft
Subbotina
Acarinina
Subbotina
Acarinina
Morozovella

Fig. 4.S6. Cont.

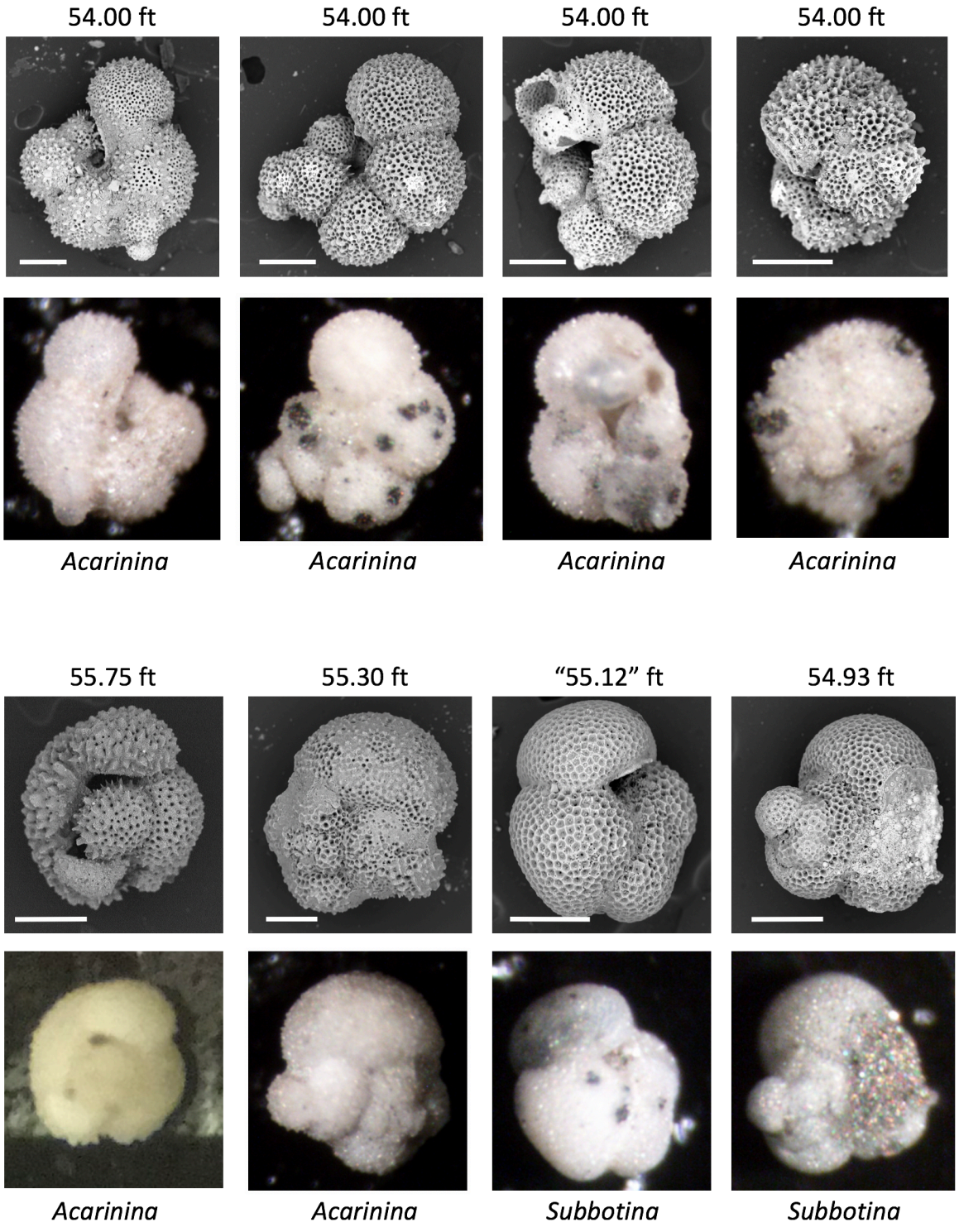

Fig. 4.S7. Scanning electron microscopy (SEM) and optical photographs of malformed tests of planktonic foraminifera with abnormal chamber morphology or abnormal additional chambers from MAP 3A core at Medford, NJ. Scale bar is 100 μm.

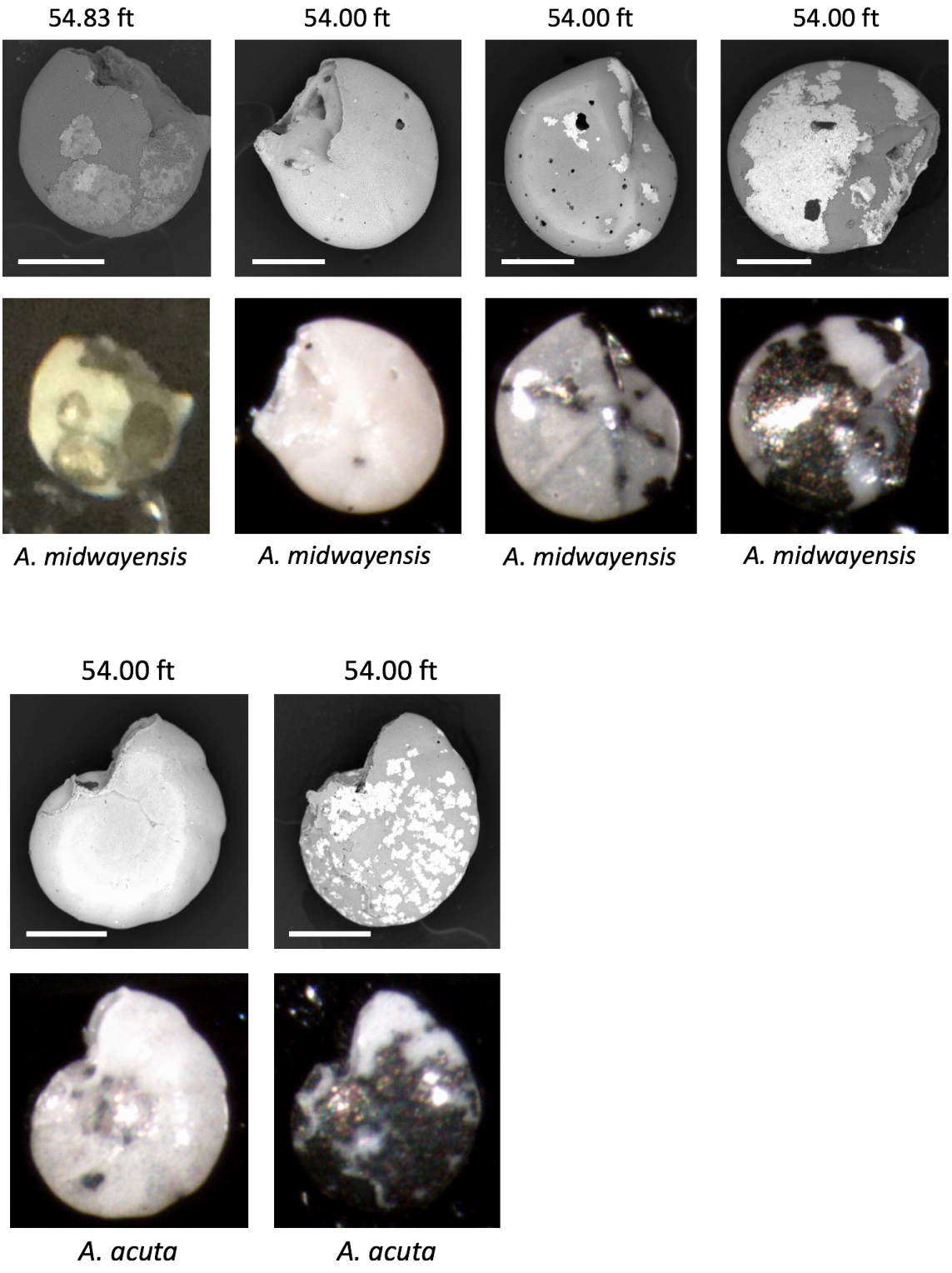

Fig. 4.S8. Scanning electron microscopy (SEM) and optical photographs of benthic foraminifera with pyrite coatings and filling from MAP 3A core at Medford, NJ. Scale bar is 100 μm.

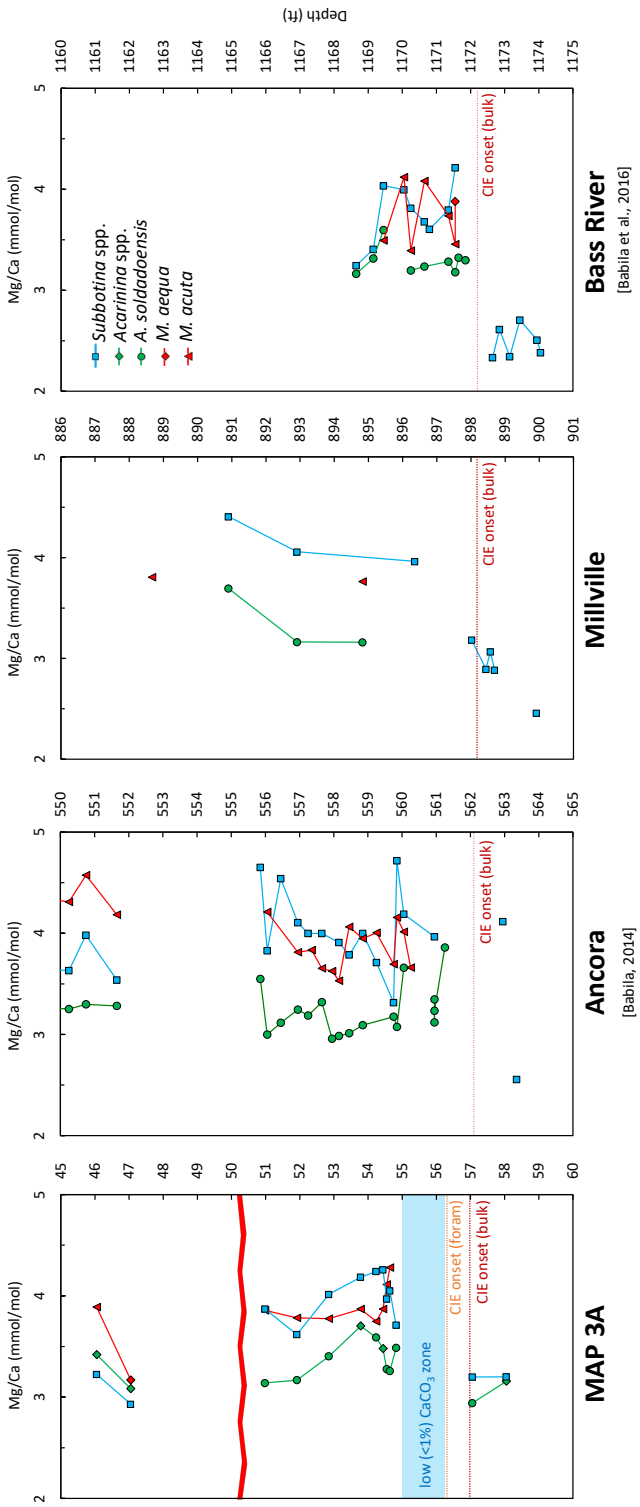

Fig. 4.S9. Mg/Ca records of planktonic foraminifera (*Morozovella* spp. in red; *Acarinina* spp. in green; *Subbotina* spp. in blue) at Medford (MAP 3A), Ancora [Babila, 2014], Millville, and Bass River [Babila et al., 2016] New Jersey coastal plain sites during the PETM.

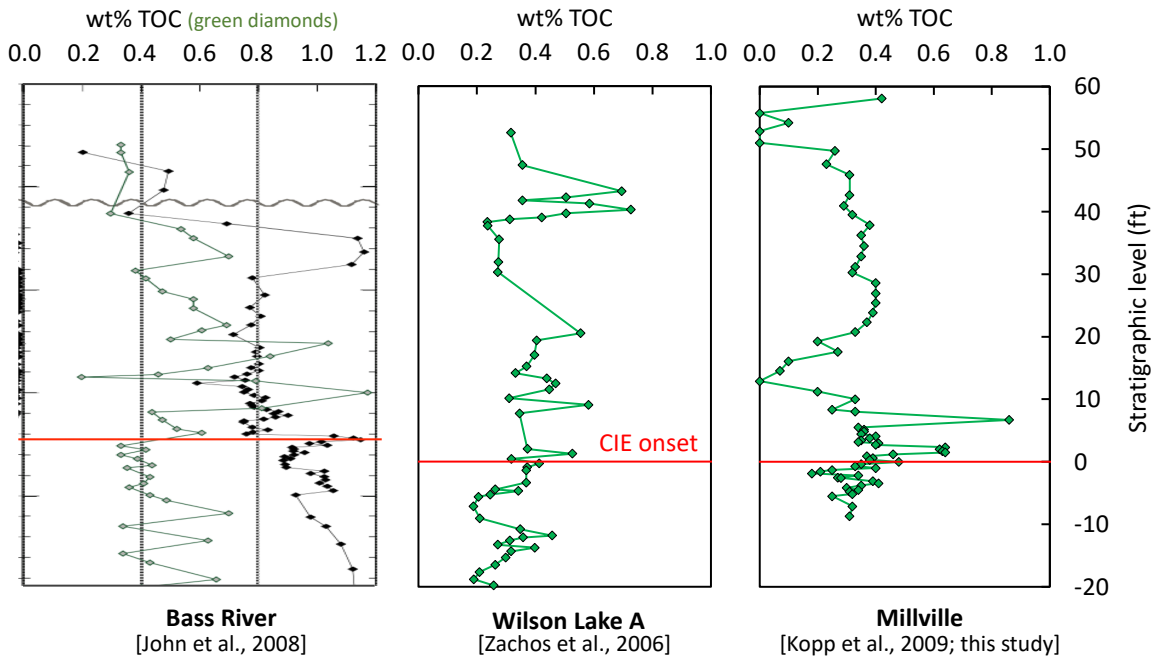

Fig. 4.S10. Percent total organic carbon (TOC) at Bass River [John et al., 2008], Wilson Lake A [Zachos et al., 2006], and Millville [Kopp et al., 2009; this study] New Jersey coastal plain sites during the PETM.

4.10 Tables

Table 4.1. Percent coarse (>63 μm) fraction at MAP 3A, 3B, and 5A, Medford, NJ. Table includes modified for core expansion depths (mcd). Samples from the core expansion are marked in quotes.

Top (ft)	Bottom (ft)	Mean depth (ft)	Mcd (ft)	Mcd (m)	Fraction > 63μm (%)
		MAP 3A			
46.00	46.10	46.05	46.05	14.04	65.0
47.00	47.10	47.05	47.05	14.34	68.9
47.95	48.05	48.00	48.00	14.63	71.5
50.10	50.20	50.15	50.14	15.28	96.7
51.00	51.10	51.05	50.98	15.54	1.1
52.00	52.10	52.05	51.92	15.82	0.6
53.00	53.10	53.05	52.85	16.11	0.9
54.00	54.10	54.05	53.79	16.39	1.6
54.50	54.57	54.54	54.24	16.53	12.1
54.70	54.80	54.75	54.44	16.59	17.3
54.83	54.90	54.87	54.55	16.63	24.0
54.93	55.00	54.97	54.64	16.65	19.3
"55.12"	"55.20"	55.16	54.82	16.71	20.6
55.10	55.17	55.14	55.14	16.81	56.7
55.30	55.37	55.34	55.34	16.87	65.8
55.55	55.62	55.59	55.59	16.94	67.5
55.75	55.82	55.79	55.79	17.00	75.2
56.00	56.10	56.05	56.05	17.08	65.2
56.50	56.57	56.54	56.54	17.23	68.8
57.00	57.10	57.05	57.05	17.39	60.5
57.19	57.26	57.23	57.23	17.44	70.3
57.35	57.41	57.38	57.38	17.49	64.6
57.50	57.57	57.54	57.54	17.54	56.9
58.00	58.10	58.05	58.05	17.69	74.7
59.00	59.10	59.05	59.05	18.00	77.8
		MAP 3B			
47.20	47.27	47.24	47.24	14.40	73.6
47.70	47.77	47.74	47.74	14.55	1.2
48.23	48.30	48.27	48.27	14.71	0.6
48.70	48.77	48.74	48.74	14.85	1.7
49.20	49.27	49.24	49.24	15.01	0.5
49.70	49.77	49.74	49.74	15.16	0.5
50.20	50.27	50.24	50.24	15.31	0.9
50.70	50.77	50.74	50.74	15.46	0.7
51.20	51.27	51.24	51.24	15.62	4.2
52.20	52.27	52.24	52.22	15.92	1.2
53.20	53.27	53.24	53.18	16.21	2.0
53.70	53.77	53.74	53.65	16.35	2.3
54.20	54.27	54.24	54.13	16.50	9.1
54.70	54.77	54.74	54.60	16.64	19.5
54.95	55.02	54.99	54.84	16.72	26.5
55.20	55.27	55.24	55.08	16.79	36.0
55.45	55.52	55.49	55.32	16.86	50.8
55.70	55.77	55.74	55.56	16.93	60.7
56.30	56.37	56.34	56.13	17.11	68.6
56.70	56.77	56.74	56.51	17.22	71.8
"57.10"	"57.17"	57.14	56.90	17.34	66.7
57.20	57.27	57.24	57.24	17.45	55.5

57.40	57.47	57.44	57.44	17.51	61.6
57.60	57.67	57.64	57.64	17.57	64.5
57.80	57.87	57.84	57.84	17.63	63.5
58.40	58.47	58.44	58.44	17.81	72.7
59.00	59.07	59.04	59.04	17.99	81.1
60.00	60.07	60.04	60.04	18.30	78.1
			MAP 5A		
15.25	15.32	15.29	15.29	4.66	62.6
15.55	15.62	15.59	15.59	4.75	60.4
15.75	15.82	15.79	15.79	4.81	65.4
16.15	16.22	16.19	16.19	4.93	75.1
16.35	16.42	16.39	16.39	4.99	80.2
16.55	16.62	16.59	16.59	5.06	77.3
16.75	16.82	16.79	16.79	5.12	74.3
16.95	17.02	16.99	16.99	5.18	74.8
17.15	17.22	17.19	17.19	5.24	73.8
17.35	17.42	17.39	17.39	5.30	72.2
17.55	17.62	17.59	17.59	5.36	72.0
17.80	17.87	17.84	17.84	5.44	0.6
18.00	18.07	18.04	18.04	5.50	0.2
18.20	18.27	18.24	18.24	5.56	0.4
18.40	18.47	18.44	18.44	5.62	0.5
20.10	20.17	20.14	20.13	6.14	0.6
20.30	20.37	20.34	20.32	6.19	0.6
20.45	20.52	20.49	20.46	6.24	0.5
20.70	20.77	20.74	20.70	6.31	0.6
20.90	20.97	20.94	20.89	6.37	0.4
21.10	21.17	21.14	21.09	6.43	0.6
21.30	21.37	21.34	21.28	6.49	0.3
21.45	21.52	21.49	21.42	6.53	0.2
21.70	21.80	21.75	21.67	6.61	0.7
21.90	22.00	21.95	21.87	6.66	0.3
22.10	22.18	22.14	22.05	6.72	0.6
22.30	22.37	22.34	22.23	6.78	0.8
22.50	22.57	22.54	22.43	6.84	0.9
22.70	22.77	22.74	22.62	6.89	1.2
22.90	22.97	22.94	22.81	6.95	0.5
23.10	23.17	23.14	23.00	7.01	0.7
23.30	23.37	23.34	23.19	7.07	0.7
23.50	23.57	23.54	23.38	7.13	0.8
23.70	23.77	23.74	23.57	7.19	0.9
23.90	23.97	23.94	23.77	7.24	0.6
24.10	24.17	24.14	23.96	7.30	0.6
24.30	24.37	24.34	24.15	7.36	0.8
24.50	24.57	24.54	24.34	7.42	0.8
24.70	24.77	24.74	24.53	7.48	0.7
24.90	24.97	24.94	24.72	7.54	0.9
25.20	25.27	25.24	25.23	7.69	2.4
25.40	25.47	25.44	25.42	7.75	2.3
25.60	25.67	25.64	25.61	7.81	7.7
25.80	25.87	25.84	25.80	7.86	4.3
26.00	26.07	26.04	26.00	7.92	5.9
26.20	26.27	26.24	26.19	7.98	15.5
26.40	26.47	26.44	26.38	8.04	22.3
26.60	26.67	26.64	26.57	8.10	27.6
26.80	26.87	26.84	26.76	8.16	31.1
27.00	27.07	27.04	26.96	8.22	30.2
27.20	27.27	27.24	27.15	8.28	52.0

27.40	27.47	27.44	27.34	8.33	66.0
27.60	27.67	27.64	27.53	8.39	66.4
27.80	27.87	27.84	27.73	8.45	71.2
28.00	28.07	28.04	27.92	8.51	75.0
28.20	28.27	28.24	28.11	8.57	76.0
28.40	28.47	28.44	28.30	8.63	80.6
28.60	28.67	28.64	28.50	8.69	76.6
28.80	28.87	28.84	28.69	8.74	65.2
29.00	29.07	29.04	28.88	8.80	73.9
29.20	29.27	29.24	29.07	8.86	72.2
29.40	29.47	29.44	29.26	8.92	72.6
29.60	29.67	29.64	29.46	8.98	70.2
29.80	29.87	29.84	29.65	9.04	69.9

Table 4.2. Stable isotopic values measured in multi-specimen samples of planktonic and benthic foraminifera at MAP 3A, Medford, NJ. Table includes modified for core expansion depths (mcd). Samples from the core expansion are marked in quotes.

Top (ft)	Bottom (ft)	Mean depth (ft)	Mcd (ft)	Mcd (m)	Species	#	Size fraction (μm)	$\delta^{13}C$ (‰)	$\delta^{18}O$ (‰)
46.00	46.10	46.05	46.05	14.04	*M. aequa*	3	250-300	2.37	-3.83
47.00	47.10	47.05	47.05	14.34	*M. aequa*	3	250-300	1.97	-2.44
47.00	47.10	47.05	47.05	14.34	*M. acuta*	4	212-250	1.80	-4.10
51.00	51.10	51.05	50.98	15.54	*M. acuta*	3	250-300	-0.11	-4.09
52.00	52.10	52.05	51.92	15.82	*M. acuta*	3	250-300	-0.36	-4.17
52.00	52.10	52.05	51.92	15.82	*M. aequa*	2	212-250	-0.65	-4.28
53.00	53.10	53.05	52.85	16.11	*M. acuta*	4	250-300	-0.40	-3.70
54.00	54.10	54.05	53.79	16.39	*M. acuta*	4	250-300	-0.51	-3.92
54.50	54.57	54.54	54.24	16.53	*M. acuta*	4	250-300	-0.63	-3.73
54.70	54.80	54.75	54.44	16.59	*M. acuta*	4	250-300	-0.27	-4.19
54.83	54.90	54.87	54.55	16.63	*M. acuta*	3	250-300	-0.45	-3.55
54.93	55.00	54.97	54.64	16.65	*M. acuta (2), M. velascoensis (1)*	3	250-300	-0.35	-3.42
"55.12"	"55.20"	55.16	54.82	16.71	*M. acuta*	3	250-300	-2.03	-3.39
57.00	57.10	57.05	57.05	17.39	*M. aequa*	2	250-300	2.49	-3.00
58.00	58.10	58.05	58.05	17.69	*M. acuta*	3	212-250	2.63	-3.47
46.00	46.10	46.05	46.05	14.04	*Acarinina* spp.	3	250-300	2.57	-3.32
47.00	47.10	47.05	47.05	14.34	*Acarinina* spp.	3	250-300	2.25	-2.96
51.00	51.10	51.05	50.98	15.54	*A. soldadoensis (2), A. angulosa (2)*	4	250-300	-0.76	-3.60
52.00	52.10	52.05	51.92	15.82	*A. soldadoensis (3), A. angulosa (1)*	4	250-300	-0.37	-3.35
53.00	53.10	53.05	52.85	16.11	*A. soldadoensis*	4	250-300	-0.75	-3.57
54.00	54.10	54.05	53.79	16.39	*A. soldadoensis*	4	250-300	-0.89	-3.68
54.50	54.57	54.54	54.24	16.53	*A. soldadoensis*	3	250-300	-0.36	-3.11
54.70	54.80	54.75	54.44	16.59	*A. soldadoensis*	4	250-300	-0.70	-3.02
54.83	54.90	54.87	54.55	16.63	*A. soldadoensis*	3	250-300	-0.51	-3.34
54.93	55.00	54.97	54.64	16.65	*A. soldadoensis*	3	250-300	-0.92	-3.06
"55.12"	"55.20"	55.16	54.82	16.71	*Acarinina* spp.	3	250-300	-1.39	-2.84
55.10	55.17	55.14	55.14	16.81	*A. soldadoensis, angulosa, coalingensis*	3	250-300 (1), 212-250 (2)	-1.25	-2.42
55.30	55.37	55.34	55.34	16.87	*A. soldadoensis*	2	250-300	-1.22	-2.69
55.55	55.62	55.59	55.59	16.94	*Acarinina* spp.	3	250-300	-1.70	-2.48
55.75	55.82	55.79	55.79	17.00	*Acarinina* spp.	3	250-300	-0.36	-2.46
56.00	56.10	56.05	56.05	17.08	*A. soldadoensis*	4	250-300	-0.44	-2.77
56.50	56.57	56.54	56.54	17.23	*Acarinina* spp.	2	250-300	1.44	-3.18
57.00	57.10	57.05	57.05	17.39	*Acarinina* spp.	3	212-250	0.76	-2.85
58.00	58.10	58.05	58.05	17.69	*Acarinina* spp.	3	250-300 (1), 212-250 (2)	2.23	-2.97
46.00	46.10	46.05	46.05	14.04	*S. roesnaesensis*	3	250-300	0.89	-2.41
47.00	47.10	47.05	47.05	14.34	*S. roesnaesensis*	4	250-300	0.13	-2.00
50.10	50.20	50.15	50.14	15.28	*Subbotina* spp.	3	212-250	-0.56	-2.04
51.00	51.10	51.05	50.98	15.54	*Subbotina* spp.	3	250-300	-1.87	-3.86
52.00	52.10	52.05	51.92	15.82	*S. roesnaesensis*	4	250-300	-2.01	-3.65
53.00	53.10	53.05	52.85	16.11	*S. roesnaesensis*	4	250-300	-2.21	-3.49
54.00	54.10	54.05	53.79	16.39	*Subbotina* spp.	4	250-300	-2.22	-3.45
54.50	54.57	54.54	54.24	16.53	*Subbotina* spp.	3	250-300	-2.44	-3.28
54.70	54.80	54.75	54.44	16.59	*Subbotina* spp.	3	250-300	-2.13	-3.56
54.83	54.90	54.87	54.55	16.63	*Subbotina* spp.	3	250-300	-2.30	-3.11
54.93	55.00	54.97	54.64	16.65	*Subbotina* spp.	2	250-300	-2.53	-3.58

"55.12"	"55.20"	55.16	54.82	16.71	*S. roesnaesensis*	3	250-300	-2.57	-2.83
55.10	55.17	55.14	55.14	16.81	*S. roesnaesensis*	2	250-300	-0.17	-1.95
56.50	56.57	56.54	56.54	17.23	*Subbotina* spp.	3	250-300	0.86	-1.96
57.00	57.10	57.05	57.05	17.39	*Subbotina* spp.	2	250-300	0.16	-2.33
58.00	58.10	58.05	58.05	17.69	*Subbotina* spp.	3	250-300	0.63	-2.54
59.00	59.10	59.05	59.05	18.00	*Subbotina* spp.	3	212-250	0.77	-1.56
46.00	46.10	46.05	46.05	14.04	*C. howelli*	3	212-250	-0.40	-1.24
47.00	47.10	47.05	47.05	14.34	*C. howelli*	3	250-300	-0.49	-1.20
47.95	48.05	48.00	48.00	14.63	*C. howelli*	4	212-250	-1.20	-1.31
50.10	50.20	50.15	50.14	15.28	*C. howelli*	2	250-300	-0.78	-1.51
55.75	55.82	55.79	55.79	17.00	*C. alleni*	3	250-300	-1.74	-1.51
56.00	56.10	56.05	56.05	17.08	*C. alleni*	4	212-250	-0.53	-1.59
56.50	56.57	56.54	56.54	17.23	*C. succedens*	2	250-300	0.08	-1.30
57.00	57.10	57.05	57.05	17.39	*C. alleni*	4	250-300	-0.67	-1.38
58.00	58.10	58.05	58.05	17.69	*C. succedens*	3	250-300	-0.48	-1.28
59.00	59.10	59.05	59.05	18.00	*C. alleni*	3	250-300	-0.49	-1.01
46.00	46.10	46.05	46.05	14.04	*Anomalinoides* spp.	3	212-250	-1.45	-1.33
47.00	47.10	47.05	47.05	14.34	*Anomalinoides* spp.	4	212-250	-1.80	-1.31
47.95	48.05	48.00	48.00	14.63	*Anomalinoides* spp.	3	212-250 (1), 150-212 (2)	-0.89	-1.01
51.00	51.10	51.05	50.98	15.54	*A. acuta*	9	150-212	-3.17	-3.44
52.00	52.10	52.05	51.92	15.82	*A. acuta*	8	150-212	-3.18	-3.30
53.00	53.10	53.05	52.85	16.11	*A. acuta*	10	150-212	-3.28	-3.23
54.00	54.10	54.05	53.79	16.39	*A. acuta*	10	150-212	-3.23	-3.13
54.50	54.57	54.54	54.24	16.53	*A. acuta*	8	150-212	-3.27	-3.04
54.70	54.80	54.75	54.44	16.59	*A. acuta*	3	212-250	-3.46	-3.26
54.70	54.80	54.75	54.44	16.59	*A. acuta*	9	150-212	-3.42	-3.05
54.83	54.90	54.87	54.55	16.63	*A. acuta*	8	150-212	-3.40	-3.09
54.93	55.00	54.97	54.64	16.65	*A. acuta*	8	150-212	-3.35	-2.96
"55.12"	"55.20"	55.16	54.82	16.71	*A. acuta*	7	150-212	-3.84	-2.90
55.10	55.17	55.14	55.14	16.81	*A. acuta*	8	150-212	-3.45	-2.74
55.10	55.17	55.14	55.14	16.81	*A. acuta*	7	150-212	-3.49	-2.75
55.30	55.37	55.34	55.34	16.87	*Anomalinoides* spp.	3	212-250	-3.87	-2.50
55.55	55.62	55.59	55.59	16.94	*Anomalinoides* spp.	4	212-250	-3.78	-2.42
56.00	56.10	56.05	56.05	17.08	*Anomalinoides* spp.	3	212-250	-3.28	-2.30
57.00	57.10	57.05	57.05	17.39	*Anomalinoides* spp.	4	150-212	-1.40	-2.03
58.00	58.10	58.05	58.05	17.69	*Anomalinoides* spp.	2	212-250	-1.67	-1.80

Table 4.3. Stable isotopic values measured in single specimens of planktonic and benthic foraminifera at MAP 3A, Medford, NJ. Table includes modified for core expansion depths (mcd).

Top (ft)	Bottom (ft)	Mean depth (ft)	Mcd (ft)	Mcd (m)	Species	#	Size fraction (µm)	$\delta^{13}C$ (‰)	$\delta^{18}O$ (‰)
50.10	50.20	50.15	50.14	15.28	*M. aequa*	1	212-250	2.38	-3.25
52.00	52.10	52.05	51.92	15.82	*M. acuta*	1	212-250	0.00	-3.93
52.00	52.10	52.05	51.92	15.82	*M. acuta*	1	212-250	-0.34	-4.19
52.00	52.10	52.05	51.92	15.82	*M. acuta*	1	212-250	-0.85	-3.54
52.00	52.10	52.05	51.92	15.82	*M. acuta*	1	212-250	-0.66	-3.38
53.00	53.10	53.05	52.85	16.11	*M. acuta*	1	212-250	0.33	-3.40
53.00	53.10	53.05	52.85	16.11	*M. acuta*	1	212-250	0.02	-3.69
53.00	53.10	53.05	52.85	16.11	*M. acuta*	1	212-250	-0.63	-4.54
53.00	53.10	53.05	52.85	16.11	*M. acuta*	1	212-250	0.22	-3.75
54.00	54.10	54.05	53.79	16.39	*M. acuta*	1	212-250	0.54	-4.16
54.00	54.10	54.05	53.79	16.39	*M. acuta*	1	212-250	-0.52	-3.17
54.00	54.10	54.05	53.79	16.39	*M. acuta*	1	212-250	0.02	-3.80
54.00	54.10	54.05	53.79	16.39	*M. acuta*	1	212-250	0.06	-3.38
54.00	54.10	54.05	53.79	16.39	*M. acuta*	1	212-250	-0.02	-3.97
54.70	54.80	54.75	54.44	16.59	*M. acuta*	1	212-250	-0.95	-3.35
54.70	54.80	54.75	54.44	16.59	*M. acuta*	1	212-250	-1.35	-3.25
54.70	54.80	54.75	54.44	16.59	*M. acuta*	1	212-250	-0.81	-3.20
56.50	56.57	56.54	56.54	17.23	*M. aequa*	1	>300	4.03	-2.35
57.00	57.10	57.05	57.05	17.39	*M. aequa*	1	212-250	2.61	-2.73
57.00	57.10	57.05	57.05	17.39	*M. aequa*	1	212-250	1.81	-2.51
51.00	51.10	51.05	50.98	15.54	*A. soldadoensis*	1	212-250	-1.57	-3.26
51.00	51.10	51.05	50.98	15.54	*A. soldadoensis*	1	212-250	-1.28	-3.12
51.00	51.10	51.05	50.98	15.54	*A. soldadoensis*	1	212-250	0.27	-3.63
51.00	51.10	51.05	50.98	15.54	*A. soldadoensis*	1	212-250	-1.12	-3.64
52.00	52.10	52.05	51.92	15.82	*A. soldadoensis*	1	212-250	-0.85	-3.51
52.00	52.10	52.05	51.92	15.82	*A. soldadoensis*	1	212-250	-0.74	-4.18
52.00	52.10	52.05	51.92	15.82	*A. soldadoensis*	1	212-250	-1.89	-4.05
52.00	52.10	52.05	51.92	15.82	*A. soldadoensis*	1	212-250	-1.11	-3.47
52.00	52.10	52.05	51.92	15.82	*A. soldadoensis*	1	212-250	-1.20	-3.30
53.00	53.10	53.05	52.85	16.11	*A. soldadoensis*	1	212-250	-0.54	-3.17
53.00	53.10	53.05	52.85	16.11	*A. soldadoensis*	1	212-250	-0.69	-3.35
53.00	53.10	53.05	52.85	16.11	*A. soldadoensis*	1	212-250	-0.76	-3.52
53.00	53.10	53.05	52.85	16.11	*A. soldadoensis*	1	212-250	-0.48	-3.54
54.00	54.10	54.05	53.79	16.39	*A. soldadoensis*	1	212-250	-1.17	-3.61
54.00	54.10	54.05	53.79	16.39	*A. soldadoensis*	1	212-250	-0.94	-4.08
54.00	54.10	54.05	53.79	16.39	*A. soldadoensis*	1	212-250	-1.24	-3.92
54.00	54.10	54.05	53.79	16.39	*A. soldadoensis*	1	212-250	-0.58	-3.27
54.70	54.80	54.75	54.44	16.59	*A. soldadoensis*	1	212-250	-1.34	-3.38
54.70	54.80	54.75	54.44	16.59	*A. soldadoensis*	1	212-250	-2.01	-3.63
54.70	54.80	54.75	54.44	16.59	*A. soldadoensis*	1	212-250	-1.86	-4.05
54.70	54.80	54.75	54.44	16.59	*A. soldadoensis*	1	212-250	-1.45	-3.57
54.70	54.80	54.75	54.44	16.59	*A. soldadoensis*	1	212-250	-1.40	-3.45
56.00	56.10	56.05	56.05	17.08	*Acarinina sp.*	1	212-250	1.30	-2.30
57.00	57.10	57.05	57.05	17.39	*A. soldadoensis*	1	212-250	1.20	-3.11
51.00	51.10	51.05	50.98	15.54	*S. roesnaesensis*	1	212-250	-1.75	-3.53
51.00	51.10	51.05	50.98	15.54	*S. roesnaesensis*	1	212-250	-1.48	-3.48
51.00	51.10	51.05	50.98	15.54	*S. roesnaesensis*	1	212-250	-2.30	-4.63
51.00	51.10	51.05	50.98	15.54	*S. roesnaesensis*	1	212-250	-1.63	-3.48
51.00	51.10	51.05	50.98	15.54	*S. roesnaesensis*	1	212-250	-1.30	-3.81
52.00	52.10	52.05	51.92	15.82	*S. roesnaesensis*	1	212-250	-2.40	-3.84
52.00	52.10	52.05	51.92	15.82	*S. roesnaesensis*	1	212-250	-2.02	-3.80

52.00	52.10	52.05	51.92	15.82	*S. roesnaesensis*	1	212-250	-2.17	-3.83
52.00	52.10	52.05	51.92	15.82	*S. roesnaesensis*	1	212-250	-2.26	-4.19
52.00	52.10	52.05	51.92	15.82	*S. roesnaesensis*	1	212-250	-2.08	-3.60
53.00	53.10	53.05	52.85	16.11	*S. roesnaesensis*	1	212-250	-2.04	-3.45
53.00	53.10	53.05	52.85	16.11	*S. roesnaesensis*	1	212-250	-1.97	-3.44
53.00	53.10	53.05	52.85	16.11	*S. roesnaesensis*	1	212-250	-2.55	-3.69
53.00	53.10	53.05	52.85	16.11	*S. roesnaesensis*	1	212-250	-2.24	-4.02
54.00	54.10	54.05	53.79	16.39	*S. roesnaesensis*	1	212-250	-2.66	-3.28
54.00	54.10	54.05	53.79	16.39	*S. roesnaesensis*	1	212-250	-2.31	-3.42
54.00	54.10	54.05	53.79	16.39	*S. roesnaesensis*	1	212-250	-2.63	-3.62
54.00	54.10	54.05	53.79	16.39	*S. roesnaesensis*	1	212-250	-2.82	-3.64
54.70	54.80	54.75	54.44	16.59	*S. roesnaesensis*	1	212-250	-2.76	-3.98
54.70	54.80	54.75	54.44	16.59	*S. roesnaesensis*	1	212-250	-2.63	-3.73
54.70	54.80	54.75	54.44	16.59	*S. roesnaesensis*	1	212-250	-2.20	-3.72
55.75	55.82	55.79	55.79	17.00	*Subbotina* sp.	1	250-300	0.86	-0.94
57.00	57.10	57.05	57.05	17.39	*Subbotina* sp.	1	212-250	0.75	-3.09
57.00	57.10	57.05	57.05	17.39	*Subbotina* sp.	1	212-250	-0.03	-3.58
57.00	57.10	57.05	57.05	17.39	*Subbotina* sp.	1	212-250	0.74	-2.60
57.00	57.10	57.05	57.05	17.39	*Subbotina* sp.	1	212-250	0.64	-1.92
57.00	57.10	57.05	57.05	17.39	*Subbotina* sp.	1	212-250	0.14	-1.59
52.00	52.10	52.05	51.92	15.82	*A. acuta*	1	150-212	-3.20	-3.33
52.00	52.10	52.05	51.92	15.82	*A. acuta*	1	150-212	-2.87	-3.56
52.00	52.10	52.05	51.92	15.82	*A. acuta*	1	150-212	-2.58	-3.06

Table 4.4. Trace elemental ratios in planktonic and benthic foraminifera at the MAP 3A core, Medford, NJ. Table includes modified for core expansion depths (mcd). Samples from the core expansion are marked in quotes.

Top (ft)	Bottom (ft)	Mean depth (ft)	Mcd (ft)	Mcd (m)	Species	#, Size (μm)	Mg25 /Ca43
46.00	46.10	46.05	46.05	14.04	*M. acuta*	7x212, 50(?)x150	3.89
47.00	47.10	47.05	47.05	14.34	*M. aequa*	4>300, 2x250, 30x212	3.17
51.00	51.10	51.05	50.98	15.54	*M. acuta*	6x250, 38x212	3.86
52.00	52.10	52.05	51.92	15.82	*M. acuta, velascoensis*	5x250, 30x212, 15x150	3.78
53.00	53.10	53.05	52.85	16.11	*M. acuta, velascoensis*	18x250, 40x212	3.77
54.00	54.10	54.05	53.79	16.39	*M. acuta, velascoensis*	12x250, 40x212	3.87
54.50	54.57	54.54	54.24	16.53	*M. acuta, velascoensis*	30x250, 10x212	3.75
54.70	54.80	54.75	54.44	16.59	*M.acuta, velascoensis*	9x250, 39x212	3.87
54.83	54.90	54.87	54.55	16.63	*M. acuta, velascoensis*	17x212, 60x150	4.11
54.93	55.00	54.97	54.64	16.65	*M. acuta, velascoensis*	8x212, 20x150	4.28
46.00	46.10	46.05	46.05	14.04	*Acarinina* spp., mostly *soldadoensis*	2>300, 5x250, 40x212	3.42
47.00	47.10	47.05	47.05	14.34	*Acarinina* spp., mostly *soldadoensis*	1>200, 4x250, 58(?)x212	3.08
51.00	51.10	51.05	50.98	15.54	*A. soldadoensis*	5>300, 30x250	3.14
52.00	52.10	52.05	51.92	15.82	*A. soldadoensis*	10x250, 15x212, 25x150	3.17
53.00	53.10	53.05	52.85	16.11	*A. soldadoensis*	25x250, 20x212	3.40
54.00	54.10	54.05	53.79	16.39	*A. esnehnsis*	7x250, 20x212, 20x150	3.70
54.50	54.57	54.54	54.24	16.53	*Acarinina* spp., mostly *soldadoensis*	20x250, 30x212	3.59
54.70	54.80	54.75	54.44	16.59	*Acarinina* spp.	9x250, 40x212	3.48
54.83	54.90	54.87	54.55	16.63	mostlly *A. soldadoensis*	5>300, 16x250, 25x212, 20x150	3.28
54.93	55.00	54.97	54.64	16.65	mostlly *A. soldadoensis*, *A. esnehensis*	2>300, 2x250, 15x212, 40x150	3.26
"55.12"	"55.20"	55.16	54.82	16.71	mostlly *A. soldadoensis*, *A. esnehensis*	4x250, 5x212, 28x150	3.49
57.00	57.10	57.05	57.05	17.39	mostlly *A. soldadoensis*	10x212, 45x150	2.94
58.00	58.10	58.05	58.05	17.69	*Acarinina* spp.	2x250, 18x212, 36x150	3.16
46.00	46.10	46.05	46.05	14.04	*Subbotina* spp.	1>300, 11x250, 40x212	3.23
47.00	47.10	47.05	47.05	14.34	*Subbotina* spp.	6x250, 42x212	2.93
51.00	51.10	51.05	50.98	15.54	*Subbotina* spp.	48x150	3.87
52.00	52.10	52.05	51.92	15.82	*Subbotina* spp.	7x250, 40x212	3.62
53.00	53.10	53.05	52.85	16.11	*Subbotina* spp.	12x250, 40x212	4.02
54.00	54.10	54.05	53.79	16.39	*Subbotina* spp.	5x212, 70x150	4.19
54.50	54.57	54.54	54.24	16.53	*Subbotina* spp.	7x212, 59x150	4.24
54.70	54.80	54.75	54.44	16.59	*Subbotina* spp.	16x250, 30x212	4.26
54.83	54.90	54.87	54.55	16.63	*Subbotina* spp.	2x250, 13x212, 55x150	3.97
54.93	55.00	54.97	54.64	16.65	*Subbotina* spp.	4x212, 60x150	4.05
"55.12"	"55.20"	55.16	54.82	16.71	*Subbotina* spp.	10x212, 42x150	3.71
57.00	57.10	57.05	57.05	17.39	*Subbotina* spp.	18x212, 60x150	3.20
58.00	58.10	58.05	58.05	17.69	*Subbotina* spp.	6x250, 19x212, 35x150	3.20
46.00	46.10	46.05	46.05	14.04	*C. alleni, C. howelli*	5x250, 31x212	3.19
47.00	47.10	47.05	47.05	14.34	*C. alleni, C. howelli*	2.300, 2x250, 38x212	3.31
47.95	48.05	48.00	48.00	14.63	*C. alleni, C. howelli*	2x250, 14x212, 30 (40?)x150	2.79
50.10	50.20	50.15	50.14	15.28	mostly *C. howelli*, *C. alleni*	8>300, 1x250, 6x212, 30x150	3.22

57.00	57.10	57.05	57.05	17.39	*C. howelli* (mosty), *C. alleni*	50x212, 30x150	3.18
58.00	58.10	58.05	58.05	17.69	*C. alleni* (mostly), *C. howelli*	5x250, 23x212, 40x150	3.37
59.00	59.10	59.05	59.05	18.00	*C. alleni* (mostly), *C. howelli*	3x250, 20x212, 60x150	3.64
46.00	47.10	46.55	46.55	14.19	*Anomalinoides* spp.	46: 1x250, 7x212, 8x150; 47: 1x250, 12x212, 15x150	2.28
51.00	51.10	51.05	50.98	15.54	*A. acuta*	80x150	4.47
53.00	53.10	53.05	52.85	16.11	*A. acuta*	70x150	4.34
54.00	54.10	54.05	53.79	16.39	*A. acuta*	70x150	3.98
54.50	54.57	54.54	54.24	16.53	*A. acuta*	70x150	3.82
54.70	54.80	54.75	54.44	16.59	*A. acuta*	80x150	3.80
54.83	54.90	54.87	54.55	16.63	*A. acuta*	70x150	3.66
54.93	55.00	54.97	54.64	16.65	*A. acuta*	70x151	3.55
"55.12"	"55.20"	55.16	54.82	16.71	*A. acuta*	67x150	3.69
55.10	55.37	55.24	55.24	16.84	*A. acuta*	55.10: 30x150; 55.30: 40x150	3.34

Table 4.4. Cont.

Mcd (ft)	Species	Mn55/Ca43	I127/Ca43	Nd143/Ca43	U238/Ca43	Fe56/Ca43
46.05	*M. acuta*	232.89	0.83	1.03	97.90	1054.06
47.05	*M. aequa*	181.56	-0.64	0.71	70.19	509.39
50.98	*M. acuta*	594.18	-1.27	5.25	50.54	523.57
51.92	*M. acuta, velascoensis*	783.72	-0.42	5.89	67.40	695.11
52.85	*M. acuta, velascoensis*	759.40	0.12	6.72	82.20	595.38
53.79	*M. acuta, velascoensis*	715.18	0.11	5.76	80.84	988.60
54.24	*M. acuta, velascoensis*	776.24	0.05	4.81	88.52	1768.40
54.44	*M.acuta, velascoensis*	690.14	-0.06	4.55	94.88	1170.80
54.55	*M. acuta, velascoensis*	861.09	-0.17	5.56	138.95	3662.97
54.64	*M. acuta, velascoensis*	841.48	0.60	5.36	137.18	4158.99
46.05	*Acarinina* spp., mostly *soldadoensis*	144.17	0.23	0.43	60.78	493.33
47.05	*Acarinina* spp., mostly *soldadoensis*	155.52	-0.41	0.51	55.76	546.54
50.98	*A. soldadoensis*	452.17	0.07	4.20	57.65	645.69
51.92	*A. soldadoensis*	461.86	-0.46	5.80	60.28	905.43
52.85	*A. soldadoensis*	474.86	-0.03	4.91	67.57	826.05
53.79	*A. esnehnsis*	619.68	-0.09	5.44	82.57	781.11
54.24	*Acarinina* spp., mostly *soldadoensis*	598.78	-0.02	4.07	74.63	1178.72
54.44	*Acarinina* spp.	463.26	-0.56	3.87	82.72	1437.77
54.55	mostlly *A. soldadoensis*	620.66	0.05	5.29	114.00	874.33
54.64	mostlly *A. soldadoensis*, *A. esnehensis*	507.20	-0.28	4.02	98.94	3147.02
54.82	mostlly *A. soldadoensis*, *A. esnehensis*	408.57	-1.81	3.10	88.98	1407.41
57.05	mostlly *A. soldadoensis*	206.27	-4.32	1.45	68.54	1843.32
58.05	*Acarinina* spp.	269.53	0.39	1.16	68.92	1162.92
46.05	*Subbotina* spp.	187.09	0.42	0.67	73.43	318.10
47.05	*Subbotina* spp.	187.43	0.22	0.92	62.43	539.18
50.98	*Subbotina* spp.	442.78	1.40	4.11	49.77	1476.80
51.92	*Subbotina* spp.	522.60	0.12	4.58	55.30	588.87
52.85	*Subbotina* spp.	495.18	0.37	4.40	52.89	795.52
53.79	*Subbotina* spp.	846.00	0.75	6.98	98.36	1419.39
54.24	*Subbotina* spp.	881.74	0.65	5.80	99.57	1423.30
54.44	*Subbotina* spp.	654.54	0.28	4.26	87.30	1173.08
54.55	*Subbotina* spp.	742.64	0.08	4.61	95.83	1928.30
54.64	*Subbotina* spp.	639.50	-0.45	4.34	97.18	1576.60
54.82	*Subbotina* spp.	629.29	-2.83	3.37	103.75	3283.73
57.05	*Subbotina* spp.	261.69	-0.22	1.58	73.77	1486.15
58.05	*Subbotina* spp.	265.89	0.59	1.06	56.68	762.61
46.05	*C. alleni, C. howelli*	201.05	17.60	0.73	85.38	479.58
47.05	*C. alleni, C. howelli*	267.57	20.02	1.03	95.44	651.96
48.00	*C. alleni, C. howelli*	146.38	16.74	2.23	104.27	592.41
50.14	mostly *C. howelli*, *C. alleni*	386.06	19.20	0.92	75.80	487.07
57.05	*C. howelli* (mosty), *C. alleni*	467.34	19.52	2.40	112.99	1082.02
58.05	*C. alleni* (mostly), *C. howelli*	462.03	11.82	1.18	62.66	794.30
59.05	*C. alleni* (mostly), *C. howelli*	430.81	10.72	1.44	96.99	1601.23
46.55	*Anomalinoides* spp.	255.32	17.60	0.92	97.87	1176.15
50.98	*A. acuta*	715.27	17.29	6.84	48.69	903.74
52.85	*A. acuta*	675.39	17.78	6.51	55.37	2192.41
53.79	*A. acuta*	748.55	17.44	6.06	62.25	3313.15
54.24	*A. acuta*	649.01	16.93	4.08	64.71	3176.93
54.44	*A. acuta*	622.34	16.32	4.16	61.05	3179.36
54.55	*A. acuta*	750.99	18.75	5.76	106.51	4592.80
54.64	*A. acuta*	661.14	17.46	7.03	95.59	4410.25
54.82	*A. acuta*	625.87	17.18	4.37	89.07	2464.97
55.24	*A. acuta*	499.26	15.69	2.37	96.33	1109.82

Table 4.5. GDGT abundances and TEX_{86} estimated temperatures [Kim et al., 2010] from the MAP 3B core at Medford, NJ. Table includes modified for core expansion depths (mcd).

Top (ft)	Bottom (ft)	Mean depth (ft)	Mcd (ft)	Mcd (m)	m/z 1302	m/z 1300	m/z 1298	m/z 1296	m/z 1292'
46.07	46.15	46.11	46.11	14.05	13269340	5385307	6690966	3206105	4914781
47.13	47.20	47.17	47.17	14.38	8424596	3416303	4367901	2077540	3075529
48.03	48.10	48.07	48.07	14.65	1941759	913449	2871290	1010788	6592713
48.99	49.06	49.03	49.03	14.94	3054912	1042977	3132958	1212528	7568874
49.99	50.05	50.02	50.02	15.25	2486119	1104122	3522998	1367654	8300755
50.98	51.05	51.02	51.02	15.55	2783317	1386234	4313546	1665680	10173581
52.13	52.20	52.17	52.16	15.90	2661881	1140066	3508255	1348560	7627030
52.99	53.06	53.03	52.98	16.15	2258522	1015117	3051972	1190677	6888301
53.25	53.32	53.29	53.22	16.22	3767997	1521748	4578094	1839277	10373064
53.50	53.55	53.53	53.45	16.29	2111591	930764	2991796	1191482	6946424
53.77	53.82	53.80	53.71	16.37	3633333	1509269	4589582	1805779	9885073
54.00	54.07	54.04	53.94	16.44	4252961	1797979	5516539	2204408	11993736
54.25	54.30	54.28	54.17	16.51	2898724	1274412	3918036	1522296	8263512
54.51	54.56	54.54	54.41	16.59	2972691	1393436	4324054	1750996	9720939
54.76	54.80	54.78	54.65	16.66	2689639	1166310	3247536	1362109	6437672
55.03	55.07	55.05	54.90	16.73	3463112	1761766	4911905	2021121	8335840
55.27	55.31	55.29	55.13	16.80	5492223	2893543	7332912	3155281	10397778
55.51	55.55	55.53	55.36	16.87	3702233	1843548	4513762	1879145	6064231
55.76	55.80	55.78	55.60	16.95	4949959	2820299	6787643	2876776	8451958
55.98	56.03	56.01	55.81	17.01	3549594	1938478	4499652	1921126	5299255
56.24	56.28	56.26	56.06	17.09	4335047	1984100	3321298	1503266	3126273
56.50	56.54	56.52	56.30	17.16	4525293	1959848	2556262	1234356	1987106
56.75	56.80	56.78	56.55	17.24	5117610	2116716	2657238	1301079	2045025
56.95	57.00	56.98	56.74	17.29	8152713	3190684	3715504	1858247	2703397
57.25	57.30	57.28	57.28	17.46	5552939	2402841	2911974	1386860	1999262
57.49	57.54	57.52	57.52	17.53	5680385	2293796	2687057	1307137	1841506
57.70	57.74	57.72	57.72	17.59	4089215	1681490	1978070	975550	1340914
57.96	58.01	57.99	57.99	17.67	3108051	1278332	1538292	714269	1067464
58.96	59.03	59.00	59.00	17.98	4592757	1803352	1953106	1005333	1227896
59.96	60.03	60.00	60.00	18.29	3964017	1498077	1603191	815626	987851
60.96	61.00	60.98	60.98	18.59	6090379	2499890	2891157	1431394	1908296
61.55	61.61	61.58	61.58	18.77	6077820	2551861	2965248	1525702	1974386

Table 4.5. Cont.

Top (ft)	Bottom (ft)	Mean depth (ft)	Mcd (ft)	Mcd (m)	GDGT ratio-1	TEX^{L}_{86}	T^{L} (°C)	GDGT ratio-2	TEX^{H}_{86}	T^{H} (°C)
46.07	46.15	46.11	46.11	14.05	0.44	-0.36	22.7	0.73	-0.13	29.4
47.13	47.20	47.17	47.17	14.38	0.44	-0.35	23.0	0.74	-0.13	29.5
48.03	48.10	48.07	48.07	14.65	0.60	-0.22	31.9	0.92	-0.04	36.1
48.99	49.06	49.03	49.03	14.94	0.58	-0.24	31.0	0.92	-0.04	36.1
49.99	50.05	50.02	50.02	15.25	0.59	-0.23	31.3	0.92	-0.03	36.2
50.98	51.05	51.02	51.02	15.55	0.59	-0.23	31.2	0.92	-0.04	36.2
52.13	52.20	52.17	52.16	15.90	0.59	-0.23	31.2	0.92	-0.04	36.0
52.99	53.06	53.03	52.98	16.15	0.58	-0.24	31.0	0.92	-0.04	36.0
53.25	53.32	53.29	53.22	16.22	0.58	-0.24	30.8	0.92	-0.04	36.0
53.50	53.55	53.53	53.45	16.29	0.59	-0.23	31.2	0.92	-0.03	36.2
53.77	53.82	53.80	53.71	16.37	0.58	-0.24	31.0	0.92	-0.04	36.0
54.00	54.07	54.04	53.94	16.44	0.58	-0.24	30.9	0.92	-0.04	36.0
54.25	54.30	54.28	54.17	16.51	0.58	-0.23	31.1	0.91	-0.04	36.0
54.51	54.56	54.54	54.41	16.59	0.58	-0.24	30.9	0.92	-0.04	36.1
54.76	54.80	54.78	54.65	16.66	0.56	-0.25	30.0	0.90	-0.04	35.6
55.03	55.07	55.05	54.90	16.73	0.56	-0.25	30.2	0.90	-0.05	35.4
55.27	55.31	55.29	55.13	16.80	0.55	-0.26	29.3	0.88	-0.06	34.7
55.51	55.55	55.53	55.36	16.87	0.55	-0.26	29.3	0.87	-0.06	34.5
55.76	55.80	55.78	55.60	16.95	0.54	-0.26	29.0	0.87	-0.06	34.3
55.98	56.03	56.01	55.81	17.01	0.54	-0.27	28.7	0.86	-0.07	34.1
56.24	56.28	56.26	56.06	17.09	0.49	-0.31	25.9	0.80	-0.10	32.0
56.50	56.54	56.52	56.30	17.16	0.44	-0.35	23.1	0.75	-0.13	29.9
56.75	56.80	56.78	56.55	17.24	0.44	-0.36	22.7	0.74	-0.13	29.6
56.95	57.00	56.98	56.74	17.29	0.42	-0.37	21.7	0.72	-0.14	28.9
57.25	57.30	57.28	57.28	17.46	0.43	-0.36	22.5	0.72	-0.14	29.0
57.49	57.54	57.52	57.52	17.53	0.43	-0.37	22.0	0.72	-0.14	28.8
57.70	57.74	57.72	57.72	17.59	0.43	-0.37	21.9	0.72	-0.14	28.8
57.96	58.01	57.99	57.99	17.67	0.44	-0.36	22.5	0.72	-0.14	28.9
58.96	59.03	59.00	59.00	17.98	0.41	-0.39	20.8	0.70	-0.16	28.0
59.96	60.03	60.00	60.00	18.29	0.41	-0.39	20.7	0.69	-0.16	27.8
60.96	61.00	60.98	60.98	18.59	0.42	-0.37	21.7	0.71	-0.15	28.6
61.55	61.61	61.58	61.58	18.77	0.42	-0.38	21.5	0.72	-0.14	28.7

Table 4.6. GDGT abundances and BIT values from the MAP 3B core at Medford, NJ. Table includes modified for core expansion depths (mcd).

Top (ft)	Bottom (ft)	Mean depth (ft)	Mcd (ft)	Mcd (m)	m/z 1292	m/z 1292'	m/z 1050	m/z 1036	m/z 1022	BIT
46.07	46.15	46.11	46.11	14.05	54580112	4914781	137105	256361	1680381	0.04
47.13	47.20	47.17	47.17	14.38	36089232	3075529	113057	209372	1363259	0.04
48.03	48.10	48.07	48.07	14.65	33728392	6592713	37722	146831	1771740	0.05
48.99	49.06	49.03	49.03	14.94	37009684	7568874	42470	137304	1639564	0.05
49.99	50.05	50.02	50.02	15.25	41217996	8300755	40137	131860	1317155	0.03
50.98	51.05	51.02	51.02	15.55	51906332	10173581	37971	145878	1491814	0.03
52.13	52.20	52.17	52.16	15.90	39902372	7627030	39086	171892	1518699	0.04
52.99	53.06	53.03	52.98	16.15	37162520	6888301	34946	132713	1209393	0.04
53.25	53.32	53.29	53.22	16.22	53360428	10373064	79051	314687	2382671	0.05
53.50	53.55	53.53	53.45	16.29	38682232	6946424	44819	174701	1565154	0.04
53.77	53.82	53.80	53.71	16.37	52273532	9885073	60268	205793	1726620	0.04
54.00	54.07	54.04	53.94	16.44	62469496	11993736	100753	404609	2922861	0.05
54.25	54.30	54.28	54.17	16.51	44671172	8263512	49162	191480	1739057	0.04
54.51	54.56	54.54	54.41	16.59	51083776	9720939	67161	241466	2005333	0.04
54.76	54.80	54.78	54.65	16.66	37359164	6437672	72063	248471	1766107	0.05
55.03	55.07	55.05	54.90	16.73	48848436	8335840	80924	247994	1874971	0.04
55.27	55.31	55.29	55.13	16.80	66587312	10397778	105557	364500	2659147	0.04
55.51	55.55	55.53	55.36	16.87	41941388	6064231	65239	235214	1645896	0.04
55.76	55.80	55.78	55.60	16.95	60276404	8451958	82045	294015	2215417	0.04
55.98	56.03	56.01	55.81	17.01	40538648	5299255	57307	190492	1431306	0.04
56.24	56.28	56.26	56.06	17.09	28347438	3126273	67992	184278	1253364	0.05
56.50	56.54	56.52	56.30	17.16	21504910	1987106	57946	106917	764945	0.04
56.75	56.80	56.78	56.55	17.24	23067130	2045025	60155	115522	775927	0.04
56.95	57.00	56.98	56.74	17.29	32925722	2703397	108480	198902	1376166	0.05
57.25	57.30	57.28	57.28	17.46	22669172	1999262	104588	197378	1845169	0.09
57.49	57.54	57.52	57.52	17.53	21977958	1841506	84186	156055	1325858	0.07
57.70	57.74	57.72	57.72	17.59	16424008	1340914	61043	120672	1028410	0.07
57.96	58.01	57.99	57.99	17.67	12574431	1067464	51483	92416	713435	0.06
58.96	59.03	59.00	59.00	17.98	16727530	1227896	56081	104342	733897	0.05
59.96	60.03	60.00	60.00	18.29	14582810	987851	53285	100654	724917	0.06
60.96	61.00	60.98	60.98	18.59	23299552	1908296	86397	170093	1462158	0.07
61.55	61.61	61.58	61.58	18.77	23933874	1974386	85181	164039	1443153	0.07

V CONCLUSIONS AND DISSERTATION FINAL REMARKS

My study of the Paleocene-Eocene Thermal Maximum (PETM) is novel and significant because I integrate chemostratigraphic correlations across paleoshelf sites using planktonic and benthic foraminiferal stable isotopic records and paleotemperature estimates from independent paleoproxies. This high-resolution research is unique in its attempt to explain variations in isotopic gradients recorded by foraminifera from both biotic and environmental perspectives and provides a new interpretation of hydrographic changes on the mid-Atlantic margin (Chapters Two and Three). Additionally, I present a detailed discussion of other possible factors that could have influenced foraminiferal stable isotopic values, such as symbiont loss, carbonate ion concentration, fresh water input, and changes in seasonality (Chapters Two and Three).

Another objective of my work is validation of different proxies for temperature estimates of past climate changes, using the PETM warming as a case study. Chapters Three and Four provide comparisons of warming anomalies estimated from $\delta^{18}O$ and Mg/Ca in planktonic and benthic foraminifera and from the organic paleothermometer TEX_{86}. Based on all proxies, I conclude that the New Jersey paleoshelf experienced a 6-7°C warming during the PETM (Chapter Three). Intersite correlation of these records shows minimal spread in absolute foraminiferal $\delta^{18}O$ and Mg/Ca values between sites and a slightly amplified TEX_{86}-based warming anomaly estimated from proximal sites versus distal sites. I suggest that the TEX_{86} values might be affected by factors other than temperature in shallow, proximal locations on the shelf (Chapter Three).

Moreover, this dissertation attempts to address the timing of the PETM onset and causal mechanism by integrating multiple proxy analyses from the most proximal site at

Medford, NJ. Correlation based on patterns of lithologic and isotopic changes in bulk sediment among New Jersey Coastal Plain (NJCP) sections suggests that the PETM onset at Medford is the most expanded of all NJCP sites. The high-resolution TEX_{86}-based temperature record from the thick onset interval in the Medford core clearly shows no warming prior to the CIE onset, rejecting the precursor warming hypothesis. I suggest conducting a survey to collect sediment coretops from the modern North Atlantic margin, analogous setting to the New Jersey paleoshelf. Such analysis of the spatial TEX_{86} variability would help to elaborate factors controlling archaeal membrane lipids distribution in shallow marine environments, improving the TEX_{86} temperature calibration.

Finally, my Ph.D. work explores the novel paleoredox proxy (I/Ca) to examine deoxygenation of the water column on the New Jersey paleoshelf during the PETM (Chapter Four). The decrease of I/Ca ratio in benthic foraminifera associated with the onset of the PETM indicates lowered O_2 concentrations in the water column that was previously suggested for shelf settings during the PETM. However, the foraminiferal I/Ca values from the Medford section did not indicate fully anoxic conditions on the shelf. My current results suggest I/Ca is a promising paleo-redox proxy that needs to be investigated more for the PETM.

A future contribution, critical to the my studies of the Medford section from Chapter Four, is to complete stable isotopes analyses in single-specimen foraminiferal samples. I suggest examining the nature of the PETM onset by investigating the lead-lags between $\delta^{13}C$ and $\delta^{18}O$ values from individual tests of foraminifera. Although the PETM onset at Medford, NJ is associated with an attendant drop in carbonate content to less

than 1% $CaCO_3$, foraminifera are rare, but well-preserved within the onset interval. Single specimens from the transitional interval of 54.5-56.5 ft (16.6-17.2 m) at the MAP 3A core from Medford, NJ are pending. Therefore, additional data from this expanded PETM onset interval characterized by a gradual decrease in bulk sediment $\delta^{13}C$ values at the Medford section are critical to reconcile the timing of the PETM onset. Study of single specimens can evaluate artifacts due to stratigraphic mixing across the Paleocene/Eocene transition by revealing bimodal distribution in $\delta^{13}C$ and $\delta^{18}O$ values versus intermediate values across the PETM onset. Also, the nature of the PETM onset, fast versus slow, could be characterized by lead/lag relationships between $\delta^{13}C$ and $\delta^{18}O$ anomalies versus synchronous decreases in carbon and oxygen isotopic records.

A corollary and important continuation of my research on the New Jersey paleoshelf would be a comparison of coastal regions with the deep ocean, including slope and basin locations. The PETM sections from NJCP display low carbonate (<1% $CaCO_3$) zones above the CIE onset varying in thickness between ~0.5 m at proximal Wilson Lake and Medford to ~0.1 m at distal Bass River. Arguing against a shelf dissolution event like in the deep sea or diagenesis, I conclude dilution of carbonate on the shelf associated with the rapid input of clay is responsible for the low carbonate zone (Chapter Four). To further address the role of dilution versus dissolution, I suggest tying New Jersey shelf records to the continental slope section from DSDP Site 605 that is located in 2,200 m water depth 100 mi southeast from Atlantic City. Analyses of percent carbonate (% $CaCO_3$) and stable isotopes of both bulk carbonate and foraminifera at DSDP Site 605 would reveal not only hydrographic and ecological responses on the continental slope, but also assist in evaluation of carbonate dilution versus dissolution on the extended mid-

Atlantic section contributing to our understanding of changes in carbon cycle during the PETM on more global scale.

In summary, my Ph.D. dissertation presents an integrated study of environmental, ecological, and hydrographic changes on the mid-Atlantic continental margin during the PETM. Combination of paleoproxies applied in this work improved our constraints in thermal evaluation and showed that the multiproxy approach is extremely useful in studies of critical transitions of past climates, such as the PETM. The proposed future work on single foraminiferal tests at the Medford can greatly contribute to our knowledge of the rapidity of the PETM onset and its causal mechanism. Supplemental research of the PETM section from DSDP Site 605 could provide insights on environmental perturbations associated with the PETM in the deep ocean. Comparison of shelf records from NJCP sites with that from continental slope at DSDP Site 605 would promote extrapolation of findings from this dissertation to the global impact of the PETM on the Earth's system.

APPENDICES

Appendix 1. Trace elements ratios in in *Morozovella*, *Acarinina*, and *Subbotina* spp. at Millville, NJ (Chapter Three).

*See attached excel spread sheet

Appendix 2. Percent coarse (>63 μm) fraction at Millville, NJ (Chapter Two). Table includes modified for core expansion depths (mcd). Samples from the core expansion are marked in quotes.

Top (ft)	Bottom (ft)	Mean depth (ft)	Mcd (ft)	Mcd (m)	Fraction > 63μm (%)
844.92	845.02	844.97	844.97	257.55	40.27
846.10	846.20	846.15	846.15	257.91	58.87
847.40	847.50	847.45	847.45	258.30	42.84
847.82	847.90	847.86	847.86	258.43	38.44
850.10	850.20	850.15	850.15	259.13	44.12
851.10	851.20	851.15	851.14	259.43	48.85
851.90	852.00	851.95	851.93	259.67	51.67
852.30	852.40	852.35	852.33	259.79	52.39
852.80	852.90	852.85	852.82	259.94	13.59
853.14	853.26	853.20	853.17	260.05	11.51
853.90	853.96	853.93	853.89	260.27	9.89
854.38	854.48	854.43	854.39	260.42	10.49
855.20	855.30	855.25	855.20	260.66	14.20
855.90	856.00	855.95	855.89	260.88	11.40
857.00	857.10	857.05	856.98	261.21	9.17
858.00	858.10	858.05	857.97	261.51	2.68
858.56	858.61	858.59	858.50	261.67	2.00
858.92	859.07	859.00	858.91	261.79	5.04
859.21	859.27	859.24	859.15	261.87	2.38
859.53	859.58	859.56	859.46	261.96	3.51
859.95	860.00	859.98	859.88	262.09	1.56
860.47	860.55	860.51	860.49	262.28	1.10
861.10	861.20	861.15	861.10	262.46	1.58
861.90	862.00	861.95	861.86	262.69	1.05
"863.00"	"863.15"	863.08	862.93	263.02	1.09
864.00	864.10	864.05	863.86	263.30	1.10
865.10	865.18	865.14	864.90	263.62	0.93
867.00	867.15	867.08	866.74	264.18	0.64
869.00	869.10	869.05	868.62	264.76	1.06
870.88	871.00	870.94	870.90	265.45	0.77
873.02	873.13	873.08	872.94	266.07	0.92
875.00	875.10	875.05	874.83	266.65	2.09
876.95	877.06	877.01	876.70	267.22	0.82
879.07	879.20	879.14	878.74	267.84	1.18
881.10	881.20	881.15	881.09	268.56	1.06
883.05	883.16	883.11	882.94	269.12	1.05
885.06	885.17	885.12	884.85	269.70	0.51
886.99	887.10	887.05	886.68	270.26	0.98
889.08	889.20	889.14	888.66	270.86	1.19
"890.35"	"890.45"	890.40	889.86	271.23	0.92
890.90	891.02	890.96	890.90	271.55	0.84
891.83	891.95	891.89	891.77	271.81	0.73
893.04	893.16	893.10	892.91	272.16	1.17
894.00	894.06	894.03	893.78	272.43	0.98
894.60	894.65	894.63	894.34	272.60	1.03
895.09	895.19	895.14	894.83	272.74	1.39
895.46	895.50	895.48	895.15	272.84	0.76
895.84	895.89	895.87	895.51	272.95	1.44
896.44	896.54	896.49	896.09	273.13	1.80
896.75	896.80	896.78	896.36	273.21	1.30
896.98	897.11	897.05	896.62	273.29	3.34
897.31	897.43	897.37	896.92	273.38	4.91

897.66	897.72	897.69	897.22	273.47	4.72
"898.16"	"898.23"	898.20	897.70	273.62	8.33
898.34	898.45	898.40	897.88	273.67	11.91
898.64	898.74	898.69	898.16	273.76	13.33
898.94	899.09	899.02	898.46	273.85	14.32
899.05	899.20	899.13	898.57	273.88	17.26
899.20	899.31	899.26	898.69	273.92	18.78
899.73	899.82	899.78	899.18	274.07	19.47
"900.16"	"900.29"	900.23	899.61	274.20	35.13
900.18	900.30	900.24	900.23	274.39	26.34
901.12	901.30	901.21	901.15	274.67	32.21
901.87	902.00	901.94	901.84	274.88	35.55
902.90	903.01	902.96	902.81	275.18	48.70
903.67	903.80	903.74	903.56	275.40	44.87
905.66	905.74	905.70	905.43	275.97	45.11
907.63	907.75	907.69	907.32	276.55	42.41
909.36	909.45	909.41	908.96	277.05	34.59

Appendix 3. Bulk sediment $\delta^{13}C$, $\delta^{18}O$, and % $CaCO_3$ at Millville, NJ (Chapter Two). Table includes modified for core expansion depths (mcd). Samples from the core expansion are marked in quotes.

Top (ft)	Bottom (ft)	Mean depth (ft)	Mcd (ft)	Mcd (m)	$\delta^{13}C$ PDB (‰)	$\delta^{18}O$ PDB (‰)	% $CaCO_3$
844.92	845.02	844.97	844.97	257.55	0.12	-1.43	8.41
846.10	846.20	846.15	846.15	257.91	0.11	-1.23	6.05
847.40	847.50	847.45	847.45	258.30	-0.14	-1.66	9.52
847.82	847.90	847.86	847.86	258.43	0.26	-1.40	8.09
850.10	850.20	850.15	850.15	259.13	0.50	-1.43	5.53
851.10	851.20	851.15	851.14	259.43	0.55	-1.28	4.74
851.90	852.00	851.95	851.93	259.67	0.29	-1.33	5.11
852.30	852.40	852.35	852.33	259.79	0.52	-1.44	4.24
852.80	852.90	852.85	852.82	259.94	0.00	-0.97	8.90
853.14	853.26	853.20	853.17	260.05	0.20	-1.24	5.53
853.90	853.96	853.93	853.89	260.27	0.20	-1.00	5.61
854.38	854.48	854.43	854.39	260.42	0.26	-1.14	5.25
		855.00	854.95	260.59	0.15	-1.35	5.57
855.20	855.30	855.25	855.20	260.66	-0.09	-1.37	5.91
855.90	856.00	855.95	855.89	260.88	-0.46	-1.50	2.99
		856.00	855.94	260.89	-0.39	-1.53	2.93
856.90	857.10	857.00	856.93	261.19	-0.65	-1.63	2.81
858.00	858.10	858.05	857.97	261.51	-0.92	-1.38	4.95
858.56	858.61	858.59	858.50	261.67	-1.00	-1.23	5.48
858.88	859.07	858.98	858.89	261.79	-1.03	-2.04	2.62
859.21	859.27	859.24	859.15	261.87	-1.16	-2.01	4.41
859.53	859.58	859.56	859.46	261.96	-1.14	-2.08	5.30
859.95	860.00	859.98	859.88	262.09	-1.26	-2.36	4.41
860.47	860.55	860.51	860.49	262.28	-1.45	-2.46	2.90
861.10	861.30	861.20	861.14	262.48	-1.42	-2.60	3.58
861.90	862.00	861.95	861.86	262.69	-2.23	-2.64	3.86
863.00	863.20	863.10	862.95	263.03	-1.69	-2.83	3.73
864.00	864.10	864.05	863.86	263.30	-1.74	-2.60	4.39
865.10	865.24	865.17	864.92	263.63	-2.02	-2.87	2.73
		866.00	865.71	263.87	-2.16	-2.84	3.03
867.00	867.25	867.13	866.79	264.20	-2.28	-2.82	2.92
869.00	869.25	869.13	868.70	264.78	-2.48	-2.75	3.07
870.82	871.00	870.91	870.87	265.44	-2.56	-2.83	3.47
872.94	873.13	873.04	872.91	266.06	-2.48	-2.99	3.28
875.00	875.20	875.10	874.88	266.66	-2.23	-3.21	3.05
		876.00	875.74	266.93	-2.42	-2.96	3.06
876.95	877.20	877.08	876.78	267.24	-2.55	-2.94	2.87
		878.00	877.66	267.51	-2.48	-2.86	2.91
879.07	879.32	879.20	878.80	267.86	-2.46	-3.01	2.53
		880.00	880.00	268.22	-2.87	-2.83	3.14
881.10	881.30	881.20	881.14	268.57	-2.81	-3.12	2.94
		882.00	881.90	268.80	-2.53	-2.91	3.82
883.05	883.23	883.14	882.98	269.13	-2.71	-3.00	2.96
		884.00	883.79	269.38	-2.83	-2.85	2.97
885.06	885.25	885.16	884.89	269.71	-3.08	-2.97	2.45
886.99	887.20	887.10	886.73	270.28	-2.78	-3.24	2.42
889.08	889.30	889.19	888.71	270.88	-3.37	-3.03	3.50
890.90	891.06	890.98	890.92	271.55	-3.08	-3.08	3.07
893.04	893.26	893.15	892.96	272.17	-2.88	-3.47	3.75
895.09	895.30	895.20	894.88	272.76	-2.54	-3.39	3.75
896.44	896.64	896.54	896.14	273.14	-2.33	-3.23	2.71
897.31	897.43	897.37	896.92	273.38	-1.99	-2.78	0.45

898.16	898.23	898.20	897.70	273.62	-0.68	-1.84	0.69
898.34	898.60	898.47	897.95	273.70	-0.26	-1.91	0.25
898.64	898.74	898.69	898.16	273.76	-0.17	-2.02	0.34
898.80	899.09	898.95	898.40	273.83	1.21	-1.77	3.03
899.20	899.40	899.30	898.73	273.93	1.01	-1.71	2.87
899.65	899.70	899.68	899.09	274.04	0.93	-1.63	2.63
899.73	899.88	899.81	899.21	274.08	0.94	-1.93	2.00
900.07	900.29	900.18	899.56	274.19	1.18	-1.50	2.41
900.18	900.40	900.29	900.28	274.40	1.34	-1.48	2.35
900.95	901.30	901.13	901.08	274.65	1.88	-1.35	2.97
901.81	902.00	901.91	901.82	274.87	1.71	-1.40	2.53
903.42	903.80	903.61	903.44	275.37	2.08	-1.20	1.90
905.50	905.74	905.62	905.35	275.95	2.30	-1.19	1.80
907.45	907.75	907.60	907.24	276.53	2.26	-1.12	2.15
		908.00	907.62	276.64	2.05	-1.44	2.00
		908.20	907.81	276.70	1.91	-1.40	2.09
		908.40	908.00	276.76	1.94	-1.42	2.06
		908.60	908.19	276.82	2.29	-1.33	2.23
		908.80	908.38	276.87	2.20	-1.55	2.12
		909.00	908.57	276.93	1.86	-1.42	2.34
		909.20	908.76	276.99	1.92	-1.44	1.16
		909.40	908.95	277.05	2.11	-1.42	2.13
909.36	909.52	909.44	908.99	277.06	2.20	-1.58	1.75
		909.60	909.14	277.11	1.97	-1.50	1.72
		909.80	909.33	277.16	2.05	-1.45	1.79
		"910.00"	909.52	277.22	1.82	-1.50	1.18
		"910.20"	909.71	277.28	1.97	-1.47	1.58
		"910.40"	909.90	277.34	2.11	-1.55	1.63
		"910.55"	910.05	277.38	2.07	-1.56	1.47
		910.08	910.08	277.39	2.09	-1.54	1.02
		910.20	910.19	277.43	2.22	-1.49	1.81
		910.40	910.39	277.49	2.13	-1.49	1.35
		910.57	910.55	277.54	2.31	-1.48	1.33
		910.80	910.78	277.60	2.48	-1.27	2.10
		911.00	910.97	277.66	2.46	-1.37	1.46
		911.20	911.17	277.72	2.77	-1.23	1.72
		911.40	911.36	277.78	2.32	-1.26	1.44
		911.60	911.55	277.84	2.37	-1.22	1.07
		911.80	911.75	277.90	2.48	-1.21	1.40
		912.00	911.94	277.96	2.26	-1.33	1.39
		912.20	912.14	278.02	2.33	-1.36	1.44
		912.40	912.33	278.08	2.39	-1.33	1.44
		912.60	912.52	278.14	2.09	-1.81	1.25
		912.80	912.72	278.20	2.16	-1.46	0.98
		913.00	912.91	278.26	2.34	-1.39	0.83
		913.20	913.11	278.31	2.36	-1.37	1.04
		913.40	913.30	278.37	2.49	-1.22	1.28
		913.60	913.50	278.43	2.41	-1.21	1.27
		913.80	913.69	278.49	2.61	-1.24	1.10
		914.00	913.88	278.55	2.60	-1.16	1.06
		914.20	914.08	278.61	2.65	-1.18	1.41
		914.40	914.27	278.67	2.69	-1.38	1.28
		914.60	914.47	278.73	2.62	-1.28	1.04
		914.80	914.66	278.79	2.54	-1.29	0.98
		915.00	914.85	278.85	2.64	-1.17	0.91
		915.20	915.05	278.91	2.24	-1.03	0.75
		915.40	915.24	278.97	2.22	-1.18	0.71
		915.60	915.44	279.03	2.43	-1.17	0.79

915.80	915.63	279.08	2.49	-1.22	1.26
916.00	915.83	279.14	2.39	-1.22	0.76
916.20	916.02	279.20	2.58	-1.19	1.27
916.40	916.21	279.26	2.52	-1.33	1.21
916.60	916.41	279.32	2.23	-1.48	1.31
916.80	916.60	279.38	2.14	-1.46	0.78
917.00	916.80	279.44	2.47	-1.39	1.03
917.20	916.99	279.50	2.62	-1.24	0.97
917.40	917.18	279.56	2.49	-1.40	1.02
917.60	917.38	279.62	2.35	-1.37	0.91
917.80	917.57	279.68	1.65	-0.95	0.29
918.00	917.77	279.74	2.41	-1.06	0.96
918.20	917.96	279.79	2.44	-1.16	0.72
918.40	918.16	279.85	2.45	-1.26	0.95
918.60	918.35	279.91	2.43	-1.30	0.98
918.80	918.54	279.97	2.44	-1.29	0.91
919.00	918.74	280.03	2.57	-1.42	0.92
919.20	918.93	280.09	2.43	-1.27	0.63
919.40	919.13	280.15	2.47	-1.36	0.74
919.60	919.32	280.21	2.38	-1.19	0.63
919.80	919.51	280.27	2.35	-1.08	0.89
920.00	919.71	280.33	1.72	-1.56	0.48
920.00	919.71	280.33	1.93	-1.23	0.39

Appendix 4. Organic carbon data (TOC, $\delta^{13}C$, Total N, C:N) at Millville, NJ (Chapter Two). Table includes modified for core expansion depths (mcd). Samples from the core expansion are marked in quotes.

Top (ft)	Bottom (ft)	Mean depth (ft)	Mcd (ft)	Mcd (m)	$\delta^{13}C$ org (‰)	TOC	N (ppm)	C:N
		855.00	854.95	260.59	-26.73	0.69	427	19.0
		856.00	855.94	260.89	-28.69	0.50	420	14.0
		857.00	856.93	261.19	-28.46	0.58	407	16.7
		858.00	857.92	261.49	-27.13	0.73	452	18.7
858.56	858.61	858.59	858.50	261.67	-27.77	0.51	425	13.9
859.21	859.27	859.24	859.15	261.87	-29.11	0.42	428	11.5
859.53	859.58	859.56	859.46	261.96	-28.96	0.31	358	10.2
859.95	860.00	859.98	859.88	262.09	-29.99	0.24	341	8.1
860.47	860.55	860.51	860.49	262.28	-29.74	0.24	360	7.7
		878.00	877.66	267.51	-29.89	0.55	535	12.1
879.07	879.32	879.20	878.80	267.86	-30.05	0.40	548	8.6
881.10	881.30	881.20	881.14	268.57	-30.18	0.40	569	8.1
883.05	883.23	883.14	882.98	269.13	-30.21	0.37	568	7.6
885.06	885.25	885.16	884.89	269.71	-30.36	0.44	594	8.6
		886.00	885.69	269.96	-30.32	0.47	591	9.3
		887.00	886.64	270.25	-30.44	0.45	579	9.0
		889.60	889.10	271.00	-30.01	0.58	615	11.0
896.44	896.64	896.54	896.14	273.14	-30.15	0.37	546	8.0
897.31	897.43	897.37	896.92	273.38	-29.48	0.53	513	12.0
899.65	899.70	899.68	899.09	274.04	-27.33	0.37	351	12.4
"900.07"	"900.29"	900.18	899.56	274.19	-27.37	0.37	337	12.8
		901.60	901.52	274.78	-28.14	0.37	205	21.0
		903.00	902.86	275.19	-28.37	0.34	146	27.4
903.42	903.80	903.61	903.44	275.37	-26.88	0.25	205	14.0
		904.00	903.81	275.48	-26.12	0.21	199	12.0
905.50	905.74	905.62	905.35	275.95	-26.26	0.19	210	10.4
907.45	907.75	907.60	907.24	276.53	-27.06	0.21	188	13.1
909.36	909.52	909.44	908.99	277.06	-27.32	0.35	275	14.8
		910.00	910.00	277.37	-27.60	0.46	345	15.4
		910.30	910.29	277.46	-27.24	0.36	249	16.8
		910.80	910.78	277.60	-26.89	0.31	249	14.6
		911.50	911.46	277.81	-26.77	0.27	243	13.0
		912.00	911.94	277.96	-27.04	0.40	297	15.6
		912.60	912.52	278.14	-26.86	0.32	260	14.2
		913.60	913.50	278.43	-27.12	0.30	216	16.1
		914.80	914.66	278.79	-26.89	0.26	218	14.0
		916.00	915.83	279.14	-26.45	0.21	215	11.4
		917.20	916.99	279.50	-26.70	0.19	197	11.3
		918.20	917.96	279.79	-26.34	0.26	244	12.4
		920.00	919.71	280.33	-27.00	0.26	228	13.5

Appendix 5. Trace elements ratios in in *Morozovella*, *Acarinina*, *Subbotina, Cibicidoides*, and *Anomalinoides* spp. at MAP 3A, Medford, NJ (Chapter Four).

*See attached excel spread sheet